

Enzymatic valorization of sustainable carbon sources

Inauguraldissertation

zur

Erlangung des akademischen Grades eines

Doktors der Naturwissenschaften (Dr. rer. nat.)

der

Mathematisch-Naturwissenschaftlichen Fakultät

der

Universität Greifswald

vorgelegt von

Henrik Terholsen

Greifswald, Februar 2023

Dekan: Prof. Dr. Gerald Kerth

1. Gutachter: Prof. Dr. Uwe T. Bornscheuer

2. Gutachter: Prof. Dr. Per-Olof Syrén

3. Gutachter: Prof. Dr. Jörg Pietruszka

Tag der Promotion: 25.04.2023

Table of contents

1. Background	1
1.1 Valorization of sustainable carbon sources	1
1.1.1 Sustainable carbon sources	1
1.1.2 Valorization of olive mill wastewater (OMWW)	2
1.1.3 Valorization of lignin from lignocellulose	3
1.1.4 Photocatalytic CO ₂ reduction	7
1.1.4.1 Homogeneous catalysts for photocatalytic CO ₂ reduction to CO	9
1.1.4.2 Enzymes and artificial metalloenzymes for photocatalytic reduction of CO ₂ to CO	10
1.2 Artificial metalloproteins (ArMs)	13
1.3 Amberlyst-15	16
1.4 Enzyme promiscuity	17
1.5 Phenolic acid decarboxylase.....	18
1.5.1 Phenolic acid decarboxylase from <i>Bacillus subtilis</i> (BsPAD).....	19
1.6 Promiscuous acyltransferases/hydrolases.....	21
1.6.1 PestE	24
2. Results	27
2.1 Valorization strategies using BsPAD.....	27
2.1.1 Photo-enzymatic catalytic CO ₂ reduction using a promiscuous decarboxylase as protein scaffold (Article I).....	27
2.1.2 Spectrophotometric and Fluorimetric High-Throughput Assays for Phenolic Acid Decarboxylase (Article II)	31
2.2 Biomass valorization using the promiscuous acyltransferase/ hydrolase PestE	33
2.2.1 Recent Insights and Future Perspectives on Promiscuous Hydrolases/ Acyltransferases (Article III)	33
2.2.2 Rational Design for Enhanced Acyltransferase Activity in Water Catalyzed by the <i>Pyrobaculum calidifontis</i> VA1 Esterase (Article IV).....	36
2.2.3 Recovery of Hydroxytyrosol from Olive Mill Wastewater using the Promiscuous Hydrolase/Acyltransferase PestE (Article V).....	39
2.2.4 An Enzyme Cascade Reaction for the Recovery of Hydroxytyrosol Derivatives from Olive Mill Wastewater (Article VI).....	42
2.2.5 Chemoenzymatic Cascade Reaction for the Valorization of the Lignin Depolymerization Product G-C2-Dioxolane Phenol (Article VII)	44
3. Conclusions	47
4. Literature	49
5. Author Contributions.....	62
6. Articles.....	65
6.1 Article I	65
6.2 Article II	103
6.3 Article III	117
6.4 Article IV	129
6.5 Article V	145
6.6 Article VI	161
6.7 Article VII	169
7. List of Publications	183
8. Acknowledgement	185

List of abbreviations

4VC	4-Vinyl catechol
4VG	4-Vinyl guaiacol
4VP	4-Vinyl phenol
4VS	4-Vinyl syringol
AAF	Aldehyde-assisted fractionation
AH	General acid
Amb-15@PDMS	Amberlyst-15 encapsulated in PDMS
ArM	Artificial metalloproteins
AT/H	Ratio acyl transfer to hydrolysis
B	General base
BpA	Benzophenone-alanine
bpy	Bipyridine
BsPAD	Phenolic acid decarboxylase from <i>Bacillus subtilis</i>
BtCA	Carbonic anhydrase from <i>Bos taurus</i>
CuA	<i>para</i> -Coumaric acid
CaA	Caffeic acid
CAL-A	Lipase A from <i>Candida antarctica</i>
CODH	Carbon monoxide dehydrogenase
CoPPIX	Cobalt protoporphyrin IX
CpLIP2	Lipase II from <i>Candida parapsilosis</i>
cyclam	1,4,8,11-Tetraazacyclotetradecane
Cyt b ₅₆₂	Cytochrome b ₅₆₂
DAF	Diol-assisted fractionation
DOX	G-C2 dioxolane phenol
<i>E. coli</i>	<i>Escherichia coli</i>
EcPanD	Aspartate-1-decarboxylase from <i>E. coli</i>
EcPPC	Phosphoenolpyruvate carboxylase from <i>E. coli</i>
EstA	Esterase A from <i>Arthrobacter nitroguajacolicus</i>
EstCE1	Esterase from a soil metagenome
EtOAc	Ethyl acetate
FA	Ferulic acid
GC	Gas chromatography
HLADH	Alcohol dehydrogenase from horse liver
HPLC	High performance liquid chromatography

HT	3-Hydroxytyrosol
HTA	3-Hydroxytyrosol acetate
HV	Homovanillin
HVA	Homovanillyl alcohol
HVB	Homovanillyl butyrate
K_M	Michaelis–Menten constant
LmrR	Multidrug resistance regulator from <i>Lactococcus lactis</i>
MD	Molecular dynamics
MES	2-(<i>N</i> -morpholino)ethanesulfonic acid
MmPPP2	Protocatechuate decarboxylase from <i>Madurella mycetomatis</i>
MsAcT	Acyltransferase from <i>Mycobacterium smegmatis</i>
NaAsch	Sodium ascorbate
OMWW	Olive mill wastewater
PAD	Phenolic acid decarboxylase
PDB	Protein Data Bank
PDMS	Polydimethylsiloxane
PestE	Esterase from <i>Pyrobaculum calidifontis</i> VA1
PFE	Esterase I from <i>Pseudomonas fluorescens</i>
PH	Product hydrolysis
<i>p</i> NP	<i>para</i> -Nitrophenol
<i>p</i> NPA	<i>para</i> -Nitrophenyl acetate
PS	Photosensitizer
RCF	Reductive catalytic fractionation
SA	Sinapic acid
ScFDC1	Ferulic acid decarboxylase 1 from <i>Saccharomyces cerevisiae</i>
SD	Sacrificial donors
sYFP	superfolder yellow fluorescent protein
SsTrpC	Indole-3-glycerol phosphate synthase from <i>Sulfolobus solfataricus</i>
TEOA	Triethanolamine
terpy	Terpyridine
TLC	Thin-layer chromatography
TON	Turnover number
TtALS	Acetolactate synthase from <i>Thermus thermophilus</i>
V_{max}	Maximum reaction rate

Scope & Outline

In this thesis, new catalysts as well as unprecedented approaches for the valorization of sustainable carbon sources were investigated. The first part deals with the design of catalysts for photocatalytic CO₂ reduction (**Articles I&II**). With the aim of designing an artificial metalloprotein for photocatalytic CO₂ reduction, we found the promiscuous activity of phenolic acid decarboxylase from *Bacillus subtilis* (BsPAD) to catalyze CO₂ reduction (Article I). This cofactor-free enzyme could facilitate the replacement of (noble) metal catalysts regularly employed in CO₂ reduction. Mutagenesis identified essential amino acids involved in CO₂ binding and electron transfer. Based on these findings, additional enzyme catalysts were identified for photocatalytic CO₂ reduction. Absorbance- and fluorescence-based assays were developed for the rapid and accurate determination of kinetic parameters for the native decarboxylation activity of BsPAD (**Article II**). The second part (**Articles III-VII**) focuses on the valorization of resources obtained from biomass by the promising acyltransferases/hydrolase PestE from *Pyrobaculum calidifontis* VA1 (**Articles IV-VII**). **Article III** is a 'perspective paper' about the discovery, development, and application of promiscuous acyltransferases/hydrolase, enzymes capable of performing acyl transfer reactions in water. Recently, the promiscuous acyltransferase activity of PestE was discovered in our group, Insight into the range of acyl transfer substrates and the development of the hyperthermostable esterase was gained by studying the acetylation of monoterpene alcohols (**Article IV**). Furthermore, PestE was engineered towards the acetylation of hydroxytyrosol from olive mill wastewater, yielding value-added hydroxytyrosol acetate (**Articles V&VI**). The use of PestE in cascade reactions was investigated as well (**Articles VI&VII**), demonstrating compatibility with other enzymes and chemical reactions for the valorization of the biomass-derived hydroxytyrosol glucoside oleuropein and the lignin depolymerization product G-C2 dioxolane phenol, respectively.

Article I Photo-enzymatic Catalytic CO₂ Reduction Using a Promiscuous Decarboxylase as Protein Scaffold

Henrik Terholsen*, Hilario Diego Huerta-Zerón*, Christina Möller, Henrik Junge, Uwe T. Bornscheuer, Matthias Beller

Nature Catal., submitted

**with equal contribution*

A new promiscuity of CO₂-binding enzymes was found for the photocatalytic reduction of CO₂ to CO. In addition, BsPAD, an enzyme with promising initial turnover numbers and high selectivity avoiding the potential by-product hydrogen, was engineered, resulting in increased activity and providing insights into the amino acids involved in the catalytic CO₂ reduction.

Article II Spectrophotometric and Fluorimetric High-Throughput Assays for Phenolic Acid Decarboxylase

Henrik Terholsen*, Kamela Myrtiliari*, Christina Möller, Robert Kourist, Uwe T. Bornscheuer, Daniel Kracher

Manuscript in preparation

**with equal contribution*

A fluorescence-based and an absorbance-based assay to detect the decarboxylation of phenolic acids to 4-vinyl phenols were developed. Both assays were validated by measuring the kinetic parameters for BsPAD.

Article III Recent Insights and Future Perspectives on Promiscuous Hydrolases/Acyltransferases

Henrik Müller, Henrik Terholsen, Simon P. Godehard, Christoffel P.S. Badenhorst, and Uwe T. Bornscheuer

ASC Catal., **2021**, *11*, 14906–14915

This ‘perspectives article’ focuses on the discovery, mechanism, synthetic application, and enzyme engineering of promiscuous acyltransferases/hydrolases.

Article IV Rational Design for Enhanced Acyltransferase Activity in Water Catalyzed by the *Pyrobaculum calidifontis* VA1 Esterase

Amanda Staudt, Henrik Terholsen, Jasmin Kaur, Henrik Müller, Simon P. Godehard,IVALDO Itabaiana Jr., Ivana C.R. Leal and Uwe T. Bornscheuer

Microorganisms, **2021**, *9*, 1790

The acyltransferase activity of the esterase from *Pyrobaculum calidifontis* VA1, PestE, was studied by screening monoterpene alcohols. PestE was modified to decrease its hydrolysis activity and increase its selectivity for the synthesis of (-)-menthyl acetate from a racemic monoterpene mixture. In addition to the reactive enol ester vinyl acetate, the non-activated acyl donor ethyl acetate was used for the acetylation of citronellol.

Article V Recovery of Hydroxytyrosol from Olive Mill Wastewater Using the Promiscuous Hydrolase/Acyltransferase PestE

Henrik Terholsen, Jasmin Kaur, Nikolaos Kaloudis, Amanda Staudt, Henrik Müller, Ioannis V. Pavlidis, and Uwe T. Bornscheuer

ChemBioChem, **2022**, 23, e202200254

PestE was engineered and investigated for the acetylation of the valuable antioxidant hydroxytyrosol, resulting in PestE_I208A_L209F_N288A. The enzyme was immobilized and used for the recovery of hydroxytyrosol acetate from Cretan olive mill wastewaters in a two-phase system with ethyl acetate.

Article VI An Enzyme Cascade Reaction for the Recovery of Hydroxytyrosol Derivatives from Olive Mill Wastewater

Henrik Terholsen, Jasmin Kaur, Nikolaos Kaloudis, Amanda Staudt, Ioannis V. Pavlidis, and Uwe T. Bornscheuer

Chem. Ing. Tech. **2022**, 94, 1860–1863

An enzymatic cascade reaction converted the hydroxytyrosol glycoside oleuropein to hydroxytyrosol acetate using a glucosidase and recently introduced acyltransferase mutant PestE_I208A_L209F_N288A, respectively. The reaction was carried out in a sequential flow setup.

Article VII Chemoenzymatic Cascade Reaction for the Valorization of the Lignin Depolymerization Product G-C2-Dioxolan Phenol

Henrik Terholsen, Jule Ruth Heike Meyer, Zhenlei Zhang, Peter J. Deuss, and Uwe T. Bornscheuer

ChemSusChem, *submitted*

A one-pot chemoenzymatic cascade was developed for the valorization of G-C2 dioxolane phenol, a lignin depolymerization product. For this purpose, a novel polydimethylsiloxane-coated solid acid catalyst based on Amberlyst-15 was used to deprotect the acetal in a buffered solution. The released homovanillin was converted to homovanillyl butyrate, using horse liver alcohol dehydrogenase and PestE_I208A_L209F_N288A.

1. Background

1.1 Valorization of sustainable carbon sources

1.1.1 Sustainable carbon sources

The stewardship of resources will be one of the most important topics in the decades to come, as also emphasized by the Sustainable Development goals of the United Nations established in 2015^[1]. Goal 12 “Responsible Consumption and Production” includes the sustainable production of chemicals, i.e., the substitution of fossil raw materials and the development of a circular economy. Recycling end-of-life materials and the use of bio-based feedstocks for chemicals could make an important contribution, as also described in one of the 12 principles of a ‘greener’ chemistry^[2]. However, the choice of bio-based feedstocks needs to be carefully considered to avoid conflict with food production through direct resource competition or land use, both negatively impacting the United Nations Sustainable Development Goal “Zero Hunger” (Goal 2). Therefore, some popular bio-based syntheses, such as the production of bio-fuels based on vegetable oils, may only be a transitional method that needs to be reconsidered in the future. In contrast, the utilization of agricultural waste, including crop residues could be an approach that is consistent with the United Nations Sustainable Development Goals 2 and 12, and, thus, is a viable path to pursue. In addition to bio-based materials, CO₂ utilization could also contribute to building a circular economy. CO₂ utilization not only has the potential to sustainably produce chemicals but to reduce the amount of environmentally harmful greenhouse gases at the same time if CO₂ is captured from the air.

1.1.2 Valorization of olive mill wastewater (OMWW)

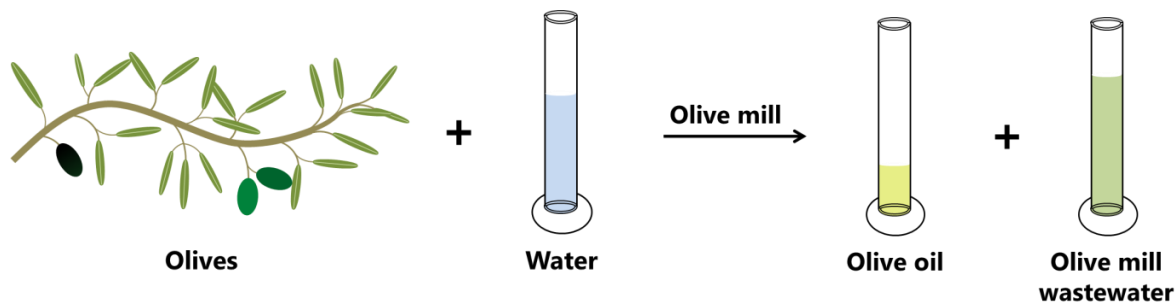


Figure 1. Schematic visualization of olive oil production.

Olive mill wastewater (OMWW) is a by-product of olive oil production (Figure 1) and is generated besides oil and solid pomace in three-phase olive mills. Annually, about 30 million m³ of OMWW are produced worldwide from October to February. Three to five liters of wastewater are produced per kilogram of olive oil; therefore, a small olive mill already produces about 1,000,000 liters of OMWW per season. The wastewater leads to environmental problems as it has a high polluting organic load, including polyphenolics, sugars, and lipids^[3]. In addition to the acidity of the OMWW (pH ~5), the phytotoxic and antimicrobial activities of polyphenolics hinder the biodegradation of organic compounds^[4,5]. Consequently, long-term incubation in open ponds, chemical treatment to decompose the organic matter, as well as illegal disposal are widespread^[3,6,7]. Besides the odor and land requirements of open pond OMWW treatment, the economic value of the phenols is also lost^[3]. Olive phenols (Figure 2), especially hydroxytyrosol (HT) and its natural derivatives such as hydroxytyrosol acetate (HTA), have gained interest due to their neuroprotective, antioxidant, and anti-inflammatory properties^[8–12]. The industrial production of these health-promoting phenols is based on fossil feedstock^[13]. Thus, there is a demand for new sustainable synthetic routes or extraction methods for HT and derivatives. Although the HT concentration in OMWW is up to 10 mM^[14], no HT derivatives are prepared from OMWW because HT is difficult to extract in high purity^[13]. The existing OMWW extraction methods (e.g., solvent extraction, membrane or adsorbent systems) fail due to economic and/or purity issues^[14–22]. Adsorbent and membrane systems for phenol recovery are costly and require pretreatment of the wastewater to remove, for example, residual solids and gelling substances that could block the systems^[3]. Solvent extractions require several steps to achieve good recovery since HT is a relatively polar compound and is difficult to extract even with relatively polar

1. Background

organic solvents such as ethyl acetate (EtOAc)^[14,15]. All methods for the valorization of OMWW suffer from poor selectivity of HT recovery due to the structural similarity to other olive phenols (Figure 2)^[14–22]. The produced phenol-rich extracts from OMWW could be used as stabilizers in the food industry^[23–27], but cannot substitute the synthesis of synthetic HT derivatives. Furthermore, HT recovery from OMWW still suffers from long duration and low recovery yields^[28]. Therefore, new methods for process intensification have to be found and will be discussed in this thesis.

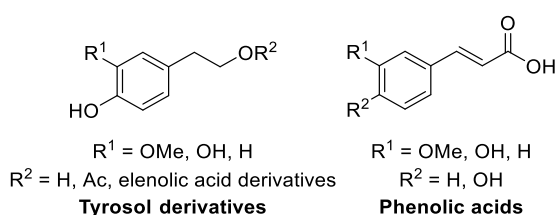


Figure 2. Main classes of olive phenols.

1.1.3 Valorization of lignin from lignocellulose

Besides hemicellulose and cellulose, lignin is part of the plant cell wall scaffolding material lignocellulose, which is one of the most abundant renewable resources on earth^[29]. Cellulose and hemicellulose are carbohydrate polymers and are used in the pulp and paper industry or the production of various sugar-based platform chemicals such as hydroxymethylfurfural^[30–32]. Valorization of the more complex hemicellulose, which is partially linked to lignin, is more difficult but is the subject of current research^[33,34]. Lignin is composed of three monolignols; *p*-coumaryl alcohol, coniferyl alcohol, and sinapyl alcohol. The composition of the building blocks and the linkages result in a very complex and structurally diverse polymer that differs according to plant species, age, and growth condition (Figure 3)^[35,36].

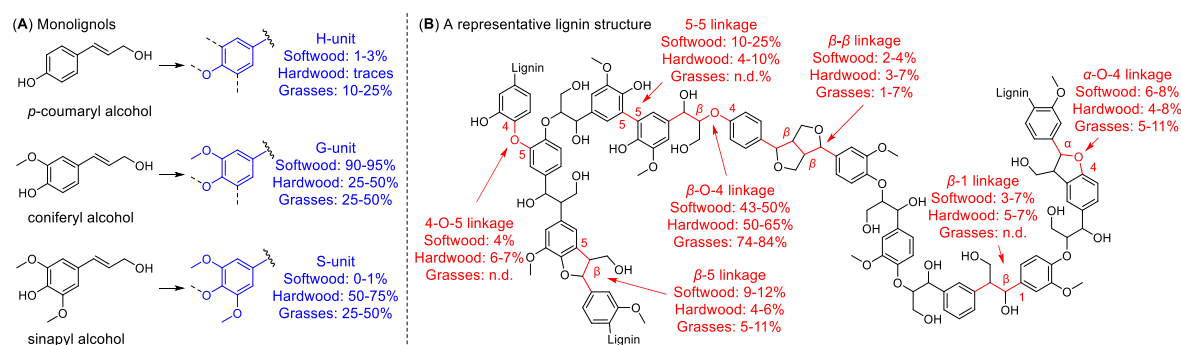


Figure 3. Structure of lignin. (A) Monolignols and composition of lignin subunits in softwoods, hardwoods, and grasses^[37,38]. (B) A representative lignin structure with common linkages and their composition in softwood, hardwood, and grasses^[39].

1. Background

In the pulp and paper industry, lignin is typically not utilized for the production of chemically defined compounds as the focus is on high-quality (hemi-)cellulose extraction. Therefore, lignin is degraded by sodium sulfite and sodium hydroxide, producing sulfonated kraft lignin, which is used as a combustible to supply energy for paper production^[40]. Kraft lignin is irreversibly modified and not a suitable source of defined phenolic compounds^[40]. Other established methods for lignin utilization, including thermal, solvolytic, and acid-catalyzed extraction/degradation, require a lot of energy or result in low phenol recovery (below 25 wt%) due to repolymerization of intermediates (Figure 4)^[29].

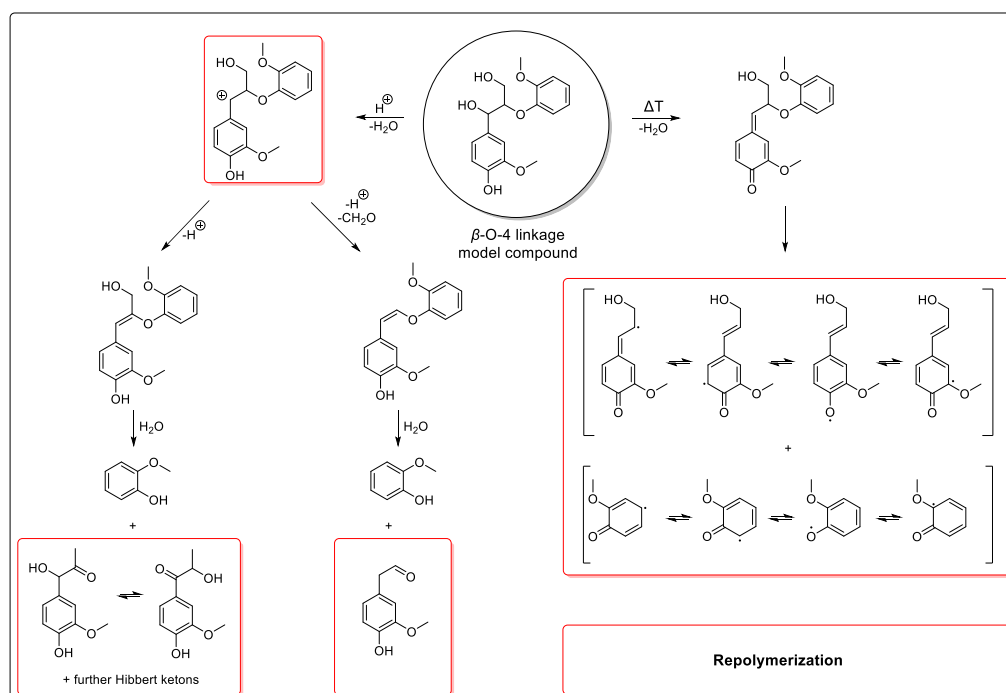


Figure 4. Reactive intermediates formed during thermal (radical) and acidic (cationic) cleavage of a β -O-4-linkage, shown for a model substrate. Intermediates that tend to repolymerize are highlighted in red^[29,41].

Therefore, besides novel extraction methods such as lignin fractionation with ammonia^[42–44], fractionation with ionic liquids^[45–48], hydrolysis with γ -valerolactone^[49], and (mild) organosolv techniques^[50–52], lignin depolymerization strategies are required that prevent the repolymerization of reactive depolymerization intermediates to form defined chemical compounds. Apart from biochemical transformations using (engineered) *Pseudomonas putida*^[53–55], modern lignin depolymerization strategies include stabilization of reactive intermediates via oxidation, reduction, or introduction of protection groups

1. Background

(Figure 5)^[38]. By preventing repolymerization, the yield of lignin monomers could be increased by 2 to 10 times^[56,57].

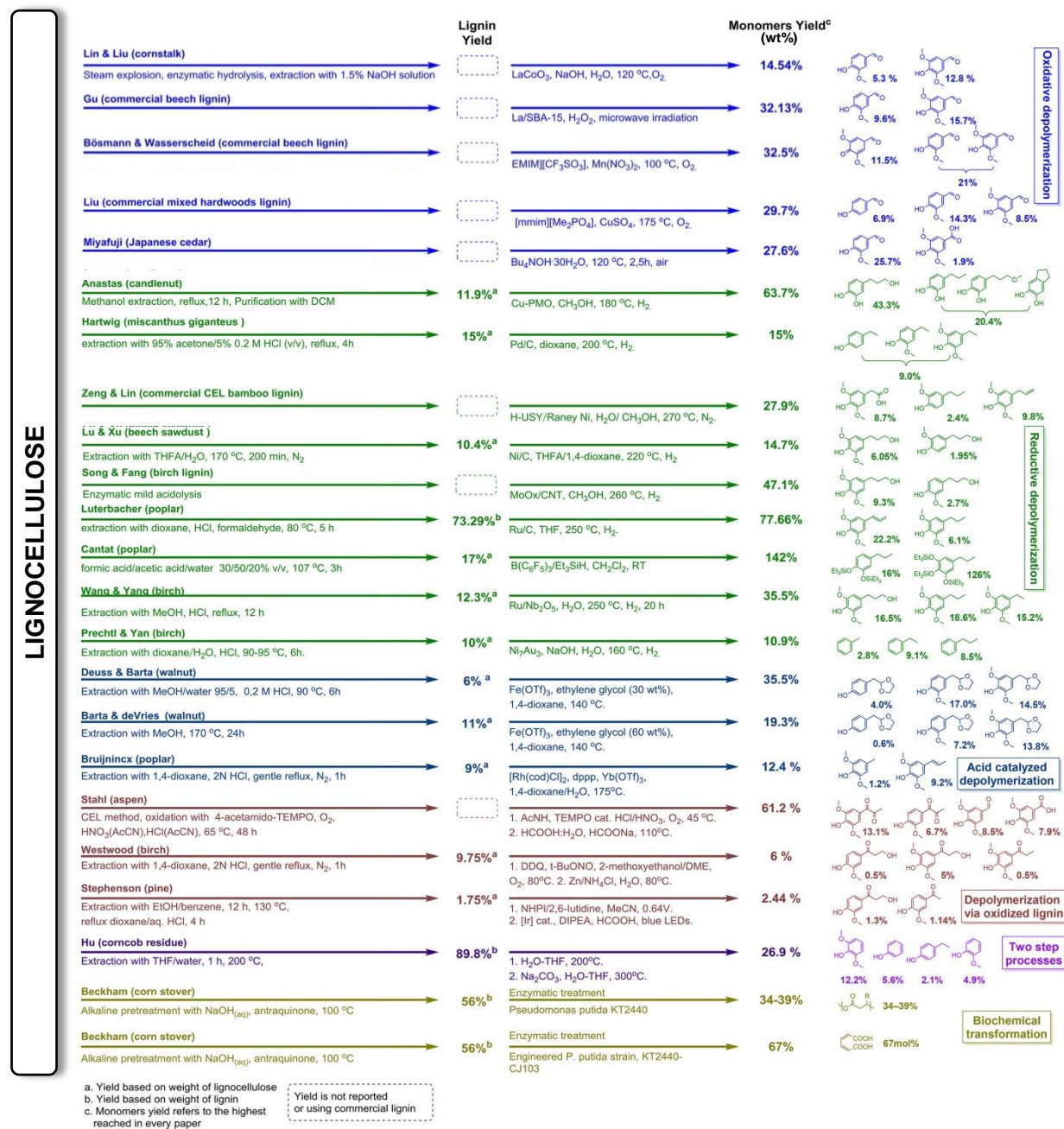


Figure 5. Examples of lignin extraction and depolymerization strategies. The figure was modified and adapted from Sun et al.^[38].

However, most of the depolymerization strategies presented in Figure 5 only focus on the valorization of lignin and neglect the (hemi-)cellulose contained in lignocellulose. In order to efficiently utilize lignocellulose as a sustainable resource, extraction, and depolymerization strategies must be developed that allow (hemi-)cellulose and lignin to be used for the production of structurally

1. Background

defined chemical compounds. In this context, the "lignin-first" concept has gained attention in recent years, which is primarily concerned with the utilization of lignin but also with the provision of high-quality (hemi-)cellulose products^[40,58]. In the recently published "Guidelines for Performing Lignin-first Biorefining", three methods are mentioned that have been successfully used to depolymerize lignin and produce (hemi-)cellulose-rich pulp (Figure 6)^[58].

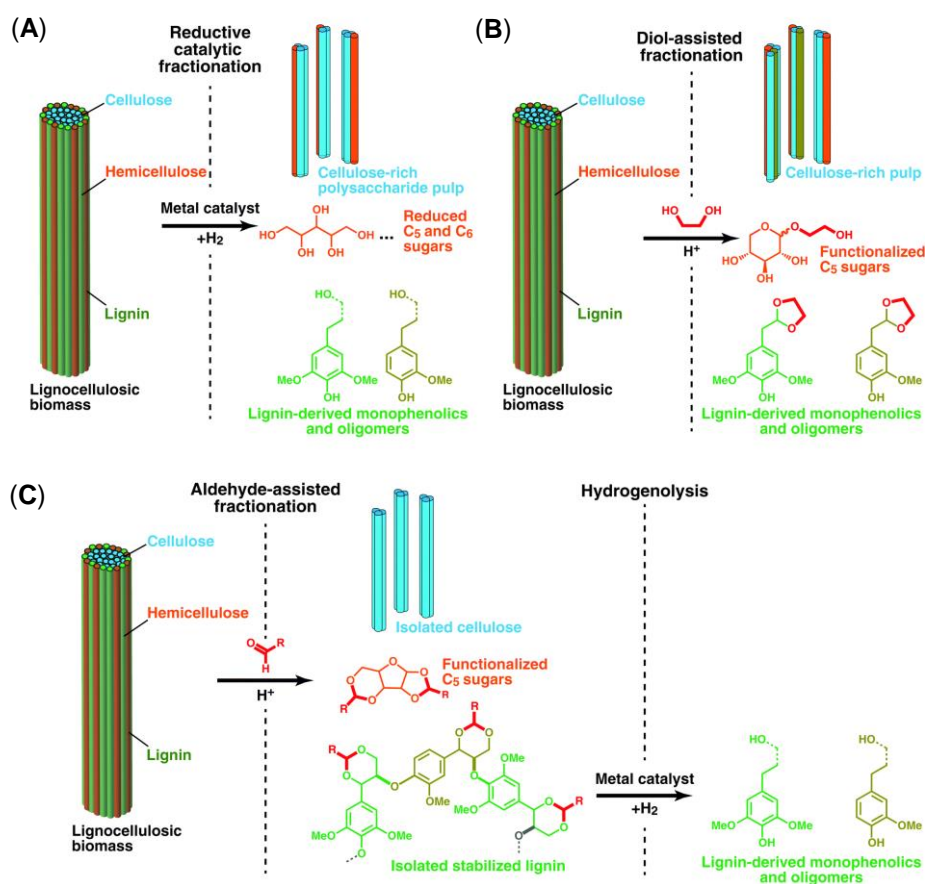


Figure 6. Three strategies following the "lignin first" strategy with solvolysis and catalytic stabilization of reactive intermediates. (A) Reductive catalytic fractionation with a metal catalyst in a polar protic solvent. (B) Diol-assisted fractionation with acid-catalyzed depolymerization in a non-protic solvent. (C) Aldehyde-assisted fractionation with acid-catalyzed depolymerization in a non-protic solvent, followed by a reductive step to obtain monomers. The figure was adapted and modified from Abu-Omar et al.^[58].

In the reductive catalytic fractionation strategy (RCF, Figure 6A) lignin is selectively extracted from the cell walls using a metal catalyst and hydrogen (or hydrogen donors) in a polar protic solvent. The depolymerization products are stabilized using reduction chemistry, leading to reduced lignin oligo- and monomers^[29,40,58–64]. On a small scale, RCF was used to analyze lignin as early as in the 1940s and has regained importance for lignin valorization in the last decades^[65–70]. In the diol-assisted

fractionation (DAF, Figure 6B) reactive intermediates from acid-catalyzed lignin depolymerization, typically catalyzed by sulfuric acid, trifluoromethanesulfonic acid, or metal triflates, are protected by diols such as ethylene glycol. DAF yield lignin mono- and oligomer derived acetals, diol-modified sugars, and cellulose-rich pulp^[50,71–74]. Similarly to DAF, in the aldehyde-assisted fractionation (AAF, Figure 6C) an acid catalyst depolymerizes lignin leads to reactive intermediates. In AAF, reactive intermediates are protected by aldehydes. However, an additional catalytic reduction step is required to generate low molecular weight lignin depolymerization products, clean cellulose, and acetal-protected sugars^[57,75]. RCF, DAF, and AAF lead to low molecular weight lignin-based phenolic compounds that can potentially be used as platform chemicals. Nonetheless, for most depolymerization products, conversion to value-added products remains to be demonstrated.

1.1.4 Photocatalytic CO₂ reduction

CO₂ is a greenhouse gas and its emission significantly contributes to global warming. In 2020 100 Mt CO₂ was emitted per day^[76]. Therefore, the utilization of CO₂ as a carbon source would decrease the negative impact on global warming and help to substitute fossil resources. However, utilizing CO₂ from the atmosphere is challenging because the concentration is only about 414 ppm (2020)^[77]. Even though CO₂ was only about 250 ppm before the industrial revolution^[77], there is still only about 0.63 g of CO₂ in a cubic meter of air, which means a large volume of air must be used and the catalysts used for CO₂ utilization would have to be both very sensitive and selective for CO₂ to yield justifiable amounts of fixation product. Therefore, methods to enrich and fix the CO₂ from air are the focus of many research projects^[78–83]. Higher CO₂ concentrations are present in gaseous waste streams, e.g., from fossil fuel power plants, although their use will be reduced in the coming decades in the wake of global warming^[81].

As mentioned earlier, besides CO₂ fixation, the development of new catalysts for CO₂ valorization is required to enable the conversion of CO₂ into value-added chemicals and substituting fossil fuel feedstocks. Since the carbon atom CO₂ is completely oxidized (+4 oxidation state), most utilization strategies, except for the

1. Background

use of carbonates, involve a (chemical) reduction, i.e., the transfer of electrons to CO₂ (hereafter referred to as "reduction"). In recent decades, many different CO₂ utilization strategies have been investigated including plasma catalytic^[84,85], electrochemical^[86,87], photocatalytic^[88–90], thermochemical^[91,92], and biochemical^[93–95] conversions. However, only photocatalytic CO₂ conversion will be discussed in detail in the following.

Photocatalytic CO₂ conversion is probably the most widely used CO₂ reduction concept in nature. The first step of photosynthesis converts atmospheric CO₂ to biomass, utilizing water as the reducing agent (Figure 7A). Since photosynthetic organisms also consume energy, the productivity of natural photosynthetic systems is relatively low, not exceeding 1% and 3% of the solar energy input on an annual basis for plants and microalgae, respectively^[96]. Therefore, synthetic systems for photocatalytic CO₂ reduction, so-called artificial photosynthetic systems (Figure 7B), could potentially have higher efficiency^[97]. Artificial photosynthetic systems that achieve the same efficiency as plants have already been discovered^[97,98]. However, extended research is needed to further increase efficiency.

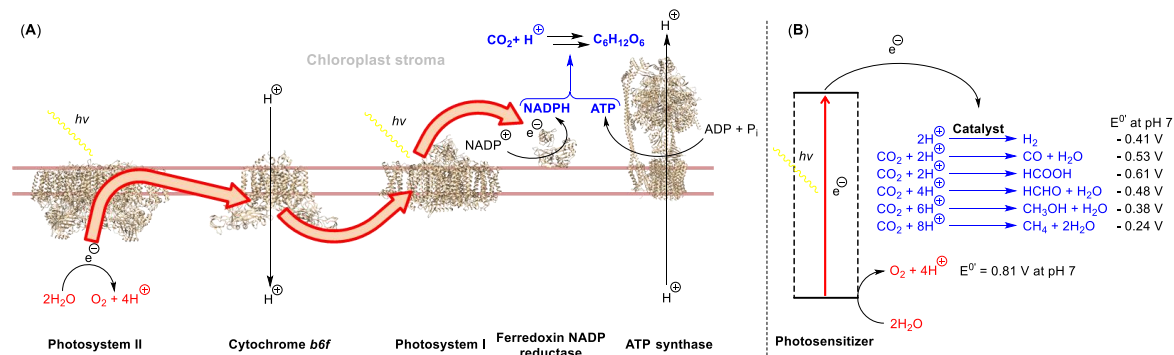


Figure 7. Comparison of photosynthesis and artificial photosynthesis^[99]. The water oxidation and CO₂ reduction reactions are highlighted in red and blue, respectively. (A) Simplified scheme for the photosynthesis showing the proteins involved, photosystem II (PDB 2AXT), cytochrome *b6f* (PDB 1Q90), photosystem I (PDB 7WFE), ferredoxin NADP reductase (PDB 5H5J), and ATP synthase (PDB 6FKH). (B) Scheme of the artificial photosynthesis with a photosensitizer that oxidizes water and transfers electrons after light excitation to the catalyst that performs CO₂ reduction. The potentials against the standard hydrogen electrode at pH 7 are given^[100].

The use of water as a reducing agent in photocatalytic CO₂ reduction is desirable because it is abundant, cheap, non-toxic, and produces only oxygen and protons as by-products. To perform photocatalytic CO₂ reduction with water as the reducing agent, the photosensitizer (PS) must at least bridge the potential difference (ΔE^0) between the water oxidation reaction and the CO₂ reduction

1. Background

reaction. Because the potential difference is relatively high and typically some overpotential is required, only a few PS can use water as a reducing agent and reduce CO_2 ^[101–104]. In addition, any PS must be able to operate in water, which is a major limitation^[101,105,106]. PS research is ongoing, and reliable PS systems that oxidize water and enable CO_2 reduction may be available in the future^[106–109]. Currently, well-established PSs are often ruthenium-based. They exhibit strong reducing power and long excited state lifetimes^[110–113]. Nonetheless, ruthenium-based PSs such as tris(bipyridine)ruthenium(II) ($[\text{Ru}(\text{bpy})_3]^{2+}$) are unable to oxidize water^[114] and, therefore, require other reducing agents to provide electrons. These sacrificial donors (SD) include sodium ascorbate (NaAscH)^[110,113], 2-(*N*-morpholino)ethanesulfonic acid (MES)^[115], or triethanolamine (TEOA)^[111,116] (Figure 8).

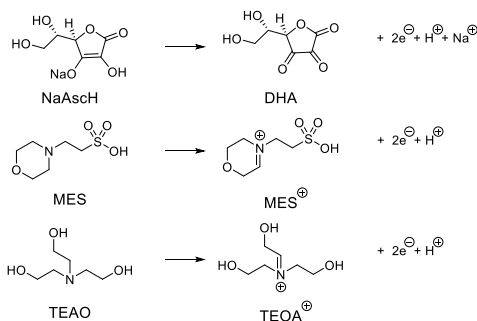


Figure 8. Selection of sacrificial donors. Oxidation of NaAscH, MES, and TEOA to dehydroascorbic acid (DHA) and the iminium forms of MES (MES^+) and TEOA (TEOA^+), respectively.

Although well-functioning PS/SD systems facilitate the development of CO_2 reduction catalysts, SD must be avoided in the long-term since stoichiometric consumption of the SD is not desirable from an atomic economy perspective.

1.1.4.1 Homogeneous catalysts for photocatalytic CO_2 reduction to CO

Photocatalytic CO_2 reduction usually leads to the formation of C_1 building blocks and hydrogen (Figure 7B) since high electron densities are required to generate $>\text{C}_2$ products^[88]. CO could be used as a precursor for $>\text{C}_2$ chemicals, e.g., through the Fischer-Tropsch synthesis, in which alkanes are produced from CO and H_2 ^[88]. Although the formation of CO and H_2 in a 1:1 ratio may be desirable for this particular application^[117], the selective formation of CO is generally targeted.

1. Background

A major obstacle in the development of homogeneous CO₂ reduction catalysts for CO formation is the selectivity between CO, other CO₂ reduction products including formate, methanol, or methane, and hydrogen production since hydrogen and CO₂ reduction products have very similar standard potentials^[100]. Therefore, the selectivity, i.e., the molar percentage of CO formed compared to other CO₂ reduction products and H₂, is monitored for each catalysis. As mentioned earlier, ideal artificial photosynthetic systems utilize water as a reductant in which they should also operate. However, since protons are abundant in aqueous solutions compared to non-protic organic solvents previously used in CO₂ reduction systems, it is more difficult to selectively reduce CO₂ in water^[118–125]. Furthermore, the low solubility of CO₂ and catalysts in aqueous solutions compared to organic solvents (e.g., acetonitrile and dimethylformamide) is a challenge for catalyst development^[126]. Therefore, photocatalytic systems that exhibited both high activity and high selectivity in fully aqueous media are rare and were predominantly depend on noble metals^[110,127–129]. Recently, a range of water-soluble cobalt-porphyrin complexes were developed as catalysts for photocatalytic CO₂ reduction in water by the group of Sakai^[110,130]. Sulfonatophenyl- and *N*-methylpyridinium modified cobalt-porphyrin complexes reached TONs of 926 and 2,680 with 82% and 77% selectivity, respectively (Figure 9)^[110,130].

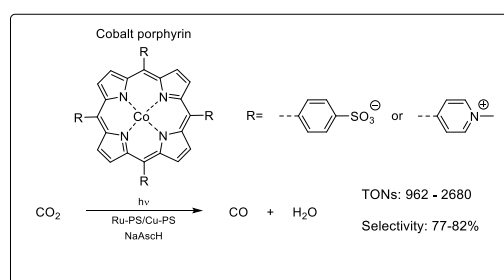


Figure 9. Photocatalytic CO₂ reduction to CO in water using cobalt porphyrin complexes. Water-soluble cobalt porphyrin complexes were prepared by attaching charged sulfonium or pyridinium groups to the catalyst^[110,130].

1.1.4.2 Enzymes and artificial metalloenzymes for photocatalytic reduction of CO₂ to CO

Enzymes have been used as selective catalysts in various applications due to their well-defined 3D structure and properties of (catalytic) amino acids^[131]. Therefore, enzymes could also be considered to solve the selectivity problem in

photocatalytic CO₂ reduction to CO. Indeed, there is a class of enzymes called carbon monoxide dehydrogenases (CODH, EC 1.2.7.4) that catalyze the reduction of CO₂ to CO using a redox partner protein like ferredoxin^[132] or redox coupling with a hydrogenase^[133]. CODHs can be divided into two classes, Ni- and Mo-dependent enzymes, which evolved separately^[134]. However, only Ni-dependent CODHs are capable of producing CO from CO₂. Ni-dependent CODHs originate from anaerobic microbes and are oxygen-sensitive^[132,133,135,136], which makes them difficult to purify and limits their application^[137–142]. Recently, however, progress has been made in increasing the oxygen tolerance of Ni-dependent CODHs^[143,144].

The CODH-I from *Carboxydotherrmus hydrogenoformans* was successfully used by the Armstrong group in 2010 for photocatalytic CO formation by providing electrons directly from a PS system^[115]. In the last decade, they have improved their photocatalytic system by changing the PS system from a Ru-PS-TiO₂ assembly to a CdS-semiconductor or TiO₂-Ag nanoclusters assembly, increasing the TON from 2,100 to 22,500 and 250,000, respectively^[115,145,146]. The selectivity of CODH-I for CO formation over the formation of formate and H₂ is about 99%^[147–149] showing that enzymes can be excellent catalysts for selective photocatalytic CO₂ reduction. However, due to the aforementioned oxygen sensitivity and associated difficulties in expressing and handling CODHs, other enzymes should be considered to carry out the reaction. Unfortunately, since the Ni-dependent CODHs are the only known enzymes that catalyze CO₂ reduction to CO, new enzymes must be discovered or artificial enzymes (see chapter “Artificial Metalloproteins”) must be developed. Schneider and Shafaat developed artificial metalloproteins (ArM) based on Cu- or Zn-loaded azurin from *Pseudomonas aeruginosa* by complexing a [Ni^{II}(cyclam)]²⁺ (cyclam = 1,4,8,11-tetraazacyclotetradecane) containing a unique surface-exposed His (H83 or H107)^[150]. [Ru^{II}(bpy)₃]²⁺ was used as a PS. The Cu-azurin-based ArM with the [Ni^{II}(cyclam)]²⁺ anchored to H107 showed the highest TON of 37, which is 2.5 times higher than the free Ni complex, considering the loading efficiency of the Ni complex of 40%. Selectivities of up to 78% were observed only in the first 20 minutes of the reaction. After 5 hours reaction time, similar CO-TONs were calculated, but a selectivity of about 20% was observed, which is as poor as the free Ni complex. The same group later addressed the problem of selectivity by

1. Background

covalently binding Ru-PS to three specific anchoring positions (S66C, S78C, or S100C)^[151]. They found complete selectivity for CO, but the applicability of this modified ArM system is low because the TONs never exceeded 2. Another group designed a genetically encoded photosensitizer by incorporating the non-natural amino acid benzophenone–alanine into the superfolder yellow fluorescent protein (sfYFP) that was autocatalytically converted to the (*E*)-4-(4-benzoylbenzylidene)-1,2-dimethyl-1H-imidazol-5(4H)-one PS (Figure 10)^[152]. The nickel-terpyridine complex was covalently bound to the protein surface and selectively converted CO₂ to CO, reaching TONs of up to 120. However, the selectivity was due to the selectivity of the nickel terpyridine complex rather than a contribution by the protein scaffold; the nickel terpyridine complex is known to catalyze selective CO₂ reductions^[153]. Since the major advantage of proteins is that they provide a well-defined molecular environment, it seems unintuitive to design an ArM with a surface-exposed, flexible metal catalyst that barely interacts with the protein. Recently, Alcalá-Torano et al. developed an ArM for the reduction of CO₂ to CO by replacing the heme of cytochrome b₅₆₂ (Cyt b₅₆₂) with an artificial cobalt protoporphyrin IX (CoPPIX) cofactor^[154]. Free [Ru^{II}(bpy)₃]²⁺ was used as PS and CO TONs of up to 42 were achieved, but the selectivity for CO over the formation of formate and hydrogen never exceeded 25%. However, it was demonstrated that the activity and selectivity could be increased by mutating the local environment of the active pocket. For example, the M7A mutation reduced hydrogen formation by 30%, while CO and formate formation remained the same.

1. Background

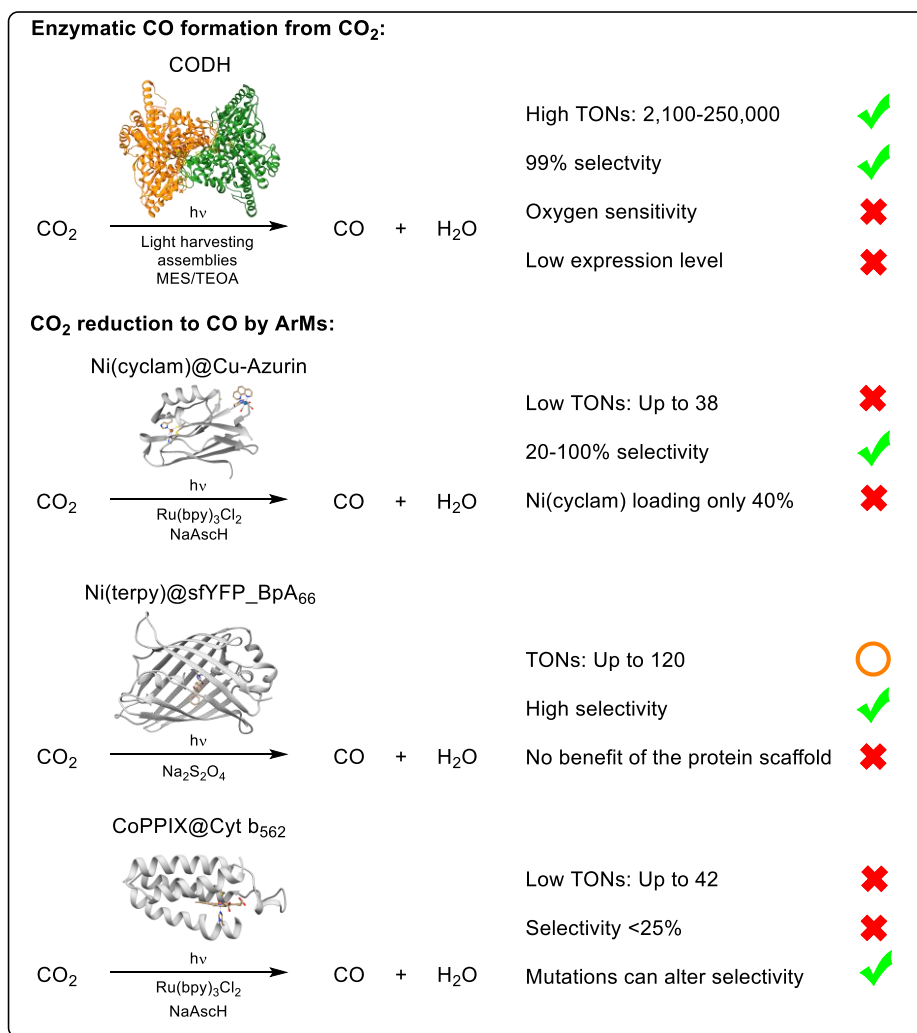


Figure 10. Comparison of enzyme and ArM catalysts for photocatalytic reduction of CO₂ to CO. The crystal structures of CODH from *Carboxydotherrmus hydrogenoformans* (PDB: 1SUF) were used with different PS systems as described above^[115,145,146]. Cu-azurin from *Pseudomonas aeruginosa* with a Ni(cyclam) complex at H107 (PDB: 1R1C) was used as ArM in combination with a Ru-PS^[150,151]. An ArM based on sfYFP bearing the (*E*)-4-(4-benzoylbenzylidene)-1,2-dimethyl-1H-imidazol-5(4H)-one-PS (PDB: 5YR3) formed autocatalytically by the incorporated non-natural amino acid benzophenone-alanine at position 66 (BpA66)^[152]. Sodium dithionite (Na₂S₂O₄) was used as the SD. An ArM based on a Cyt b₅₆₂ scaffold (PDB: 1QPU) containing a CoPPIX was reported by Alcalá-Torano et al.^[154].

In summary, to date, there is no highly active and selective ArM for the photocatalytic formation of CO from CO₂, which would be an alternative to CODH or homogeneous metal-based catalysts (Figure 10).

1.2 Artificial metalloproteins (ArMs)

Enzymes are versatile tools developed by nature to catalyze reactions required by living organisms. Their inherently high chemo-, regio-, and stereo-selectivity and substrate specificity are the key properties of enzymes that make them attractive

1. Background

for synthetic applications^[131]. Enzymes are evolutionarily adapted to convert natural compounds, but chemists have developed materials like plastics and reactions such as the Wacker oxidation that are not known to occur naturally (i.e., new-to-nature compounds and reactions, respectively). Consequently, no natural enzymes are known to catalyze the transformation of these materials or reaction pathways. While natural enzymes can be engineered to accept non-natural substrates^[155,156], it is more difficult to engineer enzymes (from scratch) that perform new-to-nature reactions^[157], especially since many of these reactions require noble transition metals such as Pd, Pt, and Ru. These are not found in natural enzymes^[158,159]. In order to combine the reactivity of metals and the selectivity of proteins, the incorporation of the metals into protein scaffolds is a feasible approach. When the resulting metalloproteins do not occur in nature, they are called artificial metalloproteins (ArM). However, artificial metalloproteins are not only developed for novel reactions but also, for example, to overcome the limitations of their natural counterpart such as stability problems^[160] or the lack of mechanistic understanding of natural enzymes^[161].

The most obvious way to create an ArM is to substitute metals in natural metal-binding proteins, for instance, the iron in heme-containing enzymes, with other metals of choice^[162,163]. Since it is known that the design of metal ligands has a great influence on the activity of metal complexes, other ArMs were developed in which not only the metal but also the natural metal-binding ligand was replaced by synthetic ligands. Among others, Rudi Fasan's group developed ArMs by replacing heme groups with various porphyrin complexes to catalyze cyclopropanylation, resulting in 99% diastereo- and enantioselectivity and TONs of up to 46,800^[164–172]. Although the binding sites of ligands can be adjusted by mutagenesis to increase selectivity and activity, the geometry or space requirement of the ligand used can only be altered to a certain extent compared to the natural ligand^[169,173,174]. Therefore, an alternative to deriving ArMs from natural metal-binding enzymes is to incorporate the desired metal complex into a protein scaffold with a suitable cavity. However, proteins can only be engineered to provide selectively if the position of the metal complex and substrate in the enzyme is known. Therefore, the metal complex needs to be anchored at a specific position in the protein. In addition to the aforementioned exchange of

1. Background

cofactors in existing metalloproteins, this anchoring can be covalent, supramolecular, or dative (Figure 11)^[175,176].

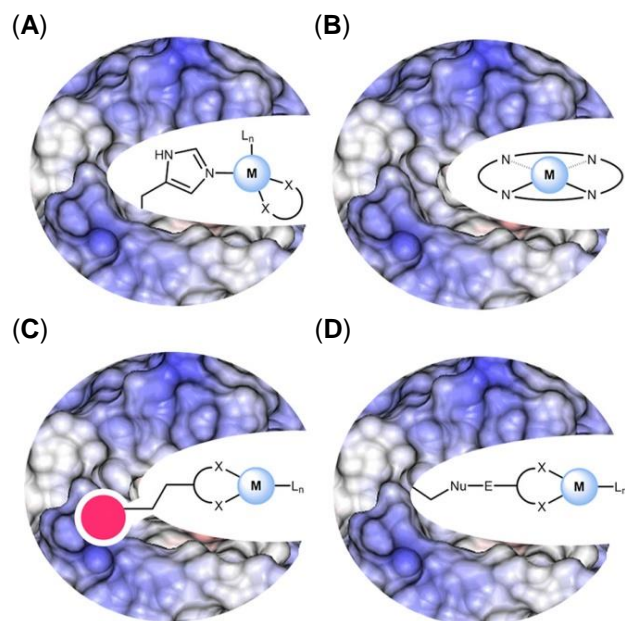


Figure 11. Anchoring strategies for the development of ArMs. (A) Dative coordination of an unsaturated metal complex by a covalently anchored ligand. (B) Metal (complex) substitution. (C) Supramolecular or affinity anchor-based coordination. (D) Covalent linkage of the metal complex. The figure was modified from Davis and Ward^[176].

Dative coordination (Figure 11A) of an unsaturated metal complex by a covalently anchored ligand (e.g., His) is a common strategy to design ArMs^[175]. To be precise, the replacement of a metal (complex) from a natural metalloprotein (Figure 11B) is always also a dative coordination at the same time, since natural metal clusters or cofactors are always anchored datively in the protein^[175]. However, when dative coordination anchoring is reported, it usually means that a new metal-binding site is created, for example, in *de novo* proteins and other small proteins^[177–180]. *De novo* protein scaffolds are unrelated to existing proteins and are partially designed computationally^[177,181,182]. Common examples of *de novo* enzymes are small proteins consisting of four parallel α -helices (four-helix bundle proteins)^[175,176]. Among others, Angela Lombardi's group has mutated four-helix bundle proteins to bind di-copper and di-iron clusters by introducing His and Asp residues to perform oxidation reactions^[183–187]. However, for synthetically useful selective catalysis, substrate binding, and protein dynamics must be considered in addition to a strong metal binding site^[187]. The same is true for supramolecular or affinity anchor-based coordi-

nation (Figure 11C), which takes advantage of the high affinity of ligands for specific scaffold proteins (e.g., biotin binding to streptavidin). This concept has been used extensively by the group of Thomas Ward^[188]. Taking advantage of the high affinity of streptavidin for binding biotin, various biotin derivatives modified with metal complexes were developed, for example, to achieve C-H hydroxylation^[189], imine reduction^[190], or metathesis reaction^[191]. However, since streptavidin is not designed to bind substrates other than biotin, the selectivity of the reactions had to be improved by multiple rounds of mutagenesis^[188]. The same is true for the supramolecular anchoring approach. A prominent example is the use of the transcription factor multidrug resistance regulator from *Lactococcus lactis* (LmrR), which was used by Gerard Roelfes' group to perform Friedel-Crafts alkylations^[192], Diels–Alder^[193] and hydration reactions^[194,195].

Since the covalent anchoring strategy (Figure 11D) is not limited to proteins that bind affinity ligands, the method could theoretically be applied to any protein, including proteins already possessing a binding pocket for the desired substrates. The metal ligand could be bound either via a unique amino acid side chain (e.g., Cys) by selective reaction of reagents such as maleimide or bromoacetamide or non-natural amino acids^[196–203]. However, unlike the other anchoring strategies, covalent anchoring *in vivo* is difficult if the catalyst is not present on the surface^[204–208].

1.3 Amberlyst-15

Many reactions in organic chemistry such as acetalization, etherification, esterification, or aldol reactions can be catalyzed by protonation under acidic conditions. Solid Brønsted acid catalysts are materials functionalized with acidic groups such as sulfonic, phosphoric, or carboxylic acid that perform acid catalyzed reactions, and allow recovery of the catalyst from the reaction medium. Amberlyst-15 is a commercially available solid Brønsted acid catalyst that has been used for many of the above applications^[209–213]. Amberlyst-15 is a polymer of sulfonated polystyrene crosslinked with 20% divinylbenzene (Figure 12), resulting in a macroporous resin with a surface area of 37.3 m²/g and a pore volume of 0.203 mL/g^[214]. The sulfonic acid residues provide a high acid capacity of

1. Background

4.7 mmol protons per gram^[215]. The resins are stable at temperatures up to 150°C and in water^[215]. However, proton solvation of the sulfonic acid residues in water results in reduced activity and prevents reuse without regeneration^[216,217].

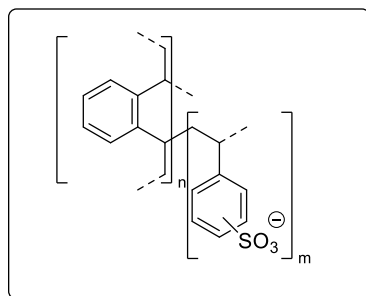


Figure 12. Representative structure of Amberlyst-15.

1.4 Enzyme promiscuity

Enzymes are nature's tools and have some similarities to man-made tools. A hammer, for example, is designed to hit nails, but the way it is handled determines whether the product is a nail in the wood or a broken finger. Transferred to enzymes, the reaction conditions, such as the solvent, pH, or temperature, have an impact on the reaction performed. Lipases, for example, preferentially hydrolyze esters in water but catalyze transesterifications or esterification reactions in the absence of water^[218]. This promiscuity is called "conditional promiscuity" and is only one type of promiscuity that can be associated with enzymes. "Substrate promiscuity" typically describes enzymes with a broad substrate spectrum that convert more than one and potentially unexpected substrates in the same reaction mode^[219]. However, the term "promiscuity" is often used when an enzyme can catalyze different types of reactions and/or uses an alternative reaction mechanism, referred to as catalytic promiscuity. Examples are pyruvate decarboxylases that also catalyze acyloin condensation^[220,221] and metalloproteins that perform different reactions if the metal is substituted^[222–224].

Moreover, enzyme promiscuity can play a central role in the natural evolution of altered – even new – enzyme functions: Firstly, an existing promiscuity is enhanced by mutation without losing the original function, and after gene amplification, the protein is further diversified^[225]. Similarly, promiscuous activities can also be enhanced by protein engineering approaches to design new enzyme-catalyzed reactions^[219,226].

1.5 Phenolic acid decarboxylase

Phenolic acids are an important class of natural phenols and occur in the biosynthesis of secondary plant compounds such as lignin. Due to their antimicrobial activity and natural occurrence, many organisms have developed strategies to degrade phenolic acids, by direct reduction^[227], coenzyme A (CoA) conjugation^[228,229], or decarboxylation^[230,231]. The latter can be carried out by phenacrylate decarboxylase (EC 4.1.1.102), which can be further subdivided into prenylated flavin cofactor-dependent (Protein family (Pfam): PF01977) and cofactor-free decarboxylases (Pfam: PF05870). In contrast to the cofactor-dependent phenacrylate decarboxylase, the cofactor-free decarboxylases, hereafter referred to as phenolic acid decarboxylases (PADs), only convert *E-para*-hydroxycinnamates, such as *p*-coumaric acid (CuA), ferulic acid, caffeic acid and sinapic acid (Figure 13A). Cinnamic acid is not accepted because it lacks the *para*-hydroxy group, which is involved in the cofactor-free decarboxylation mechanism^[232] (Figure 13B). After the initial deprotonation of the acid function in CuA by a base (B), the phenol group becomes deprotonated by a second B while the double bond receives protonation by an acid (AH) to form the intermediate *para*-quinone methide, which is decarboxylated and rearomatized to 4-vinyl phenol (4VP). Amino acids that function as B or AH can be, for example, tyrosinate or glutamic acid, but are not further specified here because the productive positioning of the substrate is still under discussion, as described below for the phenolic acid decarboxylase from *Bacillus subtilis* (BsPAD).

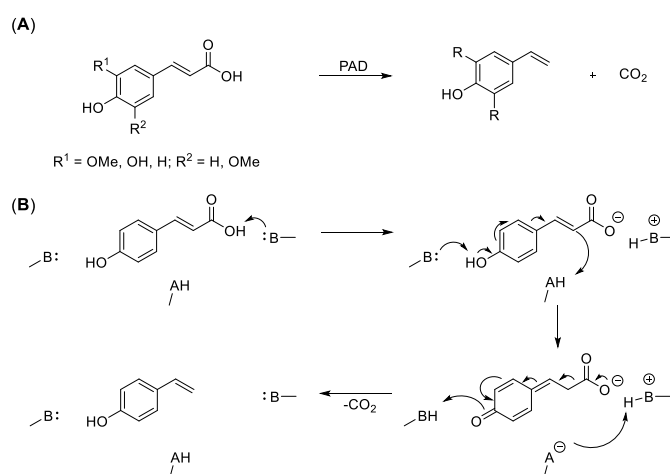


Figure 13. PAD reaction mechanism. (A) Decarboxylation reactions catalyzed by PADs. (B) Proposed general reaction mechanism of PADs according to Hashidoko and Tahara^[232] at the example of the conversion of CuA to 4VP.

1. Background

Numerous PADs have been studied and characterized^[233–243] since 4-VP derivatives of the corresponding hydroxycinnamates are value-added flavor and fragrance compounds^[244,245]. They are naturally occurring in fermented foods such as wine and beer, for example. PADs give direct access to these compounds from pretreated crude biomass such as corn cobs or rice bran^[246,247]. The best studied representative of PADs is BsPAD.

1.5.1 Phenolic acid decarboxylase from *Bacillus subtilis* (BsPAD)

BsPAD has a homodimeric structure of two catalytic monomers with a flattened barrel structure consisting of two large β -sheets. Embedded between the β -sheets is a hydrophobic cavity formed by many conserved bulky amino acids^[248]. The binding mode of phenolic acids in BsPAD remains to be discussed, although a crystal structure of the nearly inactive mutant BsPAD_Y19A with *p*-coumaric acid was solved (PDB-ID 4ALB) by Frank and co-workers^[248].

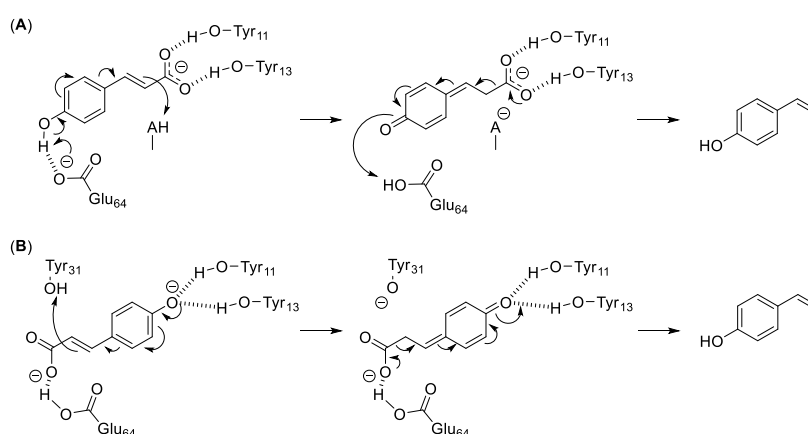


Figure 14. Proposed binding modes of CuA and the corresponding *para*-quinone methide intermediate in BsPAD (according to Frank et al.^[248] (A) and Sheng et al.^[249] (B), respectively).

Frank et al. found that the single mutations Y11F, Y13F, Y19A, and E64A decreased the activity by 96 to 100%^[248]. Therefore, in agreement with their crystal structure of BsPAD_Y19A with CuA, they proposed that Y11 and Y13 together, as well as E64, act as the general base in the reaction, while the general acid is either water or Y19 (Figure 14A). Sheng et al. performed energetic calculations based on a restored model of the wild type (WT) BsPAD and found that the energetic profile of the reaction mechanism would be favorable if the binding of the substrate occurred in a 180° rotated manner (Figure 14B)^[249]. Instead of water or Y19, which is crucial for substrate binding according to the

1. Background

simulations of Sheng et al., Y31 would act as a general acid. Stabilization of the phenolate and quinone methide intermediate by two conserved Tyr residues was also observed in the unrelated enzymes hydroxycinnamoyl-CoA hydratase/lyase and vanillyl alcohol oxidase, suggesting that the substrate binding mode proposed by Sheng et al. is the productive one. Likewise, the proposed mechanisms for the catalytic promiscuities of PADs, namely the regioselective β -carboxylation and enantioselective hydration of 4VP derivatives (Figure 15), are based on the binding mode suggested by Sheng et al.^[250–252].

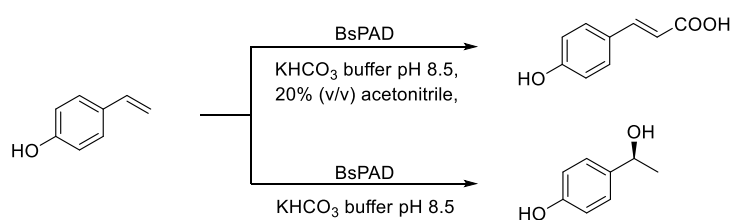


Figure 15. Comparison of BsPAD promiscuities. BsPAD catalyzes both regioselective β -carboxylation and hydration under similar reaction conditions. The figure was modified from Kourist et al.^[231].

The β -carboxylation was claimed to be a catalytic promiscuity of PAD, although it is in fact only the reverse decarboxylation reaction. The reason is that high concentrations of bicarbonate (3 M) instead of carbon dioxide were used for carboxylation^[252]. However, Sheng and Himoto showed that direct carboxylation using bicarbonate is not energetically favorable^[253]. Alternatively, they proposed that the conversion of bicarbonate to CO_2 is the first step of the regioselective β -carboxylation of 4VP derivatives, thus, representing only a reverse decarboxylation reaction as mentioned above. Therefore, the promiscuous activity would be the conversion of bicarbonate to CO_2 rather than the β -carboxylation. This conversion takes place in the bicarbonate/ CO_2 binding pocket formed by Arg41, Thr66, Glu64, and water molecules^[253]. Undeniably, BsPAD also performs direct enantioselective hydration of 4VP derivatives in the presence of bicarbonate as a catalytic promiscuity. In this reaction, the bicarbonate coordinates in the bicarbonate/ CO_2 binding pocket and abstracts a proton from a water molecule, which performs a nucleophilic attack on the quinone methide intermediate of 4VP (Figure 16).

1. Background

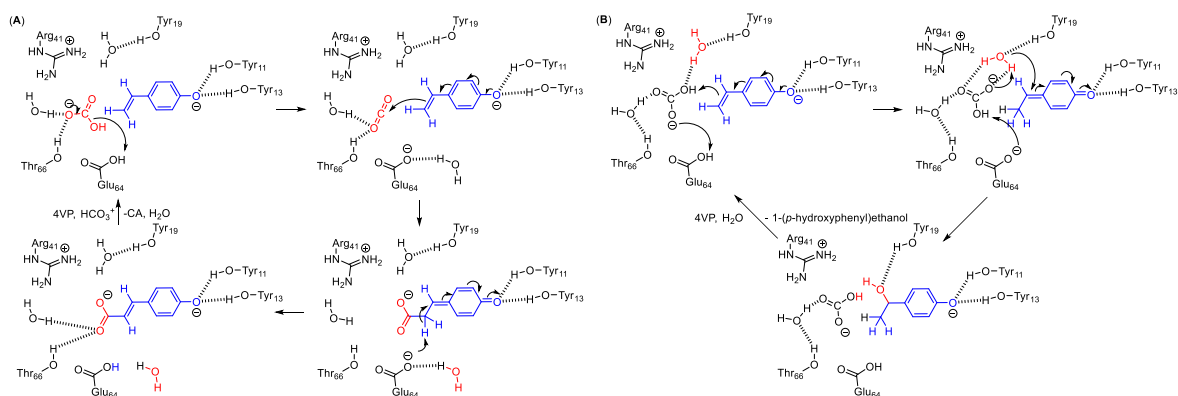


Figure 16. Reaction mechanisms of BsPAD promiscuities (according to Sheng et al.^[253].) (A) Carboxylation mechanism. (B) Hydratation mechanism.

Regardless of the catalytic activities performed by BsPAD and how the phenolic substrates are bound, the movement of the flexible $\beta 1$ - $\beta 2$ loop in the first β -sheets is critical to bring the hydroxyl groups of Y11 and Y13 close to the substrate (Figure 17)^[248]. This loop covers the active site after substrate entry and must be active as a gating mechanism^[248]. In a homologous PAD from *Enterobacter* sp. Px6-4, the Trp25 (corresponding to W17 in BsPAD) was identified as a lock in this gating mechanism^[236].

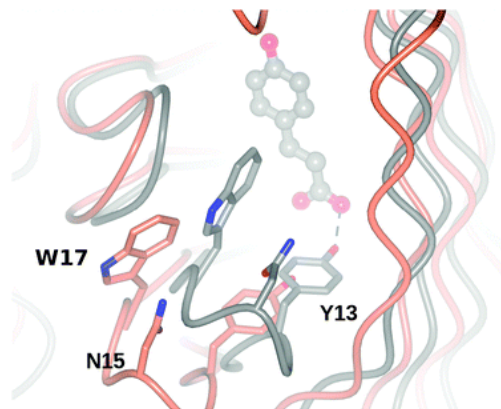


Figure 17. Superposition of BsPAD variants. BsPAD (PDB 2P8G, coral) and BsPAD_Y19A with ligand complex (PDB 4ALB, gray) are shown. The flexibility of the $\beta 1$ - $\beta 2$ -loop indicated by N15 and W17 is illustrated. Y13 comes close to the substrate within the $\beta 1$ - $\beta 2$ -loop motion. The figure is modified from Frank et al.^[248].

1.6 Promiscuous acyltransferases/hydrolases

Hydrolases are widely used in industry because they are often very robust and cofactor-free enzymes with a broad substrate spectrum that catalyze regio- and stereoselective biotransformations^[254–256]. Lipases in particular have proven to be

1. Background

synthetically useful, as they tolerate high concentrations of organic solvents. In the absence of water, they are also capable of catalyzing transesterification and reverse hydrolysis reactions, since the acyl-enzyme intermediate formed cannot be hydrolyzed and can be cleaved by attacking a nucleophile (acyl acceptor) such as alcohols, amines, and thiols^[254,257]. However, in the presence of bulk water, typically the thermodynamically more favorable hydrolysis reaction is preferred by hydrolases (Figure 18)^[258].

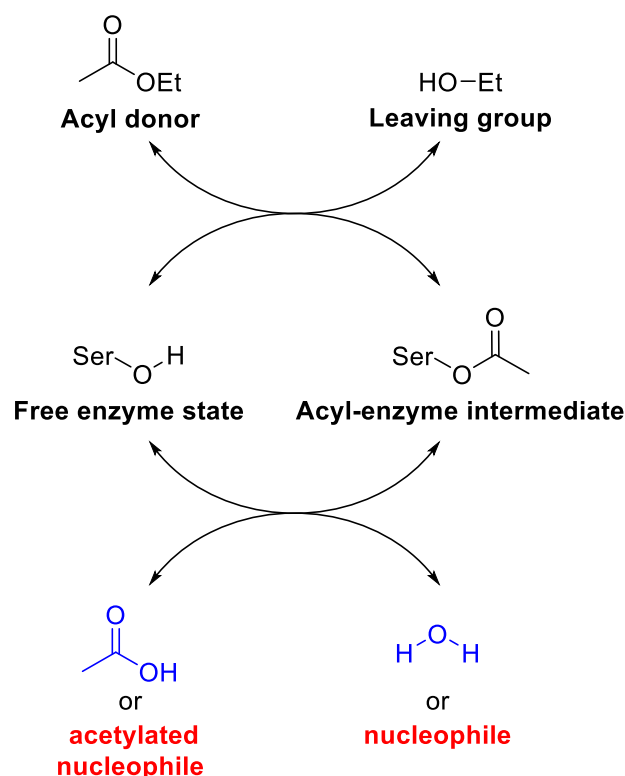


Figure 18. Schematic hydrolysis or acyl transfer reaction cycle of a serine hydrolase that uses ethyl acetate as an acyl donor. The reaction pathway for a hydrolysis and acyl transfer reaction is identical to the formation of the acyl-enzyme intermediate with the release of the leaving group. In hydrolysis, hydrolytic cleavage of the acyl-enzyme intermediate occurs to release acetic acid (blue), whereas, in an acyl transfer reaction, an organic nucleophile accepts the acetyl residue (red). Lipases prefer hydrolysis in water, whereas acyltransferases perform acyl transfer with a suitable nucleophile.

However, some hydrolases are able to carry out the acyl transfer reaction even in water by running the reaction under kinetic control in the presence of a suitable nucleophile^[259–264]. These enzymes are hereafter referred to as promiscuous acyltransferases/hydrolases. The ability of promiscuous acyltransferases/hydrolases to perform acyl transfer reactions in water makes it possible to replace organic solvents normally required for these reactions. Unlike organic solvents, water is cheap, non-toxic, and environmentally friendly^[265]. In

1. Background

addition, water is a good solvent for hydrophilic compounds such as sugars, which are usually less soluble in organic solvents. Godehard et al. demonstrated this advantage over lipases by using the optimized promiscuous acyltransferase/hydrolase EstCE1, originating from a soil metagenome^[266], and EstA from *Arthrobacter nitroguajacolicus* to selectively acetylate glucose, maltose, and maltotriose at the free 6-O positions with conversions of up to 78%^[267].

However, the best-studied promiscuous acyltransferase/hydrolase is MsAcT from *Mycobacterium smegmatis*, first described in 2007 by Mathews et al.^[264]. The application of MsAcT for the synthesis of primary and secondary esters and amides was demonstrated by the synthesis of valuable products such as flavors and fragrances, tyramine derivatives, and antioxidants^[268–271]. Moreover, the substitution of the catalytic Ser11 by Cys allowed the formation of thioesters and tertiary amides^[272]. The poor initial enantioselectivity and limited substrate scope of MsAcT were addressed by mutagenesis^[272–275]. However, the maximal conversions (kinetic maximum) achieved with some substrates remained low, since MsAcT has relatively high hydrolytic activity (Figure 19)^[275]. A high acyl transfer/hydrolysis ratio (AT/H ratio) is desired to achieve higher conversions with a lower excess of acyl donor and to prevent acidification of the medium.

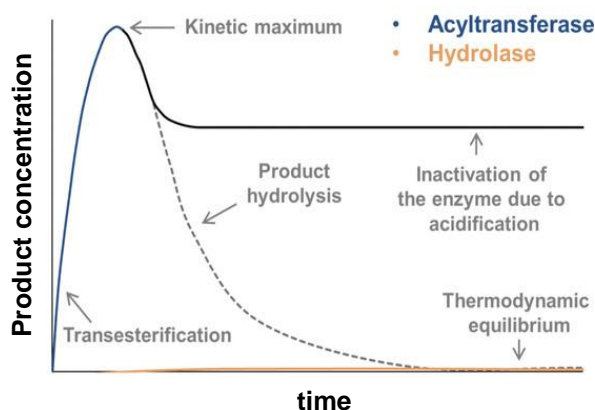


Figure 19. Schematic reaction plot in kinetically controlled reactions catalyzed by a promiscuous acyltransferases/hydrolase compared to a hydrolase. The dotted line represents the hydrolysis that would be expected if not inactivated by the acidification of the enzyme, for example. The figure was adapted and modified from Müller et al.^[276].

Müller et al. developed a colorimetric acyltransferase assay to calculate the acyl transfer and hydrolysis activity of an enzyme by measuring the formation of *p*-nitrophenolate (*p*NP) from *p*-nitrophenyl acetate (*p*NPA) in the presence or absence of an organic nucleophile^[276]. Although the assay is not an enzyme

constant and depends on the acyl donor, organic nucleophile, and concentrations of reactants^[258,275], the *p*NPA-based acyltransferase assay has proven to be a valuable tool for the development of promiscuous acyltransferases/hydrolases. For example, Godehard et al. improved the AT/H ratio of MsAcT using *p*NPA as an acyl donor for the acetylation of benzyl alcohol from 4.0 to 49.8 by rational design^[275].

The *p*NPA-based acyltransferase assay was also used to evaluate promiscuous acyltransferases/hydrolases predicted by a hydrophobicity scoring developed by Müller and co-workers^[276]. The hydrophobicity of the cap domains of several members of the bacterial hormone-sensitive lipase family was analyzed and a strong correlation was found between active site hydrophobicity and acyltransferase activity toward benzyl alcohol. Although the enzymes with the highest cap domain hydrophobicity faced stability problems, several promising new promiscuous acyltransferases/hydrolases were identified. The best newly identified promiscuous acyltransferase/hydrolase was an esterase from the hyperthermostable archaeum *Pyrobaculum calidifontis* VA1 (PestE), which exhibited a similar AT/H ratio to MsAcT in the *p*NPA assay towards benzyl alcohol^[275,276].

1.6.1 PestE

PestE belongs to the bacterial hormone-sensitive lipase family and exhibits an α/β -hydrolase fold as observed in the crystal structure (PDB 3ZWQ)^[277]. However, the name of the family is misleading because bacterial hormone-sensitive lipases, although showing some similarity to human hormone-sensitive lipases, are actually esterases^[278]. The promiscuous acyltransferase activity of PestE was identified by Müller et al. based on hydrophobicity screening of the cap domain (Figure 20)^[276] as briefly introduced above.

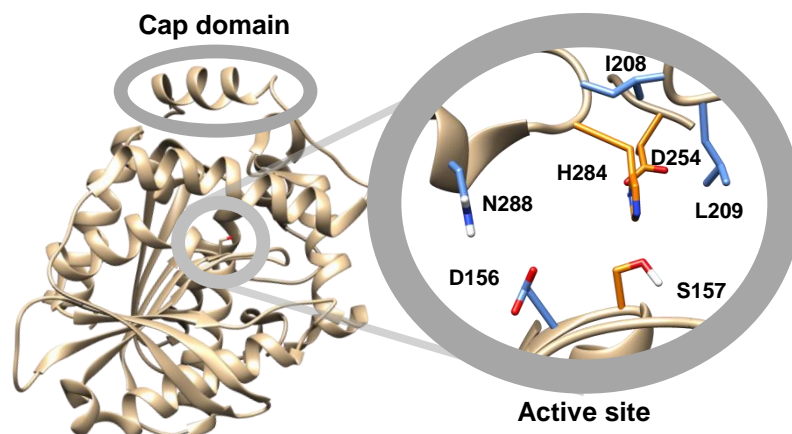


Figure 20. Structure of PestE (PDB 3ZWQ) showing the hydrophobic cap domain and active site residues. The catalytic triad formed by S157, H284, and D254 is highlighted in orange, and selected active site pocket residues are highlighted in blue.

However, apart from the initial screening for benzyl alcohol, very little is known about the substrate scope for acyl transfer reactions. Some hints can be derived from the hydrolase activity of PestE since it was originally identified as an esterase^[279]. PestE is able to hydrolyze short and medium chain aliphatic esters, tertiary esters, and bulky chiral carboxylic acid esters^[277,279,280]. Furthermore, the hyperthermophilic enzyme is very robust toward organic solvents and shows no loss of activity even after incubation at 100°C for 2 hours^[279,280]. PestE is, therefore, likely to be a versatile promiscuous acyltransferase/hydrolase whose biocatalytic potential remains to be exploited.

In the following PhD thesis, the substrate scope of PestE and its potential in synthetic applications are investigated. Furthermore, mutants with improved acyltransferase activity were engineered.

2. Results

2.1 Valorization strategies using BsPAD

2.1.1 Photo-enzymatic catalytic CO₂ reduction using a promiscuous decarboxylase as protein scaffold (Article I)

Direct utilization of the greenhouse gas CO₂ from the atmosphere could contribute to both reducing global warming and using CO₂ as a sustainable carbon source. Many pathways for catalytic CO₂ deployment have been considered. Most of them involve reduction to C₁- such as CO or C₂- and higher building blocks^[84–95]. Inspired by photosynthesis, we aim to perform photocatalytic CO₂ reduction to CO (Figure 21). In this field, besides the development of photosensitizers (PS), the development of catalysts for the selective reduction of CO₂ is a major challenge. Due to the similar reduction potential of different building blocks that can be formed from CO₂^[100], not only the activity but also the selectivity between the desired and other reduction products is a crucial optimization parameter in catalyst design. In particular, the reduction of protons to hydrogen is an undesirable side reaction that is difficult to suppress, since protons are also required for CO₂ reduction (Figure 21).

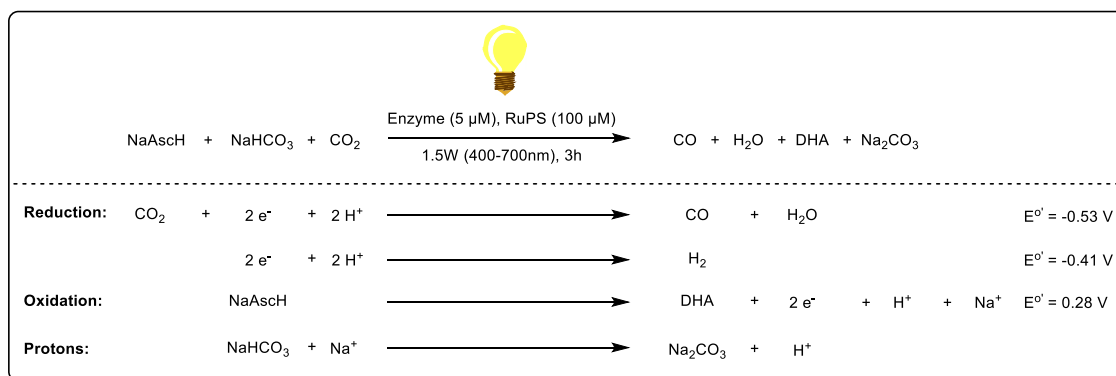


Figure 21. Reaction scheme of enzymatic photocatalytic reduction of CO₂ to CO. Sodium ascorbate (NaAscH) provides electrons and protons through its oxidation to dehydroascorbate (DHA). The 100 mM sodium bicarbonate buffer is an additional source of protons. In addition to the desired CO₂ reduction, the undesired hydrogen formation and the standard potential at pH 7 are shown^[100]. RuPS = [Ru(bpy)₃]²⁺.

Enzymes offer selectivity due to their dynamics and well-defined 3D structure^[131]. Therefore, incorporation of a metal complex capable of reducing CO₂ into a CO₂-binding enzyme – yielding an ArM – could contribute to the development of a selective catalyst for the reduction of CO₂. The phenolic acid decarboxylase from *Bacillus subtilis*, previously introduced as BsPAD, was selected as the ArM scaffold because BsPAD, has a CO₂-binding site as well as a well-defined large

2. Results

hydrophobic pocket that provides the opportunity to incorporate a metal complex. It is also easy to express recombinantly in *Escherichia coli* (*E. coli*). For the targeted incorporation of the selected Knölker-type iron catalyst, which can reduce CO₂ to CO in an organic solvent^[281], covalent anchoring using a maleimide linker was considered. Therefore, the native C100 was removed and a new Cys was introduced at position 124 (V124C). Because the latter reduced the stability of the protein scaffold, the stability-enhancing mutation A147P proposed by the online tool FireProt (<https://loschmidt.chemi.muni.cz/fireprotweb/>)^[282] was introduced. The resulting mutant BsPAD_C100W_V124C_A147P (BsPAD_WCP) was the first potential ArM scaffold. However, manual docking of the iron catalyst to the active site of BsPAD_WCP indicated that more space in the hydrophobic pocket of BsPAD might be required for the incorporation of the bulky metal catalyst. Therefore, the bulky residues W17, I85, and F87 were replaced with Ala in a combinatorial manner to increase the space in the hydrophobic cavity. After the incorporation of the metal catalyst, it was found that the enzyme itself and not the incorporated iron catalyst was responsible for the observed CO₂ reduction. The only enzymes known to reduce CO₂ to CO were Ni-dependent and oxygen-sensitive carbon monoxide dehydrogenases (CODHs). The photocatalytic CO₂ reduction activity of a cofactor-free enzyme that forms CO is a novelty. BsPAD_WCP showed a turnover number (TON) of 30 and a selectivity of 82% between CO and hydrogen (Figure 22B). No other CO₂ reduction products were detected.

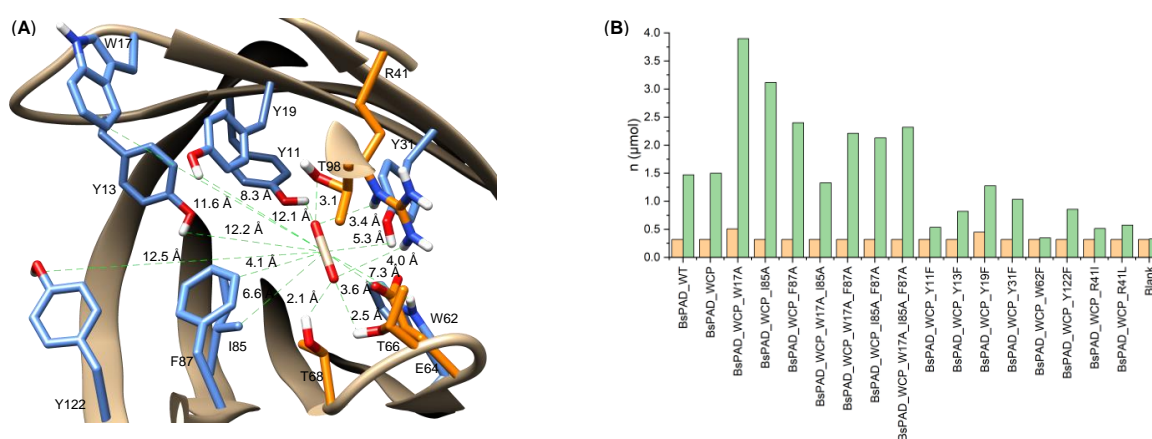


Figure 22. Mutational studies of BsPAD toward CO₂ reduction activity. (A) Visualization of residues selected for mutation (blue) in the protein cavity of BsPAD (PDB-ID: 2P8G) and amino acids involved in CO₂ binding (orange). (B) Photocatalytic carbon dioxide reduction employing BsPAD variants (without metal ligands bound). Reaction conditions: [Ru(bpy)₃Cl₂] = 100 µM; [BsPAD] = 5 µM; [NaHCO₃] = 0.1 M; [NaAsCH] = 0.05 M; total reaction volume = 10 mL; 75 mL CO₂ gas phase. The amounts of CO and H₂ produced are shown in green and orange, respectively.

2. Results

Interestingly, the single mutants W17A, I85A, and F87A, which were originally designed to increase active site space, increased the TON to 78, 62, and 48, while exhibiting selectivities of 88, 91, and 88%, respectively. By lowering the enzyme concentration from 5 to 1 μM , BsPAD_WCP_W17A achieved a TON of 196 and a selectivity of 82%.

Since the electron-transferring amino acids Trp and Tyr are known to increase the efficiency of electron transfer in proteins^[283–285], all Trp and Tyr residues near the CO₂-binding pocket were mutated to Phe. All mutations decreased activity, but Y11F and W62F decreased CO formation activity down to background activity arising from the [Ru(bpy)₃Cl₂] PS. Therefore, Y11F and W62F may play an important role in electron transfer from the PS to the CO₂-binding pocket. Further mutational studies on BsPAD_WCP revealed that the replacement of R41, which is involved in CO₂ binding (Figure 22A), with Leu or Ile, greatly reduced activity, underscoring that the architecture of the CO₂-binding pocket is critical for CO₂ reduction activity. Inspired by these results, we selected other CO₂-binding proteins and examined them for their CO₂-reducing ability (Table 1). The selected enzymes differ in CO₂-binding pockets, protein size, and origin. BsPAD and aspartate-1-decarboxylase from *E. coli* K12 (EcPanD) do not require a cofactor for CO₂ binding^[243,286]. In contrast, thiamine diphosphate, Zn²⁺ and a flavin mononucleotide are involved in CO₂ binding of acetolactate synthase from *Thermus thermophilus* (TtALS), carbonic anhydrase from *Bos taurus* (BtCA) and ferulic acid decarboxylase 1 from *Saccharomyces cerevisiae* (ScFDC1), respectively^[287–289].

2. Results

Table 1. Carbon dioxide binding enzymes investigated for photocatalytic CO₂ reduction.

#	Enzyme	nH ₂ (μmol)	nCO (μmol)	Select. (%)	TON CO
1	BsPAD_WT	<0.32	1.43	81	143
2	EcPanD	0.42	1.62	80	162
3	PFE	<0.32	0.92	74	92
4	SsTrpC	0.33	1.17	79	117
5	MmPPP2	<0.32	1.52	83	152
6	ScFDC1	<0.32	2.55	89	255
7	TtALS	0.36	2.62	88	262
8	EcPPC	<0.32	1.49	83	149
9	BtCA	0.87	2.19	72	219

Reaction conditions: 10 mL of H₂O were used for all cases (Volume of CO₂ headspace = 75 mL). [Enzyme] = 1 μM. [Ru(bpy)₃Cl₂] = 100 μM. NaHCO₃ (0.1 M) and NaAsCH (0.05 M) were employed in all cases. Reaction mixture was bubbled with CO₂ for 30 minutes before irradiation. Light input: 1.5 W (400-700 nm). Reaction time: 3 h. Standard deviations are generally 4% to 19% for TON_{CO}, except for entries 1 (26%), 4 (32%), 6 (28%), and 9 (23%), and 1% to 12% for selectivity, except for entry 6 (20%). EcPanD: Aspartate-1-decarboxylase from *Escherichia coli* K12; PFE: Esterase 1 from *Pseudomonas fluorescens*; SsTrpC: Indole-3-glycerol phosphate synthase from *Sulfolobus solfataricus*; MmPPP2: Protocatechuate decarboxylase from *Madurella mycetomatis*; ScFDC1: Ferulic acid decarboxylase 1 from *Saccharomyces cerevisiae*; TtALS: Acetolactate synthase from *Thermus thermophilus*; EcPPC: Phosphoenolpyruvate carboxylase from *Escherichia coli* K12; BtCA: Carbonic anhydrase from *Bos taurus*.

All enzymes showed CO₂ reduction activity, indicating that this might be a universal feature of CO₂-binding enzymes (Table 1). However, the selectivity and activity of these mutants were variable and did not correlate with protein size, origin, or CO₂-binding mechanism. Among the selected WT enzymes, ScFDC1, TtALS, and EcPanD showed high activities with TONs of 255, 266, and 162 and selectivities reaching 89, 88, and 80%, respectively. These WT enzymes showed similar or better performance in activities and selectivity than the engineered BsPAD_WCP_W17A variant. Therefore, in addition to BsPAD_WCP_W17A, these WT enzymes are promising targets for enzyme engineering toward photocatalytic CO₂ reduction. In particular, the cofactor-independent and well-expressible enzymes EcPanD (2.9 μmol/L) and BsPAD_WCP_W17A (8.5 μmol/L) could overcome the expression and stability problems associated with CODH. Consequently, homogeneous catalysts for CO₂ reduction, which normally contain (noble) metals^[110,127–129], could be avoided in the future by using enzymes such as BsPAD.

2.1.2 Spectrophotometric and Fluorimetric High-Throughput Assays for Phenolic Acid Decarboxylase (Article II)

To create an ArM for phenolic acid conversion, BsPAD was selected again as the protein scaffold. BsPAD has a Michaelis–Menten constant (K_M) value of 1.1, 1.3, and 2.6 mM for its natural substrates ferulic acid (FA), coumaric acid (CuA), and caffeic acid (CaA), respectively. These values demonstrate a relatively high binding affinity for phenolic acids. To ensure that the binding affinity for phenolic acids was not reduced by mutations introduced to make BsPAD a suitable ArM scaffold, the kinetic parameters of all mutants were determined. Although PADs are very interesting enzymes for the production of value-added vinyl phenols, which are used as flavor compounds^[244,245] and polymer precursors^[290,291], there is no accurate and fast activity assay for them. Hence, most kinetic studies rely on tedious and low-throughput high-performance liquid chromatography (HPLC) analysis^[234–241,292]. Only in a few cases, a spectrophotometric assay has been used to follow the substrate decrease. However, we found that the wavelengths chosen (e.g., 285 nm for CuA)^[242,243,293–295] largely overlap with the absorption wavelengths of the products (Figure 23). Therefore, the kinetic data obtained by the previous spectrophotometric method were inaccurate.

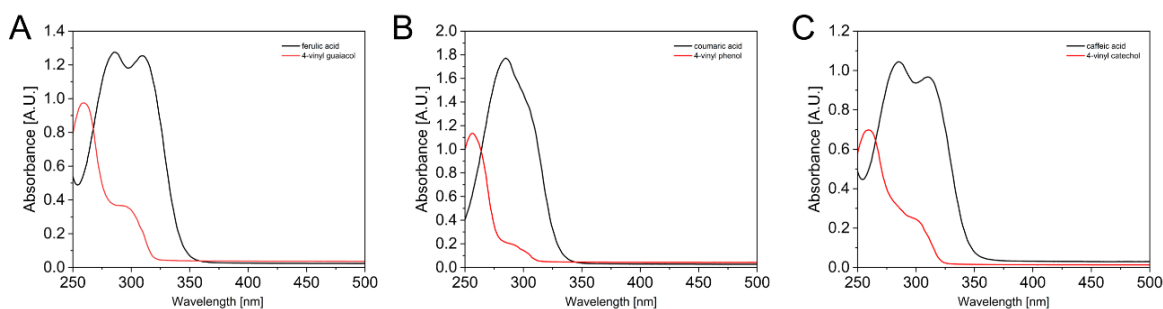


Figure 23. Results of the kinetic measurements of BsPAD using the fluorescence assay. Absorption spectra of FA (A), CuA (B), and CaA (C) and the corresponding decarboxylated products 4VG (A), 4VP (B), and 4VC (C). Spectra were recorded in 50 mM NaP_i buffer at pH 6. All species had a final concentration of 0.3 mM.

To develop a suitable activity assay with higher sample throughput, we revised the absorbance assay and found that the absorbance of FA, CuA, and CaA at 335 nm, 324 nm, and 337 nm did not overlap with the absorption wavelengths of the corresponding products (Figure 23).

In addition, an activity assay was developed based on the fluorescence of the 4VP derivatives formed. Since the fluorescence of the vinyl phenol product is in

2. Results

the range of substrate absorption, part of the fluorescence is absorbed by the residual substrate in the sample. This does not affect the outcome of qualitative high-throughput screenings (HTS), e.g., to identify a more active variant of an enzyme library. However, background adjustment is required for the characterization of kinetic parameters such as K_M and the maximum reaction rate (V_{max}). This means that a sample of the reaction is transferred to an analysis plate in which the substrate concentration is set to 0.5 mM. In addition, the detection wavelength was optimized to achieve the maximum output signal in the presence of 0.5 mM of the corresponding substrates.

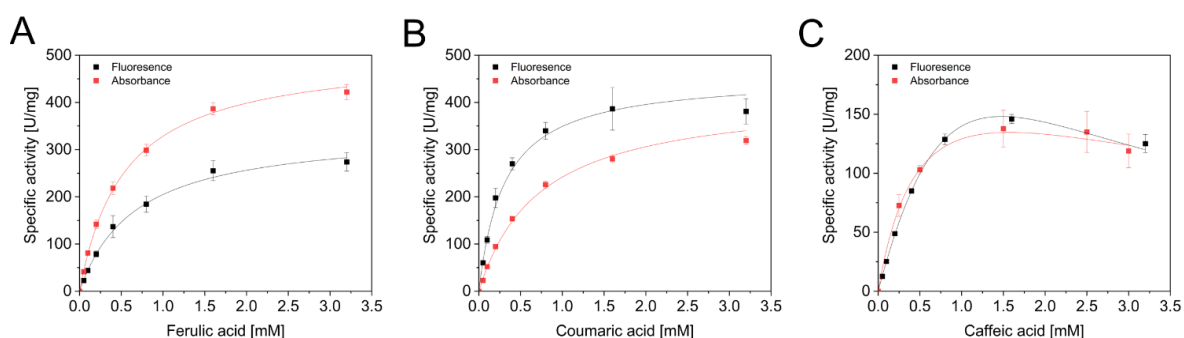


Figure 24. Kinetic measurements of BsPAD using the fluorescence- and absorbance assays with FA (A), CuA (B) and CaA (C). All measurements were performed in triplicates and incubated at 21°C (1000 rpm) for one minute (fluorescence assay) or measured in time-drive mode for 10 min (absorbance assay). Absorption wavelengths: FA: 335 nm; CuA: 324 nm; CaA: 337 nm. Fluorescence: 4VG: Ex.: 258 nm, Em.: 345 nm; 4VP: Ex.: 258 nm, Em.: 335 nm; 4VC: Ex.: 258 nm, Em.: 350 nm. Data points were fitted to the Michaelis-Menten equation without (FA and CuA) or with inhibition using Origin 2020 (OriginLab Corporation, Northampton, MA, USA).

The developed absorption and fluorescence assays were validated for FA, CuA, and CaA using the WT of BsPAD as a model PAD (Figure 24). Both assays gave similar results and were compared with kinetic data from the literature (Table 2). Only for CuA were there major differences in the kinetic data, although the data points of the two assays are similar, as substrate inhibition gave a good correlation with the fluorescence assay, whereas the spectrophotometric assay only fit the Michaelis-Menten equation well without substrate inhibition. As expected, the V_{max} values measured with the developed assays were higher than those reported in the literature because the measured apparent substrate decrease was reduced by the absorption of the formed product at the wavelengths chosen in the literature.

2. Results

Table 2. Comparison of K_M and V_{max} values from the literature and the developed absorbance and fluorescence assays.

Assay	FA		CuA		CaA	
	K_M / mM	V_{max} / U/mg	K_M / mM	V_{max} / U/mg	K_M / mM	V_{max} / U/mg
Absorbance	0.54 ± 0.02	506 ± 11	0.73 ± 0.08	417 ± 30	0.55 ± 0.15	229 ± 37
Fluorescence	0.67 ± 0.03	342 ± 10	0.31 ± 0.03	456 ± 20	2.25 ± 0.30	599 ± 71
Literature ^{[243],a}	1.1	280	1.3	265	2.6	180

a) Based on a spectrophotometric assay for substrate decrease using wavelengths that overlap with the absorption of the products.

Remarkably, both assays required less than 2 μg of enzyme to characterize the kinetic parameters for each substrate studied. Both assays have their advantages: The optimized absorbance assay can measure concentrations up to the solubility limit (about 10 mM), whereas the fluorescence assay is more sensitive in the low concentration range. In addition, both assays allow the detection of decarboxylase activity in crude cell lysate, opening a gateway for HTS library screening. Moreover, the fluorimetric assay can also be performed with whole-cells. The screening and improvement of PADs is important because of their potential application in the direct valorization of phenolic acids from natural resources^[240,246,247].

2.2 Biomass valorization using the promiscuous acyltransferase/hydrolase PestE

2.2.1 Recent Insights and Future Perspectives on Promiscuous Hydrolases/Acyltransferases (Article III)

This perspective article focuses on the discovery, mechanistic insights, synthetic applications, and engineering of promiscuous acyltransferases/hydrolases. These promising enzyme catalysts enable the production of esters, thioesters, amides, carbonates, and carbamates in water. Therefore, they can help to reduce the use of organic solvents normally required for acyl transfer reactions catalyzed by lipases, for example.

Although the activity of promiscuous acyltransferases from hydrolases in water was described as early as the 1990s for a lipase from *Candida parapsilosis* (CpLIP2) and *Pseudozyma antarctica* (CAL-A), they received less attention because they were restricted to the transfer of long-chain fatty acids^[259–262]. With the discovery of MsAcT, shorter acyl chains could also be transferred^[264].

2. Results

Therefore, MsAcT variants have been widely used for synthetic applications, such as the synthesis of valuable tryptamine derivatives, flavorants, and fragrances^[269–271,274,296,297]. The discovery of promiscuous acyltransferases/hydrolases has long been driven by accidental but careful observations and by luck^[258,262,264,298,299]. The precipitation-based acyltransferase assay by Reisky et al. was the first screening assay that allowed targeted screening of hydrolase libraries to identify new promiscuous acyltransferase/hydrolase^[300]. The formation of insoluble oligocarbonates from soluble dimethyl carbonate and 1,2-hexanediol monomers led to the discovery of Est8. EstCE1 from family VIII of carboxyesterases was also identified in a homologous manner^[301]. Müller et al. recently described a sequence-based *in silico* screening method comparing the hydrophobicity of the N-terminal cap domains in the bacterial hormone-sensitive lipase family^[276]. The discovery of numerous new promiscuous acyltransferases/hydrolases underscores that acyltransferase activity in hydrolases is a widely encountered feature rather than an exception. This is further evidenced by the fact that many promiscuous acyltransferases/hydrolases, true acyltransferases, and hydrolytic enzymes share the same catalytic Ser-His-Asp triad^[264,276,302–304].

Various explanations have been developed why acyltransferases and hydrolases prefer acyl transfer and hydrolysis, respectively. Kazlauskas et al. and Jones et al. hypothesized that subtle changes or amino acids in the hydrolase/acyltransferase structure inactivate the water molecule and, thus, stabilize the acyl-enzyme intermediate (Figure 25A)^[305,306]. The acyltransferase activity of other enzymes, including MsAcT, has been explained by water repulsion of the hydrophobic active site to prevent hydrolysis^[264]. However, computational studies with MsAcT by Kazemi and co-workers showed that the high binding affinity towards benzyl alcohol is determined by the hydrophobic pocket rather than by the shielding of water molecules^[273].

The synthetic potential of promiscuous acyltransferases/hydrolases has not yet been fully explored. The main problem in the application of these enzymes is that after the reaction reaches its kinetic maximum, hydrolysis can dominate and consequently the product is hydrolyzed (Figure 25B). Only very few systems such as the irreversible formation of amides by EstCE1 can circumvent this issue^[301]. Therefore, in acyltransferase reactions, *in situ* product removal in a two-phase

2. Results

system, a flow setup, and/or the use of an excess acyl donor are often employed to shift the equilibrium^[270,307–309]. In addition, the use of enol esters releases an enol as a leaving group, which can subsequently tautomerize into non-nucleophilic carbonyls, thus, reducing undesired back reactions of this side-product. However, leaving groups, such as acetaldehyde (i.e., the tautomer of vinyl alcohol) from vinyl acetate, not only reduces atom efficiency but are also toxic.

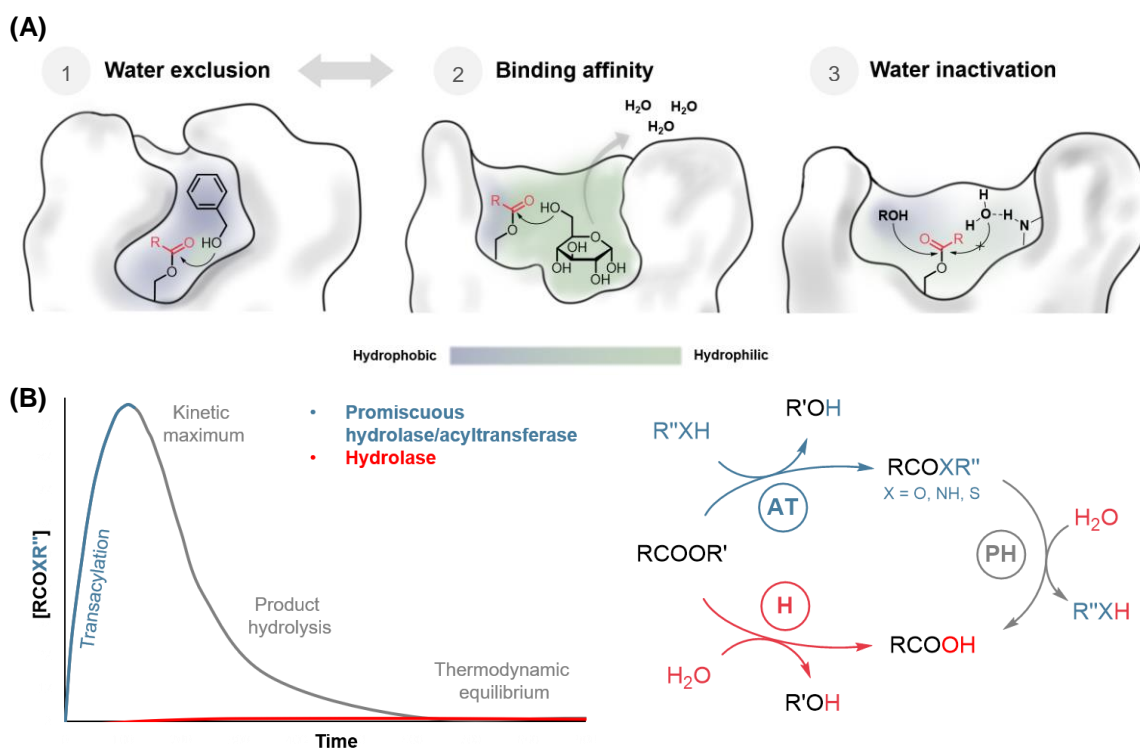


Figure 25. Mechanism and reaction pattern of promiscuous hydrolases/acetyltransferases. (A) Properties of active sites of physiologically relevant acyltransferases and promiscuous hydrolase/acetyltransferase: (1) A hydrophobic environment may provide a more favorable surrounding for organic nucleophiles than for water, (2) high binding affinity to the acyl acceptor substrate may displace water and promote acyl transfer over hydrolysis, (3) structural features may inactivate water, preventing the nucleophilic attack on the acyl-enzyme intermediate. (B) Promiscuous hydrolase/acetyltransferases catalyze acyl transfer (AT) faster than they catalyze hydrolysis (H), leading to transient accumulation of the transesterification product. If the transacylation product is a substrate to the enzyme as well, product hydrolysis (PH) will occur until the thermodynamic equilibrium is reached. A hydrolase without promiscuous acyltransferase activity will not show a kinetic maximum above the thermodynamic equilibrium. This figure was adapted from Müller et al.^[310].

The low hydrolytic activity of promiscuous acyltransferase/hydrolase is crucial for high maximum conversions and slow decay of product titer. Enzyme engineering has shown that it is possible to reduce both substrate and product hydrolysis and created enzymes with a higher acyl transfer/hydrolysis ratio (AT/H ratio)^[275,276]. Godehard et al. demonstrated that even a single mutation in MsAcT (K97A) can

increase the AT/H ratio 7.5-fold by reducing hydrolysis to one-third while increasing acyl transfer activity 2.5-fold^[275]. Further engineering of promiscuous acyltransferases/hydrolases could focus on regions/motifs near the active site since Müller et al. found that three-amino acid motifs next to the catalytic triad in EstA (HDG) and EstCE1 (WGG) had a major impact on hydrolytic activity. In the related lovastatin hydrolase, this motif was found to influence hydrolysis by affecting the hydrogen bonding network around the active site^[311].

Enzyme engineering was also used to extend the substrate range of MsAcT by replacing Ser11 in the active site with Cys. This mutant was able to form tertiary amides from secondary amines. With MsAcT_S11C, they also formed thioesters. Noteworthy, thioester hydrolysis was not observed^[272]. Apart from challenging products such as reactive thioesters, hydrophilic compounds are promising targets for acyl transfer reactions. However, the ability of most promiscuous acyltransferases/hydrolases to accept highly hydrophilic substrates is poor. Nevertheless, Godehard et al. succeeded in modifying EstEC1 to efficiently acetylate glucose, maltose, and maltotriose using ethyl acetate as an acyl donor^[267]. Moreover, the new promiscuous acyltransferases/hydrolases EstXT1 also showed acylation activity towards cyanidin-3-O-glucosides^[312]. These examples indicate that the identification of new and the engineering of known promiscuous acyltransferases/hydrolases could further enhance their synthetic utility and their use in transacylation reactions.

2.2.2 Rational Design for Enhanced Acyltransferase Activity in Water Catalyzed by the *Pyrobaculum calidifontis* VA1 Esterase (Article IV)

PestE from *Pyrobaculum calidifontis* VA1 was initially found to be an esterase and used for hydrolysis reactions of aliphatic esters, tertiary esters, and bulky chiral carboxylic acid esters^[277,279,280]. In 2020, the promiscuous acyltransferase activity of PestE was identified by Müller et al., using a hydrophobicity-based assessment of the active pocket^[276]. The nonpolar compound benzyl alcohol was the only nucleophile (acyl acceptor) known for acyl transfer reactions. In homology, nonpolar monoterpene alcohols were investigated as potential PestE substrates. The selected monoterpene alcohols (±)-citronellol, (±)-menthol, carvacrol, and (±)-

2. Results

linalool represent primary, secondary, phenolic, and tertiary alcohols, respectively (Figure 26). Consequently, their testing allows insight into the acyl transfer substrate scope of PestE.

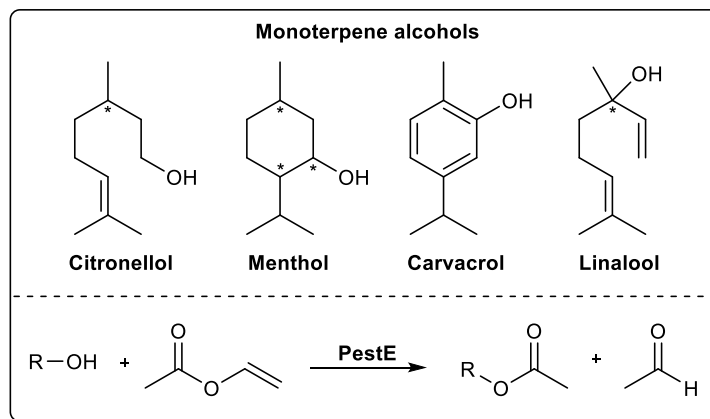


Figure 26. Monoterpene alcohol substrates and the reaction scheme of PestE-catalyzed transesterifications with vinyl acetate.

Monoterpene alcohols such as (\pm)-citronellol can be isolated from essential oils^[313] and are used as flavor and fragrance compounds^[314,315]. Generally, acetylation of monoterpene alcohols is used to alter the taste and odor perception of these compounds^[315–317]. Hence, the synthesis of monoterpene esters in water could provide a sustainable alternative to lipase-catalyzed acyl transfer reactions in organic solvents.

To screen the acyl transfer substrates of PestE, 20 mM of the desired substrate and a ten-fold excess of vinyl acetate as an acyl donor were used. The PestE_WT was remarkably active toward the primary alcohol (\pm)-citronellol. With 0.2 μ g/mL PestE_WT, complete conversion was achieved after 2 h reaction time and no enantioselectivity was observed. 40% conversion was achieved after only 5 min, indicating a specific activity in the low kU/mg range. PestE WT was also active against the secondary alcohol (\pm)-menthol, but with a maximum conversion of 38% and 57% ee (E-value 5) for (–)-menthol. The highest conversion for carvacrol was 7%, indicating high product or acyl donor hydrolysis in the presence of carvacrol. No activity towards linalool was observed. Importantly, PestE is the first promiscuous acyltransferases/hydrolases shown to form phenolic esters in water.

In order to decrease the hydrolysis activity of PestE, mutants were created by rational design. Therefore, the substrate binding pocket was detected by docking of the substrate (–)-menthol. Similar to the studies by Godehard et al. and Müller

2. Results

et al., a dependence between the acyltransferase activity and the hydrophobicity of the active site was proposed^[275,276]. Consequently, the polar residues H95 and N288 were chosen and exchanged to Ala and Phe, respectively, to increase the active site hydrophobicity. Furthermore, the bulky I208 residue, positioned at the entrance of the active site, was substituted by Ala to facilitate substrate binding. All PestE variants were investigated towards the monoterpene alcohol substrates. Figure 27 shows the results for citronellol (acyl donor: ethyl acetate (A); vinyl acetate (B)) and menthol acetylation (C).

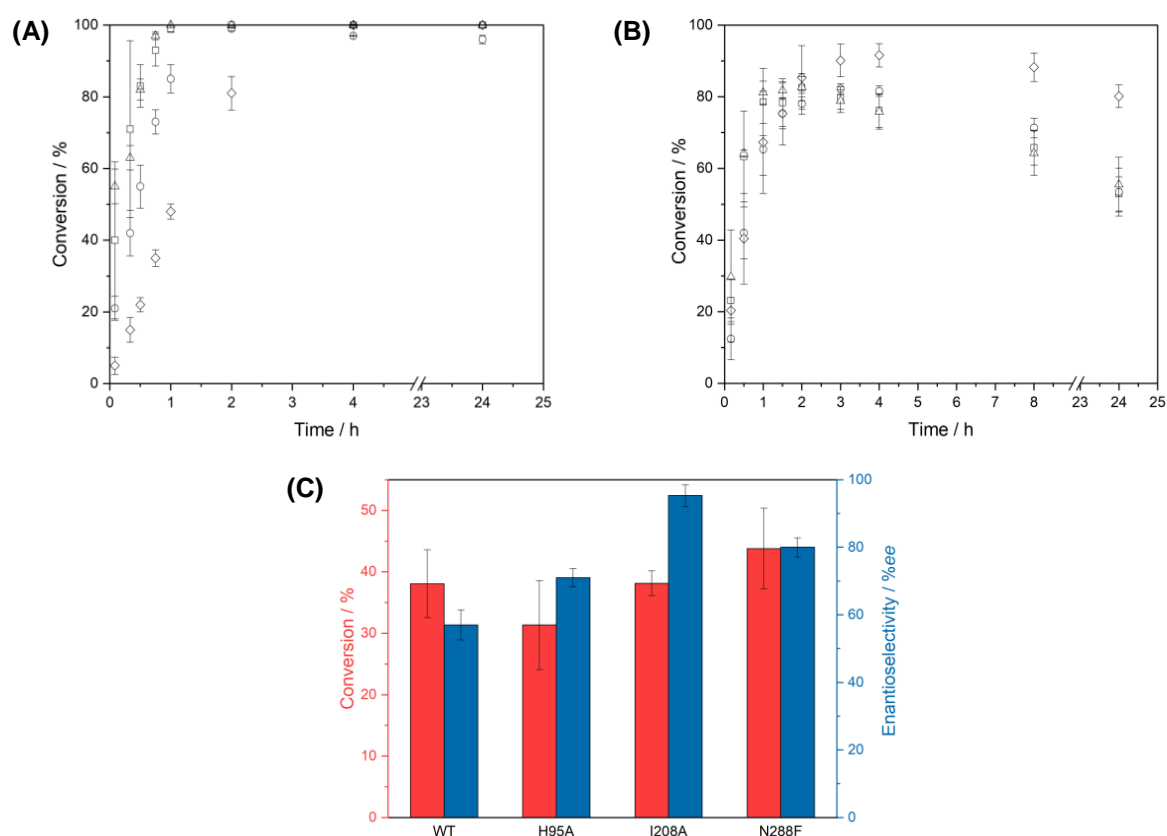


Figure 27. Acetylation of citronellol and menthol by PestE variants. (A) Acetylation of 20 mM citronellol by PestE variants with 200 mM vinyl acetate as acyl donor. PestE WT (square), H95A (circle), I208A (triangle), and N288F (diamond) were used at a loading of 0.2 $\mu\text{g/mL}$. (B) Acetylation of 20 mM citronellol by PestE variants with 200 mM ethyl acetate as acyl donor. PestE variants: WT (square), H95A (circle), I208A (triangle), and N288F (diamond) were used at an enzyme load of 20 $\mu\text{g/mL}$. (C) Acetylation of 20 mM (\pm)-menthol by PestE variants with 200 mM vinyl acetate as acyl donor. Maximum conversion and enantioselectivity are shown. The highest conversions for PestE WT, H95A, I208A, and N288F were achieved after 4, 8, 3, and 8 h, respectively. All enzymes were used at a concentration of 0.2 $\mu\text{g/mL}$. All reactions were performed in triplicates at 40°C and samples were analyzed by gas chromatography (GC). All values are given as the mean of triplicates with the corresponding standard deviation.

Interestingly, the H95A and N288F mutations decreased acyltransferase activity for all substrates, as indicated by the initial turnovers after 5 minutes. In contrast, H95A actually increased hydrolysis, as indicated by the lower maximal

conversions (Figure 27A/B). However, N288F also decreased the hydrolysis reaction and resulted in 44% maximum conversions of (\pm)-menthol and also higher selectivity over ($-$)-menthol (80%ee, E value 17). The altered hydrolysis reaction can be explained by the influence of water molecules in the active site. Molecular dynamics (MD) simulations showed that fewer water molecules and fewer hydrogen bonds are present in the active site when N288 is mutated to Phe, whereas the substitution H95A has the opposite effect. The higher acyltransferase efficiency of N288F was also demonstrated by using ethyl acetate (EtOAc) as an acyl donor for the transesterification of citronellol (Figure 27B). Unlike vinyl acetate, which releases vinyl alcohol that subsequently tautomerizes into acetaldehyde, ethyl acetate releases ethanol. The latter acts as a competing nucleophile and promotes the reverse transesterification reaction. A maximum conversion of citronellol of 92% was achieved with PestE_N288F, while the WT reached only 82% and showed faster product hydrolysis over 24 h total reaction time. The high conversions in the experiment with ethyl acetate highlight the ability of PestE to achieve high conversions even with more sustained non-activated acyl donors.

Although the I208A mutation decreased active site hydrophobicity, acyltransferase activity was increased for all substrates. Selectivity for acetylation of (\pm)-menthol was also increased towards ($-$)-menthol to 94%ee with no change in conversion from 38% (E-value 55). Mutation I208A demonstrates that, in addition to substrate binding, access to the active site is an important parameter, providing kinetic control of the target reaction.

In summary, PestE acetylates the bulky primary alcohol citronellol very rapidly. Furthermore, PestE is capable of acetylating secondary and phenolic alcohols. The (selective) conversion of bulky primary alcohols with non-activated acyl donors such as ethyl acetate could be a possible application of PestE.

2.2.3 Recovery of Hydroxytyrosol from Olive Mill Wastewater using the Promiscuous Hydrolase/Acyltransferase PestE (Article V)

The potential application of promiscuous hydrolases/acyltransferases to lipophilize hydrophilic value-added compounds to facilitate their recovery from aqueous

2. Results

waste streams has never been investigated, although wet or aqueous by-products such as fruit peels or olive mill wastewater (OMWW) are commonly produced in the agricultural industry^[318]. OMWW was targeted because the major phenolic compound hydroxytyrosol (HT) and its derivatives are valuable antioxidants with various health-promoting properties including neuroprotective, anti-cancer, and anti-inflammatory activities^[8-12,28]. The low extractability of hydrophilic HT could be overcome by acylation. PestE was chosen for the acetylation of HT to hydroxytyrosol acetate (HTA) because its ability to efficiently acetylate primary alcohols, employing ethyl acetate as the acyl donor, has been demonstrated in a previous study (**Article IV**). In addition, the robust promiscuous hydrolase/acyltransferase PestE is more likely to remain active in OMWW, which is an unbuffered solution with various reactive compounds and an acidic pH of 5^[15].

Initial screening with 5 mM HT in sodium phosphate buffer (pH 8.0) and a large excess of ethyl acetate showed that HT was accepted as a nucleophile for acyl transfer reactions, but spots on thin-layer chromatography (TLC) were weak, indicating low acyltransferase efficiency. Therefore, mutagenesis of PestE was pursued to increase acyltransferase activity. The mutants PestE_H95A, PestE_I208A, and PestE_N288F, which were previously engineered to increase acyltransferase activity toward monoterpene alcohols, were also examined. Only the PestE_I208A mutant showed stronger staining on the TLC compared to the WT. Substitution of N288 previously increased the maximum conversions obtained with ethyl acetate as an acyl donor (**Article IV**) due to the disturbance of water network formation. Since N288F did not increase conversions, the mutant N288A was created. PestE_G86A and PestE_L209F were designed based on the molecular docking of HT in the active site (Figure 28A). All mutants were tested in a two-phase system with 5 mM HT in 50 mM citrate buffer at pH 5.0 and ethyl acetate at a volumetric phase ratio of 2:1. The PestE concentration in the aqueous phase was 0.1 mg/mL. The PestE WT showed a conversion of 18% after 24 h, whereas the mutants PestE_G86A, PestE_N288A, PestE_I208A, and PestE_L209F reached 18, 21, 22, and 52% conversion, respectively (Figure 28B). Combinatorial mutagenesis revealed that the combination of I208A, L209F, and N288A (PestE_I208A_L209F_N288A) gave the best conversion of 86%.

2. Results

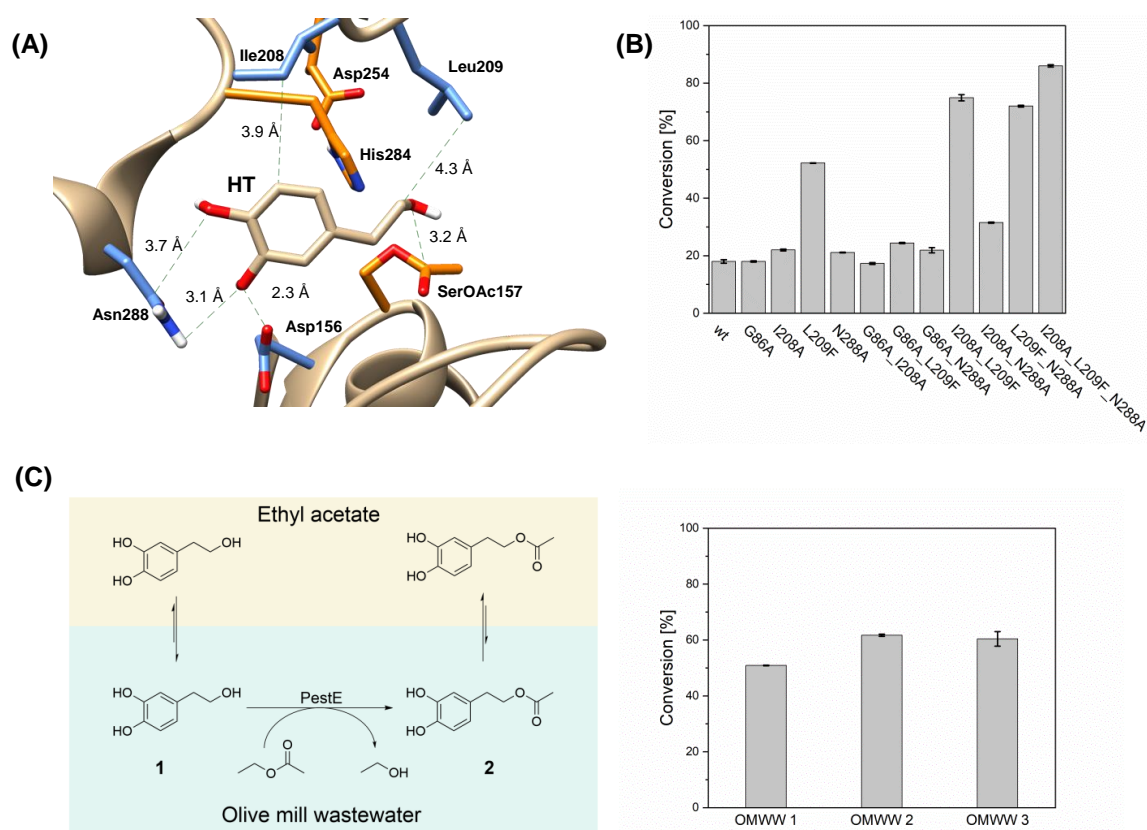


Figure 28. Acetylation of HT by PestE. (A) Docking structure of HT in PestE WT. The acetylated Ser157 was generated based on the PDB structure 3ZWQ. Residues interacting with HT are shown in light blue; residues of the catalytic triad Ser157, His284, Asp254 are highlighted in orange. (B) Conversion of HT to HTA at 25°C (1000 rpm) by 0.1 mg/mL of each PestE variant in a two-phase system of 50 mM citrate buffer and EtOAc after 24 h. (C) Reaction scheme and conversions of HT in OMWWs catalyzed by PestE_I208A_L209F_N288A (0.5 mg/mL) on EziG² beads (EnginZyme, Solna, Sweden) at 35°C (1000 rpm) after 24 h. The organic EtOAc phase was used in a 1:2 ratio to the aqueous phase. The figure was adapted from Terholsen et al.^[319].

PestE_I208A_L209F_N288A was immobilized on EziG² beads (PestE_I208A_L209F_N288A-EziG²). EziG² are commercially available porous glass beads coated with a hydrophobic polymer capable of binding his₆-tagged proteins. By using PestE_I208A_L209F_N288A-EziG² and increasing the enzyme loading to 1 mg/mL conversions of over 80% were reached within 1 h reaction time. The recyclability of the enzyme-loaded EziG² beads was demonstrated for ten reaction cycles without loss of activity. Finally, PestE_I208A_L209F_N288A-EziG² was used to generate and extract HTA from the OMWW of three olive mills from Crete (Greece). Due to inhibition by other phenols in the OMWW, the reaction was slower and only conversions of 51–62% were achieved after 24 h (Figure 28C). In a preparative scale reaction, 13.8 mg of HTA could be extracted into the organic phase, corresponding to 57 mol% of HT from the

OMWW used. Considering the additionally extracted 2.1 mg of HT, 73 mol% of HT was recovered from the OMWW in the organic phase. This is comparable to the recoveries of other extraction methods^[15,16]. However, here, only a simple one-step extraction was performed. The use of PestE_I208A_L209F_N288A could help intensify extraction processes and replace HT currently produced from fossil feedstocks^[13]. However, the total amount of HT in the OMWW samples used for extraction was relatively low due to the timing of sampling in November, as the free HT content is higher in the late season^[320]. In the early season, HT is bound in the glycoside oleuropein, for example.

2.2.4 An Enzyme Cascade Reaction for the Recovery of Hydroxytyrosol Derivatives from Olive Mill Wastewater (Article VI)

As mentioned in **Article V**, HT is found in olives in both free and bound forms^[320]. The glycoside oleuropein is the major HT glycoside and is found in olive leaves and fruits. Therefore, olive by-products such as olive leaves, OMWW, and olive seeds contain oleuropein^[321]. Its content is subject to seasonal variation and highly depends on the olive oil extraction process^[322]. To produce value-added HT from oleuropein, the glycoside must be cleaved and hydrolyzed. It is known that almond β -glucosidase cleaves oleuropein into the oleuropein aglycone and glucose^[323]. However, further cleavage is required to release HT. Because PestE_I208A_L209F_N288A has been shown to be active for the synthesis of HT esters, we exploited the hydrolytic properties of this promiscuous hydrolase/acyltransferase in the absence of an acyl donor to release HT. To enable a continuous process of OMWW produced continuously even during the olive oil season, a segmented flow setup was used to release HT from oleuropein and to produce and extract HTA from the released HT (Figure 29A). Interestingly, no further release of HT from the glucosidase-pretreated OMWW was detected under acyltransferase conditions (Figure 29B), highlighting that hydrolysis of the oleuropein aglycone is suppressed during the acyltransferase reaction. By dividing the flow reactions into a hydrolysis step of oleuropein to HT and an acyltransferase reaction (Figure 29C), the total HT(A) extraction titers relative to one liter of OMWW were increased from 130 mg/L (93 mg/L HTA and 37 mg/L HT) to 228 mg/L (166 mg/L HTA and 62 mg/L HT). Thus, similar extraction titers

2. Results

relative to one liter of OMWW were achieved as in the batch method (**Article V**; 265 mg/L). Importantly, the reaction time was reduced from 24 h to about 30 min. At the same time, the elevated temperatures used in the previous systems could be avoided.

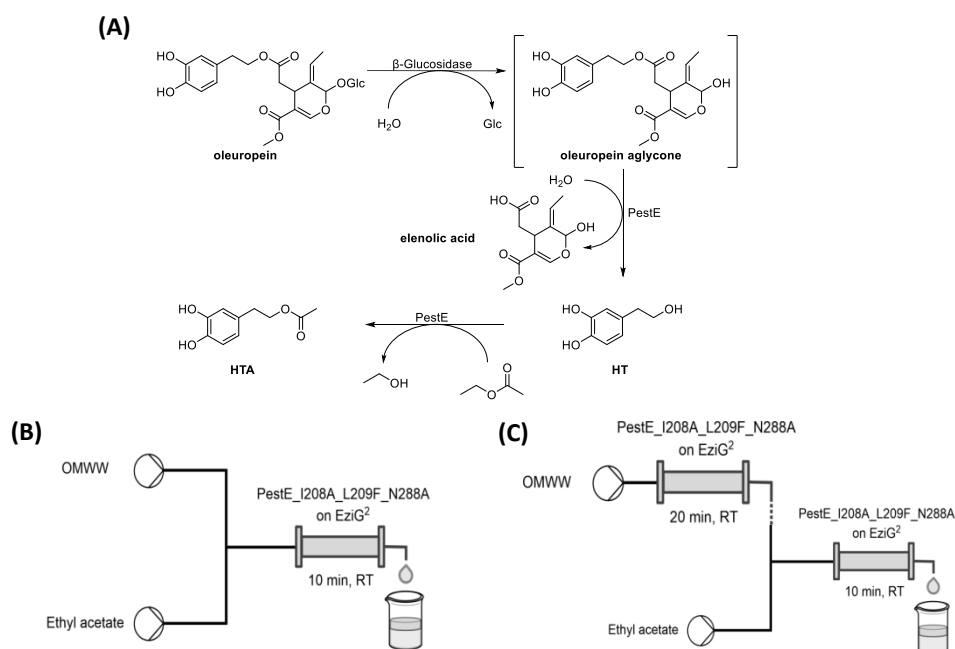


Figure 29. Schematic reaction and flow diagram of the enzymatic cascade reaction for the recovery of HT(A) from OMWW. (A) Reaction cascade for the conversion of oleuropein to HTA. The almond β -glucosidase deglycosylates oleuropein to oleuropein aglycone. PestE_I208A_L209F_N288A is intended to release elenolic acid and HT by hydrolysis and to transesterify HT to HTA using ethyl acetate as acyl donor. (B) Acetylation/extraction flow setup. Ethyl acetate and OMWW were added to the packed-bed reactor at flow rates of 1.0 mL/h and 1.6 mL/h, respectively. (C) Sequential oleuropein hydrolysis and HT acetylation/extraction setup: Hydrolysis of oleuropein was performed in a separate flow reaction at a flow rate of 1.6 mL/h. The acetylation/extraction reaction was performed as described above. The figure was adapted from Terholsen et al.^[324].

Overall, we demonstrated the coupling of almond β -glucosidase and PestE_I208A_L209F_N288A in a sequential enzyme flow cascade that utilizes both the hydrolase and acyltransferase activities of the promiscuous hydrolase/acyltransferase. The release and extraction of HT(A) from its precursor could help to recover more HTA from the by-products of industrial olive oil production. In addition, the possibility of continuous OMWW processing and extraction was demonstrated.

2.2.5 Chemoenzymatic Cascade Reaction for the Valorization of the Lignin Depolymerization Product G-C2-Dioxolane Phenol (Article VII)

Lignin is part of lignocellulose, the most abundant sustainable resource on earth^[29], and its potential for the production of certain chemicals has not yet been exhausted. In the pulp and paper industry, lignin is extracted from lignocellulose under harsh reaction conditions, irreversibly changing lignin into a chemically undefined product that is used as a combustible^[40]. The "lignin first" approach aims at extracting high quality lignin from lignocellulose while producing high quality (hemi-)cellulosic products^[40,58]. In other words, the "lignin first" strategy aims at exploiting the full potential of lignocellulose for the specific manufacturing of chemical compounds. One approach following the "lignin first" strategy is the diol-assisted fractionation of lignocellulose, which produces dioxolane products of the lignin building blocks. In softwood, the guaiacol-derived G subunit is the most abundant lignin building block^[37,38] and, therefore, the major depolymerization product. Deuss and co-workers extracted up to 16.5% (w/w) of the G-subunit derived G-C2-dioxolane phenol (DOX; Figure 30) from pinewood lignin^[50]. Our goal was to valorize the DOX to a homovanillyl alcohol-derived antioxidant. Homovanillyl alcohol (HVA) has shown protective effects on cardiovascular disease and is a natural metabolite of HT^[325,326]. In homology to HT, acylation could facilitate its transfer across membranes^[327,328]. In a one-pot chemoenzymatic cascade (Figure 30), we first deprotected the DOX with Amberlyst-15 (Merck KGaA, Darmstadt) encapsulated in polydimethylsiloxane (Amb-15@PDMS) to homovanillin (HV) and used horse liver alcohol dehydrogenase (HLADH) to generate HVA, which was subsequently acylated by the promiscuous acyltransferase/hydrolase mutant PestE_I208A_L209F_N288A described above (**Article V**). Because phenols tend to oxidize at basic pH, the cascade was performed in sodium phosphate/citrate buffer at pH 6.0.

2. Results

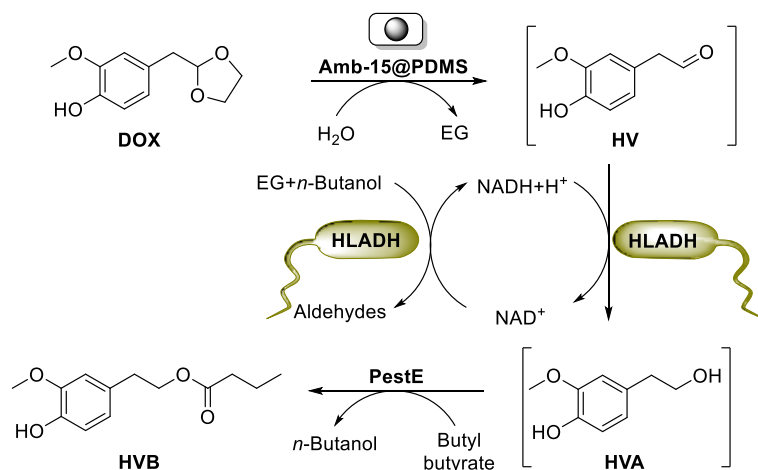


Figure 30. Chemoenzymatic cascade for the synthesis of homovanillyl butyrate from G-C2 dioxolane phenol (DOX). Polydimethylsiloxane-coated Amberlyst-15 (Amb-15@PDMS) was used to deprotect DOX, yielding homovanillin (HV). HV is reduced to homovanillyl alcohol (HVA) by lyophilized *E. coli* whole cells containing HLADH. HLADH recycled the required NADH cofactor by oxidizing ethylene glycol (EG) and *n*-butanol released during the other reaction steps. Finally, PestE_I208A_L209F_N288A acylated HVA to homovanillyl butyrate (HVB).

The deprotection of acetals by the solid acid catalyst Amberlyst-15 in pure water has been described^[211], but it was not possible to couple the deprotection and the enzyme reactions because the buffers required for the enzymatic reactions deactivated the solid acid catalyst by deprotonation. Therefore, a compartmentalization strategy was employed in which Amberlyst-15 was encapsulated with a hydrophobic polydimethylsiloxane (PDMS) polymer (Sylgard[®] 184; Merck KGaA, Darmstadt). With this strategy, it was possible to deprotect the DOX in a buffered solution at pH 6.0 and couple the deprotection with the enzymatic transformation steps (Table 3). However, the enzymatic activity of HLADH was drastically reduced in this system, which might be due to immobilization and inactivation on the PDMS surface^[329]. In general, the activity of HLADH was limiting for the cascade because a biphasic reaction with the acyl donor ethyl acetate, which was previously used to promote the acyltransferase reaction (**Articles V & VI**), inactivated the enzyme. Therefore, the acyl donor was replaced with butyl butyrate, which is less inactivating, and lyophilized *E. coli* whole cells with recombinantly expressed HLADH were used to prevent immobilization on the PDMS surface.

2. Results

Table 3. Chemoenzymatic cascade reaction for the synthesis of HVB.

Entry	HLADH	PestE	DOX	HV	HVA	HVB
1	OD ₆₀₀ 15	20 µg	13±7%	75±7%	4±0%	8±0%
2	OD ₆₀₀ 100	20 µg	14±6%	50±2%	13±3%	23±2%
3	OD ₆₀₀ 500	20 µg	3±1%	3±2%	37±1%	57±0%
4	-	-	3±0%	97±0%	n.d.	n.d.
5 ^a	-	20 µg	32±14%	57±15%	9±1%	2±0%
6	OD ₆₀₀ 500	-	64±6%	1±0%	34±6%	Traces

5 mM G-C2 dioxolane phenol, 7 mg Amb-15@PDMS (containing approximately 1.4 mg Amb-15; 10 beads), 20% (v/v) butyl butyrate, and purified PestE_I208A_L209F_N288A were added. The 100-µL-scale reaction in sodium phosphate/citrate buffer (25 mM each; pH 6.0) was performed at 20°C (1000 rpm) for 24 hours. HLADH was expressed in *E. coli* whole cells and used as a lyophilizate. All reactions were extracted twice with 200 µL ethyl acetate and Amb-15@PDMS was additionally washed twice. The values given are mean values of duplicates with the corresponding standard deviation. OD₆₀₀ was measured before lyophilization and the amount of lyophilisate added was adjusted accordingly. a) OD₆₀₀ 150 of *E. coli* whole cells containing empty vector pET28a.

Endogenous *E. coli* proteins also showed minor activity in reducing HV to HVA (Table 3, entry 5). Nevertheless, large amounts of lyophilized whole cells (OD₆₀₀ 500) containing HLADH were required to convert 97% of the HV formed. The overall conversion of 94% for the first two reaction steps indicates that deprotection, recycling of the NADH cofactor with ethylene glycol and butanol from the other reaction steps, and shifting of the equilibrium by subsequent acylation were successful. The conversions in the final acylation step reached up to 61%, which is close to the 68% conversion achieved in 24 hours in a reaction with 5 mM HVA as substrate in the presence of PestE_I208A_L209F_N288A and Amb-15@PDMS. However, it is worth noting that PestE_I208A_L209F_N288A is the HVB-forming catalyst and not Amb-15@PDMS (Table 3, entry 6). Finally, it was possible to create a one-pot chemoenzymatic cascade for the potential valorization of DOX with a total conversion of 57% to HVB. With Amb-15@PDMS and the use of the promiscuous acyltransferase/hydrolase PestE, it was possible to perform acetal cleavage and transesterification, which are typically incompatible with buffered aqueous systems, at near-neutral pH and 20°C. In addition, an enzyme-compatible solid acid catalyst was developed, which could open up the possibility of coupling various acid- and enzyme-catalyzed reactions.

3. Conclusions

In this dissertation, enzymatic valorization strategies for CO₂ and biomass-derived compounds were successfully developed.

In search of an ArM scaffold for selective photocatalytic CO₂ reduction to CO, we found a new enzymatic promiscuity of BsPAD and other CO₂-binding enzymes. It was possible to identify the essential amino acids in BsPAD – R41, Y11, and W62 – involved in CO₂ binding and electron transfer. With the best BsPAD variant, BsPAD_WCP_W17A, TONs of 196, and selectivity for CO over H₂ of 82% could be achieved. From a selection of CO₂-binding enzymes, ScFDC1, TtALS, and EcPanD showed similar or higher activity and selectivity than BsPAD_WCP_W17A. These enzymes overcome the expression and stability problems of CODH and have the potential to replace (noble) metal-containing catalysts for photocatalytic CO₂ reduction (**Article I**). During the engineering of BsPAD, two high-throughput assays for the detection of phenolic acid decarboxylation were developed, allowing fast and accurate characterization of PADs (**Article II**).

The potential of promiscuous acyltransferases/hydrolases was reviewed in a 'perspective article' (**Article III**). Along these lines of research, the acyltransferase substrate scope of PestE was investigated for the monoterpene alcohols (±)-citronellol, (±)-menthol, carvacrol, and (±)-linalool. High activity was observed toward the primary alcohol citronellol, resulting in complete conversion with vinyl acetate as the acyl donor and greater than 90% conversion with ethyl acetate using PestE_N288F. PestE_I208A increased the selectivity for acetylation of (–)-menthol and achieved E-values up to 57 (WT: 7). In addition, PestE is the first promiscuous acyltransferase/hydrolase to exhibit acyl transfer activity toward phenolic alcohols (**Article IV**). Furthermore, PestE was engineered for the acetylation of the hydrophilic antioxidant HT in a two-phase system with ethyl acetate, resulting in the optimized variant PestE_I208A_L209F_N288A. The immobilization of this PestE variant on EziG² beads yielded a potent and, importantly, reusable biocatalyst. Although the acidic, phenol-rich, and unbuffered OMWW is a very challenging reaction matrix, conversions of 51–61% HTA from OMWW samples were achieved. In a 60-mL scale batch, 73 mol% of the initial HT content (57 mol% as HTA) could be extracted into the organic phase. The

3. Conclusions

developed enzyme-assisted extraction method showed a similar yield to established extraction methods but requires only a single extraction step (**Article V**). This system was further developed to allow extraction of HT, covalently bound in its precursor oleuropein, using almond β -glucosidase and both activities of the promiscuous acyltransferase/hydrolase PestE_I208A_L209F_N288A in a flow chemistry setup (**Article VI**). PestE_I208A_L209F_N288A was also used in the final step of a chemoenzymatic cascade to convert the lignin depolymerization product DOX via HV and HVA to HVB with 57% conversion. The reaction of HV to HVA was catalyzed by recombinant HLADH from lyophilized *E. coli* whole-cells. For the acetal cleavage of DOX, an enzyme-compatible PDMS-coated Amberlyst-15 catalyst (Amb-15@PDMS) was employed, allowing the use of the solid acid catalyst under aqueous buffer conditions and mild temperatures (**Article VII**).

In conclusion, PestE has been proven to be a versatile and robust promiscuous hydrolase/acyltransferase that can operate in cascades and under challenging conditions. PestE_I208A_L209F_N288A was developed as a significantly improved variant of this acyltransferase, providing a good starting point for the valorization/extraction of other compounds, for example, resveratrol, from waste biomass. In addition, two new classes of catalysts were discovered in this work: Enzyme-compatible solid acid catalysts (Amb-15@PDMS) and CO₂ reduction catalyzing CO₂-binding enzymes. Both classes of catalysts open the door to new sustainable synthesis routes that avoid high temperatures, organic solvents, or (noble) metals. The (enzyme) catalysts presented could pave the way for sustainable synthesis of chemicals in the future.

4. Literature

- [1] United Nations, "THE 17 GOALS | Sustainable Development," can be found under <https://sdgs.un.org/goals>, **2022**.
- [2] P. T. Anastas, *Chem. Rev.* **2007**, *107*, 2167–2168.
- [3] E. Tsagaraki, H. N. Lazarides, K. B. Petrotos, in *Util. -Prod. Treat. Waste Food Ind.* (Eds.: V. Oreopoulou, W. Russ), Springer US, Boston, MA, **2007**, pp. 133–157.
- [4] A. Ramos-Cormenzana, M. Monteoliva-Sanchez, M. J. Lopez, *Int. Biodeterior. Biodegrad.* **1995**, *35*, 249–268.
- [5] H. Zbakh, A. El Abbassi, *J. Funct. Foods* **2012**, *4*, 53–65.
- [6] C. Agabo-García, N. Calderón, G. Hodaifa, *Catalysts* **2021**, *11*, 557.
- [7] K. Al-Malah, M. O. J. Azzam, N. I. Abu-Lail, *Sep. Purif. Technol.* **2000**, *20*, 225–234.
- [8] C. Qin, S. Hu, S. Zhang, D. Zhao, Y. Wang, H. Li, Y. Peng, L. Shi, X. Xu, C. Wang, J. Liu, Y. Cheng, J. Long, *Mol. Nutr. Food Res.* **2021**, *65*, 2000797.
- [9] A. H. Abuznait, H. Qosa, B. A. Busnena, K. A. El Sayed, A. Kaddoumi, *ACS Chem. Neurosci.* **2013**, *4*, 973–982.
- [10] R. Fuccelli, R. Fabiani, P. Rosignoli, *Molecules* **2018**, *23*, 3212.
- [11] G. K. Beauchamp, R. S. J. Keast, D. Morel, J. Lin, J. Pika, Q. Han, C.-H. Lee, A. B. Smith, P. A. S. Breslin, *Nature* **2005**, *437*, 45–46.
- [12] M. A. Rosillo, M. Sánchez-Hidalgo, A. González-Benjumea, J. G. Fernández-Bolaños, E. Lubberts, C. Alarcón-de-la-Lastra, *Mol. Nutr. Food Res.* **2015**, *59*, 2537–2546.
- [13] D. Diekemper, S. Schwarzer, *Nachr. Chem.* **2022**, *70*, 27–29.
- [14] N. Allouche, I. Fki, S. Sayadi, *J. Agric. Food Chem.* **2004**, *52*, 267–273.
- [15] M. O. J. Azzam, S. A. Hazaimah, *Process Saf. Environ. Prot.* **2021**, *148*, 495–523.
- [16] A. El-Abbassi, M. Khayet, A. Hafidi, *Water Res.* **2011**, *45*, 4522–4530.
- [17] D. Frascari, G. Rubertelli, F. Arous, A. Ragini, L. Bresciani, A. Arzu, D. Pinelli, *Chem. Eng. J.* **2019**, *360*, 124–138.
- [18] R. Mazzei, L. Giorno, E. Piacentini, S. Mazzuca, E. Drioli, *J. Membr. Sci.* **2009**, *339*, 215–223.
- [19] G. Ranieri, R. Mazzei, T. Poerio, F. Bazzarelli, Z. Wu, K. Li, L. Giorno, *Chem. Eng. Sci.* **2018**, *185*, 149–156.
- [20] N. Solomakou, A. M. Goula, *Rev. Environ. Sci. Biotechnol.* **2021**, *20*, 839–863.
- [21] P. Tapia-Quirós, M. F. Montenegro-Landívar, M. Reig, X. Vecino, J. Saurina, M. Granados, J. L. Cortina, *J. Environ. Manage.* **2022**, *307*, 114555.
- [22] R. Tundis, C. Conidi, M. R. Loizzo, V. Sicari, A. Cassano, *Antioxidants* **2020**, *9*, 602.
- [23] F. V. Romeo, G. Granuzzo, P. Foti, G. Ballistreri, C. Caggia, P. Rapisarda, *Molecules* **2021**, *26*, 1944.
- [24] A. Ben Saad, A. Jerbi, I. Khlif, M. Ayedi, N. Allouche, *Chem. Afr.* **2020**, *3*, 657–665.
- [25] C. Romero, E. Medina, J. Vargas, M. Brenes, A. De Castro, *J. Agric. Food Chem.* **2007**, *55*, 680–686.
- [26] C. Chaves-López, A. Serio, G. Mazzarrino, M. Martuscelli, E. Scarpone, A. Paparella, *Int. J. Food Microbiol.* **2015**, *207*, 49–56.

- [27] P. Gullón, B. Gullón, G. Astray, M. Carpena, M. Fraga-Corral, M. A. Prieto, J. Simal-Gandara, *Food Res. Int.* **2020**, *137*, 109683.
- [28] Y. Achmon, A. Fishman, *Appl. Microbiol. Biotechnol.* **2015**, *99*, 1119–1130.
- [29] M. Al-Naji, F. Brandi, M. Drieß, F. Rosowski, *Chem. Ing. Tech.* **2022**, *94*, 1611–1627.
- [30] H. Jørgensen, J. B. Kristensen, C. Felby, *Biofuels Bioprod. Biorefin.* **2007**, *1*, 119–134.
- [31] C. Megías-Sayago, S. Navarro-Jaén, F. Drault, S. Ivanova, *Catalysts* **2021**, *11*, 1395.
- [32] F. Menegazzo, E. Ghedini, M. Signoretto, *Molecules* **2018**, *23*, 2201.
- [33] P. Oinonen, L. Zhang, M. Lawoko, G. Henriksson, *Phytochemistry* **2015**, *111*, 177–184.
- [34] R. N. Monrad, J. Eklöf, K. B. R. M. Krogh, P. Biely, *Crit. Rev. Biotechnol.* **2018**, *38*, 1121–1136.
- [35] P. Ning, G. Yang, L. Hu, J. Sun, L. Shi, Y. Zhou, Z. Wang, J. Yang, *Biotechnol. Biofuels* **2021**, *14*, 102.
- [36] G. Neutelings, *Plant Sci.* **2011**, *181*, 379–386.
- [37] T. Ren, W. Qi, R. Su, Z. He, *ChemCatChem* **2019**, *11*, 639–654.
- [38] Z. Sun, B. Fridrich, A. de Santi, S. Elangovan, K. Barta, *Chem. Rev.* **2018**, *118*, 614–678.
- [39] Y. Jing, L. Dong, Y. Guo, X. Liu, Y. Wang, *ChemSusChem* **2020**, *13*, 4181–4198.
- [40] T. Renders, S. V. den Bosch, S.-F. Koelewijn, W. Schutyser, B. F. Sels, *Energy Environ. Sci.* **2017**, *10*, 1551–1557.
- [41] S. Omori, M. Aoyama, A. Sakakibara, *Holzforschung* **1998**, *52*, 391–397.
- [42] A. Mittal, R. Katahira, B. S. Donohoe, S. Pattathil, S. Kandemkavil, M. L. Reed, M. J. Bidy, G. T. Beckham, *ACS Sustain. Chem. Eng.* **2017**, *5*, 2544–2561.
- [43] L. da C. Sousa, M. Foston, V. Bokade, A. Azarpira, F. Lu, A. J. Ragauskas, J. Ralph, B. Dale, V. Balan, *Green Chem.* **2016**, *18*, 4205–4215.
- [44] F. P. Bouxin, S. David Jackson, M. C. Jarvis, *Bioresour. Technol.* **2014**, *162*, 236–242.
- [45] N. Sathitsuksanoh, K. M. Holtman, D. J. Yelle, T. Morgan, V. Stavila, J. Pelton, H. Blanch, B. A. Simmons, A. George, *Green Chem.* **2014**, *16*, 1236–1247.
- [46] K. H. Kim, B. A. Simmons, S. Singh, *Green Chem.* **2017**, *19*, 215–224.
- [47] A. Brandt, J. Gräsvik, J. P. Hallett, T. Welton, *Green Chem.* **2013**, *15*, 550–583.
- [48] L. Weigand, S. Mostame, A. Brandt-Talbot, T. Welton, J. P. Hallett, *Faraday Discuss.* **2017**, *202*, 331–349.
- [49] J. S. Luterbacher, A. Azarpira, A. H. Motagamwala, F. Lu, J. Ralph, J. A. Dumesic, *Energy Environ. Sci.* **2015**, *8*, 2657–2663.
- [50] P. J. Deuss, C. S. Lancefield, A. Narani, J. G. de Vries, N. J. Westwood, K. Barta, *Green Chem.* **2017**, *19*, 2774–2782.
- [51] C. S. Lancefield, I. Panovic, P. J. Deuss, K. Barta, N. J. Westwood, *Green Chem.* **2017**, *19*, 202–214.
- [52] E. Feghali, G. Carrot, P. Thuéry, C. Genre, T. Cantat, *Energy Environ. Sci.* **2015**, *8*, 2734–2743.

- [53] J. G. Linger, D. R. Vardon, M. T. Guarnieri, E. M. Karp, G. B. Hunsinger, M. A. Franden, C. W. Johnson, G. Chupka, T. J. Strathmann, P. T. Pienkos, G. T. Beckham, *Proc. Natl. Acad. Sci.* **2014**, *111*, 12013–12018.
- [54] D. R. Vardon, M. A. Franden, C. W. Johnson, E. M. Karp, M. T. Guarnieri, J. G. Linger, M. J. Salm, T. J. Strathmann, G. T. Beckham, *Energy Environ. Sci.* **2015**, *8*, 617–628.
- [55] M. Kumar, S. You, J. Beiyuan, G. Luo, J. Gupta, S. Kumar, L. Singh, S. Zhang, D. C. W. Tsang, *Bioresour. Technol.* **2021**, *320*, 124412.
- [56] M. D. Kärkäs, *ChemSusChem* **2017**, *10*, 2111–2115.
- [57] L. Shuai, M. T. Amiri, Y. M. Questell-Santiago, F. Héroguel, Y. Li, H. Kim, R. Meilan, C. Chapple, J. Ralph, J. S. Luterbacher, *Science* **2016**, *354*, 329–333.
- [58] M. M. Abu-Omar, K. Barta, G. T. Beckham, J. S. Luterbacher, J. Ralph, R. Rinaldi, Y. Román-Leshkov, J. S. M. Samec, B. F. Sels, F. Wang, *Energy Environ. Sci.* **2021**, *14*, 262–292.
- [59] M. V. Galkin, J. S. M. Samec, *ChemSusChem* **2014**, *7*, 2154–2158.
- [60] M. V. Galkin, A. T. Smit, E. Subbotina, K. A. Artemenko, J. Bergquist, W. J. J. Huijgen, J. S. M. Samec, *ChemSusChem* **2016**, *9*, 3280–3287.
- [61] P. Ferrini, C. A. Rezende, R. Rinaldi, *ChemSusChem* **2016**, *9*, 3171–3180.
- [62] I. Graça, R. T. Woodward, M. Kennema, R. Rinaldi, *ACS Sustain. Chem. Eng.* **2018**, *6*, 13408–13419.
- [63] S. V. den Bosch, W. Schutyser, S.-F. Koelewijn, T. Renders, C. M. Courtin, B. F. Sels, *Chem. Commun.* **2015**, *51*, 13158–13161.
- [64] T. Parsell, S. Yohe, J. Degenstein, T. Jarrell, I. Klein, E. Gencer, B. Hewetson, M. Hurt, J. I. Kim, H. Choudhari, B. Saha, R. Meilan, N. Mosier, F. Ribeiro, W. N. Delgass, C. Chapple, H. I. Kenttämä, R. Agrawal, M. M. Abu-Omar, *Green Chem.* **2015**, *17*, 1492–1499.
- [65] H. P. Godard, J. L. McCarthy, H. Hibbert, *J. Am. Chem. Soc.* **1940**, *62*, 988–988.
- [66] H. P. Godard, J. L. McCarthy, H. Hibbert, *J. Am. Chem. Soc.* **1941**, *63*, 3061–3066.
- [67] J. R. Jr. Bower, J. L. McCarthy, H. Hibbert, *J. Am. Chem. Soc.* **1941**, *63*, 3066–3068.
- [68] J. R. Jr. Bower, L. M. Cooke, H. Hibbert, *J. Am. Chem. Soc.* **1943**, *65*, 1195–1198.
- [69] C. P. Brewer, L. M. Cooke, H. Hibbert, *J. Am. Chem. Soc.* **1948**, *70*, 57–59.
- [70] J. M. Pepper, H. Hibbert, *J. Am. Chem. Soc.* **1948**, *70*, 67–71.
- [71] P. J. Deuss, M. Scott, F. Tran, N. J. Westwood, J. G. de Vries, K. Barta, *J. Am. Chem. Soc.* **2015**, *137*, 7456–7467.
- [72] A. D. Santi, M. V. Galkin, C. W. Lahive, P. J. Deuss, K. Barta, *ChemSusChem* **2020**, *13*, 4468–4477.
- [73] P. J. Deuss, C. W. Lahive, C. S. Lancefield, N. J. Westwood, P. C. J. Kamer, K. Barta, J. G. de Vries, *ChemSusChem* **2016**, *9*, 2974–2981.
- [74] C. W. Lahive, P. J. Deuss, C. S. Lancefield, Z. Sun, D. B. Cordes, C. M. Young, F. Tran, A. M. Z. Slawin, J. G. de Vries, P. C. J. Kamer, N. J. Westwood, K. Barta, *J. Am. Chem. Soc.* **2016**, *138*, 8900–8911.
- [75] W. Lan, M. T. Amiri, C. M. Hunston, J. S. Luterbacher, *Angew. Chem. Int. Ed.* **2018**, *57*, 1356–1360.
- [76] C. Le Quéré, R. B. Jackson, M. W. Jones, A. J. P. Smith, S. Abernethy, R. M. Andrew, A. J. De-Gol, D. R. Willis, Y. Shan, J. G. Canadell, P.

- Friedlingstein, F. Creutzig, G. P. Peters, *Nat. Clim. Change* **2020**, *10*, 647–653.
- [77] J. W. B. Rae, Y. G. Zhang, X. Liu, G. L. Foster, H. M. Stoll, R. D. M. Whiteford, *Annu. Rev. Earth Planet. Sci.* **2021**, *49*, 609–641.
- [78] S. Fujikawa, R. Selyanchyn, T. Kunitake, *Polym. J.* **2021**, *53*, 111–119.
- [79] X. Shi, H. Xiao, H. Azarabadi, J. Song, X. Wu, X. Chen, K. S. Lackner, *Angew. Chem. Int. Ed.* **2020**, *59*, 6984–7006.
- [80] A. I. Osman, M. Hefny, M. I. A. Abdel Maksoud, A. M. Elgarahy, D. W. Rooney, *Environ. Chem. Lett.* **2021**, *19*, 797–849.
- [81] R. Schaller, T. Markus, K. Korte, E. Gawel, *Rev. Eur. Comp. Int. Environ. Law* **2022**, *31*, 258–267.
- [82] Z. Hu, Y. Wang, B. B. Shah, D. Zhao, *Adv. Sustain. Syst.* **2019**, *3*, 1800080.
- [83] J.-T. Anyanwu, Y. Wang, R. T. Yang, *Ind. Eng. Chem. Res.* **2020**, *59*, 7072–7079.
- [84] A. George, B. Shen, M. Craven, Y. Wang, D. Kang, C. Wu, X. Tu, *Renew. Sustain. Energy Rev.* **2021**, *135*, 109702.
- [85] M. Liu, Y. Yi, L. Wang, H. Guo, A. Bogaerts, *Catalysts* **2019**, *9*, 275.
- [86] F. N. Al-Rowaili, A. Jamal, M. S. Ba Shammakh, A. Rana, *ACS Sustain. Chem. Eng.* **2018**, *6*, 15895–15914.
- [87] V. M. Badiani, C. Casadevall, M. Miller, S. J. Cobb, R. R. Manuel, I. A. C. Pereira, E. Reisner, *J. Am. Chem. Soc.* **2022**, *144*, 14207–14216.
- [88] J. Albero, Y. Peng, H. García, *ACS Catal.* **2020**, *10*, 5734–5749.
- [89] A. Wagner, C. D. Sahm, E. Reisner, *Nat. Catal.* **2020**, *3*, 775–786.
- [90] J. Zhou, J. Li, L. Kan, L. Zhang, Q. Huang, Y. Yan, Y. Chen, J. Liu, S.-L. Li, Y.-Q. Lan, *Nat. Commun.* **2022**, *13*, 4681.
- [91] D. Lee, H. Nam, M. Won Seo, S. Hoon Lee, D. Tokmurzin, S. Wang, Y.-K. Park, *Chem. Eng. J.* **2022**, *447*, 137501.
- [92] K. Feng, Y. Wang, M. Guo, J. Zhang, Z. Li, T. Deng, Z. Zhang, B. Yan, *J. Energy Chem.* **2021**, *62*, 153–171.
- [93] G. A. Aleku, G. W. Roberts, G. R. Titchiner, D. Leys, *ChemSusChem* **2021**, *14*, 1781–1804.
- [94] D. Ohde, B. Thomas, P. Bubenheim, A. Liese, *Biochem. Eng. J.* **2021**, *166*, 107825.
- [95] U. W. Liebal, L. M. Blank, B. E. Ebert, *Metab. Eng. Commun.* **2018**, *7*, e00075.
- [96] R. E. Blankenship, D. M. Tiede, J. Barber, G. W. Brudvig, G. Fleming, M. Ghirardi, M. R. Gunner, W. Junge, D. M. Kramer, A. Melis, T. A. Moore, C. C. Moser, D. G. Nocera, A. J. Nozik, D. R. Ort, W. W. Parson, R. C. Prince, R. T. Sayre, *Science* **2011**, *332*, 805–809.
- [97] D. K. Dogutan, D. G. Nocera, *Acc. Chem. Res.* **2019**, *52*, 3143–3148.
- [98] E. Edwardes Moore, V. Andrei, A. R. Oliveira, A. M. Coito, I. A. C. Pereira, E. Reisner, *Angew. Chem. Int. Ed.* **2021**, *60*, 26303–26307.
- [99] B. Zhang, L. Sun, *Chem. Soc. Rev.* **2019**, *48*, 2216–2264.
- [100] S. Berardi, S. Drouet, L. Francàs, C. Gimbert-Suriñach, M. Guttentag, C. Richmond, T. Stoll, A. Llobet, *Chem. Soc. Rev.* **2014**, *43*, 7501–7519.
- [101] L. Zou, R. Sa, H. Lv, H. Zhong, R. Wang, *ChemSusChem* **2020**, *13*, 6124–6140.
- [102] X. Liu, S. Inagaki, J. Gong, *Angew. Chem. Int. Ed.* **2016**, *55*, 14924–14950.
- [103] T. Inoue, A. Fujishima, S. Konishi, K. Honda, *Nature* **1979**, *277*, 637–638.
- [104] M. Halmann, *Nature* **1978**, *275*, 115–116.

- [105] S. Karmakar, S. Barman, F. A. Rahimi, T. K. Maji, *Energy Environ. Sci.* **2021**, *14*, 2429–2440.
- [106] C.-F. Leung, T.-C. Lau, *Energy Fuels* **2021**, *35*, 18888–18899.
- [107] N. Noll, A.-M. Krause, F. Beuerle, F. Würthner, *Nat. Catal.* **2022**, *5*, 867–877.
- [108] H. Kumagai, Y. Tamaki, O. Ishitani, *Acc. Chem. Res.* **2022**, *55*, 978–990.
- [109] H. Takeda, Y. Monma, O. Ishitani, *ACS Catal.* **2021**, *11*, 11973–11984.
- [110] A. Call, M. Cibian, K. Yamamoto, T. Nakazono, K. Yamauchi, K. Sakai, *ACS Catal.* **2019**, *9*, 4867–4874.
- [111] C. Su, Z. Chen, Q. Feng, F. Wei, M. Zhang, A. Mo, H.-H. Huang, H. Hu, D. Liu, *Inorg. Chem.* **2022**, DOI 10.1021/acs.inorgchem.2c02515.
- [112] P. De La Torre, J. S. Derrick, A. Snider, P. T. Smith, M. Loipersberger, M. Head-Gordon, C. J. Chang, *ACS Catal.* **2022**, *12*, 8484–8493.
- [113] S. Rodríguez-Jiménez, H. Song, E. Lam, D. Wright, A. Pannwitz, S. A. Bonke, J. J. Baumberg, S. Bonnet, L. Hammarström, E. Reisner, *J. Am. Chem. Soc.* **2022**, *144*, 9399–9412.
- [114] F. Kuttassery, H. Kumagai, R. Kamata, Y. Ebato, M. Higashi, H. Suzuki, R. Abe, O. Ishitani, *Chem. Sci.* **2021**, *12*, 13216–13232.
- [115] T. W. Woolerton, S. Sheard, E. Reisner, E. Pierce, S. W. Ragsdale, F. A. Armstrong, *J. Am. Chem. Soc.* **2010**, *132*, 2132–2133.
- [116] F. Arcudi, L. Đorđević, N. Schweitzer, S. I. Stupp, E. A. Weiss, *Nat. Chem.* **2022**, *14*, 1007–1012.
- [117] P. G. Alsabeh, A. Rosas-Hernández, E. Barsch, H. Junge, R. Ludwig, M. Beller, *Catal. Sci. Technol.* **2016**, *6*, 3623–3630.
- [118] Z. Guo, S. Cheng, C. Cometto, E. Anxolabéhère-Mallart, S.-M. Ng, C.-C. Ko, G. Liu, L. Chen, M. Robert, T.-C. Lau, *J. Am. Chem. Soc.* **2016**, *138*, 9413–9416.
- [119] P. L. Cheung, C. W. Machan, A. Y. S. Malkhasian, J. Agarwal, C. P. Kubiak, *Inorg. Chem.* **2016**, *55*, 3192–3198.
- [120] P. A. Forero-Cortés, M. Marx, N. G. Moustakas, F. Brunner, C. E. Housecroft, E. C. Constable, H. Junge, M. Beller, J. Strunk, *Green Chem.* **2020**, *22*, 4541–4549.
- [121] E. Boutin, L. Merakeb, B. Ma, B. Boudy, M. Wang, J. Bonin, E. Anxolabéhère-Mallart, M. Robert, *Chem. Soc. Rev.* **2020**, *49*, 5772–5809.
- [122] H. Takeda, C. Cometto, O. Ishitani, M. Robert, *ACS Catal.* **2017**, *7*, 70–88.
- [123] S.-J. Woo, S. Choi, S.-Y. Kim, P. S. Kim, J. H. Jo, C. H. Kim, H.-J. Son, C. Pac, S. O. Kang, *ACS Catal.* **2019**, *9*, 2580–2593.
- [124] W.-J. Wang, K.-H. Chen, Z.-W. Yang, B.-W. Peng, L.-N. He, *J. Mater. Chem. A* **2021**, *9*, 16699–16705.
- [125] K.-H. Chen, N. Wang, Z.-W. Yang, S.-M. Xia, L.-N. He, *ChemSusChem* **2020**, *13*, 6284–6289.
- [126] F.-Y. Ren, K. Chen, L.-Q. Qiu, J.-M. Chen, D. J. Darensbourg, L.-N. He, *Angew. Chem. Int. Ed.* **2022**, *61*, e202200751.
- [127] R. Kuriki, H. Matsunaga, T. Nakashima, K. Wada, A. Yamakata, O. Ishitani, K. Maeda, *J. Am. Chem. Soc.* **2016**, *138*, 5159–5170.
- [128] R. Kuriki, M. Yamamoto, K. Higuchi, Y. Yamamoto, M. Akatsuka, D. Lu, S. Yagi, T. Yoshida, O. Ishitani, K. Maeda, *Angew. Chem. Int. Ed.* **2017**, *56*, 4867–4871.
- [129] A. Nakada, K. Koike, T. Nakashima, T. Morimoto, O. Ishitani, *Inorg. Chem.* **2015**, *54*, 1800–1807.

- [130] X. Zhang, M. Cibian, A. Call, K. Yamauchi, K. Sakai, *ACS Catal.* **2019**, *9*, 11263–11273.
- [131] L. Hedstrom, in *ELS*, John Wiley & Sons, Ltd, **2010**.
- [132] H. L. Drake, *J. Bacteriol.* **1982**, *149*, 561–566.
- [133] D. Bonam, L. Lehman, G. P. Roberts, P. W. Ludden, *J. Bacteriol.* **1989**, *171*, 3102–3107.
- [134] M. Inoue, I. Nakamoto, K. Omae, T. Oguro, H. Ogata, T. Yoshida, Y. Sako, *Front. Microbiol.* **2019**, *9*.
- [135] D. Bonam, P. W. Ludden, *J. Biol. Chem.* **1987**, *262*, 2980–2987.
- [136] S. W. Ragsdale, J. E. Clark, L. G. Ljungdahl, L. L. Lundie, H. L. Drake, *J. Biol. Chem.* **1983**, *258*, 2364–2369.
- [137] S. Techtmann, A. Colman, A. Lebedinsky, T. Sokolova, F. Robb, *Front. Microbiol.* **2012**, *3*.
- [138] M. Merrouch, J. Hadj-Saïd, L. Domnik, H. Dobbek, C. Léger, S. Dementin, V. Fourmond, *Chem. – Eur. J.* **2015**, *21*, 18934–18938.
- [139] B. Soboh, D. Linder, R. Hedderich, *Eur. J. Biochem.* **2002**, *269*, 5712–5721.
- [140] E. S. Choi, K. Min, G.-J. Kim, I. Kwon, Y. H. Kim, *Sci. Rep.* **2017**, *7*, 44323.
- [141] J. Eun Hyeon, S. Wook Kim, C. Park, S. Ok Han, *Chem. Commun.* **2015**, *51*, 10202–10205.
- [142] B. Sundara Sekar, S. Mohan Raj, E. Seol, S. K. Ainala, J. Lee, S. Park, *Int. J. Hydrog. Energy* **2014**, *39*, 15446–15454.
- [143] S. M. Kim, J. Lee, S. H. Kang, Y. Heo, H.-J. Yoon, J.-S. Hahn, H. H. Lee, Y. H. Kim, *Nat. Catal.* **2022**, 1–11.
- [144] E. C. Wittenborn, C. Guendon, M. Merrouch, M. Benvenuti, V. Fourmond, C. Léger, C. L. Drennan, S. Dementin, *ACS Catal.* **2020**, *10*, 7328–7335.
- [145] Y. S. Chaudhary, T. W. Woolerton, C. S. Allen, J. H. Warner, E. Pierce, S. W. Ragsdale, F. A. Armstrong, *Chem. Commun.* **2011**, *48*, 58–60.
- [146] L. Zhang, M. Can, S. W. Ragsdale, F. A. Armstrong, *ACS Catal.* **2018**, *8*, 2789–2795.
- [147] H. A. Hansen, J. B. Varley, A. A. Peterson, J. K. Nørskov, *J. Phys. Chem. Lett.* **2013**, *4*, 388–392.
- [148] F. A. Armstrong, J. Hirst, *Proc. Natl. Acad. Sci.* **2011**, *108*, 14049–14054.
- [149] V. C.-C. Wang, S. T. A. Islam, M. Can, S. W. Ragsdale, F. A. Armstrong, *J. Phys. Chem. B* **2015**, *119*, 13690–13697.
- [150] C. R. Schneider, H. S. Shafaat, *Chem. Commun.* **2016**, *52*, 9889–9892.
- [151] C. R. Schneider, A. C. Manesis, M. J. Stevenson, H. S. Shafaat, *Chem. Commun.* **2018**, *54*, 4681–4684.
- [152] X. Liu, F. Kang, C. Hu, L. Wang, Z. Xu, D. Zheng, W. Gong, Y. Lu, Y. Ma, J. Wang, *Nat. Chem.* **2018**, *10*, 1201–1206.
- [153] M. F. Kuehnel, K. L. Orchard, K. E. Dalle, E. Reisner, *J. Am. Chem. Soc.* **2017**, *139*, 7217–7223.
- [154] R. Alcalá-Torano, N. Halloran, N. Gwerder, D. J. Sommer, G. Ghirlanda, *Front. Mol. Biosci.* **2021**, *8*, 17.
- [155] Z. Li, Y. Zhao, P. Wu, H. Wang, Q. Li, J. Gao, H.-M. Qin, H. Wei, U. T. Bornscheuer, X. Han, R. Wei, W. Liu, *Biochem. Biophys. Res. Commun.* **2022**, *626*, 100–106.
- [156] G. von Haugwitz, X. Han, L. Pfaff, Q. Li, H. Wei, J. Gao, K. Methling, Y. Ao, Y. Brack, J. Mican, C. G. Feiler, M. S. Weiss, D. Bednar, G. J. Palm, M. Lalk, M. Lammers, J. Damborsky, G. Weber, W. Liu, U. T. Bornscheuer, R. Wei, *ACS Catal.* **2022**, 15259–15270.

- [157] S. V. Athavale, K. Chen, F. H. Arnold, in *Transition Metal-Catalyzed Carbene Transformations*, John Wiley & Sons, Ltd, **2022**, pp. 95–138.
- [158] A. Cvetkovic, A. L. Menon, M. P. Thorgersen, J. W. Scott, F. L. Poole II, F. E. Jenney Jr, W. A. Lancaster, J. L. Praissman, S. Shanmukh, B. J. Vaccaro, S. A. Trauger, E. Kalisiak, J. V. Apon, G. Siuzdak, S. M. Yannoni, J. A. Tainer, M. W. W. Adams, *Nature* **2010**, *466*, 779–782.
- [159] S. M. Yannoni, S. Hartung, A. L. Menon, M. W. Adams, J. A. Tainer, *Curr. Opin. Biotechnol.* **2012**, *23*, 89–95.
- [160] P. Dydio, H. M. Key, A. Nazarenko, J. Y.-E. Rha, V. Seyedkazemi, D. S. Clark, J. F. Hartwig, *Science* **2016**, *354*, 102–106.
- [161] C. Van Stappen, Y. Deng, Y. Liu, H. Heidari, J.-X. Wang, Y. Zhou, A. P. Ledray, Y. Lu, *Chem. Rev.* **2022**, *122*, 11974–12045.
- [162] G. Sreenilayam, E. J. Moore, V. Steck, R. Fasan, *Adv. Synth. Catal.* **2017**, *359*, 2076–2089.
- [163] H. M. Key, P. Dydio, D. S. Clark, J. F. Hartwig, *Nature* **2016**, *534*, 534–537.
- [164] H. M. Key, P. Dydio, Z. Liu, J. Y.-E. Rha, A. Nazarenko, V. Seyedkazemi, D. S. Clark, J. F. Hartwig, *ACS Cent. Sci.* **2017**, *3*, 302–308.
- [165] G. Sreenilayam, E. J. Moore, V. Steck, R. Fasan, *ACS Catal.* **2017**, *7*, 7629–7633.
- [166] K. Oohora, H. Meichin, L. Zhao, M. W. Wolf, A. Nakayama, J. Hasegawa, N. Lehnert, T. Hayashi, *J. Am. Chem. Soc.* **2017**, *139*, 17265–17268.
- [167] M. W. Wolf, D. A. Vargas, N. Lehnert, *Inorg. Chem.* **2017**, *56*, 5623–5635.
- [168] M. Bordeaux, V. Tyagi, R. Fasan, *Angew. Chem. Int. Ed.* **2015**, *54*, 1744–1748.
- [169] S. Huang, W.-H. Deng, R.-Z. Liao, C. He, *ACS Catal.* **2022**, *12*, 13725–13731.
- [170] D. M. Carminati, R. Fasan, *ACS Catal.* **2019**, *9*, 9683–9697.
- [171] A. Tinoco, Y. Wei, J.-P. Bacik, D. M. Carminati, E. J. Moore, N. Ando, Y. Zhang, R. Fasan, *ACS Catal.* **2019**, *9*, 1514–1524.
- [172] A. L. Chandgude, X. Ren, R. Fasan, *J. Am. Chem. Soc.* **2019**, *141*, 9145–9150.
- [173] T. D. Rapson, H. Ju, P. Marshall, R. Devilla, C. J. Jackson, S. Giddey, T. D. Sutherland, *Sci. Rep.* **2020**, *10*, 3774.
- [174] S. Hirota, Y.-W. Lin, *JBIC J. Biol. Inorg. Chem.* **2018**, *23*, 7–25.
- [175] F. Schwizer, Y. Okamoto, T. Heinisch, Y. Gu, M. M. Pellizzoni, V. Lebrun, R. Reuter, V. Köhler, J. C. Lewis, T. R. Ward, *Chem. Rev.* **2018**, *118*, 142–231.
- [176] H. J. Davis, T. R. Ward, *ACS Cent. Sci.* **2019**, *5*, 1120–1136.
- [177] H. Kries, R. Blomberg, D. Hilvert, *Curr. Opin. Chem. Biol.* **2013**, *17*, 221–228.
- [178] M. R. Ghadiri, C. Soares, C. Choi, *J. Am. Chem. Soc.* **1992**, *114*, 4000–4002.
- [179] S. Basler, S. Studer, Y. Zou, T. Mori, Y. Ota, A. Camus, H. A. Bunzel, R. C. Helgeson, K. N. Houk, G. Jiménez-Osés, D. Hilvert, *Nat. Chem.* **2021**, *13*, 231–235.
- [180] M. J. Chalkley, S. I. Mann, W. F. DeGrado, *Nat. Rev. Chem.* **2022**, *6*, 31–50.
- [181] J. R. Desjarlais, T. M. Handel, *Protein Sci.* **1995**, *4*, 2006–2018.
- [182] P.-S. Huang, S. E. Boyken, D. Baker, *Nature* **2016**, *537*, 320–327.

- [183] A. Lombardi, F. Pirro, O. Maglio, M. Chino, W. F. DeGrado, *Acc. Chem. Res.* **2019**, *52*, 1148–1159.
- [184] F. Pirro, S. La Gatta, F. Arrigoni, A. Famulari, O. Maglio, P. Del Vecchio, M. Chiesa, L. De Gioia, L. Bertini, M. Chino, F. Nastri, A. Lombardi, *Angew. Chem. Int. Ed.* **2023**, *135*, e202211552.
- [185] M. Chino, O. Maglio, F. Nastri, V. Pavone, W. F. DeGrado, A. Lombardi, *Eur. J. Inorg. Chem.* **2015**, *2015*, 3371–3390.
- [186] M. Faiella, C. Andreatti, R. T. M. de Rosales, V. Pavone, O. Maglio, F. Nastri, W. F. DeGrado, A. Lombardi, *Nat. Chem. Biol.* **2009**, *5*, 882–884.
- [187] M. Chino, L. Leone, O. Maglio, D. D'Alonzo, F. Pirro, V. Pavone, F. Nastri, A. Lombardi, *Angew. Chem. Int. Ed.* **2017**, *56*, 15580–15583.
- [188] T. Heinisch, T. R. Ward, *Acc. Chem. Res.* **2016**, *49*, 1711–1721.
- [189] J. Serrano-Plana, C. Rumo, J. G. Rebelein, R. L. Peterson, M. Barnet, T. R. Ward, *J. Am. Chem. Soc.* **2020**, *142*, 10617–10623.
- [190] S. Wu, Y. Zhou, J. G. Rebelein, M. Kuhn, H. Mallin, J. Zhao, N. V. Igareta, T. R. Ward, *J. Am. Chem. Soc.* **2019**, *141*, 15869–15878.
- [191] A. Kajetanowicz, A. Chatterjee, R. Reuter, T. R. Ward, *Catal. Lett.* **2014**, *144*, 373–379.
- [192] J. Bos, W. R. Browne, A. J. M. Driessen, G. Roelfes, *J. Am. Chem. Soc.* **2015**, *137*, 9796–9799.
- [193] J. Bos, F. Fusetti, A. J. M. Driessen, G. Roelfes, *Angew. Chem. Int. Ed.* **2012**, *51*, 7472–7475.
- [194] G. Roelfes, *Acc. Chem. Res.* **2019**, *52*, 545–556.
- [195] J. Bos, A. García-Herraiz, G. Roelfes, *Chem. Sci.* **2013**, *4*, 3578–3582.
- [196] C. Mayer, D. G. Gillingham, T. R. Ward, D. Hilvert, *Chem. Commun.* **2011**, *47*, 12068–12070.
- [197] E. N. Mirts, A. Bhagi-Damodaran, Y. Lu, *Acc. Chem. Res.* **2019**, *52*, 935–944.
- [198] A. Stein, A. D. Liang, R. Sahin, T. R. Ward, *J. Organomet. Chem.* **2022**, *962*, 122272.
- [199] P. J. Deuss, G. Popa, A. M. Z. Slawin, W. Laan, P. C. J. Kamer, *ChemCatChem* **2013**, *5*, 1184–1191.
- [200] A. Thiel, D. F. Sauer, U. Markel, M. A. Stephanie Mertens, T. Polen, U. Schwaneberg, J. Okuda, *Org. Biomol. Chem.* **2021**, *19*, 2912–2916.
- [201] U. Markel, D. F. Sauer, J. Schiffels, J. Okuda, U. Schwaneberg, *Angew. Chem. Int. Ed.* **2019**, *58*, 4454–4464.
- [202] C. Jatmika, K. Wakabayashi, R. Tamaki, N. Akiyama, I. Nakamura, S. Hirota, H. Yamaguchi, T. Matsuo, *Chem. Lett.* **2020**, *49*, 1490–1493.
- [203] G. T. Hermanson, in *Bioconjugate Techniques (Third Edition)*, Academic Press, Boston, **2013**, pp. 229–258.
- [204] D. M. Carminati, E. J. Moore, R. Fasan, in *Methods in Enzymology*, Academic Press, **2020**, pp. 35–61.
- [205] M. Diéguez, J.-E. Bäckvall, O. Pàmies, *Artificial Metalloenzymes and MetalloDNazymes in Catalysis: From Design to Applications*, John Wiley & Sons, **2018**.
- [206] T. Heinisch, F. Schwizer, B. Garabedian, E. Csibra, M. Jeschek, J. Vallapurackal, V. B. Pinheiro, P. Marlière, S. Panke, T. R. Ward, *Chem. Sci.* **2018**, *9*, 5383–5388.
- [207] J. G. Rebelein, Y. Cotellet, B. Garabedian, T. R. Ward, *ACS Catal.* **2019**, *9*, 4173–4178.

- [208] S. Kato, A. Onoda, A. R. Grimm, U. Schwaneberg, T. Hayashi, *J. Inorg. Biochem.* **2021**, *216*, 111352.
- [209] R. M. Quinta Ferreira, C. A. Almeida-Costa, A. E. Rodrigues, *Ind. Eng. Chem. Res.* **1996**, *35*, 3827–3841.
- [210] L.-M. Tau, B. H. Davis, *Appl. Catal.* **1989**, *53*, 263–271.
- [211] G. M. Coppola, *Synthesis* **1984**, *1984*, 1021–1023.
- [212] R. Reddy Kuchukulla, F. Li, Z. He, L. Zhou, Q. Zeng, *Green Chem.* **2019**, *21*, 5808–5812.
- [213] A. Lahyani, M. Chtourou, M. H. Frikha, M. Trabelsi, *Ultrason. Sonochem.* **2013**, *20*, 1296–1301.
- [214] P. F. Siril, H. E. Cross, D. R. Brown, *J. Mol. Catal. Chem.* **2008**, *279*, 63–68.
- [215] G. Busca, *Chem. Rev.* **2007**, *107*, 5366–5410.
- [216] R. Thornton, B. C. Gates, *J. Catal.* **1974**, *34*, 275–287.
- [217] V. C. Malshe, E. S. Sujatha, *React. Funct. Polym.* **1997**, *35*, 159–168.
- [218] K. Hult, P. Berglund, *Trends Biotechnol.* **2007**, *25*, 231–238.
- [219] U. T. Bornscheuer, R. J. Kazlauskas, in *Enzyme Catalysis in Organic Synthesis*, John Wiley & Sons, Ltd, **2012**, pp. 1693–1733.
- [220] D. H. G. Crout, H. Dalton, D. W. Hutchinson, M. Miyagoshi, *J. Chem. Soc. Perkin 1* **1991**, 1329–1334.
- [221] H. Sahm, *Biocatalysis* **1988**, *1*, 321–331.
- [222] K. Okrasa, R. J. Kazlauskas, *Chem. – Eur. J.* **2006**, *12*, 1587–1596.
- [223] U. T. Bornscheuer, R. J. Kazlauskas, *Angew. Chem. Int. Ed.* **2004**, *43*, 6032–6040.
- [224] M. S. Humble, P. Berglund, *Eur. J. Org. Chem.* **2011**, *2011*, 3391–3401.
- [225] A. Aharoni, L. Gaidukov, O. Khersonsky, S. M. Gould, C. Roodveldt, D. S. Tawfik, *Nat. Genet.* **2005**, *37*, 73–76.
- [226] I. Nobeli, A. D. Favia, J. M. Thornton, *Nat. Biotechnol.* **2009**, *27*, 157–167.
- [227] L. Santamaría, I. Reverón, F. López de Felipe, B. de las Rivas, R. Muñoz, *Appl. Environ. Microbiol.* **2018**, *84*, e01123-18.
- [228] T. M. Lowe, F. Ailloud, C. Allen, *Mol. Plant. Microbe Interact.* **2015**, *28*, 286–297.
- [229] T. Campillo, S. Renoud, I. Kerzaon, L. Vial, J. Baude, V. Gaillard, F. Bellvert, C. Chamignon, G. Comte, X. Nesme, C. Lavire, F. Hommais, *Appl. Environ. Microbiol.* **2014**, *80*, 3341–3349.
- [230] H. Rodríguez, J. A. Curiel, J. M. Landete, B. de las Rivas, F. L. de Felipe, C. Gómez-Cordovés, J. M. Mancheño, R. Muñoz, *Int. J. Food Microbiol.* **2009**, *132*, 79–90.
- [231] R. Kourist, A. Schweiger, H. Büchsenschütz, in *Lipid Modification by Enzymes and Engineered Microbes*, AOCS Press, **2018**, pp. 89–118.
- [232] Y. Hashidoko, S. Tahara, *Arch. Biochem. Biophys.* **1998**, *359*, 225–230.
- [233] H. Hu, L. Li, S. Ding, *Appl. Microbiol. Biotechnol.* **2015**, *99*, 5071–5081.
- [234] S. Gao, H.-N. Yu, Y.-F. Wu, X.-Y. Liu, A.-X. Cheng, H.-X. Lou, *Biochem. Biophys. Res. Commun.* **2016**, *481*, 239–244.
- [235] J. M. Landete, H. Rodríguez, J. A. Curiel, B. de las Rivas, J. M. Mancheño, R. Muñoz, *J. Ind. Microbiol. Biotechnol.* **2010**, *37*, 617–624.
- [236] W. Gu, J. Yang, Z. Lou, L. Liang, Y. Sun, J. Huang, X. Li, Y. Cao, Z. Meng, K.-Q. Zhang, *PLoS ONE* **2011**, *6*, e16262.
- [237] G. Degrassi, P. Polverino De Laureto, C. V. Bruschi, *Appl. Environ. Microbiol.* **1995**, *61*, 326–332.
- [238] L. Li, L. Long, S. Ding, *Front. Microbiol.* **2019**, *10*, 1798.

- [239] J. Ni, Y.-T. Wu, F. Tao, Y. Peng, P. Xu, *J. Am. Chem. Soc.* **2018**, *140*, 16001–16005.
- [240] K. L. Morley, S. Grosse, H. Leisch, P. C. K. Lau, *Green Chem.* **2013**, *15*, 3312.
- [241] D.-H. Jung, W. Choi, K.-Y. Choi, E. Jung, H. Yun, R. J. Kazlauskas, B.-G. Kim, *Appl. Microbiol. Biotechnol.* **2013**, *97*, 1501–1511.
- [242] J. Cavin, *FEMS Microbiol. Lett.* **1997**, *147*, 291–295.
- [243] J. F. Cavin, V. Dartois, C. Diviès, *Appl. Environ. Microbiol.* **1998**, *64*, 1466–1471.
- [244] S. van Beek, F. G. Priest, *Appl. Environ. Microbiol.* **2000**, *66*, 5322–5328.
- [245] S. Mathew, T. E. Abraham, S. Sudheesh, *J. Mol. Catal. B Enzym.* **2007**, *44*, 48–52.
- [246] J. M. Salgado, R. Rodríguez-Solana, J. A. Curiel, B. de las Rivas, R. Muñoz, J. M. Domínguez, *Bioresour. Technol.* **2012**, *117*, 274–285.
- [247] L.-H. Sun, S.-W. Lv, F. Yu, S.-N. Li, L.-Y. He, *J. Biotechnol.* **2018**, *281*, 144–149.
- [248] A. Frank, W. Eborall, R. Hyde, S. Hart, J. P. Turkenburg, G. Grogan, *Catal. Sci. Technol.* **2012**, *2*, 1568.
- [249] X. Sheng, M. E. S. Lind, F. Himo, *FEBS J.* **2015**, *282*, 4703–4713.
- [250] C. Wuensch, S. M. Glueck, J. Gross, D. Koszelewski, M. Schober, K. Faber, *Org. Lett.* **2012**, *14*, 1974–1977.
- [251] C. Wuensch, J. Gross, G. Steinkellner, K. Gruber, S. M. Glueck, K. Faber, *Angew. Chem. Int. Ed.* **2013**, *52*, 2293–2297.
- [252] C. Wuensch, T. Pavkov-Keller, G. Steinkellner, J. Gross, M. Fuchs, A. Hromic, A. Lyskowski, K. Fauland, K. Gruber, S. M. Glueck, K. Faber, *Adv. Synth. Catal.* **2015**, *357*, 1909–1918.
- [253] X. Sheng, F. Himo, *ACS Catal.* **2017**, *7*, 1733–1741.
- [254] U. T. Bornscheuer, R. J. Kazlauskas, *Hydrolases in Organic Synthesis: Regio- and Stereoselective Biotransformations*, John Wiley & Sons, **2006**.
- [255] E. L. Bell, W. Finnigan, S. P. France, A. P. Green, M. A. Hayes, L. J. Hepworth, S. L. Lovelock, H. Niikura, S. Osuna, E. Romero, K. S. Ryan, N. J. Turner, S. L. Flitsch, *Nat. Rev. Methods Primer* **2021**, *1*, 1–21.
- [256] S. Wu, R. Snajdrova, J. C. Moore, K. Baldenius, U. T. Bornscheuer, *Angew. Chem. Int. Ed.* **2021**, *60*, 88–119.
- [257] S. Zeng, J. Liu, S. Anankanbil, M. Chen, Z. Guo, J. P. Adams, R. Snajdrova, Z. Li, *ACS Catal.* **2018**, *8*, 8856–8865.
- [258] L. Mestrom, J. G. R. Claessen, U. Hanefeld, *ChemCatChem* **2019**, *11*, 2004–2010.
- [259] J. Müller, M. A. Sowa, M. Dörr, U. T. Bornscheuer, *Eur. J. Lipid Sci. Technol.* **2015**, *117*, 1903–1907.
- [260] J. Müller, M. A. Sowa, B. Fredrich, H. Brundiek, U. T. Bornscheuer, *ChemBioChem* **2015**, *16*, 1791–1796.
- [261] A.-H. Jan, E. Dubreucq, J. Drone, M. Subileau, *Biochim. Biophys. Acta - Proteins Proteom.* **2017**, *1865*, 1105–1113.
- [262] A. Riaublanc, R. Ratomahenina, P. Galzy, M. Nicolas, *J. Am. Oil Chem. Soc.* **1993**, *70*, 497–500.
- [263] Y. Lv, S. Sun, J. Liu, *ACS Omega* **2019**, *4*, 20064–20071.
- [264] I. Mathews, M. Soltis, M. Saldajeno, G. Ganshaw, R. Sala, W. Weyler, M. A. Cervin, G. Whited, R. Bott, *Biochemistry* **2007**, *46*, 8969–8979.
- [265] D. Prat, J. Hayler, A. Wells, *Green Chem.* **2014**, *16*, 4546–4551.

- [266] C. Elend, C. Schmeisser, C. Leggewie, P. Babiak, J. D. Carballeira, H. L. Steele, J.-L. Reymond, K.-E. Jaeger, W. R. Streit, *Appl. Environ. Microbiol.* **2006**, *72*, 3637–3645.
- [267] S. P. Godehard, H. Müller, C. P. S. Badenhorst, C. Stanetty, C. Suster, M. D. Mihovilovic, U. T. Bornscheuer, *ACS Catal.* **2021**, *11*, 2831–2836.
- [268] H. Land, P. Hendil-Forsell, M. Martinelle, P. Berglund, *Catal. Sci. Technol.* **2016**, *6*, 2897–2900.
- [269] I. C. Perdomo, S. Gianolio, A. Pinto, D. Romano, M. L. Contente, F. Paradisi, F. Molinari, *J. Agric. Food Chem.* **2019**, *67*, 6517–6522.
- [270] M. L. Contente, S. Farris, L. Tamborini, F. Molinari, F. Paradisi, *Green Chem.* **2019**, *21*, 3263–3266.
- [271] F. Annunziata, M. L. Contente, C. Pinna, L. Tamborini, A. Pinto, *Antioxidants* **2021**, *10*, 1142.
- [272] M. L. Contente, D. Roura Padrosa, F. Molinari, F. Paradisi, *Nat. Catal.* **2020**, *3*, 1020–1026.
- [273] M. Kazemi, X. Sheng, W. Kroutil, F. Himo, *ACS Catal.* **2018**, *8*, 10698–10706.
- [274] E. Jost, M. Kazemi, V. Mrkonjić, F. Himo, C. K. Winkler, W. Kroutil, *ACS Catal.* **2020**, *10*, 10500–10507.
- [275] S. P. Godehard, C. P. S. Badenhorst, H. Müller, U. T. Bornscheuer, *ACS Catal.* **2020**, *10*, 7552–7562.
- [276] H. Müller, A.-K. Becker, G. J. Palm, L. Berndt, C. P. S. Badenhorst, S. P. Godehard, L. Reisky, M. Lammers, U. T. Bornscheuer, *Angew. Chem. Int. Ed.* **2020**, *59*, 11607–11612.
- [277] G. J. Palm, E. Fernández-Álvaro, X. Bogdanović, S. Bartsch, J. Sczodrok, R. K. Singh, D. Böttcher, H. Atomi, U. T. Bornscheuer, W. Hinrichs, *Appl. Microbiol. Biotechnol.* **2011**, *91*, 1061–1072.
- [278] T. D. Kim, *J. Microbiol. Biotechnol.* **2017**, *27*, 1907–1915.
- [279] Y. Hotta, S. Ezaki, H. Atomi, T. Imanaka, *Appl. Environ. Microbiol.* **2002**, *68*, 3925–3931.
- [280] S. Hari Krishna, M. Persson, U. T. Bornscheuer, *Tetrahedron Asymmetry* **2002**, *13*, 2693–2696.
- [281] A. Rosas-Hernández, C. Steinlechner, H. Junge, M. Beller, *Green Chem.* **2017**, *19*, 2356–2360.
- [282] M. Musil, J. Stourac, J. Bendl, J. Brezovsky, Z. Prokop, J. Zendulka, T. Martinek, D. Bednar, J. Damborsky, *Nucleic Acids Res.* **2017**, *45*, W393–W399.
- [283] C. C. Page, C. C. Moser, X. Chen, P. L. Dutton, *Nature* **1999**, *402*, 47–52.
- [284] C. Shih, A. K. Museth, M. Abrahamsson, A. M. Blanco-Rodriguez, A. J. Di Bilio, J. Sudhamsu, B. R. Crane, K. L. Ronayne, M. Towrie, A. Vlček, J. H. Richards, J. R. Winkler, H. B. Gray, *Science* **2008**, *320*, 1760–1762.
- [285] C. Shipps, H. R. Kelly, P. J. Dahl, S. M. Yi, D. Vu, D. Boyer, C. Glynn, M. R. Sawaya, D. Eisenberg, V. S. Batista, N. S. Malvankar, *Proc. Natl. Acad. Sci.* **2021**, *118*, e2014139118.
- [286] F. Schmitzberger, M. L. Kilkeny, C. M. C. Loble, M. E. Webb, M. Vinkovic, D. Matak-Vinkovic, M. Witty, D. Y. Chirgadze, A. G. Smith, C. Abell, T. L. Blundell, *EMBO J.* **2003**, *22*, 6193–6204.
- [287] M. Cheng, H. Yoshiyasu, K. Okano, H. Ohtake, K. Honda, *PLOS ONE* **2016**, *11*, e0146146.

- [288] R. Saito, T. Sato, A. Ikai, N. Tanaka, *Acta Crystallogr. D Biol. Crystallogr.* **2004**, *60*, 792–795.
- [289] K. A. P. Payne, M. D. White, K. Fisher, B. Khara, S. S. Bailey, D. Parker, N. J. W. Rattray, D. K. Trivedi, R. Goodacre, R. Beveridge, P. Barran, S. E. J. Rigby, N. S. Scrutton, S. Hay, D. Leys, *Nature* **2015**, *522*, 497–501.
- [290] G. G. Barclay, C. J. Hawker, H. Ito, A. Orellana, P. R. L. Malenfant, R. F. Sinta, *Macromolecules* **1998**, *31*, 1024–1031.
- [291] J. van Schijndel, D. Molendijk, K. van Beurden, L. A. Canalle, T. Noël, J. Meuldijk, *Eur. Polym. J.* **2020**, *125*, 109534.
- [292] L. Li, L. Long, S. Ding, *ACS Sustain. Chem. Eng.* **2020**, *8*, 14732–14742.
- [293] S. Noda, Y. Kawai, T. Tanaka, A. Kondo, *Bioresour. Technol.* **2015**, *180*, 59–65.
- [294] J. J. Williamson, N. Bahrin, E. M. Hardiman, T. D. H. Bugg, *Biotechnol. J.* **2020**, *15*, 1900571.
- [295] L. Barthelmebs, C. Diviès, J.-F. Cavin, *Appl. Environ. Microbiol.* **2001**, *67*, 1063–1069.
- [296] M. Finnveden, S. Semlitsch, O. He, M. Martinelle, *Catal. Sci. Technol.* **2019**, *9*, 4920–4927.
- [297] N. de Leeuw, G. Torrelo, C. Bisterfeld, V. Resch, L. Mestrom, E. Straulino, L. van der Weel, U. Hanefeld, *Adv. Synth. Catal.* **2018**, *360*, 242–249.
- [298] W. M. Fitch, *J. Biol. Chem.* **1964**, *239*, 1328–1334.
- [299] R. Willstätter, A. Stoll, *Justus Liebigs Ann. Chem.* **1911**, *378*, 18–72.
- [300] L. Reisky, V. S. T. Srinivasamurthy, C. P. S. Badenhorst, S. P. Godehard, U. T. Bornscheuer, *Catalysts* **2019**, *9*, 64.
- [301] H. Müller, S. P. Godehard, G. J. Palm, L. Berndt, C. P. S. Badenhorst, A.-K. Becker, M. Lammers, U. T. Bornscheuer, *Angew. Chem. Int. Ed.* **2021**, *60*, 2013–2017.
- [302] T. H. Yeats, L. B. B. Martin, H. M.-F. Viart, T. Isaacson, Y. He, L. Zhao, A. J. Matas, G. J. Buda, D. S. Domozych, M. H. Clausen, J. K. C. Rose, *Nat. Chem. Biol.* **2012**, *8*, 609–611.
- [303] W. Koeller, P. E. Kolattukudy, *Biochemistry* **1982**, *21*, 3083–3090.
- [304] M. Subileau, A.-H. Jan, H. Nozac'h, M. Pérez-Gordo, V. Perrier, E. Dubreucq, *Biochim. Biophys. Acta - Proteins Proteom.* **2015**, *1854*, 1400–1411.
- [305] Y. Jiang, K. L. Morley, J. D. Schrag, R. J. Kazlauskas, *ChemBioChem* **2011**, *12*, 768–776.
- [306] C. S. Jones, D. Sychantha, P. L. Howell, A. J. Clarke, *J. Biol. Chem.* **2020**, *295*, 8204–8213.
- [307] J. Rodrigues, V. Perrier, J. Lecomte, E. Dubreucq, S. Ferreira-Dias, *Bioresour. Technol.* **2016**, *218*, 1224–1229.
- [308] R. Okachi, Y. Hashimoto, M. Kawamori, R. Katsumata, K. Takayama, T. Nara, in *Enzyme Eng.* (Eds.: I. Chibata, S. Fukui, L.B. Wingard), Springer US, Boston, MA, **1982**, pp. 81–90.
- [309] M. L. Contente, L. Tamborini, F. Molinari, F. Paradisi, *J. Flow Chem.* **2020**, *10*, 235–240.
- [310] H. Müller, H. Terholsen, S. P. Godehard, C. P. S. Badenhorst, U. T. Bornscheuer, *ACS Catal.* **2021**, *11*, 14906–14915.
- [311] Y. Liang, X. Lu, *J. Biol. Chem.* **2020**, *295*, 1047–1055.
- [312] Y. Zhang, L. Ding, Z. Yan, D. Zhou, J. Jiang, J. Qiu, Z. Xin, *Appl. Biochem. Biotechnol.* **2021**, DOI 10.1007/s12010-021-03614-9.

- [313] K. P. Solanki, M. A. Desai, J. K. Parikh, *Chem. Pap.* **2020**, *74*, 145–156.
- [314] A. Lapczynski, S. P. Bhatia, C. S. Letizia, A. M. Api, *Food Chem. Toxicol.* **2008**, *46*, 103-109.
- [315] K. Bauer, D. Garbe, H. Surburg, *Common Fragrance and Flavor Materials: Preparation, Properties and Uses*, John Wiley & Sons, **2008**.
- [316] S. A. Elsharif, A. Buettner, *J. Agric. Food Chem.* **2018**, *66*, 2324–2333.
- [317] S. A. Elsharif, A. Banerjee, A. Buettner, *Front. Chem.* **2015**, *3*.
- [318] L. M. Reguengo, M. K. Salgaço, K. Sivieri, M. R. Maróstica Júnior, *Food Res. Int.* **2022**, *152*, 110871.
- [319] H. Terholsen, J. Kaur, N. Kaloudis, A. Staudt, H. Müller, I. V. Pavlidis, U. T. Bornscheuer, *ChemBioChem* **2022**, *23*, e202200254.
- [320] E. López-Huertas, J. Lozano-Sánchez, A. Segura-Carretero, *Food Chem.* **2021**, *342*, 128291.
- [321] M. A. Nunes, F. B. Pimentel, A. S. G. Costa, R. C. Alves, M. B. P. P. Oliveira, *Innov. Food Sci. Emerg. Technol.* **2016**, *35*, 139–148.
- [322] E. Vierhuis, M. Servili, M. Baldioli, H. A. Schols, A. G. J. Voragen, Montedoro, *J. Agric. Food Chem.* **2001**, *49*, 1218–1223.
- [323] A. V. Chatzikonstantinou, E. Gkantzou, E. Thomou, N. Chalmpes, K.-M. Lyra, V. G. Kontogianni, K. Spyrou, M. Patila, D. Gournis, H. Stamatis, *Nanomaterials* **2019**, *9*, 1166.
- [324] H. Terholsen, J. Kaur, N. Kaloudis, A. Staudt, I. V. Pavlidis, U. T. Bornscheuer, *Chem. Ing. Tech.* **2022**, *94*, 1860–1863.
- [325] R. De la Torre, D. Corella, O. Castañer, M. A. Martínez-González, J. Salas-Salvador, J. Vila, R. Estruch, J. V. Sorli, F. Arós, M. Fiol, E. Ros, L. Serra-Majem, X. Pintó, E. Gómez-Gracia, J. Lapetra, M. Ruiz-Canela, J. Basora, E. M. Asensio, M. I. Covas, M. Fitó, *Am. J. Clin. Nutr.* **2017**, *105*, 1297–1304.
- [326] R. Mateos, L. Goya, L. Bravo, *J. Agric. Food Chem.* **2005**, *53*, 9897–9905.
- [327] R. Mateos, G. Pereira-Caro, S. Saha, R. Cert, M. Redondo-Horcajo, L. Bravo, P. A. Kroon, *Food Chem.* **2011**, *125*, 865–872.
- [328] R. Bernini, E. Mincione, M. Barontini, F. Crisante, *J. Agric. Food Chem.* **2008**, *56*, 8897–8904.
- [329] K. A. Heyries, C. A. Marquette, L. J. Blum, *Langmuir* **2007**, *23*, 4523–4527.

5. Author Contributions

Article I **Photo-enzymatic Catalytic CO₂ Reduction Using a Promiscuous Decarboxylase as Protein Scaffold**

Henrik Terholsen*, Hilario Diego Huerta-Zerón*, Christina Möller, Henrik Junge, Uwe T. Bornscheuer, Matthias Beller

Nature Catal., submitted

**equal contribution*

U.T.B, H.J., H.D.H.-Z., and H.T. conceived the project. H.T. selected, engineered, and expressed most proteins investigated. C.M. created and expressed some mutants of BsPAD. H.D.H.-Z. performed all CO₂ reduction experiments. U.T.B and M.B. directed the project. H.D.H.-Z. and H.T. created the manuscript to which all authors contributed. H.D.H.-Z. and H.T. share the first authorship.

Article II **Spectrophotometric and Fluorimetric High-Throughput Assays for Phenolic Acid Decarboxylase**

Henrik Terholsen*, Kamela Myrtiollari*, Mirna Larva, Christina Möller, Robert Kourist, Uwe T. Bornscheuer, Daniel Kracher

Manuscript in preparation

**equal contribution*

D.K. and H.T. conceived the project. H.T., C.M., M.L., K.M., and D.K. performed most experiments. C.M. expressed BsPAD. U.T.B., R.K., and D.K. directed the project. D.K. and H.T. created the manuscript to which all authors contributed. K.M. and H.T. share the first authorship.

Article III **Recent Insights and Future Perspectives on Promiscuous Hydrolases/Acyltransferases**

Henrik Müller, Henrik Terholsen, Simon P. Godehard, Christoffel P.S. Badenhorst, and Uwe T. Bornscheuer

ASC Catal., 2021, 11, 14906–14915

U.T.B. and C.P.S.B. conceived the Perspective paper. H.M. developed the outline for the paper. H.M., C.P.S.B., and H.T. drafted the manuscript to which all authors contributed.

Article IV Rational Design for Enhanced Acyltransferase Activity in Water Catalyzed by the *Pyrobaculum calidifontis* VA1 Esterase

Amanda Staudt, [Henrik Terholsen](#), Jasmin Kaur, Henrik Müller, Simon P. Godehard,IVALDO Itabaiana Jr, Ivana C.R. Leal and Uwe T. Bornscheuer

Microorganisms, **2021**, *9*, 1790

U.T.B. and A.S. conceived the project; A.S. and H.T. equally designed the methodology and performed the investigation; J.K. performed the investigation; H.M. executed formal analysis; S.P.G. contributed to the methodology; I.I.J., I.C.R.L., and U.T.B. accomplished the funding; U.T.B. administered and supervised the project; A.S. and H.T. wrote the original draft that all authors contributed to. All authors have read and agreed to the published version of the manuscript.

Article V Recovery of Hydroxytyrosol from Olive Mill Wastewater using the Promiscuous Hydrolase/Acyltransferase PestE

[Henrik Terholsen](#), Jasmin Kaur, Nikolaos Kaloudis, Amanda Staudt, Henrik Müller, Ioannis V. Pavlidis, and Uwe T. Bornscheuer

ChemBioChem, **2022**, *23*, e202200254

H.T. conceived the project. H.T. and J.K. designed and performed most of the experiments. N.K. and I.V.P. organized the olive mill wastewater sampling. U.T.B. directed the project. H.T. created the manuscript to which all authors contributed.

Article VI An Enzyme Cascade Reaction for the Recovery of Hydroxytyrosol Derivatives from Olive Mill Wastewater

[Henrik Terholsen](#), Jasmin Kaur, Nikolaos Kaloudis, Amanda Staudt, Ioannis V. Pavlidis, and Uwe T. Bornscheuer

Chem. Ing. Tech. **2022**, *94*, 1860–1863

U.B. and H.T. conceived the project. H.T. designed and performed all experiments. N.K. and I.V.P. organized the olive mill wastewater sampling. U.T.B. directed the project. H.T. created the manuscript to which all authors contributed.

Article VII Chemoenzymatic Cascade Reaction for the Valorization of the Lignin Depolymerization Product G-C2-Dioxolane Phenol

Henrik Terholsen, Jule Ruth Heike Meyer, Zhenlei Zhang, Peter J. Deuss, and Uwe T. Bornscheuer

ChemSusChem, submitted

H.T. conceived the project. H.T. designed and J.R.H.M performed most of the experiments. Z.Z. and P.J.D. provided the G-C2-dioxolane phenol. U.T.B. directed the project. H.T. created the manuscript to which all authors contributed.

6. Articles

Article I

Photo-enzymatic catalytic CO₂ reduction using a promiscuous decarboxylase as protein scaffold

Henrik Terholsen^{1*}, Hilario Diego Huerta-Zerón^{2*}, Christina Möller¹, Henrik Junge^{2§}, Uwe Bornscheuer^{1§}, Matthias Beller^{2§}

¹Institute of Biochemistry, Department of Biotechnology and Enzyme Catalysis
University Greifswald
Felix-Hausdorff-Straße 4, 17487 Greifswald (Germany)
E-mail: uwe.bornscheuer@uni-greifswald.de

²Leibniz Institute for Catalysis e.V.
Albert-Einstein-Straße 29a, 18059 Rostock (Germany)
Email: matthias.beller@catalysis.de

*Equal contribution.

§Corresponding authors.

Abstract

The application of carbon dioxide and its derivatives e.g., carbonate, bicarbonate, which are so far widely seen as waste, is required to reach a circular carbon economy and minimize environmental issues. Currently many research efforts focus on new concepts for utilizations of such materials. To achieve these goals, photo-, electro-, thermal-, and biocatalysis are key tools to realize the desired transformations, especially in aqueous solution. Nevertheless, catalytic systems that operate efficiently in water are scarce. Here, we present a general concept for the identification of suitable and stable enzymes for CO₂ reduction based on structural analysis for potential carbon dioxide binding sites and subsequent mutation. Following this idea, we discovered that the wild-type of phenolic acid decarboxylase from *Bacillus subtilis* (BsPAD_WT) promotes the aqueous photocatalytic CO₂ reduction selectively to carbon monoxide in the presence of a ruthenium photosensitizer and sodium ascorbate. Crucial for this ability are a CO₂-binding pocket containing arginine and in close proximity redox active amino acids, e.g., tyrosine or tryptophane. By mutating the active site of BsPAD_WT, improved turnover numbers for CO generation up to 196 were achieved (BsPAD_WCP_W17A). Further investigations of the influence of mutations gained insights into the working mode showing that electron transfer occurs via multistep tunneling. The generality of this concept was then proven by using eight other decarboxylases containing CO₂-binding sites, which all showed the desired activity underlining that a range of proteins are capable of photocatalytic CO₂ reduction.

Introduction

An efficient and economic carbon valorization is a prerequisite for a circular carbon economy that includes reducing, reusing, and recycling¹. This is substantial for sustaining and improving human economy activity and life quality. In general, any carbon-containing materials are finally transformed into carbonates, bicarbonates, and carbon dioxide, which were so far only seen as waste. To realize the desired circular carbon economy, the application of the above-mentioned carbon sources is essential and can contribute to minimizing consumption of fossil resources and emission of pollutants².

In addition to the direct application of gaseous CO₂, less works focused on the utilization of bicarbonates and carbonates³. Thermal hydrogenations^{4,5} as well as electro-⁶ and photocatalytic reactions constitute the most viable options for reduction of carbon dioxide⁷⁻⁹. Valorization of the resulting C1 products (CO, HCO₂H, CH₃OH, CH₄) allows to produce carbon-neutral fuels and chemicals and thereby enable an anthropogenic carbon cycle¹⁰. Many research efforts were undertaken developing active photocatalytic systems containing either noble or base metal catalysts and/or photosensitizers to generate carbon monoxide¹¹, formates^{12,13}, methanol or methane¹⁴. Most of those transformations were performed in organic solvents like acetonitrile, dimethylformamide or *N*-methyl-2-pyrrolidone (NMP). However, from a sustainable and practical perspective, water-based systems are highly desired and offer the possibility to couple CO₂ reduction with water oxidation as a kind of artificial photosynthesis¹⁵⁻¹⁷. Low solubility of catalysts and photosensitizers is the major drawback for transferring known photocatalytic systems to aqueous media, although some progress has been made¹⁸. Among the few examples of successful photocatalytic carbon dioxide reduction in water, Sakai et al. reported the application of a ruthenium photosensitizer¹⁹ and, more recently, a copper photosensitizer²⁰ in combination with a water-soluble cobalt porphyrin complex and sodium ascorbate as sacrificial electron donor. Catalyst turnover numbers TON_{CO} of 926 and 2680, respectively, were obtained. Due to the comparable potentials of carbon dioxide reduction to CO ($E = -0.52$ V, pH = 7) or formate ($E = -0.61$ V, pH = 7) compared to proton reduction ($E = -0.41$ V, pH = 7), hydrogen formation is expected to take place as competing reaction, especially in aqueous solution (Figures 1a and b). Indeed, hydrogen generation was observed in the above-mentioned examples with catalyst TON_{H₂} of 197 and 820. Obviously, high selectivity for CO₂ reduction over hydrogen generation is an important parameter for any catalyst performance. To achieve a more chemoselective reaction of carbon dioxide in aqueous media an appropriate microenvironment with CO₂ binding sites in close proximity to a catalytic reduction center seems to be a promising concept^{9,21}. Although such well-defined 3D-structures can be found in enzymes, these have been studied only scarcely for photocatalytic carbon dioxide reduction. Advantageously, enzymes are stable in an aqueous environment and organic solvents which are commonly used in artificial systems for photocatalytic CO₂ reduction can be avoided. Among the few known examples, mainly enzymes with natural carbon dioxide reducing activity, such as carbon monoxide dehydrogenases (CODH) or formate dehydrogenases (FDH)²²⁻²⁴, have been proposed for photocatalytic CO₂ reduction (Figure 1c). FDH and CODH are both highly selective in their CO₂-reducing activity and yield formate and carbon monoxide, respectively²⁵. In these systems, electrons from the photocatalysts were used to regenerate redox cofactors such as NAD(P)H, which naturally provide electrons for CO₂ reduction, or to directly supply electrons to the proteins. For the latter concept, photosensitizer-semiconductor assemblies, such as metal oxide nanoparticles^{26,27}, cadmium sulfide nanocrystals²⁸, and titanium dioxide combined with silver nanoclusters²⁹ were used for carbon monoxide generation by CODH. Unfortunately, only anaerobic oxygen-sensitive Ni-Fe-CODHs are capable of catalyzing CO₂ reduction to CO³⁰, which substantially limits the potential applications of these enzymes in waste gas treatment or direct air capture and makes purification of them costly and their practical handling cumbersome³¹⁻³⁴. Although significant progress has recently been made in reducing the oxygen sensitivity of CODH-II from *Carboxydotherrmus hydrogenoformans*³⁵, modifying CODHs remains very limited, as even minor changes in CODH result in a complete loss of activity³⁶, hampering further development of these enzymes.

As an alternative to natural CO₂-reducing enzymes, proteins that originally do not have CO₂-reducing activity, such as azurin or the yellow fluorescent superfolder protein, were modified with photosensitizers (PS) such as [Ru^{II}(bpy)₃]²⁺ or (E)-4-(4-benzoylbenzylidene)-1,2-dimethyl-1H-imidazol-5(4H)-one and used for CO₂ reduction with an attached Ni catalyst³⁷⁻³⁹. These systems were typically run on nanomolar-scale and TONs for CO formation did not exceed 120. The high selectivity for CO

formation was mainly attributed to the applied Ni catalysts^{40,41}. Recently, Alcalá-Torano et al. developed another artificial metalloprotein (ArM) for CO₂ reduction to CO by replacing the heme unit of cytochrome b₅₆₂ by an artificial cobalt protoporphyrin IX cofactor using free [Ru^{II}(bpy)₃]²⁺ as PS⁴².

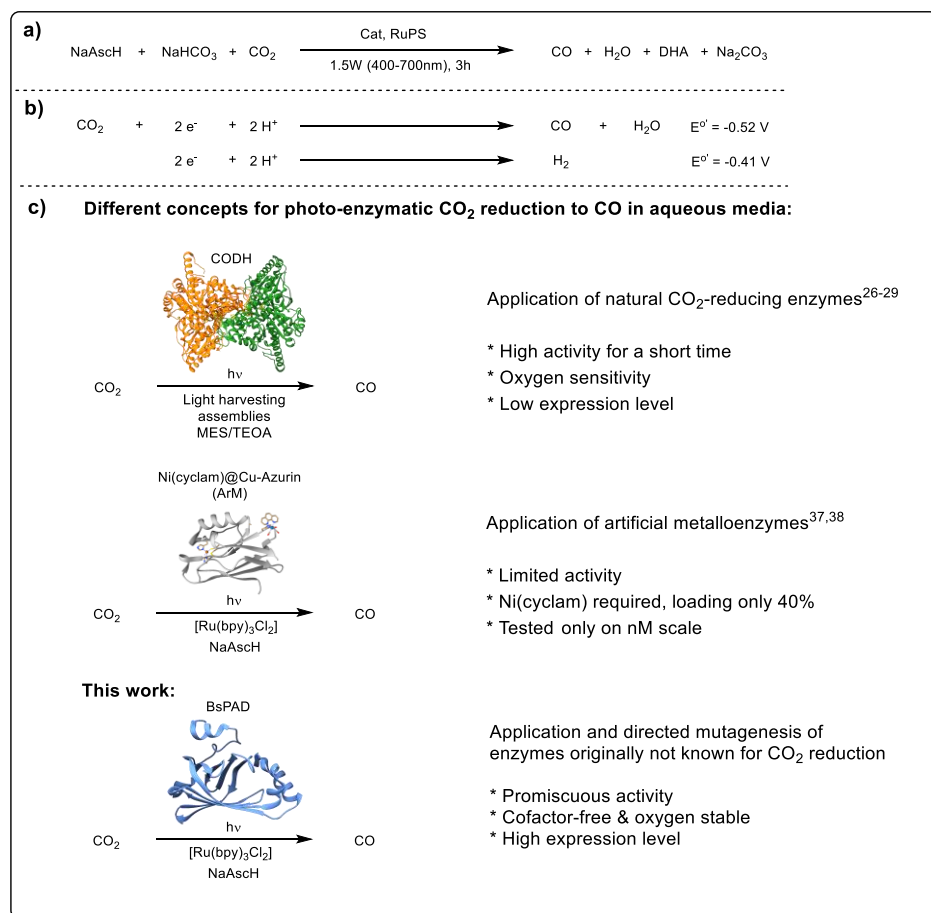


Fig. 1 Photocatalytic enzyme-based CO₂ reduction in aqueous media. **a**, General equation for photocatalytic CO₂ reduction to CO. **b**, Reduction potentials for competing reactions: Proton coupled carbon dioxide reduction to carbon monoxide and proton reduction. **c**, Different concepts for photo-enzymatic CO₂ reduction to CO in aqueous media: Selected examples from literature.

Although the selectivity and TONs were comparatively low, they proved that mutating amino acids in the first coordination sphere of the metal complex prevents competitive formation of hydrogen.

Inspired by these works, we here describe a metal-free enzyme with a well-defined reduction center and CO₂ binding pocket for efficient and selective photocatalytic carbon dioxide reduction in the presence of a common photosensitizer. Conceptually, we started our catalyst development with an enzyme not known for carbon dioxide reduction, which was further improved via site-directed mutagenesis. For this purpose, we chose phenolic acid decarboxylase from *Bacillus subtilis* (BsPAD) as the protein scaffold because of its high expressability in *E. coli* and stability as well as for having a well-defined CO₂-binding site and protein cavity⁴³⁻⁴⁵.

Results and discussion

In order to develop a carbon dioxide reduction system able to work under aqueous conditions we initially applied our previously reported photocatalytic system consisting of an iron cyclopentadienone Knölker type complex⁴⁶ in combination with a copper photosensitizer and 1,3-

dimethyl-2-phenyl-2,3-dihydro-1H-benzimidazole (BIH) as sacrificial electron donor. However, applying water and water-soluble Cu-PS-2 instead of NMP and CuPS-1 limited the overall productivity (TON = 12) and a very poor selectivity was obtained (Table S-2, entry 7) due to the low solubility of the sacrificial electron donor (BIH). Different approaches to overcome these problems were performed, e.g., application of phase transfer catalysts, different sacrificial donors (ascorbate, ascorbic acid or triethanolamine) resulting in limited success (Table S-2, entries 2-6). Finally, tests employing [Ru(bpy)₃Cl₂] as photosensitizer (PS) in combination with sodium ascorbate as sacrificial electron donor were performed, achieving improved turnover numbers (Table 1, entry 1), representing only less than 10% of the productivity obtained for the original system applying NMP as solvent. Notably, utilizing a lower ratio of PS to Fe-1 (20:1) only 12 turnovers for CO formation were obtained (Table 1, entry 7). Similarly, the ability of Fe-2 to promote the photocatalytic CO₂ reduction was proven both in NMP (Table S-3, entry 2; TON 118) as well as in water (Table 1, entries 2 and 8; TON 41 and 18).

Table 1. Carbon dioxide photocatalytic reduction in water							
Entry	Catalyst	PS (μM)	Cat/Enzyme (μM)	H ₂ (μmol)	CO (μmol)	Select. (%)	TON CO
1	Fe-1	500	5	0.71	1.95	73	38
2	Fe-2	500	5	0.35	2.05	85	41
3	BsPAD_WT	500	5	<0.32	1.80	85	36
4	BsPAD_WCP	500	5	0.48	2.25	82	44
5	BsPAD_WCP@Fe-2	500	5	0.39	1.84	82	37
6	–	500	–	0.33	0.98	75	0.1 ^a
7	Fe-1	100	5	0.44	0.63	59	12
8	Fe-2	100	5	0.85	0.9	51	18
9	BsPAD_WT	100	5	<0.32	1.47	82	29
10	BsPAD_WCP	100	5	<0.32	1.48	82	30
11	BsPAD_WCP@Fe-2	100	5	0.33	1.62	83	32
12	–	100	–	<0.32	0.33	51	0.3 ^a

Reaction conditions: 10 mL H₂O were used for all cases (Volume of headspace = 75 mL). [Ru(bpy)₃Cl₂] was employed as PS for all reactions. NaHCO₃ (0.1 M) and NaAsCh (0.05 M) were employed in all cases. The reaction mixtures were bubbled with carbon dioxide for 30 minutes prior to irradiation. Light output: 1.5W (400-700nm). Reaction time: 3 hours. TON CO calculated by nCO/nCat based on the amount of Ru-PS. To proof reproducibility of experiments exemplarily the experiments in entries 3, 6, 10 and 12 were performed at least twice. Standard deviations are 7-14% of the average for TON(CO) in enzyme-based reactions and up to 18% in the absence of enzyme as well as for selectivity in enzyme-based reactions 0.3 to 1% and up to 5% in the absence of enzyme, respectively.

After the activity of Fe-1 and Fe-2 in water were proven, the next step was to incorporate the latter complex into a protein scaffold with a carbon dioxide binding site. BsPAD was found to be a suitable scaffold as it is a well-characterized enzyme (2P8G) possessing a large nonpolar substrate binding pocket.^{43,44} Obviously, the Fe-based reduction catalyst should be incorporated into the substrate binding pocket in close proximity to the CO₂ binding pocket, which is expected enabling high selectivity against proton reduction due to shielding from the solvent. To achieve covalent binding to a cysteine residue of the protein, the complex Fe-1 was modified with a short linker and a maleimide group (Fe-2)⁴⁷. Since the BsPAD wild-type (BsPAD_WT) naturally has a cysteine (C100) that is not in the active site and therefore was not suitable for anchoring the metal complex, C100 was replaced by tryptophan (W). Additionally, a new cysteine was introduced at position 124 because this position has access to the active site but is not so close to it so that incorporation of Fe-2 would block the CO₂-binding site. Unfortunately, this mutation decreased protein stability and was recovered using the stabilizing mutation A147P suggested by the Fireprot onlinetool⁴⁸. The resulting BsPAD differs

from the WT in the mutations C100W, V124C, and A147P and is therefore in the following named as BsPAD_WCP.

Next, the Fe-2-modified BsPAD_WCP and, for comparison, the BsPAD_WT, BsPAD_WCP were tested in the photocatalytic carbon dioxide reduction under our standard conditions (Table 1). Applying the artificial metalloenzyme system (BsPAD_WCP@Fe-2) resulted in significantly higher TON_{CO} (Table 1, entries 7, 8, 11; PS:Cat = 20:1) compared to the molecularly-defined metal complexes Fe-1 and Fe-2. Surprisingly, the metal-free BsPAD_WT and BsPAD_WCP showed turnover numbers almost equal to BsPAD_WCP@Fe-2. Noteworthy, BsPAD_WT, BsPAD_WCP and BsPAD_WCP@Fe-2 outperform the Fe catalysts with respect to the carbon monoxide selectivity (Table 1, entries 9-11). These interesting results encouraged us to focus on the application of the metal free enzymes. To improve the performance of this promiscuous enzyme, next we performed single, two- and three-fold mutations at different positions (Table 2, Tables S-1, S-4 and Figure S-6). Those experiments revealed interesting structure activity relationships regarding CO productivity and selectivity and the photocatalytic tests of the further mutated BsPAD_WCP are summarized in Table 2.

Table 2. Photocatalytic carbon dioxide reduction by BsPAD variants					
#	Enzyme	nH ₂ (μmol)	nCO (μmol)	Select. (%)	TON CO
1	BsPAD_WT	<0.32	1.47	82	29
2 ^a	BsPAD_WT	<0.32	1.43	81	143
3	BsPAD_WCP	<0.32	1.48	82	30
4	BsPAD_WCP_W17A	0.51	3.90	88	78
5 ^a	BsPAD_WCP_W17A	0.42	1.96	82	196
6	BsPAD_WCP_I85A	<0.32	3.12	91	62
7 ^a	BsPAD_WCP_I85A	0.32	1.19	78	119
8	BsPAD_WCP_F87A	<0.32	2.40	88	48
9	BsPAD_WCP_W17A_I85A	<0.32	1.33	81	27
10	BsPAD_WCP_W17A_F87A	<0.32	2.21	87	44
11	BsPAD_WCP_I85A_F87A	<0.32	2.13	87	42
12	BsPAD_WCP_W17A_I85A_F87A	<0.32	2.32	88	46

Reaction conditions: 10 mL H₂O were used for all cases (Volume of headspace = 75 mL). [Enzyme] = 5 μM. [Ru(bpy)₃Cl₂] = 100 μM. NaHCO₃ (0.1 M) and NaAsch (0.05 M) were employed in all cases. Reaction mixtures were bubbled with carbon dioxide for 30 minutes prior to irradiation. Light output: 1.5W (400-700 nm). Reaction time: 3 hours; a) Conditions: 10 mL H₂O containing 1 μmol [Ru(bpy)₃Cl₂] [100 μM]; 0.01 μmol enzyme [1 μM]; 1 mmol NaHCO₃ [0.1 M] and 500 μmol NaAsch [0.05 M]. The experiments in entries 2 to 5 and 7 were performed at least twice. Standard deviations are 7 to 11 % (except for entries 2 and 7: 26% and 20%, respectively) of the average for TON(CO) as well as 1% to 5% for selectivity, respectively.

First, the amino acids tryptophan, isoleucine, and phenylalanine in positions 17, 85, and/or 87 of BsPAD_WCP were replaced by alanine to increase the CO₂ binding pocket. Among the obtained mutants especially the single mutated BsPAD_WCP_W17A, BsPAD_WCP_I85A and BsPAD_WCP_F87A, showed increased CO productivities and still high CO selectivity (Table 2, entries 4, 6, 8). For the double and triple mutants, lower TON values and comparable selectivities were obtained (Table 2, entries 9-12).

Mutating W17A, I85A and/or F87A at the entry site of the protein lead to a change in the opening/closing mechanism of the enzyme, as previously described for the W25A mutation (corresponding to W17A in BsPAD) in the phenolic acid decarboxylase from *Enterobacter sp.* Px6-4⁴⁹. To demonstrate the effect on protein dynamics, molecular dynamics simulations were also performed. These simulations showed that W17A, I85A, and F87A appear to stabilize the open enzyme conformation, while BsPAD_WT undergoes closing of the entry site within the simulated 10 ns (Figure S-2). Therefore, W17A, I85A, and F87A facilitate the access of CO₂ into the binding site

and the availability of protons⁵⁰; however, the combinatorial mutations did not result in synergistic effects regarding the TONs.

To figure out optimal reaction conditions, experiments with the wild-type and two modified proteins (BsPAD_WCP_W17A and BsPAD_WCP_I85A) were done at lower BsPAD concentration while keeping the same amount of photosensitizer (Table 2, entries 2, 5, and 7). Higher ratios of PS to catalyst resulted in a better activity due to more efficient electron transfer for the best variant BsPAD_WCP_W17A. Notably, further irradiation of the solution (>3 h) showed residual activity of the biocatalysts, underlining the high stability of the modified enzymes.

To proof the photocatalytic activity of BsPAD and its variants, potential contaminants resulting from the expression were tested. Using pure phosphate buffer as solvent (pH = 7.5) did result in very low activity. In the presence of 5 μmol imidazole under standard conditions 0.73 μmol of CO were detected with 70% selectivity (Table S-5; entry 4). Next, the effect of nickel(II) chloride, which can also be present as a contaminant derived from the purification method, was tested in high concentration. Again, only low activity was observed (Table S-5; entry 5). To exclude the possibility that the CO₂-reducing activity is caused by nonspecific interactions with protein backbones or amino acids, the effect of bovine serum albumin (BSA), a relatively large protein (66.5 kDa), and free amino acids known to interact with CO₂, such as Arg and Lys were investigated. Here, the amount of CO generated was close to blank volumes without any additive present (Table S-6). In conclusion all these control experiments suggest that the reduction of carbon dioxide is indeed a result of the catalytic promiscuity⁵¹ of BsPAD.

To proof if BsPAD_WT is still natively folded, we studied the decarboxylation of ferulic acid under optimal photocatalytic conditions in the presence of CO₂. While complete decarboxylation occurred, carbon dioxide reduction was decreased by 26% (Table S-7), suggesting that photocatalytic CO₂ reduction takes place in the same binding pocket as decarboxylation. The importance of the native folding of the protein was also demonstrated by heat treatment of BsPAD_WCP at 60°C for 30 min (such mild heat treatment was used to prevent protein aggregation and precipitation), which resulted in 60% activity decrease. Although no melting point could be determined by nano-differential scanning fluorimetry (NanoDSF) after the heat treatment, the residual activity could be explained by refolding of the protein after mild denaturation at 60°C (Table S-8).

In general, the electron transfer in the Ru-PS/BsPAD-based system might occur via direct single-step electron tunneling from the PS to carbon dioxide in the active site or secondly via multi-step tunneling through redox-active amino acid side chains. Typically, single-step electron tunneling in proteins is only observed within 14 Å, as the electron transfer rate decreases exponentially with distance^{52,53}. If the electron is not transferred directly in the active site, electron-conducting amino acids (Tyr or Trp) must be involved in electron transport.⁵⁴ Such multistep tunneling through redox-active amino acid side chains, often referred to as electron hopping, allows for higher electron transfer rates over long distances^{52,53}. Considering that the Ru-PS is too large to enter the protein cavity and that the CO₂ in the CO₂-binding pocket of BsPAD is located at least 8 Å from the protein surface, efficient one-step electron tunneling from the PS to the bound CO₂ is only possible if the PS is located close to a specific position on the protein surface. Since many Tyr and Trp amino acids are located in the binding pocket closer than 14 Å to the CO₂ (Figure 2A), multistep tunneling is more likely. To determine if any of the five tyrosines (Y11, Y13, Y19, Y31, Y122) and two tryptophans (W17, W62) in the cavity of the BsPAD_WCP (Figure 2A) is involved in multistep tunneling, they were replaced stepwise. Since BsPAD_WCP_W17A has already shown increased activity, tryptophan W17 is not essential for electron transfer. All other residues were replaced by phenylalanine (Phe), which has an aromatic character and a similar space requirement to Trp and Tyr, but does not conduct electrons. While substitution at positions Y13, Y19, Y31, and Y122 resulted in only slight decrease in

activity, the substitution of Y11 and W62 almost completely deactivated the system. These results suggest that Y11 and W62 mainly contribute to a multistep electron tunneling pathway within the protein.

Table 3. Influence of removal of redox active and CO₂ binding amino acids in WCP mutants applied in photocatalytic carbon dioxide reduction

#	Enzyme	nH ₂ (μmol)	nCO (μmol)	Select. (%)	TON CO
1	BsPAD_WT	<0.32	1.47	82	29
2	BsPAD_WCP	<0.32	1.48	82	30
3	BsPAD_WCP_Y11F	<0.32	0.52	62	10
4	BsPAD_WCP_Y13F	<0.32	0.82	72	16
5	BsPAD_WCP_Y19F	0.45	1.28	75	26
6	BsPAD_WCP_Y31F	<0.32	1.14	78	23
7	BsPAD_WCP_W62F	<0.32	0.35	52	7.0
8	BsPAD_WCP_Y122F	<0.32	0.80	71	16
9	BsPAD_WCP_R41I	<0.32	0.51	62	10
10	BsPAD_WCP_R41L	<0.32	0.58	64	12

Reaction conditions: 10 mL H₂O were used for all cases (Volume of headspace = 75 mL). [Enzyme] = 5 μM. [Ru(bpy)₃Cl₂] = 100 μM. NaHCO₃ (0.1 M) and NaAsch (0.05 M) were employed in all cases. Reaction mixtures were bubbled with carbon dioxide for 30 minutes prior to irradiation. Light output: 1.5 W (400-700 nm). Reaction time: 3 hours. The experiments in entries 2, 3, 5, 6 and 8 were performed at least twice. Standard deviations are 2 to 14 % of the average for TON(CO) as well as 1% to 4% (except entry 5: 11%) for selectivity, respectively.

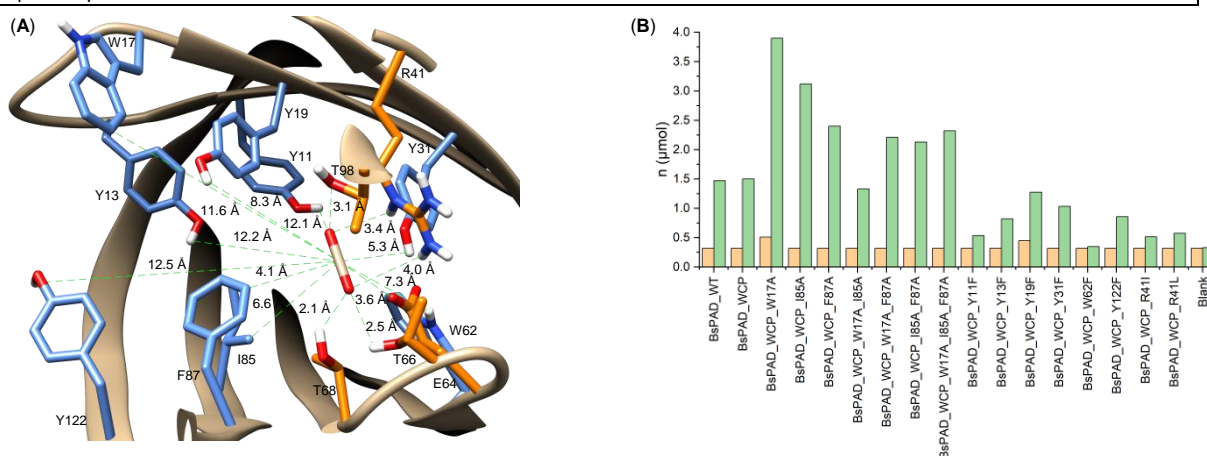


Figure 2. Mutation studies on BsPAD. (A) Visualization of residues selected for mutation (blue) in the protein cavity of BsPAD (PDB-ID: 2P8G) and amino acids involved in CO₂ binding (orange). (B) Overview of results in photocatalytic carbon dioxide reduction employing BsPAD derived mutants according to Tables 2 and 3. Reaction conditions: [Ru(bpy)₃Cl₂] = 100 μM; [Enz] = 5 μM; [NaHCO₃] = 0.1 M; [NaAsch] = 0.05 M; total reaction volume = 10 mL. Carbon monoxide produced is shown in green color, hydrogen production is shown in orange color.

Next, we turned our attention to the amino acid Arg41 (R41) which is known to be essential for the phenolic acid decarboxylation activity of BsPAD⁴³ and is expected to be involved in carbon dioxide binding⁵⁵⁻⁵⁷. Thus, a loss of activity is expected exchanging Arg41 by leucine or isoleucine. Indeed, the BsPAD_WCP_R41I and BsPAD_WCP_R41L variants showed significantly decreased productivity in CO formation (Table 3; entries 9 and 10). Therefore, besides the redox active amino acids also the carbon dioxide binding site of BsPAD is essential for the obtained catalytic performance.

To proof the presence of accessible and stable radicals, a photocatalytic experiment was carried in the presence of a high concentration of hydroxy TEMPO as radical scavenger. Interestingly, there is no complete inhibition and the system still showed half of the activity (Table S-9).

Table 4. Carbon dioxide binding enzymes (wild-types) studied for photocatalytic CO₂ reduction					
#	Enzyme	nH ₂ (μmol)	nCO (μmol)	Select. (%)	TON CO
1	BsPAD_WT	<0.32	1.43	81	143
2 ^{a)}	EcPanD	0.42	1.62	80	162
3	PFE	<0.32	0.92	74	92
4 ^{a)}	SsTrpC	0.33	1.17	79	117
5	MmPPP2	<0.32	1.52	83	152
6	ScFDC1	<0.32	2.55	89	255
7	TtALS	0.36	2.62	88	262
8	EcPPC	<0.32	1.49	83	149
9	BtCA	0.87	2.19	72	219

Reaction conditions: 10 mL H₂O were used for all cases (Volume of headspace = 75 mL). [Enzyme] = 1 μM. [Ru(bpy)₃Cl₂] = 100 μM. NaHCO₃ (0.1 M) and NaAsCH (0.05 M) were employed in all cases. Reaction mixtures were bubbled with carbon dioxide for 30 minutes prior to irradiation. Light output: 1.5 W (400-700 nm). Reaction time: 3 hours. a) Different enzyme batches were applied. All experiments (except entry 3) were performed twice, and average values are shown. Standard deviations are in general 4% to 19% for TON(CO) except for entries 1 (26%), 4 (32%), 6 (28%) and 9 (23%) as well as 1% to 12% for selectivity except for entry 6 (20%). Details about the applied enzyme batches are provided in the supplementary information (Table S-10).

Obviously, the carbon dioxide reduction activity of BsPAD is favored by the proximity of electron-conducting amino acids and the CO₂ binding pocket. Since a total of about 5% of amino acids in proteins are Tyr and Trp⁵⁸, CO₂ reduction might occur also in other proteins capable of binding carbon dioxide⁵⁹. To prove this, exemplarily eight other proteins that release or utilize CO₂ were selected and investigated for their carbon dioxide-reducing activity (Table 4). In addition, *Pseudomonas fluorescens* esterase 1⁶⁰ (PFE) was included in the selection, although it naturally releases carboxylic acids rather than CO₂ during ester hydrolysis. As shown in a docking experiment, CO₂ binding occurs at the same position between the oxyanion hole and the catalytic Ser, as expected for carboxylic acids (Figure S-3)⁶¹. Among the selected proteins, the carbon dioxide binding mechanism, protein size, and origin differed. While e.g., acetolactate synthase from *Thermus thermophilus* (TtALS), carbonic anhydrase from *Bos taurus* (BtCA), and ferulic acid decarboxylase 1 from *Saccharomyces cerevisiae* (ScFDC1) require thiamine diphosphate, Zn²⁺, and flavin mononucleotide cofactors, respectively, in substrate or CO₂ binding, no cofactors are necessary for the other enzymes studied. Interestingly, all enzymes with CO₂-binding sites exhibited some activity regardless of the binding mechanism. CO₂-binding pockets in enzymes serve to stabilize transition states in CO₂-releasing or -utilizing reactions, therefore charged intermediates of CO₂ reduction could also be stabilized by interacting with the CO₂-binding site. Indeed, indole-3-glycerol phosphate synthase from *Sulfolobus solfataricus* (SsTrpC) showed activity (TON 117) and selectivity (79%) for CO formation, albeit somewhat lower compared to the BsPAD_WT (Table 4, entry 4). Protocatechuate decarboxylase from *Madurella mycetomatis* (MmPPP2) showed comparable TON and selectivity to BsPAD_WT (Table 4, entry 5). Higher TON and selectivity were obtained applying TtALS, while PFE showed lower TON and selectivity (Table 4, entries 7 and 3). BtCA and ScFDC1 showed high activity (TON 219 and 255, respectively; Table 4, entries 9 and 6) combined with low or high selectivity at 72% and 89%, respectively. Phosphoenolpyruvate carboxylase (EcPPC) and aspartate-1-decarboxylase from *Escherichia coli* K12 (EcPanD) showed TONs around 150 and selectivity for CO

formation of 83% and 80%, respectively (Table 4, entries 8 and 2). Especially the wild-type enzymes ScFDC1, TtALS, and EcPanD showed similar or even better performance in terms of activity and selectivity than the engineered variant BsPAD_WCP_W17A and therewith constitute potential targets for further engineering studies of the newly found enzymatic promiscuity. In particular, EcPanD and BsPAD_WCP_W17A, which do not require external cofactors^{44,62}, could overcome expression and stability issues associated with enzymatic CO₂ reduction by CODH. Noteworthy, the expression level of WT_BsPAD reaches more than 8 μmol_{Enzyme}/L_{Medium} (Table S-10).

At this point it is worth mentioning that the productivity of BsPAD decreased substituting Arg41; thus, it seems that Arg plays an important role in carbon dioxide activation in enzymes, as also suggested for CO₂ activation catalyzed by Arg in the synthesis of quinazoline-2,4(1H,3H)-diones in water⁶³. Therefore, analyses of the structures of all other tested enzymes regarding Arg were performed. However, both Arg-rich enzymes, as well as those where Arg is not involved in CO₂ binding, showed activity and selectivity for CO₂ reduction, e.g., in PFE or BtCA. Therefore, a specific role of Arg in enzyme-based photocatalytic CO₂ reduction seems not to be necessary. The presence of Arg in many CO₂-binding pockets might appear due to the fact that Arg is the most abundant amino acid in CO₂-binding motifs⁶⁴ and is known to be efficient for carbon dioxide capture⁶⁵.

Conclusions

Here, we present a concept identifying enzymes with promiscuous CO₂ reducing activity by functional and structural analysis and optimizing their activity via mutations. We believe this approach opens the way for developing new and improved biocatalysts for this important transformation based on profound knowledge of enzymes structures and mechanism. More specifically, it is demonstrated that the wild-type as well as the mutants of the phenolic acid decarboxylase from *Bacillus subtilis* (BsPAD_WT) constitute practical alternatives for air-sensitive and difficult to handle enzymes like so far applied CODH. BsPAD_WT, originally not expected to possess CO₂-reducing activity, promotes the aqueous photocatalytic CO₂ reduction to carbon monoxide in the presence of a ruthenium photosensitizer and sodium ascorbate (TON up to 143) in good selectivity (81%). By mutating the active site of this enzyme, improved turnover numbers and higher selectivity for CO were achieved for BsPAD_WCP_W17A. Further investigations of the influence of mutations substituting either the redox active amino acids tyrosine and tryptophane or arginine gained insights into the working mode of the enzyme. A multistep electron tunneling was identified to be the most certain mechanism. Based on determined structural and functional analyses, eight other enzymes with CO₂-binding pockets were chosen and successfully examined for their ability to perform photocatalytic CO₂ reduction; thus, demonstrating the viability of our concept.

References

- 1 Meys, R. *et al.* Achieving net-zero greenhouse gas emission plastics by a circular carbon economy. *Science* **374**, 71-76 (2021).
- 2 Stahel, W. R. Circular economy. *Nature* **531**, 435-437 (2016).
- 3 Wei, D., Shi, X., Sponholz, P., Junge, H. & Beller, M. Manganese promoted (bi)carbonate hydrogenation and formate dehydrogenation: Toward a circular carbon and hydrogen economy. *ACS Cent. Sci.* **8**, 1457-1463 (2022). <https://doi.org:10.1021/acscentsci.2c00723>
- 4 Bai, S. T. *et al.* Homogeneous and heterogeneous catalysts for hydrogenation of CO₂ to methanol under mild conditions. *Chem. Soc. Rev.* **50**, 4259-4298 (2021). <https://doi.org:10.1039/d0cs01331e>

- 5 Wang, W. H., Himeda, Y., Muckerman, J. T., Manbeck, G. F. & Fujita, E. CO₂ hydrogenation to formate and methanol as an alternative to photo- and electrochemical CO₂ reduction. *Chem. Rev.* **115**, 12936-12973 (2015). <https://doi.org/10.1021/acs.chemrev.5b00197>
- 6 Benson, E. E., Kubiak, C. P., Sathrum, A. J. & Smieja, J. M. Electrocatalytic and homogeneous approaches to conversion of CO₂ to liquid fuels. *Chem. Soc. Rev.* **38**, 89-99 (2009). <https://doi.org/10.1039/b804323j>
- 7 Takeda, H., Cometto, C., Ishitani, O. & Robert, M. Electrons, photons, protons and earth-abundant metal complexes for molecular catalysis of CO₂ reduction. *ACS Catal.* **7**, 70-88 (2016). <https://doi.org/10.1021/acscatal.6b02181>
- 8 Morris, A. J., Meyer, G. J. & Fujita, E. Molecular approaches to the photocatalytic reduction of carbon dioxide for solar fuels. *Acc. Chem. Res.* **42**, 1983-1994 (2009). <https://doi.org/10.1021/ar9001679>
- 9 Dalle, K. E. *et al.* Electro- and solar-driven fuel synthesis with first row transition metal complexes. *Chem. Rev.* **119**, 2752-2875 (2019). <https://doi.org/10.1021/acs.chemrev.8b00392>
- 10 Olah, G. A., Prakash, G. K. & Goepfert, A. Anthropogenic chemical carbon cycle for a sustainable future. *J. Am. Chem. Soc.* **133**, 12881-12898 (2011). <https://doi.org/10.1021/ja202642y>
- 11 Arcudi, F., Dordevic, L., Nagasing, B., Stupp, S. I. & Weiss, E. A. Quantum dot-sensitized photoreduction of CO₂ in water with turnover number > 80,000. *J. Am. Chem. Soc.* **143**, 18131-18138 (2021). <https://doi.org/10.1021/jacs.1c06961>
- 12 Cauwenbergh, R. & Das, S. Photochemical reduction of carbon dioxide to formic acid. *Green Chem.* **23**, 2553-2574 (2021). <https://doi.org/10.1039/d0gc04040a>
- 13 Kuriki, R., Sekizawa, K., Ishitani, O. & Maeda, K. Visible-light-driven CO₂ reduction with carbon nitride: enhancing the activity of ruthenium catalysts. *Angew. Chem., Int. Ed.* **54**, 2406-2409 (2015). <https://doi.org/10.1002/anie.201411170>
- 14 Habisreutinger, S. N., Schmidt-Mende, L. & Stolarczyk, J. K. Photocatalytic reduction of CO₂ on TiO₂ and other semiconductors. *Angew. Chem., Int. Ed.* **52**, 7372-7408 (2013). <https://doi.org/10.1002/anie.201207199>
- 15 Kim, D., Sakimoto, K. K., Hong, D. & Yang, P. Artificial photosynthesis for sustainable fuel and chemical production. *Angew. Chem., Int. Ed.* **54**, 3259-3266 (2015). <https://doi.org/10.1002/anie.201409116>
- 16 Zhang, B. & Sun, L. Artificial photosynthesis: opportunities and challenges of molecular catalysts. *Chem. Soc. Rev.* **48**, 2216-2264 (2019). <https://doi.org/10.1039/c8cs00897c>
- 17 Ye, S. *et al.* Mimicking the key functions of photosystem II in artificial photosynthesis for photoelectrocatalytic water splitting. *J. Am. Chem. Soc.* **140**, 3250-3256 (2018). <https://doi.org/10.1021/jacs.7b10662>
- 18 Ren, F. Y. *et al.* Amphiphilic polycarbonate micellar rhenium catalysts for efficient photocatalytic CO₂ reduction in aqueous media. *Angew. Chem., Int. Ed.* **61**, e202200751 (2022). <https://doi.org/10.1002/anie.202200751>
- 19 Call, A. *et al.* Highly efficient and selective photocatalytic CO₂ reduction to CO in water by a cobalt porphyrin molecular catalyst. *ACS Catal.* **9**, 4867-4874 (2019). <https://doi.org/10.1021/acscatal.8b04975>
- 20 Zhang, X., Cibian, M., Call, A., Yamauchi, K. & Sakai, K. Photochemical CO₂ reduction driven by water-soluble copper(I) photosensitizer with the catalysis accelerated by multi-electron chargeable cobalt porphyrin. *ACS Catal.* **9**, 11263-11273 (2019). <https://doi.org/10.1021/acscatal.9b04023>
- 21 Segev, G. *et al.* The 2022 solar fuels roadmap. *J. Phys. D: Appl. Phys.* **55** (2022). <https://doi.org/10.1088/1361-6463/ac6f97>
- 22 Yadav, R. K. *et al.* A photocatalyst-enzyme coupled artificial photosynthesis system for solar energy in production of formic acid from CO₂. *J. Am. Chem. Soc.* **134**, 11455-11461 (2012). <https://doi.org/10.1021/ja3009902>

- 23 Edwardes Moore, E. *et al.* A semi-artificial photoelectrochemical tandem leaf with a CO₂ -to-formate efficiency approaching 1. *Angew. Chem., Int. Ed.* **60**, 26303-26307 (2021).
<https://doi.org/10.1002/anie.202110867>
- 24 Parkinson, B. A. & Weaver, P. F. Photoelectrochemical pumping of enzymatic CO₂ reduction
Nat. Chem. **309**, 148-149 (1984). [https://doi.org:https://doi.org/10.1038/309148a0](https://doi.org/10.1038/309148a0)
- 25 Beller, M. & Bornscheuer, U. T. CO₂ fixation through hydrogenation by chemical or enzymatic
methods. *Angew. Chem., Int. Ed.* **53**, 4527-4528 (2014).
<https://doi.org/10.1002/anie.201402963>
- 26 Woolerton, T. W., Sheard, S., Pierce, E., Ragsdale, S. W. & Armstrong, F. A. CO₂
photoreduction at enzyme-modified metal oxide nanoparticles. *Energy Environ. Sci.* **4** (2011).
<https://doi.org/10.1039/c0ee00780c>
- 27 Woolerton, T. W. *et al.* Efficient and clean photoreduction of CO₂ to CO by enzyme-modified
TiO₂ nanoparticles using visible light. *J. Am. Chem. Soc.* **132**, 2132-2133 (2010).
- 28 Chaudhary, Y. S. *et al.* Visible light-driven CO₂ reduction by enzyme coupled CdS nanocrystals.
Chem. Commun. **48**, 58-60 (2012). <https://doi.org/10.1039/c1cc16107e>
- 29 Zhang, L., Can, M., Ragsdale, S. W. & Armstrong, F. A. Fast and selective photoreduction of
CO₂ to CO catalyzed by a complex of carbon monoxide dehydrogenase, TiO₂, and Ag
nanoclusters. *ACS Catal.* **8**, 2789-2795 (2018). <https://doi.org/10.1021/acscatal.7b04308>
- 30 Ghosh, D., Sinhababu, S., Santarsiero, B. D. & Mankad, N. P. A W/Cu synthetic model for the
Mo/Cu cofactor of aerobic CODH indicates that biochemical CO oxidation requires a
frustrated Lewis acid/base pair. *J. Am. Chem. Soc.* **142**, 12635-12642 (2020).
<https://doi.org/10.1021/jacs.0c03343>
- 31 Soboh, B., Linder, D. & Hedderich, R. Purification and catalytic properties of a CO-oxidizing:
H₂-evolving enzyme complex from *Carboxydothemus hydrogenoformans*. *Eur. J. Biochem.*
269, 5712-5721 (2002). <https://doi.org/10.1046/j.1432-1033.2002.03282.x>
- 32 Choi, E. S., Min, K., Kim, G. J., Kwon, I. & Kim, Y. H. Expression and characterization of
Pantoea CO dehydrogenase to utilize CO-containing industrial waste gas for expanding the
versatility of CO dehydrogenase. *Sci. Rep.* **7**, 44323 (2017).
<https://doi.org/10.1038/srep44323>
- 33 Hyeon, J. E., Kim, S. W., Park, C. & Han, S. O. Efficient biological conversion of carbon
monoxide (CO) to carbon dioxide (CO₂) and for utilization in bioplastic production by
Ralstonia eutropha through the display of an enzyme complex on the cell surface. *Chem.*
Commun. **51**, 10202-10205 (2015). <https://doi.org/10.1039/c5cc00832h>
- 34 Svetlitchnyi, V., Peschel, C., Acker, G. & Meyer, O. Two membrane-associated NiFeS-carbon
monoxide dehydrogenases from the anaerobic carbon-monoxide-utilizing eubacterium
Carboxydothemus hydrogenoformans. *J. Bacteriol.* **183**, 5134-5144 (2001).
<https://doi.org/10.1128/JB.183.17.5134-5144.2001>
- 35 Kim, S. M. *et al.* O₂-tolerant CO dehydrogenase via tunnel redesign for the removal of CO
from industrial flue gas. *Nat. Catal.* **5**, 807-817 (2022). <https://doi.org/10.1038/s41929-022-00834-y>
- 36 Jeoung, J. H. *et al.* A morphing [4Fe-3S-nO]-cluster within a Carbon Monoxide
Dehydrogenase Scaffold. *Angew. Chem., Int. Ed.* **61**, e202117000 (2022).
<https://doi.org/10.1002/anie.202117000>
- 37 Schneider, C. R., Manesis, A. C., Stevenson, M. J. & Shafaat, H. S. A photoactive semisynthetic
metalloenzyme exhibits complete selectivity for CO₂ reduction in water. *Chem. Commun.* **54**,
4681-4684 (2018). <https://doi.org/10.1039/c8cc01297k>
- 38 Schneider, C. R. & Shafaat, H. S. An internal electron reservoir enhances catalytic CO₂
reduction by a semisynthetic enzyme. *Chem. Commun.* **52**, 9889-9892 (2016).
<https://doi.org/10.1039/c6cc03901d>
- 39 Liu, X. *et al.* A genetically encoded photosensitizer protein facilitates the rational design of a
miniature photocatalytic CO₂-reducing enzyme. *Nat. Chem.* **10**, 1201-1206 (2018).
<https://doi.org/10.1038/s41557-018-0150-4>

- 40 Kuehnel, M. F., Orchard, K. L., Dalle, K. E. & Reisner, E. Selective photocatalytic CO₂ Reduction in water through anchoring of a molecular Ni catalyst on CdS nanocrystals. *J. Am. Chem. Soc.* **139**, 7217-7223 (2017). <https://doi.org:10.1021/jacs.7b00369>
- 41 Froehlich, J. D. & Kubiak, C. P. Homogeneous CO₂ reduction by Ni(cyclam) at a glassy carbon electrode. *Inorg. Chem.* **51**, 3932-3934 (2012). <https://doi.org:10.1021/ic3001619>
- 42 Alcalá-Torano, R., Halloran, N., Gwerder, N., Sommer, D. J. & Ghirlanda, G. Light-driven CO₂ reduction by Co-cytochrome b 562. *Front. Mol. Biosci.* **8**, 609654 (2021). <https://doi.org:10.3389/fmolb.2021.609654>
- 43 Frank, A. *et al.* Mutational analysis of phenolic acid decarboxylase from *Bacillus subtilis* (BsPAD), which converts bio-derived phenolic acids to styrene derivatives. *Catal. Sci. Technol.* **2** (2012). <https://doi.org:10.1039/c2cy20015e>
- 44 Cavin, J.-F. Gene cloning, transcriptional analysis, purification, and characterization of phenolic acid Decarboxylase from *Bacillus subtilis*. *Appl. Environ. Microbiol.* **64**, 1466-1471 (1998).
- 45 Bierbaumer, S. *et al.* Enzymatic conversion of CO₂: From natural to artificial utilization. *Chem. Rev.* (2023). <https://doi.org:10.1021/acs.chemrev.2c00581>
- 46 Rosas-Hernández, A., Steinlechner, C., Junge, H. & Beller, M. Earth-abundant photocatalytic systems for the visible-light-driven reduction of CO₂ to CO. *Green Chem.* **19**, 2356-2360 (2017). <https://doi.org:10.1039/c6gc03527b>
- 47 Kariyawasam, K. *et al.* Artificial iron hydrogenase made by covalent grafting of Knölker's complex into xylanase: Application in asymmetric hydrogenation of an aryl ketone in water. *Biotechnol. Appl. Biochem.* **67**, 563-573 (2020). <https://doi.org:10.1002/bab.1906>
- 48 Musil, M. *et al.* FireProt: web server for automated design of thermostable proteins. *Nucleic Acids Res.* **45**, W393-W399 (2017). <https://doi.org:10.1093/nar/gkx285>
- 49 Gu, W. *et al.* Structural basis of enzymatic activity for the ferulic acid decarboxylase (FADase) from *Enterobacter sp.* Px6-4. *PLoS One* **6**, e16262 (2011). <https://doi.org:10.1371/journal.pone.0016262>
- 50 Nilsen-Moe, A. *et al.* Proton-coupled electron transfer from tyrosine in the interior of a *de novo* protein: Mechanisms and primary proton acceptor. *J. Am. Chem. Soc.* **142**, 11550-11559 (2020). <https://doi.org:10.1021/jacs.0c04655>
- 51 Bornscheuer, U. T. & Kazlauskas, R. J. Catalytic promiscuity in biocatalysis: using old enzymes to form new bonds and follow new pathways. *Angew. Chem., Int. Ed.* **43**, 6032-6040 (2004). <https://doi.org:10.1002/anie.200460416>
- 52 Page, C. C., Moser, C. C., Chen, X. & Leslie, D. P. Natural engineering principles of electron tunnelling in biological oxidation-reduction. *Nature* **402**, 47-52 (1999). <https://doi.org:10.1038/46972>
- 53 Crystal, S. A. K., Museth; Malin, Abrahamsson; Ana Maria, Blanco-Rodriguez; Harry B. Gray. Tryptophan-accelerated electron flow through proteins. *Science* **320**, 1760-1762 (2008). <https://doi.org:10.1126/science.1158241>
- 54 Shipps, C. *et al.* Intrinsic electronic conductivity of individual atomically resolved amyloid crystals reveals micrometer-long hole hopping via tyrosines. *Proc. Natl. Acad. Sci. U. S. A.* **118** (2021). <https://doi.org:10.1073/pnas.2014139118>
- 55 Wuensch, C. *et al.* Asymmetric enzymatic hydration of hydroxystyrene derivatives. *Angew. Chem., Int. Ed.* **52**, 2293-2297 (2013). <https://doi.org:10.1002/anie.201207916>
- 56 Sheng, X., Lind, M. E. & Himo, F. Theoretical study of the reaction mechanism of phenolic acid decarboxylase. *FEBS J.* **282**, 4703-4713 (2015). <https://doi.org:10.1111/febs.13525>
- 57 Sheng, X. & Himo, F. Theoretical study of enzyme promiscuity: Mechanisms of hydration and carboxylation activities of phenolic acid decarboxylase. *ACS Catal.* **7**, 1733-1741 (2017). <https://doi.org:10.1021/acscatal.6b03249>
- 58 Kozłowski, L. P. Proteome-pl: proteome isoelectric point database. *Nucleic Acids Res.* **45**, D1112-D1116 (2017). <https://doi.org:10.1093/nar/gkw978>
- 59 Lindsay, S. Ubiquitous electron transport in non-electron transfer proteins. *Life (Basel)* **10** (2020). <https://doi.org:10.3390/life10050072>

- 60 N., K., F., Z., J., A. & Bornscheuer, U. T. Characterization and enantioselectivity of a
recombinant esterase from *Pseudomonas Fluorescens*. *Enzyme Microb. Technol.* **22**, 641-646
(1998). [https://doi.org:10.1016/S0141-0229\(98\)00004-0](https://doi.org:10.1016/S0141-0229(98)00004-0)
- 61 Cheeseman, J. D., Tocilj, A., Park, S., Schrag, J. D. & Kazlauskas, R. J. Structure of an aryl
esterase from *Pseudomonas fluorescens*. *Acta Crystallogr., Sect. D: Biol. Crystallogr.* **60**, 1237-
1243 (2004). <https://doi.org:10.1107/S0907444904010522>
- 62 Schmitzberger, F. *et al.* Structural constraints on protein self-processing in L-aspartate-alpha-
decarboxylase. *EMBO J.* **22**, 6193-6204 (2003). <https://doi.org:10.1093/emboj/cdg575>
- 63 Lu, W. *et al.* Choline hydroxide promoted chemical fixation of CO₂ to quinazoline-2,4(1H,3H)-
diones in water. *RSC Adv.* **4**, 50993-50997 (2014). <https://doi.org:10.1039/c4ra08551e>
- 64 Cundari, T. R. W., Angela K.; Drummond, Michael L.; Gonzalez, Hector Emanuel; Jorgensen,
Kameron R.; Payne, Stacy; Braunfeld, Jordan; De Jesus, Margarita; Johnson, Vanessa M. CO₂-
formatics: How do proteins bind carbon dioxide? *J. Chem. Inf. Model.* **49**, 2111-2115 (2009).
- 65 Moazezbarabadi, A., Wei, D., Junge, H. & Beller, M. Improved CO₂ capture and catalytic
hydrogenation using amino acid based ionic liquids. *ChemSusChem*, e202201502 (2022).
<https://doi.org:10.1002/cssc.202201502>

Supplementary Information

Photo-enzymatic catalytic CO₂ reduction using a promiscuous decarboxylase as protein scaffold

Henrik Terholsen^{1*}, Hilario Diego Huerta-Zerón^{2*}, Christina Möller¹,
Dr. Henrik Junge^{2§}, Prof. Dr. Uwe Bornscheuer^{1§}, Prof. Dr. Matthias
Beller^{2§}

¹Department of Biotechnology and Enzyme Catalysis, Institute of Biochemistry
University Greifswald
Felix-Hausdorff-Straße 4, 17487 Greifswald (Germany)
Email: uwe.bornscheuer@uni-greifswald.de

¹Leibniz Institute for Catalysis e.V.
Albert-Einstein-Straße 29a, 18059 Rostock (Germany)
Email: matthias.beller@catalysis.de

- 1. General information**
 - 1.1 Chemicals**
 - 1.2 Analysis (include limits of detection/quantification)**
 - 1.3 Calculation of product amounts (CO, H₂) and TON**
 - 1.4 Demonstrative calculation example**

- 2. Enzymes and mutations**
 - 2.1. Protein preparation**
 - 2.2. *In silico* experiments**
 - 2.3. Enzyme loading with Fe-2 and analysis**

- 3. Photocatalytic CO₂ reduction**
 - 3.1. Photocatalytic setup**
 - 3.2. Protocol for Photocatalytic CO₂ reduction**
 - 3.3. Transferring the reaction to fully aqueous media**
 - 3.4. Application of Fe-1 and Fe-2 in photocatalytic CO₂ reduction in NMP**
 - 3.5. Application of BsPAD derivatives and Fe-2 modified BsPAD derivatives in photocatalytic CO₂ reduction in H₂O**
 - 3.6. Aqueous photocatalytic CO₂ reduction in the presence of potential enzyme impurities**
 - 3.7. Aqueous photocatalytic CO₂ reduction applying potential alternative compounds to BsPAD (Bovine Serum Albumin, amino acids)**
 - 3.8. Control experiment: Decarboxylation of ferulic acid by BsPAD_WT**
 - 3.9. Control experiment: Aqueous photocatalytic CO₂ reduction applying heat treated BsPAD_WT**
 - 3.10. Poisoning experiment applying hydroxy TEMPO**
 - 3.11. Carbon dioxide binding enzymes (wild types) tested in photocatalytic CO₂ reduction**

- 4. State of the art of relevant systems in aqueous homogeneous photocatalytic CO₂ reduction**

- 5. References**

1. General information

1.1 Chemicals

All reagents and solvents were purchased from different suppliers and used without further purification. Carbon dioxide was purchased from Linde with 99.998% or 99.9994% purity, $^{13}\text{CO}_2$ (99.9% purity) was purchased from Merck (Sigma-Aldrich). Schlenk techniques were used for handling metallic complexes.

Fe-1^1 , Fe-2^2 , CuPS-1^3 , CuPS-2^4 and 1,3-dimethyl-2-phenyl-2,3-dihydro-1H-benzimidazole⁵ (BIH) were synthesized according to previously reported literature procedures. $[\text{Ru}(\text{bpy})_3\text{Cl}_2] \cdot 6\text{H}_2\text{O}$ was purchased from Strem Chemicals, transferred to a Schlenk tube, and stored under argon.

1.2 Analysis

Liquid samples were analyzed by NMR. ^1H NMR spectra were recorded on 300 MHz (Avance 300 and Fourier 300) Bruker spectrometers for liquid phase of each photocatalytic experiment.

The headspace of each reaction was analyzed by gas chromatography. An Agilent Technologies 7890A gas chromatograph, a HP Plot-Q column, a TCD, and Ar carrier gas was used for this purpose. Calibration of the GC was performed using the following gas concentrations:

- (1) H_2 : 25.3%, 10.0%, 5.0%, 1.01%, 0.51%, 0.25%, 1000 ppm, 500 ppm, 262 ppm, 105 ppm
- (2) CO : 10.1%, 5.82%, 0.99%, 993 ppm, 237 ppm, 78 ppm
- (3) CH_4 : 9.89%, 5.05%, 1.02%, 993 ppm, 81 ppm
- (4) CO_2 : 100%, 95%, 50%, 25%, 10%, 5%, 1%

Limits of quantification are: 0.32 μmol for hydrogen and 0.24 μmol for carbon monoxide resulting in quantification limits of 4.8 TON(CO) and 6.4 TON(H_2) applying 5 μmol catalyst/enzyme as well as 24 TON(CO) and 32 TON(H_2) applying 1 μmol catalyst/enzyme, respectively.

1.3 Calculation of product amounts and TON

Headspace of each reaction was analyzed using a calibrated GC. For each sample, 5 mL of gas were injected.

Carbon monoxide and hydrogen were quantified considering the following van der Waals molar volumes: 24.44323 L/mol for CO ($a = 1.505 \text{ L}^2 \cdot \text{bar} \cdot \text{mol}^{-2}$; $b = 0.03985 \text{ L} \cdot \text{mol}^{-1}$) and 24.48068 L/mol for H_2 ($a = 0.2476 \text{ L}^2 \cdot \text{bar} \cdot \text{mol}^{-2}$; $b = 0.02661 \text{ L} \cdot \text{mol}^{-1}$). Photocatalytic vessels contain a total volume of 85 mL, and for all tests the solvent volume was 10 mL, therefore we considered a volume of 75 mL for the headspace.

$$n_{\text{CO}} = \frac{(\% \text{CO}) \cdot V_{\text{Headspace}}}{100 \cdot V_m \text{CO}} = \frac{(\% \text{CO}) \cdot 0.075 \text{L}}{2444.323 \text{ L} \cdot \text{mol}^{-1}} = \% \text{CO} \cdot 3.068 \times 10^{-5} \text{mol}$$

$$n_{\text{H}_2} = \frac{(\% \text{H}_2) \cdot V_{\text{Headspace}}}{100 \cdot V_m \text{H}_2} = \frac{(\% \text{H}_2) \cdot 0.075 \text{L}}{2448.068 \text{ L} \cdot \text{mol}^{-1}} = \% \text{H}_2 \cdot 3.063 \times 10^{-5} \text{mol}$$

Turnover numbers (TON) for carbon monoxide and hydrogen were calculated using the following equation:

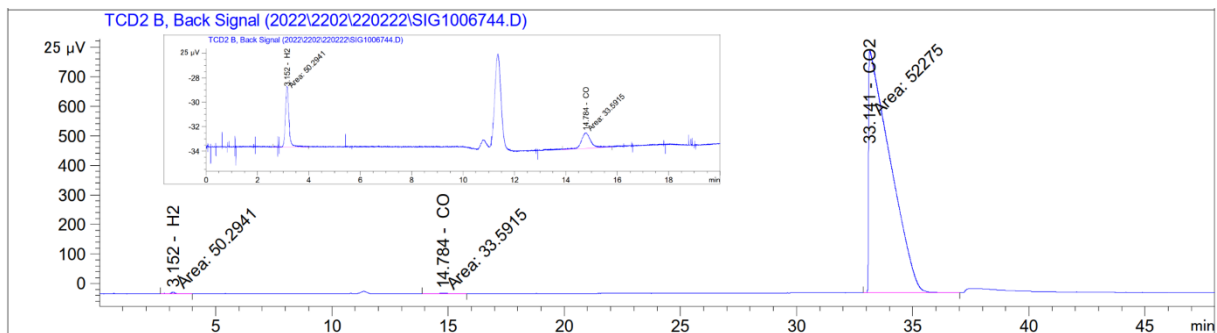
$$TON = \frac{n_{product}}{n_{catalyst}}$$

Selectivity towards carbon monoxide on each experiment was calculated using the following equation:

$$\% \text{ Selectivity} = \frac{n_{CO}}{n_{CO} + n_{H_2}} \times 100$$

1.4 Demonstrative calculation example

The following values were obtained from the corresponding chromatogram in Figure S-1.



RetTime [min]	Type	Area [25 µV*s]	Amt/Area	Amount [% Vol.]	Grp	Name
3.152	MM	50.29408	3.35612e-4	1.68793e-2		H2
10.770		-	-	-		O2
11.339		-	-	-		N2
14.784	MM	33.59151	3.47685e-3	1.16793e-1		CO
26.900		-	-	-		CH4
33.141	MM	5.22750e4	1.87687e-3	98.11364		CO2
Totals :				98.24731		

Figure S-1. Typical GC of a sample and obtained volume percentage of carbon monoxide and hydrogen.

Based on the %Vol of each gas the amounts of CO and H₂ can be calculated by the corresponding equation:

$$n_{CO} = 1.16793 \times 10^{-1} \cdot 3.068 \times 10^{-5} \text{ mol} = 3.58 \times 10^{-6} \text{ mol}$$

$$n_{H_2} = 1.68793 \times 10^{-2} \cdot 3.063 \times 10^{-5} \text{ mol} = 5.17 \times 10^{-7} \text{ mol}$$

Selectivity is calculated using the previously provided equation:

$$\% \text{ Selectivity} = \frac{3.58 \mu\text{mol}}{(3.58 \mu\text{mol} + 0.517 \mu\text{mol})} \times 100 = 87.4\%$$

2. Enzymes and mutations

2.1 Protein preparation

Plasmid construction and site-directed mutagenesis

Synthetic genes of the BsPAD wild-type (GeneBank: WP_003243190.1), EcPanD (GeneBank: NP_414673.1), SsTrpC (GeneBank: WP_009992313.1), MmPP2 (GeneBank: KXX81388.1), ScFDC1 (GeneBank: NP_010828.1), TtALS (GeneBank: WP_011228519.1), and EcPPC (GeneBank: NP_418391.1) in pET28a were ordered from BioCat (Heidelberg, Germany) using seamless cloning with the flanking regions 5' GTGCCGCGCGGCAGC 3' (5' flanking) and 5' CACCACCACCACCAC CACTGAGATCCG 3' (3' flanking). The amino acid numberings given are based on the original protein sequences.

The mutant BsPAD_C100W_V124C_A147P (BsPAD_WCP) was created by sequential mutagenesis of C100W, V124C, and A147P. BsPAD_WCP was used as the basis to introduce W17A, I85A, and F87A. Combinatorial mutagenesis of W17A, I85A, and F87A was performed sequentially, but adapted primers were used for the combination of I85A and F87A (I85A_F87A_fw/rv; table S-1). All site-directed mutagenesis were performed using the Q5[®] Site-Directed Mutagenesis Kit (New England Biolabs GmbH, Ipswich, UK). Non-overlapping DNA-oligonucleotides were designed using the online NEBaseChanger tool. The list of primers used for mutagenesis is given in the Table S-1. The annealing temperatures suggested by NEBaseChanger online were used for the polymerase chain reaction (PCR), which was performed according to the manufacturer's protocol. Obtained constructs were amplified in *E. coli* Top10 and used for heat-shock transformation of *E. coli* BL21 (DE3). The BsPAD variants BsPAD_WCP_Y11F, BsPAD_WCP_Y13F, BsPAD_WCP_Y19F, BsPAD_WCP_Y31F, BsPAD_WCP_W62F, BsPAD_WCP_Y122F, BsPAD_WCP_Y11F_Y13F_W17F_Y19F_Y31F_W62F_Y122F (BsPAD_WCP_7F), BsPAD_WCP_R41I, and BsPAD_WCP_R41L were ordered as synthetic genes as described above.

Table S-1. Primers used for the construction of the BsPAD variants.

Primer	Sequence (5'→3')	T _a [°C]
W17A_fw	TGAAAATGGTgcgGAATATGAAATCTATATC	57
W17A_rv	TAGGTATAGATCATATGGC	57
I85A_fw	GCATGGCATTgcgTTCCTTCCGAAATG	57
I85A_rv	ATACGTTTTTCATTCGGC	57
I85A_F87A_fw	GCATGGCATTgcgTTCGCGCCGAAATG	63
I85A_F87A_rv	ATACGTTTTTCATTCGGCATAAAATTC	63

F87A_fw	CATTATTTTCgcgCCGAAATGGGTTTCATG	58
F87A_rv	CCATGCATACGTTTTTCATTC	58
C100W_fw	AATTACCGTGtggTATCAGAATG	61
C100W_rv	TCCGGATGTTTCATGAACC	61
V124C_fw	GAAATATGTGtgtCCGGAATTTGCAGAAATTAC	57
V124C_rv	GGATAGGTTTCATATTTTTTCG	57
A147P_fw	TATTAGCAAAccgCCGTATGAAG	57
A147P_rv	ACTTCTTCATTATCAACGC	57

Protein expression

All BsPAD variants were produced recombinantly in *E. coli*. Pre-cultures (4 mL LB containing kanamycin) of *E. coli* BL21 (DE3) colonies harboring the constructs for the expression of the desired proteins were incubated overnight (37°C, 180 rpm). LB medium (50-200 mL containing kanamycin) was inoculated with 1% (v/v) of the preculture and incubated (37°C, 180 rpm) until it reached an OD₆₀₀ of 0.6. Protein expression was induced by the addition of isopropyl-β-D-thiogalactopyranoside (IPTG) to a final concentration of 0.5 mM followed by incubation for ~20 h at 18°C at 180 rpm. Cells were harvested by centrifugation at 10,000 × g and 4°C for 3 minutes, and cell pellets were resuspended with 4 mL of equilibration buffer per gram of cell pellet (50 mM potassium phosphate, 300 mM sodium chloride, 10 mM imidazole, pH 8.0). Cells were disrupted by sonication on ice (five cycles of 1 min sonication (30% intensity, 50% pulsed cycle)) using a SONOPULS HD 2070 (BANDELIN Electronic GmbH & Co. KG, Berlin, Germany), and the lysates were clarified by centrifugation at 10,000 × g and 4°C for 30 min. For purification, the crude lysates were applied to 1.5 mL Roti® Garose-His/Ni Beads (Carl Roth, Karlsruhe, Germany). The resins were washed with 15 mL washing buffer (50 mM sodium phosphate, 300 mM sodium chloride, 20 mM imidazole, pH 8.0) before target proteins were eluted with elution buffer (50 mM sodium phosphate, 300 mM sodium chloride, 250 mM imidazole, pH 8.0). Protein-containing fractions were pooled, 1 mM ethylenediaminetetraacetic acid added, and re-buffered in 50 mM KP, pH 7.5 using PD10 columns (GE Healthcare, Buckinghamshire, UK) to a final volume of 3.5 mL. Protein concentrations were determined using the NanoDrop1000™ (Thermo Fisher Scientific, Waltham, MA, USA), with molecular weights and extinction coefficients calculated by the ExPASy ProtParam tool.

PFE wild-type was expressed as previously reported⁶.

2.2 *In silico* experiments

MD simulations

Mutations were introduced into the BsPAD structure (PDB-ID 2P8G) and MD simulation was performed with YASARA (YASARA Biosciences, Vienna, Austria) using the AMBER14 force field. The simulated temperature was set to 328 K and a pH of 6.0 was used. Snapshots were taken every 100 ps during the 10 ns simulation. The snapshots were visualized using UCSF Chimera 1.14 (San Francisco, USA).

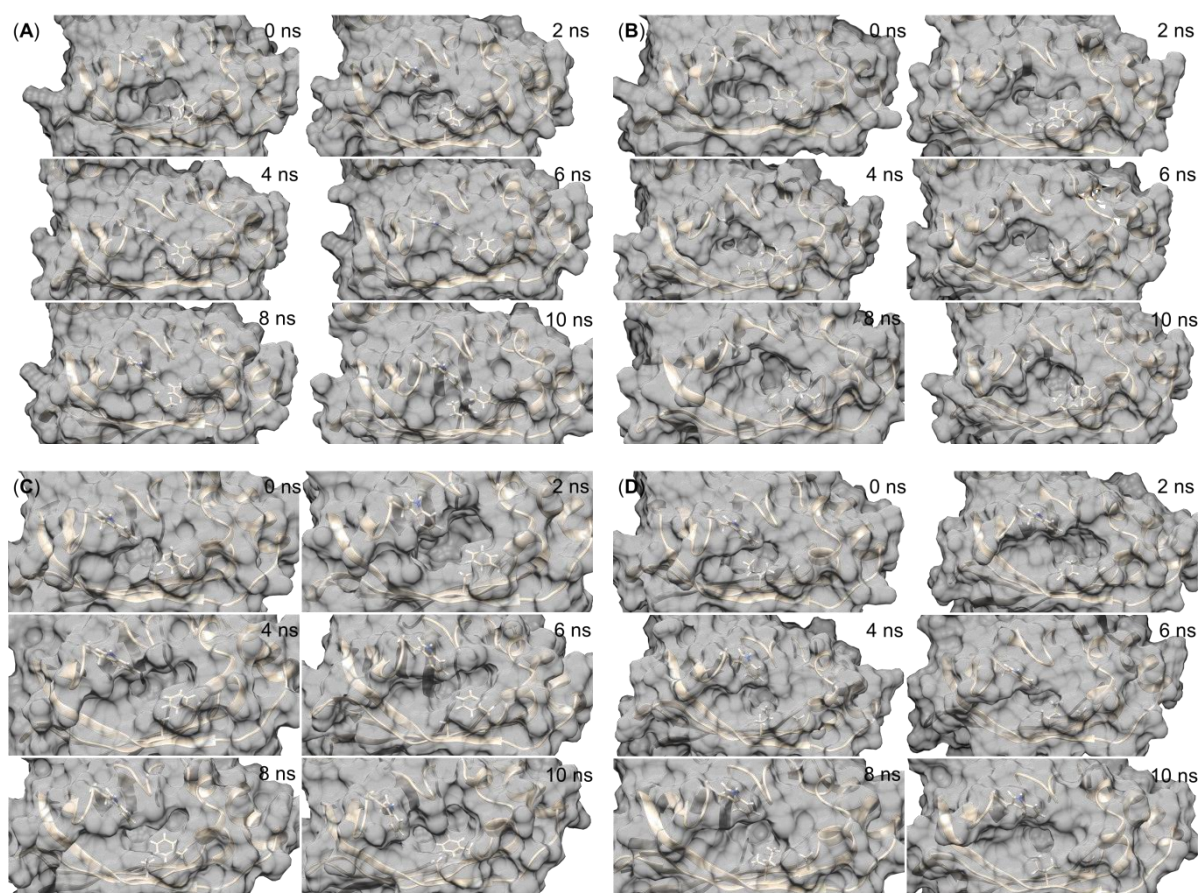


Figure S-2. Snapshots of BsPAD-MD simulations at different time points based on PDB 2P8G. **A)** MD simulation of WCP. **B)** MD simulation of WCP_W17A. **C)** MD simulation of WCP_I85A. **D)** MD simulation of WCP_F87A.

Molecular docking experiments

The docking of carbon dioxide into the crystal structure of the *Pseudomonas fluorescens* esterase I (PFE; PDB-ID 1VA4) or BsPAD (PDB-ID 2P8G) and the docking experiments of CO₂ was performed with YASARA (YASARA Biosciences, Vienna, Austria). 100 docking runs were performed using force field AMBER03. A simulation cell was defined at least 5 Å around all atoms of the crystal structure. The snapshots were visualized using UCSF Chimera 1.14 (San Francisco, USA).

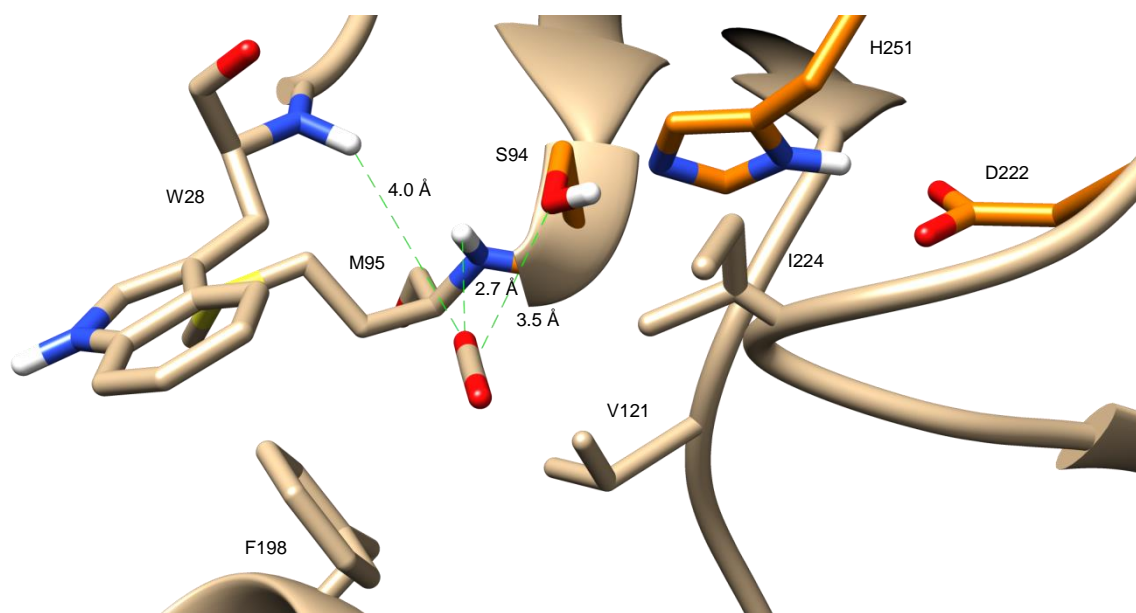


Figure S-3. Docking structure of carbon dioxide in PFE (PDB ID: 1VA4). The residues of the catalytic triad are highlighted in orange, and the distances to the oxyanion hole (W28 and M95 peptide backbone) and catalytic S94 are shown.

2.3 Enzyme loading with Fe-2 and analysis

For loading BsPAD_WCP with Fe-2, 1 mM dithiothreitol from a 1 M stock was added to the purified enzyme in loading buffer (50 mM NaPi, 300 mM NaCl, pH 6.0). After 30 min at 20°C and 160 rpm in the incubator (Infors HT, Infors AG, Bottmingen, Switzerland), the buffer was replaced with PD10 columns (GE Healthcare, Buckinghamshire, UK). To quantify the concentration of free thiols before loading, a sample of 20 μL was added to 255 μL of Ellman reagent (0.2 mM 5,5'-dithiobis-2-nitrobenzoic acid, 1 mM EDTA, 100 mM NaPi, pH 8.0) in a microtiter plate, incubated at RT for 15 minutes, and absorbance was measured at 412 nm. The reaction was performed in triplicate. Subsequently, 300 μL of the protein solution was withdrawn as an autooxidation control. Five equivalents of Fe-2 from a 50 mM stock solution in methanol was added to the residual solution. After incubation for 17 h at 20°C and 160 rpm, the buffer was exchanged for loading buffer and the concentration of free thiols was quantified, and the percentage of iron loading determined. Respective resulted loadings are provided in table S-4.

3. Photocatalytic CO₂ reduction

3.1 Photocatalytic setup

Three necked, double-wall vessels of 85 mL or 65 mL internal volume were used for photocatalytic experiments. One neck was used as a gas inlet with the help of a septum and a needle (A), a septum was adapted to the second neck and a valve was placed on top (B), the third neck was used as a gas outlet for the bubbling (C), and all vessels contained a plain borosilicate-glass window intended for light irradiation (D). Reaction temperature was controlled with the help of a thermostat (Phoenix 300). Photocatalytic experiments were carried out using Lumatec Superlite 400 Hg-lamps with different filters (400-700 nm, 320-400 nm, and 415 nm) and the light output for each reaction was measured using a Laserpoint Plus+ power meter with a thermopile detector.

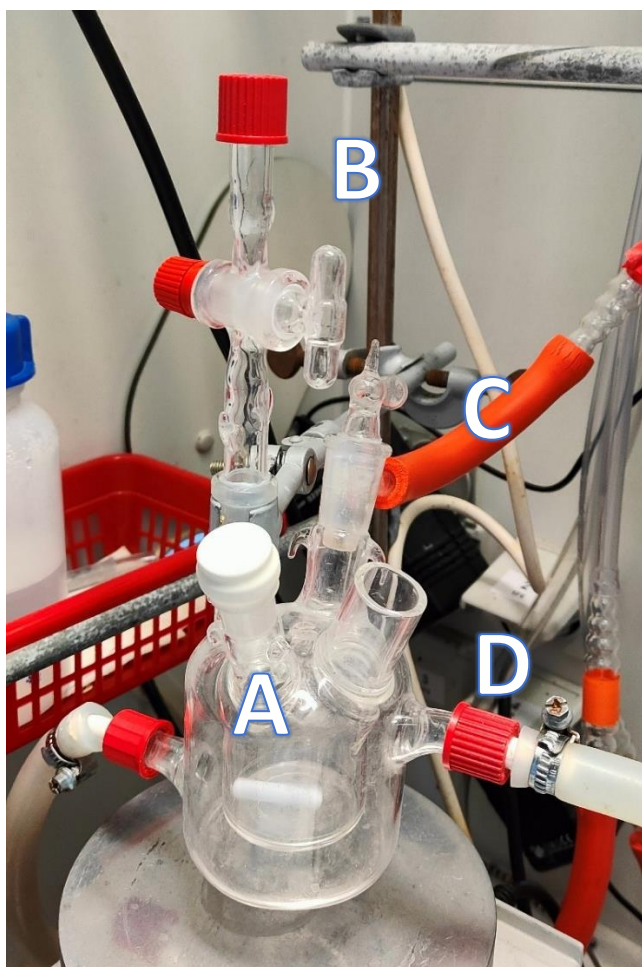


Figure S-4. Photocatalytic vessel. Total volume 85 mL, A) Gas inlet. B) Sampling valve. C) Gas outlet. D) Borosilicate-glass window.

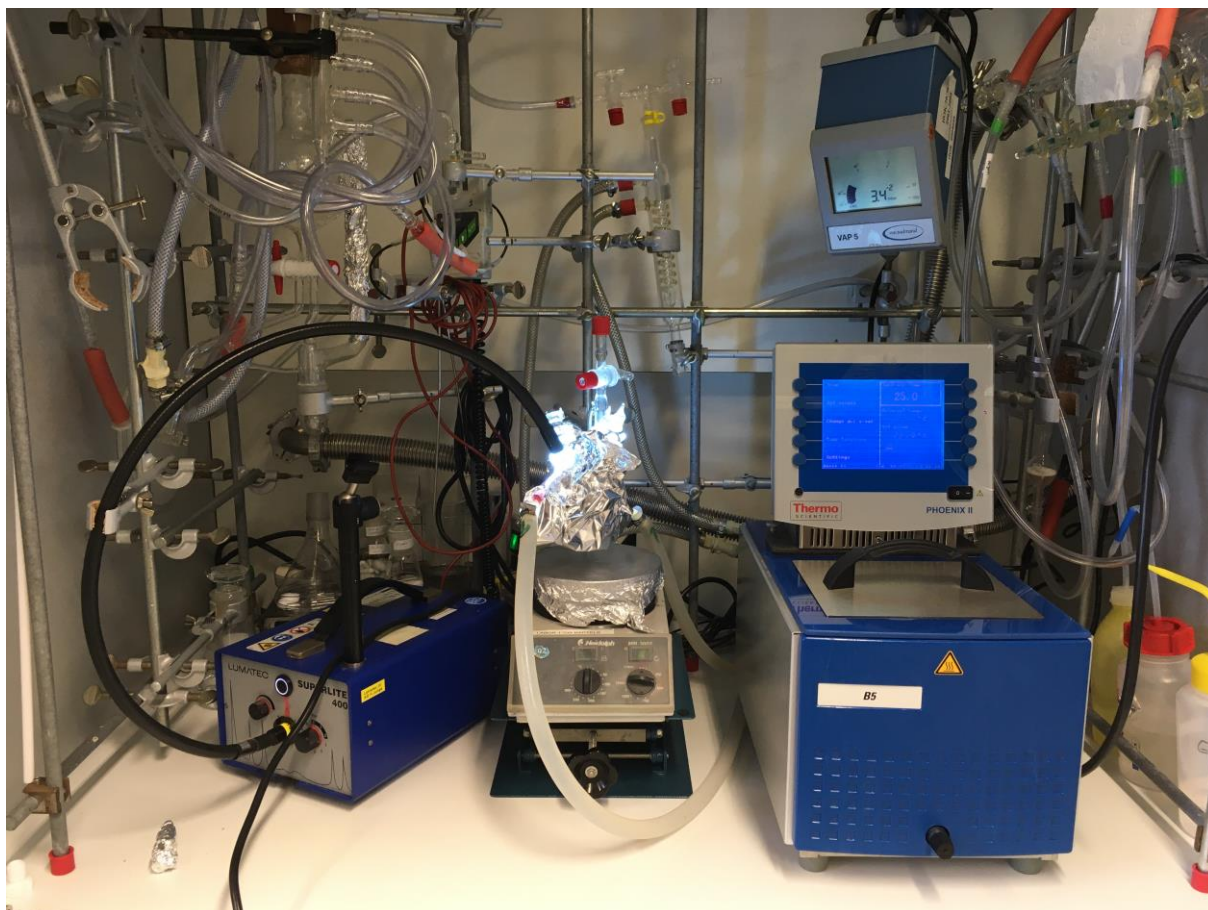


Figure S-5. Photocatalytic setup. Light was applied using a Lumatec lamp (left), temperature on the photocatalytic vessel was controlled using a thermostat (right).

3.2 Protocol for photocatalytic CO₂ reduction

The thermostat was connected to the photocatalytic vessel and temperature was set at 25°C for the whole procedure. Three cycles of vacuum and argon were performed through the gas outlet C (see Figure S-3) connected directly to a Schlenk line, and then three cycles of vacuum and carbon dioxide (4.8 purity) were performed using vacuum on the outlet C and introducing carbon dioxide through inlet A using a needle.

For a typical photocatalytic experiment three different solutions were prepared:

- Buffer solution: Solution was prepared on an Erlenmeyer flask using 84 mg of NaHCO₃ (1 mmol) and 99 mg of sodium ascorbate (0.5 mmol) in 9 mL distilled water. Solution must be freshly prepared before each experiment, due to light sensitivity of sodium ascorbate.
- Photosensitizer solution: 7.49 mg of [Ru(bpy)₃Cl₂] (1 μmol) were dissolved in distilled water under inert atmosphere conditions, and solution was mildly bubbled with argon for 10 minutes.
- Enzyme/catalyst solution: Enzymes were provided in a sodium phosphate buffer (0.05 M), and the range of concentrations was between 9.3 and 350 μM.

The buffer solution was introduced under carbon dioxide atmosphere and bubbled using a 0.8 x 120 mm hypodermic needle. Bubbling of the solution was kept under mild conditions (avoiding

evaporation of the solvent) for at least 30 minutes. During the bubbling time, 1 mL of photosensitizer solution was added to the reaction mixture. Catalyst was added employing micropipettes (when necessary) as the last step. Once the bubbling time was finished, the system was closed at atmospheric pressure and light was applied to the vessel through a borosilicate-glass window employing a mercury lamp (Lumatec SuperLite 400, 400-700 nm, 1.5 W). Lamp was turned off after 3 hours.

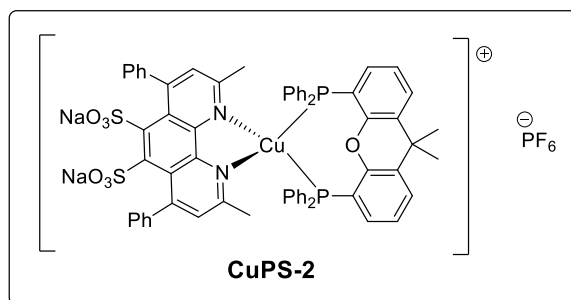
After irradiation was stopped, a 5 mL gas sample from the headspace was taken and analyzed by gas chromatography. The solution was analyzed by ^1H NMR using dimethylformamide (DMF) as internal standard in D_2O .

3.3 Transferring photocatalytic reaction to fully aqueous media

Reaction conditions: 10 mL total solvent were used for all cases (Volume of headspace = 75 mL). Catalyst was added in NMP solution to achieve a final concentration of 100 μM for most cases. The photosensitizer CuPS-2 was dissolved directly using the solvent of choice. Addition of 220 mg 1,3-dimethyl-2-phenyl-2,3-dihydro-1H-benzimidazole (BIH) was performed directly to the photocatalytic vessel. NaHCO_3 (0.1 M) and NaAscH (0.1 M) were employed in all cases. The reaction mixture was bubbled with carbon dioxide for 30 minutes prior to irradiation. Light output: 1.5W (400-700 nm). Reaction time: 5 hours.

Table S-2. Carbon dioxide photocatalytic reduction in aqueous media							
$2 \text{CO}_2 + \text{BIH} \xrightarrow[\text{Solvent}]{\text{Cat (100 } \mu\text{M), CuPS-2 (500 } \mu\text{M), 1.5W (400-700nm), 5h}} \text{CO} + \text{BI}^{\oplus} + \text{HCO}_3^{\ominus}$							
#	Cat	Additives	Solvent	$n\text{H}_2$ (μmol)	$n\text{CO}$ (μmol)	Select. (%)	TON CO
1	Fe-1	-	H_2O	31	5.3	15	5.3
2 ^a	Fe-1	10 μmol of TBAI	$\text{H}_2\text{O}/\text{NMP}$ (9:1)	1.5	7.1	83	7.1
3 ^a	Fe-1	CuPS-1 + 10 μmol TBAI	$\text{H}_2\text{O}/\text{NMP}$ (9:1)	<0.32	3.7	92	3.7
4 ^a	Fe-1	Water. SD = NaAscH/ NaHCO_3 (0.1 M) TBAI (0.01 M). No BIH	$\text{H}_2\text{O}/\text{NMP}$ (9:1)	0.6	8.0	93	8.0
5 ^b	Fe-1	Water. SD = NaAscH/ NaHCO_3 (0.1 M). TBAB (0.01 M). No BIH	$\text{H}_2\text{O}/\text{NMP}$ (9:1)	3.0	7.3	71	7.3
6	Fe-1	No BIH. Triethanolamine (0.1 M)	$\text{H}_2\text{O}/\text{NMP}$ (9:1)	<0.32	3.7	92	3.7
7	Fe-1	Low concentration of Cat (5 μM)	H_2O	10	0.6	5.6	12

- a) Tetrabutylammonium iodide was added directly to the reaction mixture to achieve a final concentration of 1 mM (for entries 2-3). For entry 4, 100 μmol TBAI were added.
- b) Tetrabutylammonium bromide was tested under the same conditions as entry 4.

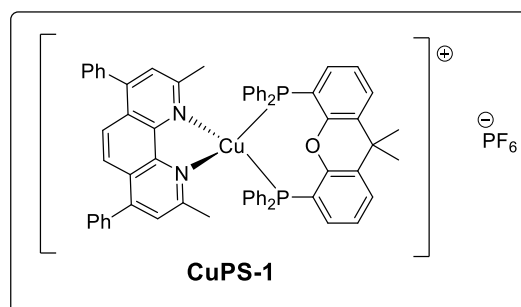


3.4 Application of Fe-1 and Fe-2 in photocatalytic CO₂ reduction in NMP

Reaction conditions: 10 mL NMP were used in all cases (volume of headspace = 75 mL). [Cat] = 100 μM. [CuPS-1] = 500 μM. BIH = 0.1 M. Reaction mixture was bubbled with carbon dioxide for 30 minutes prior to irradiation. Light output: 1.5W (400-700 nm). Reaction time: 5 hours.

Table S-3. Evaluation of iron cyclopentadienone complexes as catalysts for CO₂ photocatalytic reduction						
$2 \text{ CO}_2 + \text{Catalyst} \xrightarrow[\text{NMP}]{\text{Cat (100 } \mu\text{M), CuPS-1 (500 } \mu\text{M), 1.5W (400-700nm), 5h}} \text{CO} + \text{Catalyst} + \text{HCO}_3^-$						
#	Cat	Structure	nH ₂ (μmol)	nCO (μmol)	Select. (%)	TON CO
1	Fe-1		1.2	410	>99	410
2	Fe-2		2.6	118	98	118

*CuPS-1 = Molecularly defined [Cu(xantphos)(bcp)]PF₆, structure shown below. Reaction volume: 10 mL for all cases. Bubbling with CO₂ was performed for 30 minutes.



3.5. Application of BsPAD derivatives and Fe-2 modified BsPAD derivatives in photocatalytic CO₂ reduction in H₂O

Docking studies of the Fe complex suggested that some of the bulky residues in the entry site of WCP need to be replaced by alanine to allow binding of the complex in close proximity to the CO₂-binding pocket (data not shown). Therefore, W17, I85, and F87 were replaced with alanine and all combinatorial mutants were created to allow proper alignment of the metal complex in the active site. The modification of all these protein scaffolds was successful and lead to soluble expressed protein in *E. coli*. Their photocatalytic carbon dioxide reduction activity was demonstrated, however, this did not lead to improved productivities compared to the respective mutated enzymes without the Fe complex (Table S-4).

Table S-4. Photocatalytic carbon dioxide reduction employing ArMs and BsPAD modified enzymes						
Cat (5 μM), RuPS (100 μM) NaHCO ₃ (0.1M), NaAsch (0.05M) $\text{CO}_2 \xrightarrow[1.5\text{W (400-700nm), 3h}]{\text{CO}_2 \rightarrow \text{CO}}$						
#	Enzyme	Fe-2 loading (%)	nH ₂ (μmol)	nCO (μmol)	Select. (%)	TON CO
1	BsPAD_WCP	-	<0.32	1.48	82	28
2	BsPAD_WCP@Fe-2	55	0.33	1.45	81	29
3	BsPAD_WCP_W17A	-	0.51	3.90	88	78
4	BsPAD_WCP_W17A@Fe-2	88	1.20	1.59	57	32
5	BsPAD_WCP_I85A	-	0.32	3.12	91	62
6	BsPAD_WCP_I85A@Fe-2	75	<0.32	1.46	82	29
7	BsPAD_WCP_F87A	-	<0.32	2.40	88	48
8	BsPAD_WCP_F87A@Fe-2	38	1.38	2.05	60	41
9	BsPAD_WCP_W17A_I85A	-	<0.32	1.33	81	27
10	BsPAD_WCP_W17A_I85A@Fe-2	59	<0.32	0.88	63	18
11	BsPAD_WCP_W17A_F87A	-	<0.32	2.21	87	44
12	BsPAD_WCP_W17A_F87A@Fe-2	80	<0.32	0.98	75	20
13	BsPAD_WCP_I85A_F87A	-	<0.32	2.13	87	42
14	BsPAD_WCP_I85A_F87A@Fe-2	20	3.54	2.03	37	41
15	BsPAD_WCP_W17A_I85A_F87A	-	<0.32	2.32	88	46
16	BsPAD_WCP_W17A_I85A_F87A@Fe-2	44	<0.32	1.54	83	31
17	-	-	<0.32	0.33	51	-

Fe-2 loading was determined using Ellman's test for quantification of free thiol residues. Reaction conditions: 10 mL H₂O were used in all cases (volume of headspace = 75 mL). [Enzyme] = 5 μM. [Ru(bpy)₃Cl₂] = 100 μM. NaHCO₃ (0.1 M) and NaAsch (0.05 M) were employed in all cases. The reaction mixture were bubbled with carbon dioxide for 30 minutes prior to irradiation. Light output: 1.5 W (400-700 nm). Reaction time: 3 hours.

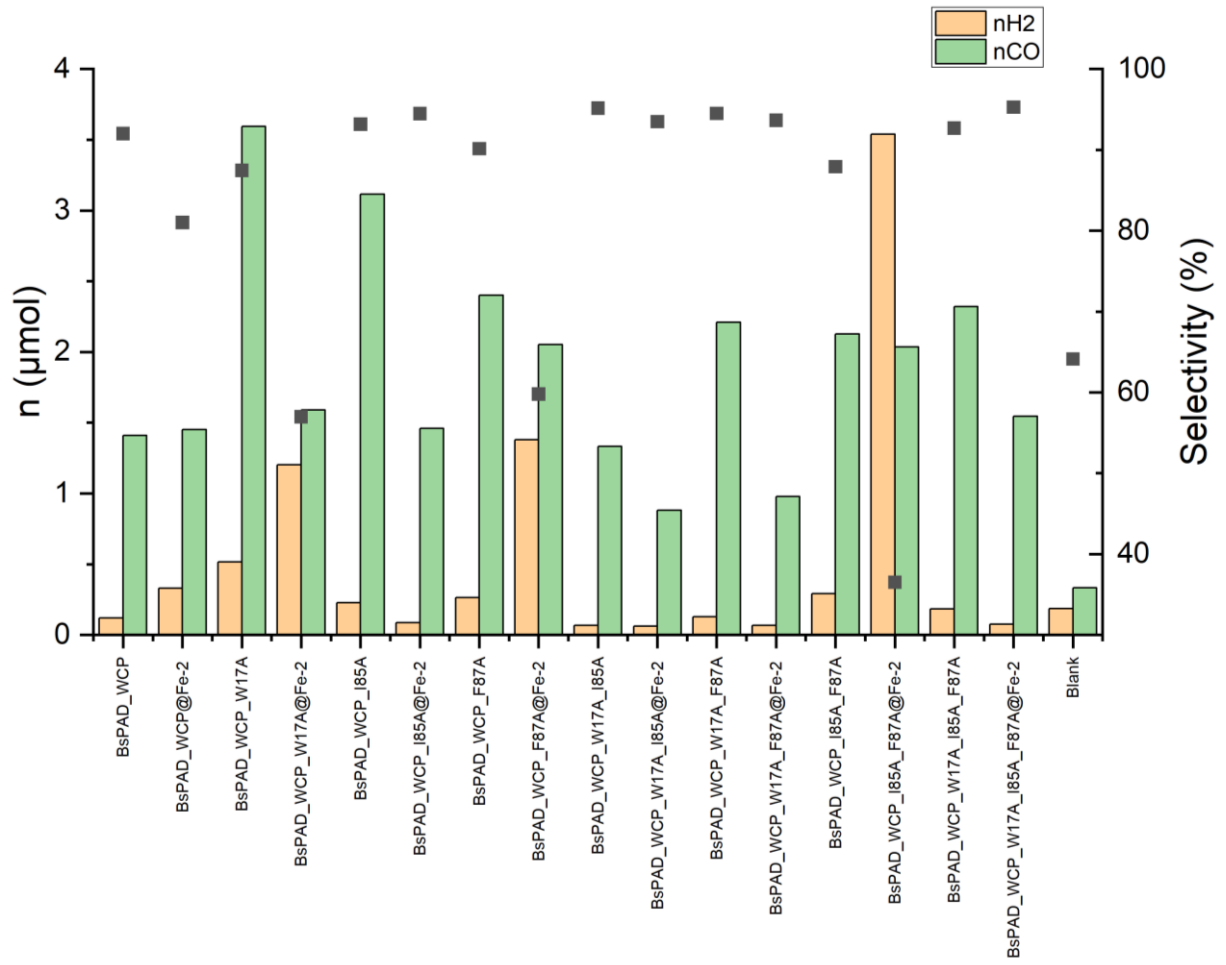


Figure S-6. Graphical representation of Table S-4.

3.6. Aqueous photocatalytic CO₂ reduction in the presence of potential enzyme impurities

Reaction conditions: 10 mL H₂O were used for all cases (volume of headspace = 75 mL). [Ru(bpy)₃Cl₂] = 100 μM. NaHCO₃ (0.1 M) and NaAscH (0.05 M) were employed in all cases. The reaction mixtures were bubbled with carbon dioxide for 30 minutes prior to irradiation. Light output: 1.5 W (400-700 nm). Reaction time: 3 hours.

#	Conditions	nH ₂ (μmol)	nCO (μmol)	Select. (%)	TON CO
1	BsPAD_WCP (5μM)	<0.32	1.41	82	28
2 ^a	50 mM Sodium phosphate buffer pH 7.5	4.34	0.32	7	-
3 ^a	Phosphate buffer as solvent + Imidazole (1 mM)	<0.32	0.51	61	-
4	Imidazole (5 μM)	<0.32	0.73	70	-
5	NiCl ₂ (1 mM)	<0.32	0.50	61	-

a) NaHCO₃ was not employed in these reactions.

3.7. Aqueous photocatalytic CO₂ reduction applying potential alternative compounds to BsPAD (Bovine Serum Albumin, amino acids)

Reaction conditions: 10 mL H₂O were used for all cases (volume of headspace = 75 mL). [Ru(bpy)₃Cl₂] = 100 μM. NaHCO₃ (0.1 M) and NaAsCH (0.05 M) were employed in all cases. The reaction mixtures were bubbled with carbon dioxide for 30 minutes prior to irradiation. Light output: 1.5 W (400-700 nm). Reaction time: 3 hours.

#	Conditions	nH ₂ (μmol)	nCO (μmol)	Select. (%)	*TON CO
1	BSA (5 μM)	<0.32	0.59	65	12
2	Lysine (0.05 M)	<0.32	0.27	46	-
3	Arginine (0.05 M)	<0.32	0.30	48	-

*Calculated based on the added compound (BSA, lysine or arginine)

3.8. Control experiment: Decarboxylation of ferulic acid by BsPAD_WT

Reaction conditions: 10 mL H₂O were used for all cases (volume of headspace = 75 mL). [Ru(bpy)₃Cl₂] = 100 μM. NaHCO₃ (0.1 M) and NaAsCH (0.05 M) were employed in all cases. The reaction mixtures were bubbled with carbon dioxide for 30 minutes prior to irradiation. Light output: 1.5 W (400-700 nm). Reaction time: 3 hours.

#	Conditions	nH ₂ (μmol)	nCO (μmol)	Select. (%)	TON CO
1	BsPAD_WT (5μM)	<0.32	1.47	82	29
2	BsPAD_WT (5μM) + Ferulic acid (10 mM)	<0.32	1.08	77	22



After irradiation, 500 μmol DMF were added to the reaction mixture as internal standard. Next, 100 μL of the reaction mixture were transferred to an NMR tube and 500 μL D₂O were added. No signals corresponding to ferulic acid were found in the NMR analysis, assuming that it was all converted to 4-vinylguaiacol, which in fact can be detected in a similar concentration as the starting material (10 mM).

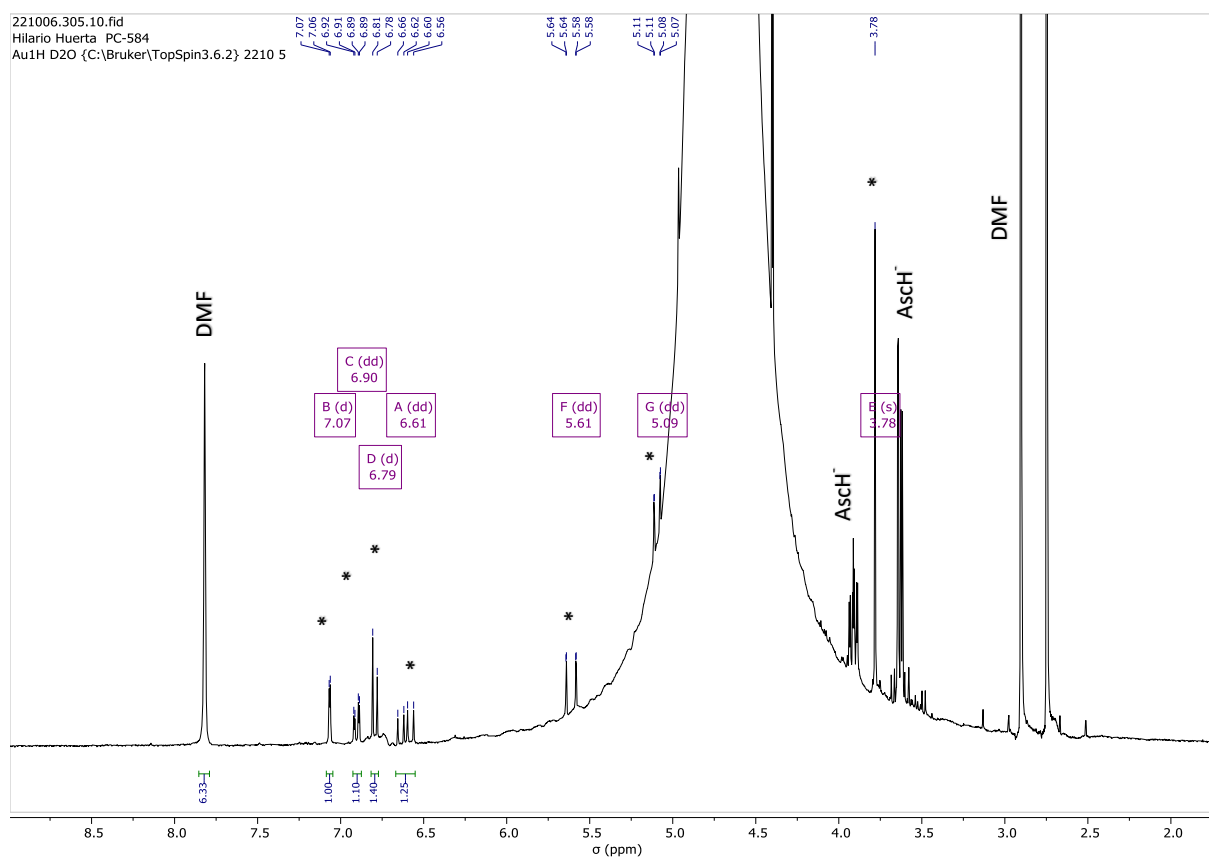


Figure S-7. NMR spectra for photocatalytic CO₂ reduction employing BsPAD_WT in the presence of 10 mM ferulic acid. Purple boxes are only indicated for the product 4-vinylguaiacol.

3.9. Control experiment: aqueous photocatalytic CO₂ reduction using heat treated BsPAD_WT

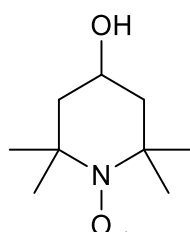
Reaction conditions: 10 mL H₂O were used for all cases (Volume of headspace = 75 mL). [Enzyme] = 5 μM. [Ru(bpy)₃Cl₂] = 100 μM. NaHCO₃ (0.1 M) and NaAsCH (0.05 M) were employed in all cases. The reaction mixtures were bubbled with carbon dioxide for 30 minutes prior to irradiation. Light output: 1.5 W (400-700 nm). Reaction time: 3 hours.

Table S-8. Control experiments for aqueous photocatalytic CO ₂ reduction					
#	Catalyst	nH ₂ (μmol)	nCO (μmol)	Select. (%)	TON CO
1	BsPAD_WCP	<0.32	1.41	82	28
2	Heat treated BsPAD_WCP	<0.32	0.57	64	11

3.10. Poisoning experiment applying hydroxy TEMPO

Reaction conditions: 10 mL H₂O were used for all cases (volume of headspace = 75 mL). [Ru(bpy)₃Cl₂] = 100 μM. NaHCO₃ (0.1 M) and NaAsCH (0.05 M) were employed in all cases. Hydroxy-TEMPO (1.72 mg) was added directly as solid and completely dissolved in the reaction mixture. The reaction mixtures were bubbled with carbon dioxide for 30 minutes prior to irradiation. Light output: 1.5 W (400-700 nm). Reaction time: 3 hours.

Table S-9. Poisoning experiment employing hydroxy TEMPO					
#	Catalyst	nH ₂ (μmol)	nCO (μmol)	Select. (%)	TON CO
1	BsPAD_WCP (5μM)	<0.32	1.41	82	28
2	BsPAD_WCP (5μM) + Hydroxy-TEMPO (1mM)	<0.32	0.88	73	17.6



4-hydroxy TEMPO

3.11 Carbon dioxide binding enzymes (wild types) tested in photocatalytic CO₂ reduction

Procedure for the expression of the enzymes used

All enzymes except carbonic anhydrase (>95% purity, >3,500 U/mg; Sigma-Aldrich, Saint Louis, MO, USA) were produced recombinantly in *E. coli*. Pre-cultures (4 mL LB containing kanamycin) of *E. coli* BL21 (DE3) colonies harboring the constructs for the expression of the desired proteins were incubated overnight (37°C, 180 rpm). Proteins are either expressed in 50 mL LB medium, 100 mL LB medium as described above (Section 2.1) or using an autoinduction expression protocol: 150 mL LB medium was supplemented with 0.5 g/L glucose and 2 g/L lactose (Table S-10). After inoculation with 1% (v/v) of the appropriate preculture, cells were grown at 37°C for 4 h and another 72 h at 15°C (140 rpm). The purification was performed described above (Section 2.1). After buffer exchange, 3.5 mL of protein solution was generated in both expression batches. The protein concentrations are listed in Table S-10.

Table S-10. Details about enzyme batches applied in photocatalytic CO₂ reduction and expression levels

#	Enzyme	Concentration (expression levels) of the first expression batch	Concentration (expression levels) of the second expression batch
1	BsPAD_WT	242 μM (8.47 μmol _{Enzyme} /L _{Medium} ^a)	-
2	EcPanD	25.9 μM (1.81 μmol _{Enzyme} /L _{Medium} ^b)	123.4 μM (2.88 μmol _{Enzyme} /L _{Medium} ^c)
3	PFE	15.8 μM (1.11 μmol _{Enzyme} /L _{Medium} ^b)	-
4	SsTrpC	12.2 μM (2.12 μmol _{Enzyme} /L _{Medium} ^b)	29.2 μM (0.68 μmol _{Enzyme} /L _{Medium} ^c)
5	MmPPP2	19.3 μM (1.35 μmol _{Enzyme} /L _{Medium} ^b)	
6	ScFDC1	28.7 μM (0.67 μmol _{Enzyme} /L _{Medium} ^c)	
7	TtALS	20.4 μM (1.43 μmol _{Enzyme} /L _{Medium} ^b)	
8	EcPPC	9.3 μM (0.22 μmol _{Enzyme} /L _{Medium} ^c)	
9	BtCA	68.7 μM (commercial enzyme)	-

a) Expression volume: 100 mL LB medium

b) Expression volume: 50 mL LB medium

c) Expression volume: 150 mL LB autoinduction medium

4. State of the art of relevant systems in aqueous homogeneous photocatalytic CO₂ reduction

Catalyst (μM)	Photosensitizer (μM)	Sacrificial donor (M)	Solvent	CO (μmol)	Selectivity (%)	TON (h)	Corr. Author References
Co(pTMpyP) (5)	Cu complex (500)	NaAsCH (0.1)	NaHCO ₃ aq. buffer	200	90	4000 (12)	Sakai ⁷
Co(pTPPS) (10)	[Ru(bpy) ₃] ²⁺ (500)	NaAsCH (0.1)	NaHCO ₃ aq. buffer	92	82	926 (4)	Sakai ⁸
CODH (<0.1nmol)	CdS	MES (0.35)	MES aq. buffer	2	n.r.	22,500	Armstrong ⁹
CODH (117)	RuP/TiO ₂	MES (0.2)	MES aq. buffer	6	n.r.	2100	Armstrong/Reisner ¹⁰
Ni(cyclam)@Cu-Azurin (4)	[Ru(bpy) ₃] ²⁺ (1000)	NaAsCH (0.1)	Phosphate aq. buffer	0.12	n.r.	38 (2)	Shafaat ¹¹
BsPAD_WCP_W17A (1)	[Ru(bpy) ₃] ²⁺ (100)	NaAsCH (0.05)	NaHCO ₃ aq. buffer	1.96	81	196 (3)	This work
BsPAD_WCP_W17A (5)				3.94	89	78 (3)	
Carbonic anhydrase	[Ru(bpy) ₃] ²⁺ (100)	NaAsCH (0.05)	NaHCO ₃ aq. buffer	2.19	68	219 (3)	This work

5. References:

- 1 Rosas-Hernández, A., Steinlechner, C., Junge, H. & Beller, M. Earth-abundant photocatalytic systems for the visible-light-driven reduction of CO₂ to CO. *Green Chem.* **19**, 2356-2360 (2017). <https://doi.org:10.1039/c6gc03527b>
- 2 Kariyawasam, K. *et al.* Artificial iron hydrogenase made by covalent grafting of Knölker's complex into xylanase: Application in asymmetric hydrogenation of an aryl ketone in water. *Biotechnol. Appl. Biochem.* **67**, 563-573 (2020). <https://doi.org:10.1002/bab.1906>
- 3 Luo, S. P. *et al.* Photocatalytic water reduction with copper-based photosensitizers: a noble-metal-free system. *Angew. Chem., Int. Ed.* **52**, 419-423 (2013). <https://doi.org:10.1002/anie.201205915>
- 4 Karnahl, M. *et al.* Photocatalytic hydrogen production with copper photosensitizer-titanium dioxide composites. *ChemCatChem* **6**, 82-86 (2014). <https://doi.org:10.1002/cctc.201300459>
- 5 Marx, M. *et al.* Addressing the reproducibility of photocatalytic carbon dioxide reduction. *ChemCatChem* **12**, 1603-1608 (2020). <https://doi.org:10.1002/cctc.201901686>
- 6 Schliessmann, A., Hidalgo, A., Berenguer, J. & Bornscheuer, U. T. Increased enantioselectivity by engineering bottleneck mutants in an esterase from *Pseudomonas fluorescens*. *ChemBioChem* **10**, 2920-2923 (2009). <https://doi.org:10.1002/cbic.200900563>
- 7 Zhang, X., Yamauchi, K. & Sakai, K. Earth-abundant photocatalytic CO₂ reduction by multielectron chargeable cobalt porphyrin catalysts: High CO/H₂ selectivity in water based on phase mismatch in frontier MO association. *ACS Catal.* **11**, 10436-10449 (2021). <https://doi.org:10.1021/acscatal.1c02475>
- 8 Call, A. *et al.* Highly efficient and selective photocatalytic CO₂ reduction to CO in water by a cobalt porphyrin molecular catalyst. *ACS Catal.* **9**, 4867-4874 (2019). <https://doi.org:10.1021/acscatal.8b04975>
- 9 Chaudhary, Y. S. *et al.* Visible light-driven CO₂ reduction by enzyme coupled CdS nanocrystals. *Chem. Commun.* **48**, 58-60 (2012). <https://doi.org:10.1039/c1cc16107e>
- 10 Woolerton, T. W. *et al.* Efficient and clean photoreduction of CO₂ to CO by enzyme-modified TiO₂ nanoparticles using visible light. *J. Am. Chem. Soc.* **132**, 2132-2133 (2010).
- 11 Schneider, C. R. & Shafaat, H. S. An internal electron reservoir enhances catalytic CO₂ reduction by a semisynthetic enzyme. *Chem. Commun.* **52**, 9889-9892 (2016). <https://doi.org:10.1039/c6cc03901d>

Article II

Spectrophotometric and fluorimetric high-throughput assays for phenolic acid decarboxylase

Henrik Terholsen^{‡[a]}, Kamela Myrtollari^{‡[b][c]}, Mirna Larva^[b], Christina Möller^[a], Robert Kourist^[b], Uwe T. Bornscheuer^{*[a]}, Daniel Kracher^{*[b]}.

[a] University of Greifswald, Biotechnology and Enzyme Catalysis, Felix-Hausdorff-Straße 4, 17487 Greifswald, Germany

[b] Graz University of Technology, Institute of Molecular Biotechnology, Petersgasse 14, 8010 Graz, Austria

[c] Henkel AG & Co. KGaA, Adhesive Research/Bioconjugates, Henkelstraße 67, 40191 Düsseldorf, Germany

*Corresponding authors: uwe.bornscheuer@uni-greifswald.de & daniel.kracher@tugraz.at

‡ These authors contributed equally to this work.

ABSTRACT: Biocatalytic decarboxylation of hydroxycinnamic acids yields *p*-vinylphenol derivatives, which are important precursors for antioxidants, epoxy coatings, adhesives and other polymeric materials. *Bacillus subtilis* decarboxylase (*BsPAD*) is a cofactor-independent enzyme that catalyzes the cleavage of carbon dioxide from *p*-coumaric-, caffeic-, and ferulic acid with high catalytic efficiency. Current methods to biochemically characterize the decarboxylation reactions rely on HPLC, mass spectrometry, gas chromatography, or NMR, which require extensive sample workup while measuring only endpoint concentrations. This work presents two robust and sensitive assays based on photometry and fluorimetry that allow following decarboxylation reactions with high sensitivity while avoiding product extraction and long analysis times. Optimized assay procedures were used to measure *BsPAD* activity in cell lysates and to determine the kinetic constants (K_M and V_{max}) of the purified enzyme for *p*-coumaric-, caffeic- and ferulic acid.

INTRODUCTION

Hydroxycinnamates are a ubiquitous class of natural phenols with diverse biological roles. They are important building blocks that contribute to the rigidity of plant cell walls by connecting hemicelluloses to lignin¹. Due to their broad natural abundance and antimicrobial activity, many organisms have developed strategies to degrade hydroxycinnamic acids, e.g. via direct reduction², CoA conjugation of hydroxycinnamates^{3,4}, or decarboxylation^{5,6}. Phenolic acid decarboxylases (PADs) convert hydroxycinnamates to the corresponding 4-vinylphenol (4VP) derivatives, which also serve as value-added flavor and fragrance compounds^{7,8}, e.g. in fermented foods like wine and beer^{9,10} or as precursors for epoxy-coatings, adhesives, and other polymeric materials^{11,12}. PADs have gained academic and industrial attention because they can be used to directly valorize phenolic acids from natural resources^{13–19}. Several PADs have been discovered and characterized over the past decades and have been used for various biotransformation reactions^{14,15,20–22}. However, the biochemical and kinetic characterization of these enzymes has mainly relied on HPLC analyses, or NMR-, MS-, or GC- methods for product quantification^{15,19–21,23–29}, which are time-consuming and largely unsuitable for application in high-throughput screenings (HTS). In addition to these commonly used analysis methods, UV-vis detection of hydroxycinnamate substrates has been used in a few cases^{30–35}. For example, spectral shifts in the UV range upon substrate decarboxylation

have been used to measure PAD activity in stopped assays³⁰ or to screen a PAD library generated by site-saturation mutagenesis³⁶. However, the overlapping UV absorbance spectra of the hydroxycinnamates and their corresponding 4VP derivatives complicate kinetic measurements. Here, we present an improved UV-absorbance assay and a novel fluorimetric assay that overcome these issues by using non-overlapping spectral and fluorescent features to detect hydroxycinnamate products. Both assays allow fast evaluation of decarboxylation reactions while avoiding time-consuming workup procedures such as product extraction. Kinetics of natural substrates of phenolic acid decarboxylase from *Bacillus subtilis* (*BsPAD*), namely ferulic acid (FA), coumaric acid (CuA), and caffeic acid (CaA), were successfully measured with both assay procedures. Compared to currently used methods, the photometric and fluorimetric decarboxylase assays offer the advantage of greatly reduced sample analysis times, making these procedures suitable for HTS and biochemical applications.

MATERIALS AND METHODS

Chemicals

All chemicals were purchased from commercial suppliers (Sigma-Aldrich, TCI, Roth, VWR) at the highest purity available. 4-Vinyl phenol (10% (w/w) in propylene glycol) and 4-vinyl guaiacol (>98% purity) were purchased from Sigma-Aldrich (St. Louis, MO,

USA). 4-Vinyl catechol (with 1% (w/w) BHT) was obtained from Toronto Research Chemicals (Toronto, ON, Canada).

Protein preparation

Precultures (4 mL LB containing kanamycin) of *E. coli* BL21 (DE3) colonies harboring the pET28a constructs (Gene ID: 938579)¹⁶ for the expression of wild-type BsPAD with an N-terminal 6xHis-tag were incubated overnight (37°C, 180 rpm). LB medium (200 mL containing 50 µg/mL kanamycin) was inoculated with 1% (v/v) of the preculture and incubated at 37°C and 180 rpm until it reached an OD₆₀₀ of 0.6. Protein expression was induced by the addition of isopropyl-β-D-thiogalactopyranoside (IPTG) to a final concentration of 0.5 mM, followed by incubation for 20 h at 20°C and 180 rpm. Cells were harvested by centrifugation at 10,000 × g and 4°C for 3 minutes, and cell pellets were resuspended with 4 mL of equilibration buffer per gram of cell pellet (50 mM potassium phosphate, 300 mM sodium chloride, 10 mM imidazole, pH 8.0). Cells were disrupted by sonication on ice (two cycles of 5 min sonication (30% intensity, 50% pulsed cycle)) using a SONOPULS HD 2070 (BANDELIN Electronic GmbH & Co. KG, Berlin, Germany), and the lysates were clarified by centrifugation at 10,000 × g and 4°C for 30 min. For purification, the crude lysates were applied to 1.5 mL Roti[®] Agarose-His/Ni Beads (Carl Roth, Karlsruhe, Germany). The resins were washed with 15 mL washing buffer (50 mM sodium phosphate, 300 mM sodium chloride, 20 mM imidazole, pH 8.0) before target proteins were eluted with elution buffer (50 mM sodium phosphate, 300 mM sodium chloride, 250 mM imidazole, pH 8.0). Protein-containing fractions were pooled and re-buffered in 50 mM sodium phosphate buffer (NaP_i) pH 6.0 using PD10 columns (GE Healthcare, Buckinghamshire, UK). Protein concentration was determined using the NanoDrop1000[™] (Thermo Fisher Scientific, Waltham, MA, USA), and molecular weight and extinction coefficient were calculated by the ExPASy ProtParam tool (<https://web.expasy.org/protparam/>)³⁷ using the mature protein sequence of BsPAD.

UV-Vis spectra of hydroxycinnamic acids

Electronic absorption spectra of FA, CaA, and CuA and 4-vinyl guaiacol (4VG), 4-vinyl phenol (4VP) and 4-vinyl catechol (4VC) (0.5 mM) were recorded at room temperature (21°C) on a BioTek Synergy HTX plate reader (Agilent Technologies, USA) from 220 to 700 nm.

Fluorescence spectra of hydroxysterene products

The fluorescence emission spectra (300 to 400 nm, 2 nm steps) of 4VG (20 µM), 4VP (20 µM), and 4VC (10 µM) in the presence of 0.5 mM FA, CaA, and CuA, respectively, were acquired using TecanReader infinite M200PRO (Tecan Trading AG, Männedorf, Switzerland). The fluorescence was excited at 258, 254, and 258 nm for 4VG, 4VP, and 4VC, respectively. All samples were prepared in 50 mM NaP_i pH 6.0 with 10% (v/v) acetonitrile.

High-performance liquid chromatography (HPLC) measurements

Decarboxylation reactions were analyzed on an Agilent 1200 Gradient HPLC System (Agilent Technologies, Austria) connected to a reversed-phase Nucleodur C18 Pyramid column (5 µm, 250 ×

4.6 mm; Macherey Nagel, Germany). The absorption of residual hydroxycinnamic acids was followed at 305 nm using a DAD detector. An isocratic HPLC method using a mixture of ddH₂O and acetonitrile (40% (v/v); flow rate: 1 mL/min) was used. Samples from enzymatic conversions (150 µL) were mixed with 150 µL of acetonitrile to quench the reaction. Calibration standards (0.5 – 10 mM) were prepared in the measurement buffer (50 mM NaP_i pH 6.0) and analyzed in triplicates.

Fluorescence assay procedure

Enzyme reactions were performed in 96-well plates at room temperature (21°C) and had a total volume of 200 µL. Reactions were started by mixing 20 µL of a BsPAD solution (0.25, 1, 4, or 60 µg/mL) with the respective substrate solution in 50 mM NaP_i at pH 6.0. The final substrate concentrations ranged from 0.05 mM to 3.2 mM FA, CaA and CuA. All reactions were carried out in triplicates. The reactions were stopped after a total reaction time of one minute by adding 100 µL of acetonitrile.

40 µL of the reaction mix was transferred to black polystyrene 96-well plates (Fluotrac[™], Greiner Bio-One, Kremsmünster, Austria). To guarantee accurate results, concentrations of the substrates in the reaction mixtures were adjusted by adding 160 µL of a solution containing 0.5 mM of the respective hydroxycinnamic acids in 50 mM NaP_i, pH 6.0. The difference between the initial substrate concentration and the residual substrate concentration is negligible because the reaction was stopped at conversions below 10%. Only at higher concentrations, where the relative conversion of the reactions was at the lowest, substantial portions of the final substrate came from the reaction sample. The decarboxylation products of FA, CuA and CaA; 4VG, 4VP, and 4VC were excited at 258, 254, and 258 nm, respectively. The fluorescence of 4VG, 4VP, and 4VC was monitored at 345, 335 and 350 nm, respectively.

Product formation was calculated using a standard curve of 4VG, 4VP, and 4VC in 50 mM NaP_i pH 6.0 in the presence of 0.5 mM FA, CuA, and CaA and 10% (v/v) acetonitrile.

Kinetic constants (K_M and V_{max} values) were calculated with the Origin 2020 software (Northampton, MA, USA) using the Michaelis-Menten or substrate inhibition fit functions.

Photometric conversion of hydroxycinnamic acids to the corresponding 4-vinylphenol substrates

PAD activity was followed by the time-resolved quantification of substrate consumption. Measurements were carried out on a BioTek Synergy HTX plate reader (Agilent Technologies, USA) in UV-transparent 96 well-plates. Reactions had a final volume of 100 µL and were performed at ambient temperature (21°C) in 50 mM NaP_i, pH 6.0. Reactions were started by adding 10 µL of a PAD solution to reach a final concentration of 0.5 µg/mL. The decrease in absorbance was followed for 10 min at 324 nm for *p*-coumaric acid ($\epsilon_{324nm}=3.57 \text{ mM}^{-1} \text{ cm}^{-1}$), at 337 nm for caffeic acid ($\epsilon_{337nm}=3.63 \text{ mM}^{-1} \text{ cm}^{-1}$) and at 335 nm for ferulic acid ($\epsilon_{335nm}=3.77 \text{ mM}^{-1} \text{ cm}^{-1}$). All reactions were performed at least in triplicates. Control reactions contained substrates in the absence of PAD. One unit of enzyme activity is defined as the amount of enzyme required to convert 1 µmol of the substrate per minute.

Measurement of PAD activity in cell lysates

E. coli cells expressing *BsPAD* or an empty pET28 vector (control) and lysates thereof were used for activity measurements. Assays were performed in 50 mM NaP_i using UV-transparent 96-well plates (photometric assay, cell lysates) or black polystyrene plates (fluorimetric assay, cell lysates and whole cells). Assays had a final volume of 200 μ L and contained CA at a concentration of 0.5 mM. Reactions were started by adding 10 μ L of 20-fold diluted lysates or 10 μ L of whole cells (final OD₆₀₀=0.1). After mixing, fluorescence (excitation: 254 nm; emission: 335 nm) was measured after a total reaction time of 10 min at 25°C, and absorbance was recorded for 10 min at 329 nm and room temperature. All measurements were carried out in triplicates.

RESULTS AND DISCUSSION

A fluorimetric decarboxylation assay

Here we show that vinyl phenol compounds generated upon carbon dioxide cleavage from FA, CuA and CaA possess an intrinsic fluorescence, which can be used to follow enzymatic decarboxylation reactions. Fluorescence emission spectra of FA, CuA and CaA and their respective decarboxylation products 4-vinyl guaiacol (4VG), 4-vinyl phenol (4VP) and 4-vinyl catechol (4VC) are shown in **Figure S1**. The vinyl species showed high fluorescence compared to the hydroxycinnamic acids, which allowed us to specifically quantify the reaction products in PAD-catalyzed biotransformations.

Table 1. Wavelengths used for the fluorimetric and photometric measurements of *BsPAD* activity.

Substrate	Fluorescence assay		Photometric assay	
	Excitation (nm)	Emission (nm)	Wavelength (nm)	Mol. abs. coeff. (mM ⁻¹ cm ⁻¹)
<i>p</i> -Coumaric acid	254	335	324	3.57
Caffeic acid	258	350	337	3.63
Ferulic acid	258	345	335	3.77

The strong fluorescence of the vinyl products allow real-time measurements for HTS (as described below). However, the fluorescence output is higher at lower residual substrate concentrations (preferably 0.5 mM) because the fluorescence

emission spectra of the 4VP derivatives overlap with the absorption spectra of the corresponding hydroxycinnamates (**Figure S2**). Therefore, accurate quantification of enzyme activity is not possible in real-time measurements. To overcome this problem, we established a stopped assay in which the biocatalytic reactions were performed in a separate microtiter plate (reaction plate) and were stopped at low conversion rates by adding acetonitrile after a total reaction time of 1 minute. Reaction aliquots were transferred to an analysis plate where the substrate concentration was adjusted to the same level by adding the respective hydroxycinnamic acid substrate to a concentration of 0.5 mM. Calibration curves generated with pure 4VP compounds indicate that the fluorescence signals of all decarboxylation products are proportional to their concentration within a range of 64 μ M (**Figure S3**). While substrate absorbance became a problem at high concentrations, detecting low, micromolar concentrations was always possible in the presence of 0.5 mM FA, CA, and CaA. The high fluorescence of 4VG, 4VP and 4VC, allowed the measurement of FA, CA, and CaA substrate concentrations of 0.05 mM. Emission- and excitation wavelengths used for kinetic measurements are shown in **Table 1**. The ability to measure at low substrate concentrations is of particular interest for the determination of the kinetics of enzymes with K_M values below 1 mM, as reported for decarboxylases from *Conocephalum japonicum*, *Bacillus amyloliquefaciens* and *Lactobacillus brevis* RM84^{15,28,29}. The K_M value of decarboxylases is usually in the range of 0.8 to 2 mM³⁸, as is the case for *BsPAD*.

A photometric decarboxylation assay

To overcome some of the limitations of the fluorimetric PAD assay, we also established kinetic measurements based on the known absorbance changes that occur upon decarboxylation of hydroxycinnamic acids³⁰. **Figure S1** shows the electronic UV-Vis absorbance spectra of FA, CuA and CaA and the respective decarboxylation products. For each investigated substrate, decarboxylation leads to a significant loss of absorbance in the far UV range. While this pronounced absorbance change has been previously used, for example to screen PAD variants in a mutagenesis library³⁶, the overlap of substrate- and product absorption complicates kinetic measurements. Here, we used the wavelength region from 320-340 nm, where none of the products interfered with the absorption of the hydroxycinnamic acids. This allowed us to establish an assay that detects the activity of *BsPAD* in real-time. The concentrations of

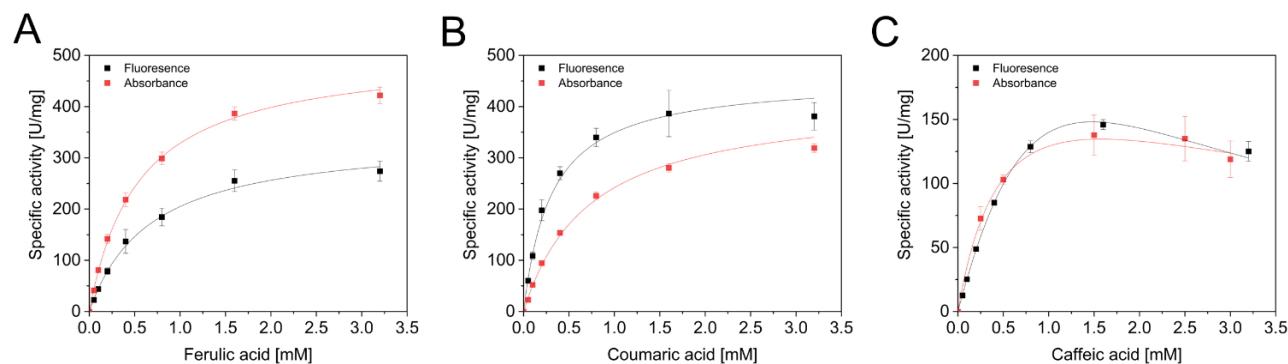


Figure 1 Kinetic measurements of *BsPAD* using the fluorescence- and absorbance assays with ferulic acid (A), coumaric acid (B) and caffeic acid (C). Enzyme concentration used ranged from 0.05 μ g/ml (FA) to 0.8 μ g/ml (CaA). All measurements were performed in triplicates and incubated at 21°C (1000 rpm) for one minute (fluorescence assay) or measured in time-drive mode for 10 min (absorbance assay). Data points were fitted to the Michaelis-Menten equation without (FA and CuA) or with inhibition using Origin 2020 (OriginLab Corporation, Northampton, MA, USA).

hydroxycinnamic acids at the selected wavelengths were proportional to the absorbance (**Figure S4**), and molar absorption coefficients used for kinetic measurement (**Table 1**) were determined from the absorption spectra. Importantly, the assay does not require the removal of intermittent samples or product extraction. Biotransformations at a 1 mL scale containing 2.5 mM of the hydroxycinnamic acids were followed with the photometric assay, which was in excellent agreement with the residual substrate concentrations determined by HPLC analysis (**Figures S5 and S6**).

Determination of kinetic constants

Both assays were used for the measurement of kinetic constants. Michaelis-Menten curves of both assays with FA, CuA and CaA

consumption and can be used as an orthogonal method.

Notably, the K_M values calculated with the two assays agree well with the values known from the literature³². Slight differences in the V_{max} values can be explained by different protein preparation strategies and the fact that Cavin et al. used wavelengths that overlap with the absorption of the products (Figure S2), e.g., 285 nm to follow CuA decrease, which slows down the absorption decrease and leads to lower V_{max} values.

In summary, using the improved version of the absorbance assay presented here is more suitable to determine the kinetics of decarboxylase enzymes with high K_M values, e.g., decarboxylase from *Candida guilliermondii* with K_M values above 5 mM³⁹. The measurement of substrate concentrations higher than 3.5 mM in the fluorescence assay would also necessitate an increase in the substrate concentration in the analysis plate, resulting in a

Table 1. Comparison of K_M and v_{max} values from the literature and the developed absorbance and fluorescence assays. a Based on a UV absorption assay with wavelength that overlap with the absorption of the products

	FA		CuA		CaA	
Assay	K_M / mM	V_{max} / U/mg	K_M / mM	V_{max} / U/mg	K_M / mM	V_{max} / U/mg
Absorbance	0.54 ± 0.02	506 ± 11	0.73 ± 0.08	417 ± 30	0.55 ± 0.15	229 ± 37
Fluorescence	0.67 ± 0.03	342 ± 10	0.31 ± 0.03	456 ± 20	2.25 ± 0.30	599 ± 71
Literature ^{32,a}	1.1	280	1.3	265	2.6	180

are shown in Figure 1, and kinetic constants are given in **Table 3**. For comparison, the same substrate ranges were used for both assays. Overall, similar results were obtained with both procedures. K_M and V_{max} values for FA and CuA were in the same order of magnitude, while for CaA there is a notable discrepancy. However, for the latter substrate, kinetic traces were fit to the Michaelis Menten inhibition model, thus resulting in deviating values. It should also be noted that the fluorescence assay measures the formation of reaction products and thus depends on the calibration curves of the vinyl phenol derivatives. In

notable decrease in signal intensity. The fluorescence assay, however, could be more reliable for enzymes with low K_M values because it has a favorable signal-to-noise ratio at low substrate concentrations. Both assays significantly reduce the effort and analysis time when compared to routinely used HPLC methods, while yielding comparable results. The kinetic measurements of BsPAD required only 0.1 to 1.6 µg of the enzyme towards a single substrate. The time required to measure a full well plate, including pipetting, is approximately 10-30 min, depending on the availability of liquid handling equipment and the

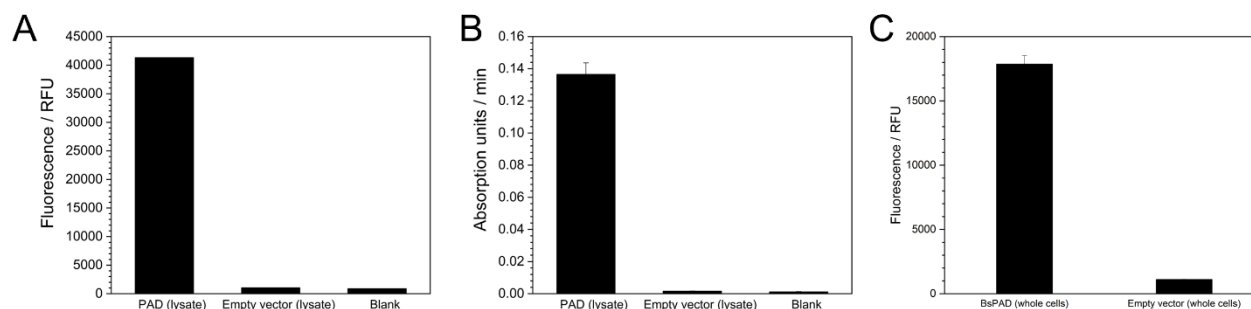


Figure 2. Measurement of BsPAD activity with cell lysate of *E. coli* cells using the fluorescence assay (A) or the absorbance assay (B). Whole cell assays (final OD₆₀₀=0.1) are shown in C. Control reactions contained *E. coli* cells transformed with an “empty” pET28 vector or were performed without lysate (Blank). All cell lysates were diluted 20 times. All reactions were carried out in triplicates.

contrast, the photometric assay quantifies the substrate

Measurement of BsPAD activity in cell lysates

To test the utility of the photometric and fluorimetric PAD assays for HTS applications, the activity of PAD was measured with both

instrumentation used.

procedures using *E. coli* lysate (**Figure 2 A and B**) or whole cells with the more sensitive fluorescence assay. With both assays, PAD activity could be reliably detected in cell lysates or in whole cells. Control reactions carried out under identical conditions with *E. coli* cells transformed with a pET28 vector without any

insert showed no apparent side reactions that interfere with the assay.

CONCLUSIONS

Using BsPAD as a model decarboxylase, it was shown that the absorption- and fluorescence-based assays provide reliable kinetic data for FA, CuA, and CaA. The developed assays were performed in microtiter plates, allowing faster measurement of enzyme activities with lower amounts of enzyme and less sample workup than, for example, HPLC-based analyses. While the fluorescence assay is particularly suitable for the application at low substrate concentrations, it also requires pure decarboxylation products to generate calibration curves. Both assays can also be used in cell lysates, which is particularly important for HTS applications aiming to identify new decarboxylase enzymes or screen for improved enzyme variants from screening libraries.

ASSOCIATED CONTENT

Supporting Information

Figure S1, Fluorescence emission spectra of all substrates and products used, **Figure S2**, Electronic absorption spectra of all substrates and products used, **Figure S3**. Standard curves of 4VG, 4VP, and 4VC (fluorimetric assay), **Figure S4**. Standard curves of FA, CuA, and CaA (spectrophotometric assay), **Figure S5**. HPLC validation of the spectrophotometric assay, **Figure S6**. Standard curves of FA, CuA, and CaA (HPLC).

Scheme S1. Reaction scheme of BsPAD-catalyzed decarboxylation.

The Supporting Information is available free of charge on the ACS Publications website.

Supporting Information (PDF)

AUTHOR INFORMATION

Corresponding Author

* (Word Style "FA_Corresponding_Author_Footnote"). Give contact information for the author(s) to whom correspondence should be addressed.

Present Addresses

†If an author's address is different than the one given in the affiliation line, this information may be included here.

Author Contributions

D.K. and H.T. conceived the project. H.T., C.M., M.L., K.M., and D.K. performed experiments. C.M. expressed BsPAD. U.T.B., R.K., and D.K. directed the project. D.K. and H.T. created the manuscript to which all authors contributed. / All authors have given approval to the final version of the manuscript. / ‡These authors contributed equally. (match statement to author names with a symbol)

Notes

Any additional relevant notes should be placed here.

ACKNOWLEDGMENT

H.T. was funded by the Leibniz Association's strategic networking funding program Leibniz ScienceCampus ComBioCat. D.K. acknowledges funding from BioTechMed-Graz within the framework of the "Young Researcher Group" program. K.M. was funded by the European Union's Horizon 2020 research and innovation program under the Marie Skłodowska-Curie grant agreement no. 860414.

REFERENCES

- (1) Gu, H.; Zhu, Y.; Peng, Y.; Liang, X.; Liu, X.; Shao, L.; Xu, Y.; Xu, Z.; Liu, R.; Li, J. Physiological Mechanism of Improved Tolerance of *Saccharomyces Cerevisiae* to Lignin-Derived Phenolic Acids in Lignocellulosic Ethanol Fermentation by Short-Term Adaptation. *Biotechnol. Biofuels* **2019**, *12* (1), 268. <https://doi.org/10.1186/s13068-019-1610-9>.
- (2) Santamaría, L.; Reverón, I.; López de Felipe, F.; de las Rivas, B.; Muñoz, R. Unravelling the Reduction Pathway as an Alternative Metabolic Route to Hydroxycinnamate Decarboxylation in *Lactobacillus Plantarum*. *Appl. Environ. Microbiol.* **2018**, *84* (15), e01123-18. <https://doi.org/10.1128/AEM.01123-18>.
- (3) Lowe, T. M.; Ailloud, F.; Allen, C. Hydroxycinnamic Acid Degradation, a Broadly Conserved Trait, Protects *Ralstonia Solanacearum* from Chemical Plant Defenses and Contributes to Root Colonization and Virulence. *Mol. Plant. Microbe Interact.* **2015**, *28* (3), 286–297. <https://doi.org/10.1094/MPMI-09-14-0292-FI>.
- (4) Campillo, T.; Renoud, S.; Kerzaon, I.; Vial, L.; Baude, J.; Gaillard, V.; Bellvert, F.; Chamignon, C.; Comte, G.; Nesme, X.; Lavire, C.; Hommais, F. Analysis of Hydroxycinnamic Acid Degradation in *Agrobacterium Fabrum* Reveals a Coenzyme A-Dependent, Beta-Oxidative Deacetylation Pathway. *Appl. Environ. Microbiol.* **2014**, *80* (11), 3341–3349. <https://doi.org/10.1128/AEM.00475-14>.
- (5) Rodríguez, H.; Curiel, J. A.; Landete, J. M.; de las Rivas, B.; de Felipe, F. L.; Gómez-Cordovés, C.; Mancheño, J. M.; Muñoz, R. Food Phenolics and Lactic Acid Bacteria. *Int. J. Food Microbiol.* **2009**, *132* (2), 79–90. <https://doi.org/10.1016/j.ijfoodmicro.2009.03.025>.
- (6) Kourist, R.; Schweiger, A.; Büchenschütz, H. Chapter 5 - Enzymatic Decarboxylation as a Tool for the Enzymatic Defunctionalization of Hydrophobic Bio-Based Organic Acids. In *Lipid Modification by Enzymes and Engineered Microbes*; Bornscheuer, U. T., Ed.; AOCs Press, 2018; pp 89–118. <https://doi.org/10.1016/B978-0-12-813167-1.00005-0>.
- (7) van Beek, S.; Priest, F. G. Decarboxylation of Substituted Cinnamic Acids by Lactic Acid Bacteria Isolated during Malt Whisky Fermentation. *Appl. Environ. Microbiol.* **2000**, *66* (12), 5322–5328. <https://doi.org/10.1128/AEM.66.12.5322-5328.2000>.
- (8) Mathew, S.; Abraham, T. E.; Sudheesh, S. Rapid Conversion of Ferulic Acid to 4-Vinyl Guaiacol and Vanillin Metabolites by *Debaryomyces Hansenii*. *J. Mol. Catal. B Enzym.* **2007**, *44* (2), 48–52. <https://doi.org/10.1016/j.molcatb.2006.09.001>.
- (9) Tsapou, E. A.; Ntourtoglou, G.; Drosou, F.; Tataridis, P.; Dourtoglou, T.; Lalas, S.; Dourtoglou, V. In Situ Creation of the Natural Phenolic Aromas of Beer: A Pulsed Electric Field Applied to Wort-Enriched Flax Seeds. *Front. Bioeng. Biotechnol.* **2020**, *8*.
- (10) Bowen, A. J.; Reynolds, A. G. Aroma Compounds in Ontario Vidal and Riesling Icewines. I. Effects of Harvest Date. *Food Res.*

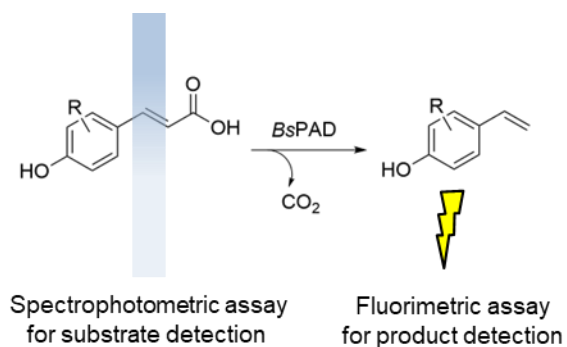
- Int.* **2015**, *76*, 540–549. <https://doi.org/10.1016/j.foodres.2015.06.046>.
- (11) van Schijndel, J.; Molendijk, D.; van Beurden, K.; Canalle, L. A.; Noël, T.; Meuldijk, J. Preparation of Bio-Based Styrene Alternatives and Their Free Radical Polymerization. *Eur. Polym. J.* **2020**, *125*, 109534. <https://doi.org/10.1016/j.eurpolymj.2020.109534>.
- (12) Barclay, G. G.; Hawker, C. J.; Ito, H.; Orellana, A.; Malenfant, P. R. L.; Sinta, R. F. The “Living” Free Radical Synthesis of Poly(4-Hydroxystyrene): Physical Properties and Dissolution Behavior. *Macromolecules* **1998**, *31* (4), 1024–1031. <https://doi.org/10.1021/ma961129p>.
- (13) Yang, J.; Wang, S.; Lorrain, M.-J.; Rho, D.; Abokitse, K.; Lau, P. C. K. Bioproduction of Lauryl Lactone and 4-Vinyl Guaiacol as Value-Added Chemicals in Two-Phase Biotransformation Systems. *Appl. Microbiol. Biotechnol.* **2009**, *84* (5), 867–876. <https://doi.org/10.1007/s00253-009-2026-4>.
- (14) Chen, Y.; Li, L.; Long, L.; Ding, S. High Cell-Density Cultivation of Phenolic Acid Decarboxylase-Expressing *Escherichia Coli* and 4-Vinyl Guaiacol Bioproduction from Ferulic Acid by Whole-Cell Catalysis. *J. Chem. Technol. Biotechnol.* **2018**, *93* (8), 2415–2421. <https://doi.org/10.1002/jctb.5590>.
- (15) Jung, D.-H.; Choi, W.; Choi, K.-Y.; Jung, E.; Yun, H.; Kazlauskas, R. J.; Kim, B.-G. Bioconversion of *p*-Coumaric Acid to *p*-Hydroxystyrene Using Phenolic Acid Decarboxylase from *B. Amyloliquefaciens* in Biphasic Reaction System. *Appl. Microbiol. Biotechnol.* **2013**, *97* (4), 1501–1511. <https://doi.org/10.1007/s00253-012-4358-8>.
- (16) Schweiger, A. K.; Ríos-Lombardía, N.; Winkler, C. K.; Schmidt, S.; Moris, F.; Kroutil, W.; González-Sabín, J.; Kourist, R. Using Deep Eutectic Solvents to Overcome Limited Substrate Solubility in the Enzymatic Decarboxylation of Bio-Based Phenolic Acids. *ACS Sustain. Chem. Eng.* **2019**, *7* (19), 16364–16370. <https://doi.org/10.1021/acssuschemeng.9b03455>.
- (17) Salgado, J. M.; Rodríguez-Solana, R.; Curiel, J. A.; Rivas, B. de las; Muñoz, R.; Domínguez, J. M. Production of Vinyl Derivatives from Alkaline Hydrolysates of Corn Cobs by Recombinant *Escherichia Coli* Containing the Phenolic Acid Decarboxylase from *Lactobacillus Plantarum* CECT 748T. *Bioresour. Technol.* **2012**, *117*, 274–285. <https://doi.org/10.1016/j.biortech.2012.04.051>.
- (18) Sun, L.-H.; Lv, S.-W.; Yu, F.; Li, S.-N.; He, L.-Y. Biosynthesis of 4-Vinyl Guaiacol from Crude Ferulic Acid by *Bacillus Licheniformis* DLF-17056. *J. Biotechnol.* **2018**, *281*, 144–149. <https://doi.org/10.1016/j.jbiotec.2018.07.021>.
- (19) Morley, K. L.; Grosse, S.; Leisch, H.; Lau, P. C. K. Antioxidant Canolol Production from a Renewable Feedstock via an Engineered Decarboxylase. *Green Chem.* **2013**, *15* (12), 3312. <https://doi.org/10.1039/c3gc40748a>.
- (20) Li, L.; Long, L.; Ding, S. Bioproduction of High-Concentration 4-Vinyl Guaiacol Using Whole-Cell Catalysis Harboring an Organic Solvent-Tolerant Phenolic Acid Decarboxylase from *Bacillus Atrophaeus*. *Front. Microbiol.* **2019**, *10*, 1798. <https://doi.org/10.3389/fmicb.2019.01798>.
- (21) Hu, H.; Li, L.; Ding, S. An Organic Solvent-Tolerant Phenolic Acid Decarboxylase from *Bacillus Licheniformis* for the Efficient Bioconversion of Hydroxycinnamic Acids to Vinyl Phenol Derivatives. *Appl. Microbiol. Biotechnol.* **2015**, *99* (12), 5071–5081. <https://doi.org/10.1007/s00253-014-6313-3>.
- (22) Petermeier, P.; Bittner, J. P.; Müller, S.; Byström, E.; Kara, S. Design of a Green Chemoenzymatic Cascade for Scalable Synthesis of Bio-Based Styrene Alternatives. *Green Chem.* **2022**, *24* (18), 6889–6899. <https://doi.org/10.1039/D2GC01629J>.
- (23) Ni, J.; Wu, Y.-T.; Tao, F.; Peng, Y.; Xu, P. A Coenzyme-Free Biocatalyst for the Value-Added Utilization of Lignin-Derived Aromatics. *J. Am. Chem. Soc.* **2018**, *140* (47), 16001–16005. <https://doi.org/10.1021/jacs.8b08177>.
- (24) Li, L.; Long, L.; Ding, S. Direct Affinity-Immobilized Phenolic Acid Decarboxylase by a Linker Peptide on Zeolite for Efficient Bioconversion of Ferulic Acid into 4-Vinyl Guaiacol. *ACS Sustain. Chem. Eng.* **2020**, *8* (39), 14732–14742. <https://doi.org/10.1021/acssuschemeng.0c03489>.
- (25) Degrassi, G.; Polverino De Laureto, P.; Bruschi, C. V. Purification and Characterization of Ferulate and *p*-Coumarate Decarboxylase from *Bacillus Pumilus*. *Appl. Environ. Microbiol.* **1995**, *61* (1), 326–332. <https://doi.org/10.1128/aem.61.1.326-332.1995>.
- (26) Rodrigues, R. C.; Berenguer-Murcia, Á.; Carballares, D.; Morellon-Sterling, R.; Fernandez-Lafuente, R. Stabilization of Enzymes via Immobilization: Multipoint Covalent Attachment and Other Stabilization Strategies. *Biotechnol. Adv.* **2021**, *52*, 107821. <https://doi.org/10.1016/j.biotechadv.2021.107821>.
- (27) Gu, W.; Yang, J.; Lou, Z.; Liang, L.; Sun, Y.; Huang, J.; Li, X.; Cao, Y.; Meng, Z.; Zhang, K.-Q. Structural Basis of Enzymatic Activity for the Ferulic Acid Decarboxylase (FADase) from *Enterobacter Sp.* Px6-4. *PLoS One* **2011**, *6* (1), e16262. <https://doi.org/10.1371/journal.pone.0016262>.
- (28) Landete, J. M.; Rodríguez, H.; Curiel, J. A.; de las Rivas, B.; Mancheño, J. M.; Muñoz, R. Gene Cloning, Expression, and Characterization of Phenolic Acid Decarboxylase from *Lactobacillus Brevis* RM84. *J. Ind. Microbiol. Biotechnol.* **2010**, *37* (6), 617–624. <https://doi.org/10.1007/s10295-010-0709-6>.
- (29) Gao, S.; Yu, H.-N.; Wu, Y.-F.; Liu, X.-Y.; Cheng, A.-X.; Lou, H.-X. Cloning and Functional Characterization of a Phenolic Acid Decarboxylase from the Liverwort *Conocephalum Japonicum*. *Biochem. Biophys. Res. Commun.* **2016**, *481* (3), 239–244. <https://doi.org/10.1016/j.bbrc.2016.10.131>.
- (30) Cavin, J.; Andioc, V.; Etiévant, P.; Diviès, C. Ability of Wine Lactic Acid Bacteria to Metabolize Phenol Carboxylic Acids. *Am J Enol Vitic. January* **1993**, *44*, 76-80. <https://doi.org/10.5344/ajev.1993.44.1.76>.
- (31) Cavin, J. Purification and Characterization of an Inducible *p*-Coumaric Acid Decarboxylase from *Lactobacillus Plantarum*. *FEMS Microbiol. Lett.* **1997**, *147* (2), 291–295. [https://doi.org/10.1016/S0378-1097\(97\)00004-9](https://doi.org/10.1016/S0378-1097(97)00004-9).
- (32) Cavin, J. F.; Dartois, V.; Diviès, C. Gene Cloning, Transcriptional Analysis, Purification, and Characterization of Phenolic Acid Decarboxylase from *Bacillus Subtilis*. *Appl. Environ. Microbiol.* **1998**, *64* (4), 1466–1471.
- (33) Noda, S.; Kawai, Y.; Tanaka, T.; Kondo, A. 4-Vinylphenol Biosynthesis from Cellulose as the Sole Carbon Source Using Phenolic Acid Decarboxylase- and Tyrosine Ammonia Lyase-Expressing *Streptomyces Lividans*. *Bioresour. Technol.* **2015**, *180*, 59–65. <https://doi.org/10.1016/j.biortech.2014.12.064>.
- (34) Williamson, J. J.; Bahrin, N.; Hardiman, E. M.; Bugg, T. D. H. Production of Substituted Styrene Bioproducts from Lignin and Lignocellulose Using Engineered *Pseudomonas Putida* KT2440. *Biotechnol. J.* **2020**, *15* (7), 1900571. <https://doi.org/10.1002/biot.201900571>.
- (35) Barthelmebs, L.; Diviès, C.; Cavin, J. F. Knockout of the *p*-Coumarate Decarboxylase Gene from *Lactobacillus Plantarum* Reveals the Existence of Two Other Inducible Enzymatic Activities Involved in Phenolic Acid Metabolism. *Appl. Environ. Microbiol.* **2000**, *66* (8), 3368–3375. <https://doi.org/10.1128/AEM.66.8.3368-3375.2000>.
- (36) Frank, A.; Eborall, W.; Hyde, R.; Hart, S.; Turkenburg, J. P.; Grogan, G. Mutational Analysis of Phenolic Acid Decarboxylase from *Bacillus Subtilis* (BsPAD), Which Converts Bio-Derived Phenolic Acids to Styrene Derivatives. *Catal. Sci. Technol.* **2012**, *2* (8), 1568. <https://doi.org/10.1039/C2CY20015E>.
- (37) Gasteiger, E.; Hoogland, C.; Gattiker, A.; Duvaud, S.; Wilkins, M. R.; Appel, R. D.; Bairoch, A. Protein Identification and Analysis Tools on the ExPASy Server. In *The Proteomics Protocols*

Handbook; Walker, J. M., Ed.; Humana Press: Totowa, NJ, 2005; pp 571–607. <https://doi.org/10.1385/1-59259-890-0-571>.

- (38) Pesci, L.; Baydar, M.; Glueck, S.; Faber, K.; Liese, A.; Kara, S. Development and Scaling-Up of the Fragrance Compound 4-Ethylguaiacol Synthesis via a Two-Step Chemo-Enzymatic Reaction Sequence. *Org. Process Res. Dev.* **2017**, *21* (1), 85–93. <https://doi.org/10.1021/acs.oprd.6b00362>.

- (39) Huang, H.-K.; Chen, L.-F.; Tokashiki, M.; Ozawa, T.; Taira, T.; Ito, S. An Endogenous Factor Enhances Ferulic Acid Decarboxylation Catalyzed by Phenolic Acid Decarboxylase from *Candida Guilliermondii*. *AMB Express* **2012**, *2* (1), 4. <https://doi.org/10.1186/2191-0855-2-4>.

Table of Contents (TOC)



SUPPORTING INFORMATION

Spectrophotometric and fluorimetric high-throughput assays for phenolic acid decarboxylase

Henrik Terholsen^{‡[a]}, Kamela Myrtollari^{‡[b][c]}, Mirna Larva^[b], Christina Möller^[a], Robert Kourist^[b], Uwe T. Bornscheuer^{*[a]}, Daniel Kracher^{*[b]}

[a] University of Greifswald, Biotechnology and Enzyme Catalysis, Felix-Hausdorff-Straße 4, 17487 Greifswald, Germany

[b] Graz University of Technology, Institute of Molecular Biotechnology, Petersgasse 14, 8010 Graz, Austria

[c] Henkel AG & Co. KGaA, Adhesive Research/Bioconjugates, Henkelstraße 67, 40191 Düsseldorf, Germany

*Corresponding authors: uwe.bornscheuer@uni-greifswald.de & daniel.kracher@tugraz.at

‡ These authors contributed equally to this work.

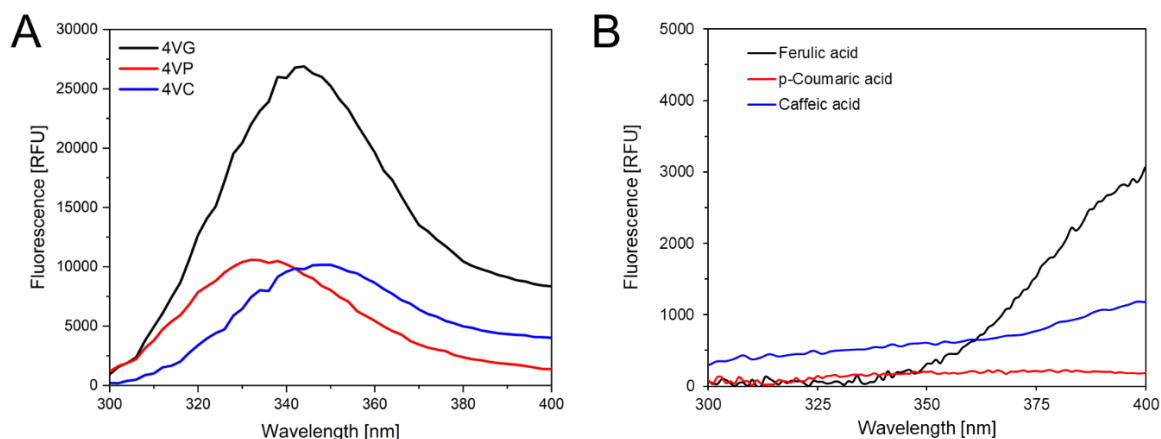


Figure S1. Fluorescence emission spectra of 4VG (20 μM), 4VP (20 μM), and 4VC (10 μM) in the presence of 0.5 mM ferulic acid, *p*-coumaric acid and caffeic acid (A) and emission spectra of 0.5 mM ferulic acid, *p*-coumaric acid and caffeic acid (B). Spectra were recorded in 50 mM NaP_i buffer, pH 6.

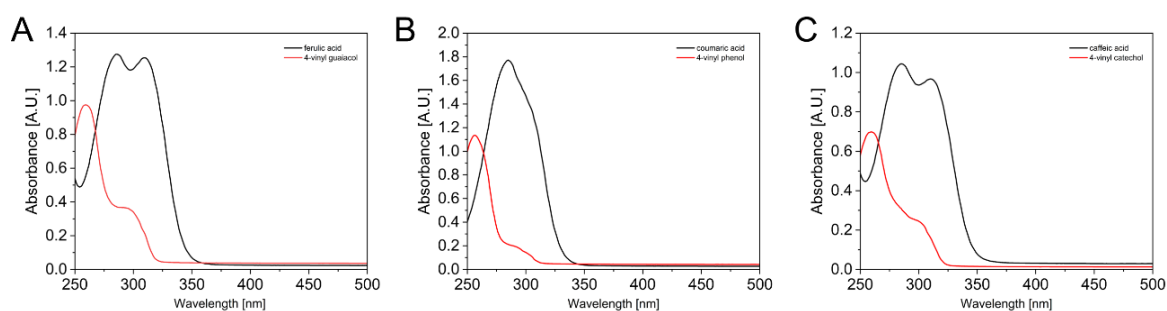


Figure S2. Electronic absorption spectra of ferulic acid (A), *p*-coumaric acid (B), and caffeic acid (C) and the decarboxylated reaction products 4VG (A), 4VP (B), and 4VC (C). Spectra were recorded in 50 mM NaP_i buffer, pH 6. All species had a final concentration of 0.3 mM.

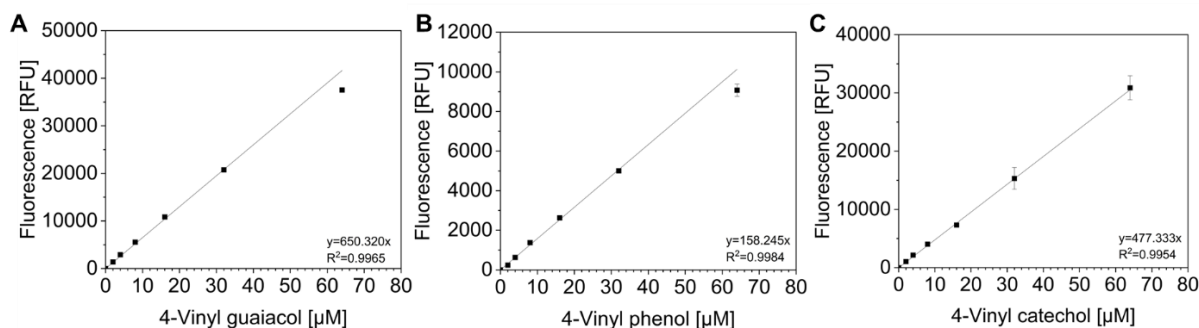


Figure S3. Calibration curves of 4VG (A), 4VP (B), and 4VC (C) in 50 mM NaP_i pH 6.0 in the presence of 0.5 mM FA, CuA, and CaA, and 10% (v/v) acetonitrile, respectively (Figure S1).

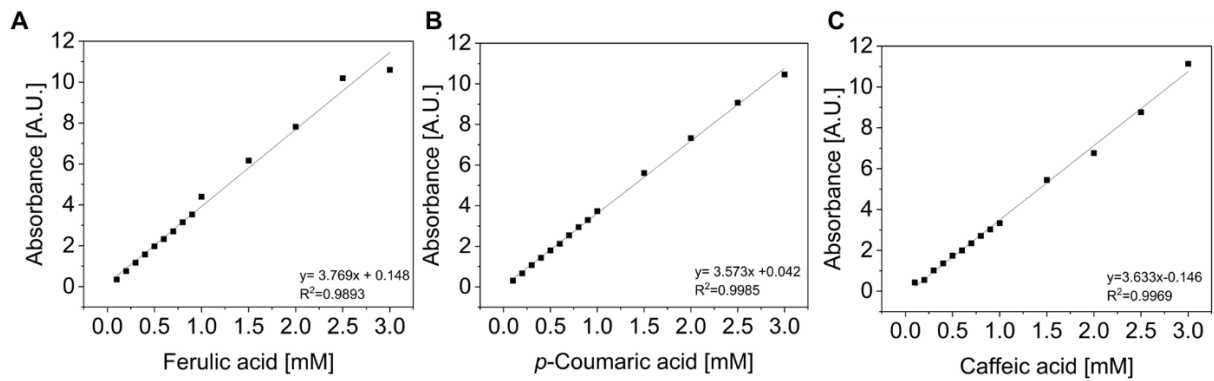


Figure S4. Calibration curves of ferulic acid at 335 nm (A), *p*-coumaric acid at 324 nm (B), and caffeic acid at 337 nm (C) measured in 50 mM NaP_i pH 6.0 with the photometric assay.

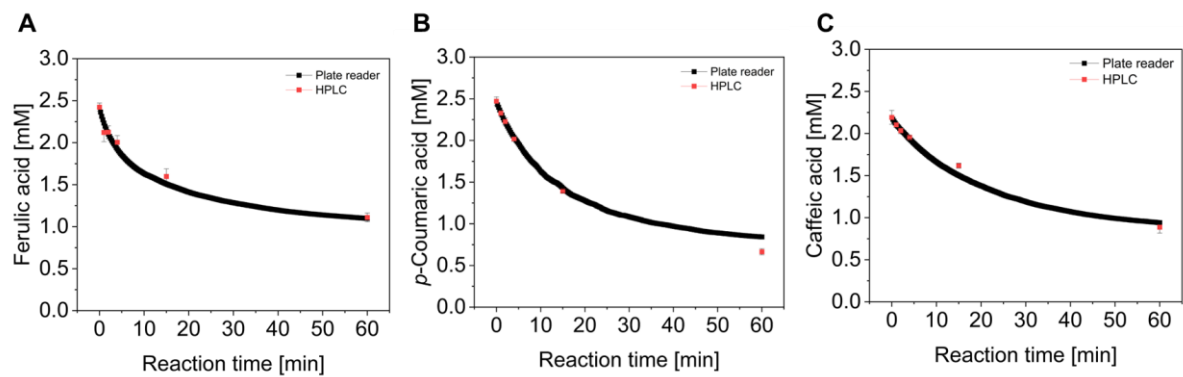


Figure S5. Biotransformation of 2.5 mM ferulic acid (A), 2.5 mM *p*-coumaric acid (B), and 2.1 mM caffeic acid (C). Residual substrate concentration was followed continuously with the photometric assay (red line) and by withdrawing samples which were analyzed by HPLC.

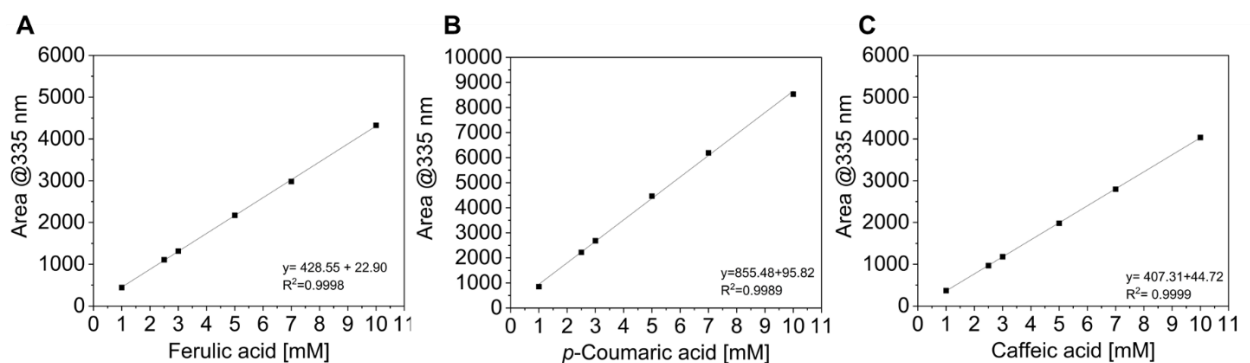
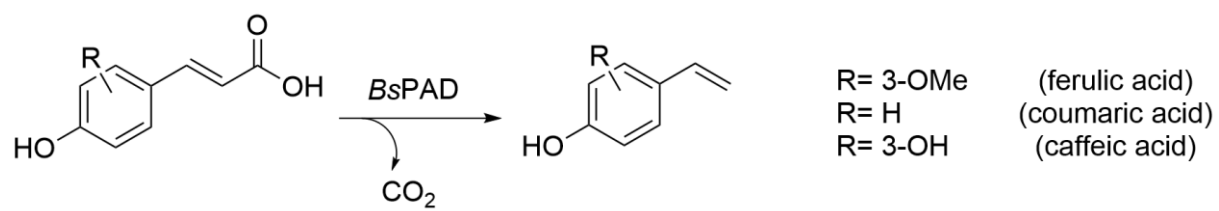


Figure S6. HPLC calibration curves for ferulic acid (A), *p*-coumaric acid (B), and caffeic acid (C). The injection volume was 2 μ L, and all hydroxycinnamic acids were detected at 335 nm. Error bars show the standard deviation from three independent replicates.



Scheme S1. Reaction scheme of *BsPAD*-catalyzed decarboxylation.

Article III

Recent Insights and Future Perspectives on Promiscuous Hydrolases/Acyltransferases

Henrik Müller, Henrik Terholsen, Simon P. Godehard, Christoffel P. S. Badenhorst,* and Uwe T. Bornscheuer*

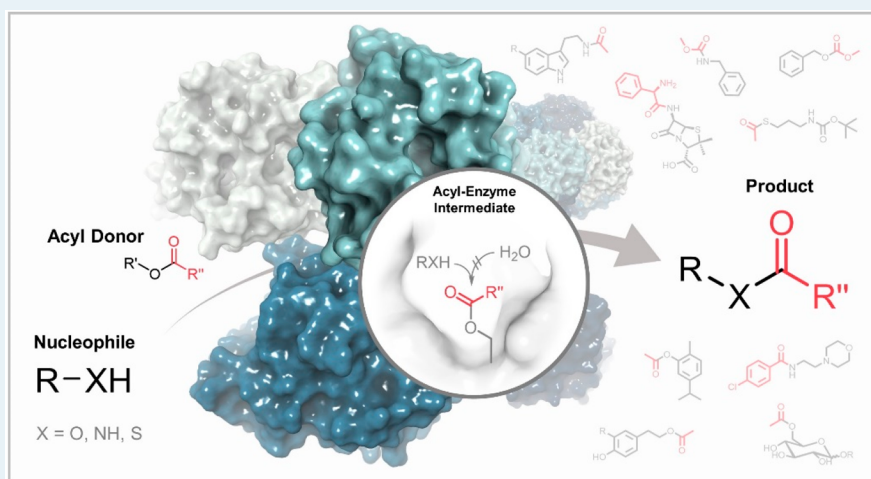
Cite This: *ACS Catal.* 2021, 11, 14906–14915

Read Online

ACCESS |

Metrics & More

Article Recommendations



ABSTRACT: Promiscuous hydrolases/acyltransferases have attracted attention for their ability to efficiently catalyze selective transacylation reactions in water to produce esters, thioesters, amides, carbonates, and carbamates. Promiscuous hydrolases/acyltransferases can be implemented into aqueous enzyme cascades and are ideal biocatalysts for the acylation of hydrophilic substrates that are barely soluble in dry organic solvents. This activity was thought to be rare, and recent research has focused on just a small number of accidentally identified promiscuous hydrolases/acyltransferases. High-throughput screening for acyltransferases and an *in silico* sequence-based method for prediction of acyltransferase activity provided access to many efficient promiscuous hydrolases/acyltransferases, thereby demonstrating that promiscuous acyltransferase activity is rather common in hydrolases. These synthetically valuable enzymes could further be enhanced by protein engineering. This Perspective aims to demonstrate the synthetic potential of these enzymes and raise awareness of the frequency of this activity.

KEYWORDS: biocatalysis, hydrolase, acyltransferase, acyl-enzyme intermediate, catalytic promiscuity

INTRODUCTION

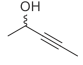
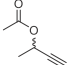
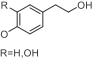
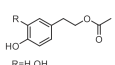
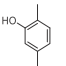
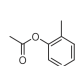
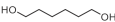
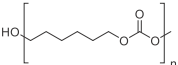
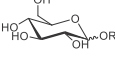
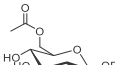

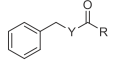
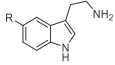
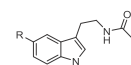
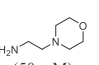
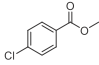
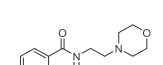
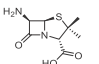
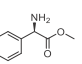
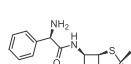
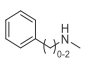
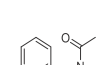
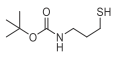
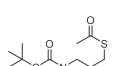
Hydrolases are synthetically useful stereo- and regioselective biocatalysts with a wide substrate scope. They usually do not require cofactors, and many of them are very robust, making them outstandingly suitable for industrial applications.^{1–3} Many hydrolases, especially lipases and esterases, even maintain activity in virtually water-free organic solvents, which enables them to also catalyze valuable “reverse hydrolysis” or transesterification reactions.⁴ However, the use of organic solvents has several drawbacks, including high costs, negative environmental impact, and incompatibility with food and cosmetic applications due to toxicity.⁵ Furthermore, while enzymes can catalyze the very challenging selective acylation of hydrophilic compounds like sugars, the low solubility of these

compounds in dry organic solvents largely limits this approach.⁶ Integration of lipase-catalyzed transesterifications into biocatalytic reaction cascades is also complicated by the incompatibility of most other enzymes with organic solvents.⁷ Therefore, selective biocatalytic acylation in bulk water is highly desirable as it would allow enzyme cascades to synthesize hydrophilic esters, thioesters, amides, carbonates,

Received: October 2, 2021

Revised: November 16, 2021

Table 1. Selected Examples of Synthetic Applications of Various Promiscuous Hydrolases/Acyltransferases in Water^a

Acyl Acceptor (conc.)	Acyl Donor (conc.)	Product	Remarks	Enzyme (conc.)	Conversion (time)	Reference
 (100 mM)	ViOAc (9.2% (v/v))		Kinetic resolution of secondary alcohols; biphasic	MsAcT WT (0.5 mg/mL CFE)	40%, (5 h) E-value = 39 (<i>S</i>)	41
				MsAcT_F154A (0.5 mg/mL CFE)	6%, (5 h) E-value >200 (<i>R</i>)	
 (250 mM)	EtOAc (30 % v/v)	 R=H,OH	Aliphatic alcohol; hydroxytyrosol (antioxidant); flow conditions	Immobilized MsAcT (0.2 mg/mL)	75-81 % (10 min)	40
 (20 mM)	ViOAc (200 mM)		Phenolic alcohol	PestE_I208A (0.2 µg/mL)	11 % (45 min)	60
 (50 mM)	DMC (50 mM)		Oligocarbonate mixture	Est8 (3.2 mg/mL lyophilized crude lysate)	~4 % isolated yield (23.5 h)	23
MeOH (2 M)	Crude jatropha oil (triacylglycerols; 30% w/v)	Fatty acid methyl esters (FAME)	Biodiesel, biphasic	Immobilized CpLIP2 (10% w/v)	93% (8 h)	61
 (25-100 mM)	EtOAc (500 mM), IPOAc (200 mM)		Biosurfactant	EstA, EstCE1_MAA (93 µg/mL)	17-77 % (15-240 min)	62
 Y = OH, NH ₂ (50 mM)	ViOAc (200 mM), EtOAc (500 mM) DMC (500 mM)	 Y = O, NH R = Me, OMe	Ester, Amide, Carbonate, Carbamate	EstCE1 (0.34 mg/mL)	90-100 % (5-60 min)	22
 R=H,OH,OMe (500 mM)	EtOAc, ViOAc (10 % v/v)	 R=H,OH,OMe	Tryptamine derivatives; flow conditions	Immobilized MsAcT (1.25 mg/mL)	62-99 % (5 min)	63
 (50 mM)	 (200 mM)		Moclobemide (antidepressant)	EstCE1 (0.25 mg/mL)	20 % (42 h)	22
 (46 mM)	 (151 mM)		Ampicillin (antibiotic)	Penicillin acylase (30 mg/mL CFE)	70 % (4 h)	64
 (250 mM)	ViOAc (10 % v/v)		Tertiary amide; biphasic	MsAcT_S11C (1 mg/mL)	30-99 % (2-24 h)	65
 (250 mM)	ViOAc (10 % v/v)		Thioester; biphasic	MsAcT_S11C (1 mg/mL)	>99 % (30 min)	65
CoA (100 mM)	ViOAc (10% v/v)	Acetyl-CoA	Acyl-CoA regeneration system; biphasic	MsAcT_S11C (1 mg/mL)	80 % (48 h)	65

^aAbbreviations: ViOAc: vinyl acetate, EtOAc: ethyl acetate, IPOAc: isopropenyl acetate, DMC: dimethyl carbonate; CFE: cell free extract; WT: wild type.

and carbamates in water (Table 1). However, typical acyltransferases are not synthetically valuable because they often have narrow substrate specificities and depend on complex and expensive acyl donors like acyl-CoA thioesters or even acyl-carrier proteins.^{8,9} Consequently, there is a demand for hydrolases with the ability to catalyze (trans-)acylation in water, using simple and readily available acyl donors like methyl-, ethyl-, and vinyl esters. This Perspective is about such “promiscuous hydrolases/acyltransferases”.

Acyltransferases use either a concerted mechanism¹⁰ or a ping-pong bi-bi mechanism involving the formation of a covalent acyl-enzyme intermediate that can acylate organic nucleophiles like alcohols, amines, and thiols.^{11,12} The ping-pong bi-bi mechanism and acyl-enzyme intermediate are also employed by hydrolases and hydrolysis can be seen as acyl transfer to water.¹³ As pointed out long ago, the mechanisms of hydrolysis and acyl transfer are closely related by a shared acyl-enzyme intermediate^{14,15} (Figure 1), explaining why promis-

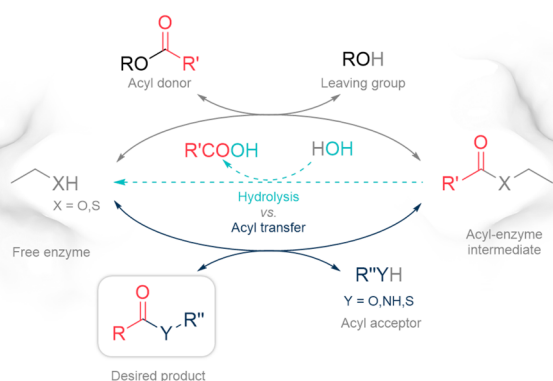


Figure 1. Mechanisms of acyl transfer and hydrolysis by promiscuous hydrolases/acyltransferases both involve a covalent acyl-enzyme intermediate.

cus hydrolase/acyltransferase activity is widespread in nature.^{16–18} The ability of some hydrolases to catalyze acyl transfer reactions in bulk water has been known for over a century¹⁹ but has recently received considerable attention as a number of synthetically valuable promiscuous hydrolases/acyltransferases have been discovered.^{20–24}

When the first promiscuous hydrolases/acyltransferases were discovered, the lack of protein structures and modern protein engineering tools like rational design and directed evolution meant that these properties could not be altered. Today, however, we can enhance the acyltransferase activity of hydrolases by directed evolution and rational engineering, providing access to a vast number of novel acylation catalysts.

This Perspective summarizes the recently discovered promiscuous hydrolases/acyltransferases and their synthetic applications, provides structural and mechanistic insights, and discusses how to find more of these useful enzymes. We also discuss how protein engineering has enabled tailoring the activity, substrate scope, and stereoselectivity of these enzymes. Most importantly, protein engineering has been used to reduce undesired hydrolytic activity while maintaining or improving acyltransferase activity.^{22,25–27} This can dramatically slow down the hydrolysis of the acyl donor and the transacylation products, resulting in higher conversions and more stable product accumulation over prolonged reaction times. This greatly increases the attractiveness of promiscuous hydrolases/

acyltransferases to synthetic chemists. It is important to note that acyltransferases must not necessarily have hydrolase activity. For example, cutin synthases make use of the same serine-histidine-aspartate catalytic triad employed by the cutin-hydrolyzing cutinases, yet they do not have any detectable cutinase activity.²⁸ Inspired by natural evolution, we know that it is possible to transform hydrolases into excellent acyltransferases.^{29,30}

RECENT RESEARCH ON PROMISCUOUS HYDROLASES/ACYLTRANSFERASES

Recent research on promiscuous hydrolases/acyltransferases started in 1993 when CpLIP2, a lipase from *Candida parapsilosis*, was discovered and shown to be able to catalyze the synthesis of oleoylesters of ethylene glycol, ethanol, *n*-propanol, and isopropanol in aqueous systems.²⁴ Homologous lipases, phylogenetically related to *Pseudozyma antarctica* (formerly named *Candida antarctica*) lipase A (CAL-A), shared this promiscuous acyltransferase activity, which could be used to produce fatty acid methyl or ethyl esters (biofuels) in the presence of water.^{31–33} The acyltransferase activity of CAL-A could be improved by a single mutation (D122L), allowing up to 95% fatty acid ethyl ester to be produced from palm kernel oil in the presence of aqueous ethanol.^{32–34} CAL-A’s promiscuous acyltransferase activity was further used in a cascade reaction with an alcohol dehydrogenase and a Baeyer–Villiger monoxygenase (BVMO) to reduce product inhibition and shift the reaction equilibrium toward product formation by catalyzing the oligomerization of the ϵ -caprolactone produced from cyclohexanol.³⁵ This example demonstrates the value of acyltransferases that can be employed in biocatalytic cascades in water. As lipases/acyltransferases, the CpLIP2-related enzymes are limited to the transfer of long-chain fatty acyl groups.²⁴ The esterase/acyltransferase MsAcT from *Mycobacterium smegmatis* extended the range of enzymatic acyl transfer reactions in water by also catalyzing the transfer of shorter acyl chains.²⁰ Because of its versatility, the synthetic potential of MsAcT has been studied extensively, making it the most thoroughly characterized promiscuous hydrolase/acyltransferase. It was used together with a transaminase in a one-pot reaction cascade to synthesize *N*-benzylacetamide from benzaldehyde, thereby shifting the unfavorable equilibrium of the transaminase reaction toward amine formation, again demonstrating the potential of promiscuous hydrolases/acyltransferases in reaction cascades.³⁶ MsAcT also has potential applications in wastewater treatment,³⁷ but this Perspective will focus on synthetic applications. MsAcT has been used for the acylation of several primary and secondary alcohols and amines, producing various compounds including valuable tryptamine derivatives, flavors, and fragrances (Table 1).^{36,38–42} However, MsAcT also has significant hydrolase activity, a limited substrate scope, and poor enantioselectivity.^{36,41} This has prompted researchers to engineer MsAcT variants with impressively high enantioselectivity and significantly reduced hydrolase activity, demonstrating that these problems can be addressed by modern protein engineering methods.^{25,41}

DISCOVERY OF NOVEL PROMISCUOUS HYDROLASES/ACYLTRANSFERASES

Historically, the discovery of the promiscuous acyltransferase activity of hydrolases has been unintentional and based on

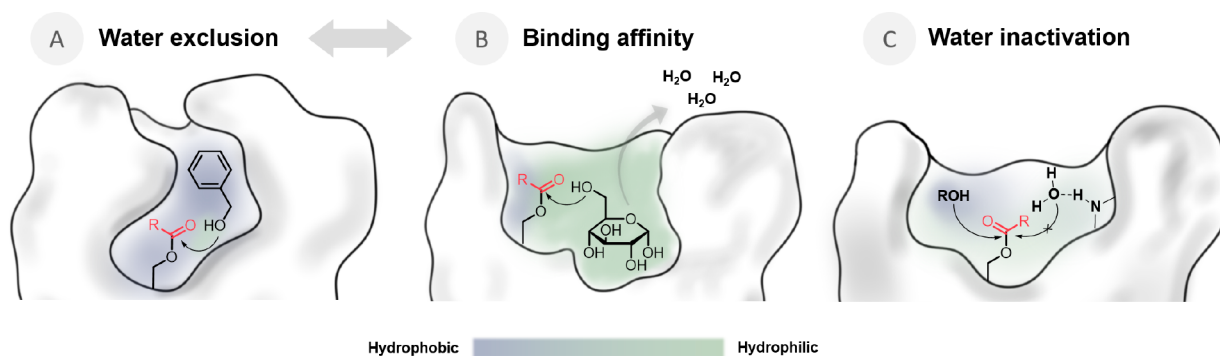


Figure 2. Factors affecting acyltransferase activity in physiologically relevant acyltransferases and in promiscuous hydrolases/acyltransferases. (A) A hydrophobic environment may provide a more favorable surrounding for organic nucleophiles than for water. (B) High binding affinity to the acyl acceptor substrate may displace water and promote acyl transfer over hydrolysis. (C) Structural features may inactivate water, preventing nucleophilic attack on the acyl-enzyme intermediate.

fortuitous observations.^{14,19,43} For example, the acyltransferase activity of CpLIP2 was discovered by observation of extra spots by thin layer chromatography.²⁴ MsAcT was identified in reactions containing neopentyl glycol and ethyl acetate, which are converted to the insoluble neopentyl glycol diacetate, which opacifies the reaction mixture.^{20,44} We realized that this concept could be used to deliberately search for novel acyltransferases. Reisky et al. used a clear, monophasic solution of dimethyl carbonate and 1,2-hexanediol to identify Est8 as an acyltransferase capable of producing insoluble oligocarboxylates.²³ Similarly, Müller et al. discovered the acyltransferase activity of EstCE1 by screening for opacification using an initially transparent solution of vinyl acetate and 2-phenylethanol.²² On the basis of our understanding that promiscuous acyltransferase activity is a fundamental feature of hydrolases that use an acyl-enzyme intermediate, we set out to find homologues of Est8 and EstCE1 which also have acyltransferase activity. EstCE1 is closely related to naturally occurring acyltransferases like Lovastatin synthase (LovD) and CapW, which use methyl esters as acyl donors for the synthesis of Capuramycin-type antibiotics.^{8,45,46} Interestingly, most of the homologous family VIII carboxylesterases we tested were also excellent acyltransferases with very high acyl transfer to hydrolysis (AT/H) activity ratios.²² The structure of Est8 revealed it to be a bacterial hormone-sensitive lipase with a hydrophobic active site.²¹ This was reminiscent of the hydrophobic active sites of MsAcT and the CpLIP2-related lipases/acyltransferases, which are thought to repel water, preventing hydrolysis of the acyl-enzyme intermediate and thereby facilitating acyl transfer.^{20,24,47} We therefore hypothesized that the hydrophobicity of Est8's active site was responsible for its promiscuous acyltransferase activity. We then tested several homologues with known structures and found that there was an excellent correlation between active site hydrophobicity and the acetylation of 2-phenylethanol, a model acyl acceptor substrate. On the basis of this correlation, we developed a sequence-based method for predicting the promiscuous acyltransferase activity of homologous esterases from the bacterial hormone-sensitive lipase family. The method is based on estimating active-site hydrophobicity, which is believed to reflect binding affinity to hydrophobic acyl acceptors, from the sequence of the N-terminal cap domain.²¹ Therefore, promiscuous acyltransferase activity could be predicted from the sequence of the N-terminal cap domain alone, allowing several other homologues with acyltransferase

activity to be identified. Most importantly, these results suggested that, just in the small sequence library we studied, there must be several thousand more promiscuous acyltransferases with synthetically valuable activities. As far as we know, this is the first example of the sequence-based prediction of promiscuous acyltransferase activity of hydrolases, which is usually considered to be very challenging.²¹

MECHANISTIC DIFFERENCES BETWEEN HYDROLASES AND TRANSFERASES

Hydrolases and acyltransferases often employ the same catalytic residues. For example, the serine-histidine-aspartate triad employed by the promiscuous hydrolases/acyltransferases CpLIP2, MsAcT, and the bacterial hormone-sensitive lipases is shared with true acyltransferases like cutin synthase and with the hydrolytic cutinases.^{20,21,28,48,49} The molecular mechanisms differentiating acyl transfer from hydrolysis are still poorly understood. Physiologically relevant acyltransferases employ three general strategies to favor acyl transfer over hydrolysis of the acyl-enzyme intermediate. These strategies are high affinity to the acyl acceptor substrate, water inactivation mediated by a different orientation of the oxyanion loop in the active site, and active site hydrophobicity, which is supposed to repel water from the active site (Figure 2).

Kazlauskas et al. argued that subtle structural variations can affect the balance between acyl transfer and hydrolysis by inactivation of attacking water molecules, thereby stabilizing the acyl-enzyme intermediate.¹¹ For example, a reorientation of the oxyanion hole of the thioesterase domain of the *Bacillus subtilis* surfactin synthase favors macrolactonization over hydrolysis.⁵⁰ Another example is the acyltransferase DynE8, which forms a stable acyl-enzyme intermediate visible in its crystal structure.⁵¹ DynE8 and related acyltransferases have a GHSxG motif, corresponding to the GxSxG esterase motif. Mutation of the histidine in this motif to alanine led to a 7-fold increased hydrolysis rate, without affecting the rate of acyl transfer. Jones et al. proposed that an active site aspartate residue in OatA-related SGNH family acyltransferases is a conserved feature, limiting esterase activity by coordination of a water molecule that would otherwise hydrolyze the acyl-enzyme intermediate.⁵² We can assume that enzymes that act as hydrolases *in vivo* did not experience evolutionary pressure to inactivate hydrolytic water, suggesting that applying such pressure in the laboratory could significantly enhance their acyltransferase activities.

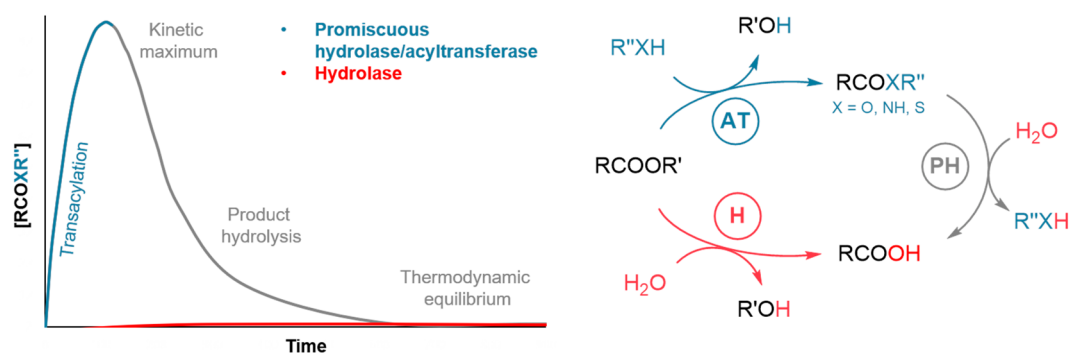


Figure 3. Promiscuous hydrolases/acetyltransferases catalyze acyl transfer (AT) faster than they catalyze hydrolysis (H), leading to transient accumulation of the transesterification product. If the transesterification product is a substrate to the enzyme as well, product hydrolysis (PH) will occur until the thermodynamic equilibrium is reached. A hydrolase without promiscuous acyltransferase activity will not show a kinetic maximum above the thermodynamic equilibrium.

A concept that has received considerably more attention is active site hydrophobicity, which formed the basis for the hydrophobicity scoring system we used to predict acyltransferase activity in the bacterial hormone-sensitive lipases (see section above). Some physiological acyltransferases seem to limit the access of water to the active site by hydrophobic shielding. Lecithin-retinol acyltransferase (LRAT) uses an N-terminal α -helix to bind to the cell membrane, thereby shielding the acyl-enzyme intermediate from water in a highly hydrophobic microenvironment.⁵³ However, Kazlauskas et al. demonstrated that this is not a general feature of acyltransferases and that water inactivation and substrate affinity are more important.¹¹ This is clearly demonstrated by comparison of homoserine *O*-acetyltransferases and two close homologues, MekB and CgHle. The MekB and CgHle sequences were initially annotated as homoserine *O*-acetyltransferases but later found to be unable to acetylate homoserine.⁵⁴ These enzymes are hydrolases but have narrow hydrophobic active sites, while the homologous *O*-acetyltransferases have large polar active sites. Therefore, acyltransferase activity in homoserine *O*-acetyltransferases is explained by a high binding affinity of the acyl acceptor substrate homoserine, which displaces water and increases the effective concentration of the acyl acceptor. The fact that CpLIP2, MsAcT, and the bacterial hormone-sensitive lipases/acetyltransferases are all also hydrolases clearly demonstrates that even very hydrophobic binding pockets are not capable of entirely excluding water from the active site and preventing hydrolysis of the acyl-enzyme intermediate. In fact, a computational approach by Kazemi et al. revealed that the determining factor for acyltransferase activity in MsAcT is not hydrophobic shielding of the active site from water but rather the higher binding affinity toward benzyl alcohol resulting from active-site hydrophobicity.⁵⁵ Thus, the water-repelling effect of active-site hydrophobicity on promiscuous acyltransferase activity may be largely overrated.

■ SYNTHETIC APPLICATIONS AND CHOICE OF ACYL DONOR

Promiscuous hydrolases/acetyltransferases can be used to synthesize esters, thioesters, amides, carbonates, and carbamates in water. Table 1 lists a selection of interesting reactions and valuable products, highlighting the synthetic potential of these enzymes. EstCE1 was shown to efficiently catalyze the formation of *N*-benzylacetamide from ethyl acetate and

benzylamine, and *N*-benzyl carbamate from dimethyl carbonate and benzylamine, while lacking amidase and carbamate-hydrolyzing activities.²² This ability to catalyze the irreversible conversion of esters to amides is synthetically very valuable.⁴⁵ While esters may be irreversibly converted to amides, the interconversion of two esters or amides by transacylation is often reversible.^{56,57} Therefore, transacylation equilibria are often shifted by using activated acyl donors like cyanomethyl, trifluoroethyl, and enol esters.⁴⁴ Enol esters became very popular acyl donors because they are cheap, highly reactive, and release byproducts that quickly tautomerize to their non-nucleophilic carbonyl form, making the reactions virtually irreversible. However, in all of these strategies, the leaving groups or byproducts are toxic/explosive and negatively impact the atom economy of the reactions. The application of less-activated acyl donors like ethyl acetate is considered to be more environmentally friendly, but requires considerably larger amounts of acyl donor to be used. A more recent approach involves the use of cheap, biobased α -angelica lactones as acyl donors. These cyclic enol lactones do not produce any byproducts, theoretically enabling 100% atom economy. In contrast to other lactones, the transesterification product quickly tautomerizes into a more stable methyl ketone, making the acylation irreversible and preventing further acylation of the reaction product. Angelica lactones are attractive for kinetic resolutions, especially since the methyl ketones can be derivatized to allow chromatography-free separations of the acylated and unacylated enantiomers.^{58,59}

Perhaps the most exciting application of promiscuous hydrolases/acetyltransferases is the acylation of hydrophilic substrates. Therefore, the inability of MsAcT and the CpLIP2-related enzymes to acylate hydrophilic compounds like sugars in water is a significant limitation. Realizing that active site hydrophobicity may not be as critical as previously thought and that the acylation of very hydrophilic acceptors has been reported,^{24,29,66,67} we decided to test the ability of the family VIII carboxylesterases/acetyltransferases, which have less hydrophobic active sites, to acylate sugars. We found that EstA, a family VIII carboxylesterase/acetyltransferase related to EstCE1, was capable of acylating glucose in bulk water with good yields and selectivity. EstA also acylated maltose and maltotriose, but less efficiently.⁶² EstA has a large, polar, and well-solvated ligand-binding site due to an active site aspartate which seems to promote sugar binding, as suggested by induced-fit docking.⁶² The sugars were acetylated at the most

reactive C6 hydroxyl group. However, EstA also formed a small amount of diester product, and protein engineering could be used to change this regioselectivity. The potential to expand the range of sugar-acylating enzymes is further demonstrated by our protein engineering of EstCE1, which does not efficiently acylate sugars, into a catalyst that efficiently acetylates glucose, maltose, and maltotriose using ethyl acetate or isopropenyl acetate as acyl donors.⁶² The engineered EstCE1 had a preference for the larger sugars maltose and maltotriose, compared to EstA that preferentially acylated glucose. Interestingly, the family VIII carboxylesterase EstXT1 has subsequently been shown to acylate cyanidin-3-O-glucoside, suggesting that sugar acylating activities are not rare among the family VIII carboxylesterases.⁶⁸

■ CURRENT CHALLENGES AND PROTEIN ENGINEERING

Despite the synthetic advantages of promiscuous hydrolases/acyltransferases in water, the use of lipases in anhydrous solvents is still more common. At the moment this is almost certainly due to the relatively small number of well-studied promiscuous hydrolases/acyltransferases and their synthetic limitations. A major limitation of promiscuous hydrolases/acyltransferases is that transacylation reactions proceed under kinetic control in water, which means that the transesterification product rapidly accumulates to a transient maximum concentration before being hydrolyzed (Figure 3).⁶⁹ To be synthetically useful, acyltransferases must catalyze acyl transfer much faster than hydrolysis, which means that the higher the AT/H ratio, the more valuable the biocatalyst is for synthetic application in water.^{13,69}

Even if a promiscuous hydrolases/acyltransferase catalyzes acyl transfer faster than hydrolysis, its synthetic application is very limited if it also has a high product hydrolysis rate. In contrast to lipases in anhydrous organic solvents, acyl donor hydrolysis must be compensated by the use of a significant excess of acyl donor (Table 1), and the reaction has to be quenched at the kinetic maximum to prevent enzymatic hydrolysis of the product. Part of the problem can be overcome by applying immobilized promiscuous hydrolases/acyltransferases in flow reactors, since the reaction duration can be accurately controlled. Furthermore, biphasic systems with immiscible acyl donors like ethyl acetate, may also serve to extract the reaction products, preventing subsequent hydrolysis.^{61,63,64,70} Much more importantly, several recent examples demonstrated that protein engineering can reduce both acyl donor and product hydrolysis to the extent that they play an almost negligible role in batch reactions. Engineering approaches aim at modulating one or more of the factors that may influence the balance of acyl transfer to hydrolysis (Figure 2). For example, rational design of MsAcT and EstCE1 produced variants with dramatically increased AT/H ratios, making acyl donor hydrolysis a minor side reaction. A high AT/H ratio means that a lower molar ratio of acyl donor to acyl acceptor can be used, which is important for the atom economy of reactions. For the MsAcT K97A/R150I variant, it was shown that the improved AT/H ratio toward benzyl alcohol was also accompanied by slower hydrolysis of the benzyl acetate formed. This means faster synthesis of more product that is more stable than when the wild-type MsAcT is used as the catalyst. A single mutation can be sufficient to shift the balance of acyltransferase and hydrolase activities or even completely invert it. A K97A variant of MsAcT had less than a

third of the wild-type hydrolase activity, while acyltransferase activity was improved 2.5-fold, resulting in a 7.5-fold higher AT/H ratio. K97 is involved in the coordination of a water molecule by N94 and mutation of K97 presumably destabilizes a hydrogen bond network required for the hydrolysis reaction. Interestingly, the D192N variant of MsAcT, which lacks the charge-relay acid of the catalytic triad, showed a 100-fold lower activity but a doubled AT/H ratio.²⁵

Wild-type EstA does not acetylate benzyl alcohol, but a single mutation (HDG to HGG) transformed EstA into a benzyl alcohol acyltransferase almost as efficient as MsAcT. This mutation aimed at increasing affinity to benzyl alcohol as acyl acceptor by increasing active site hydrophobicity.²² Acyltransferase activity in family VIII carboxylesterases/acyltransferases appears to be linked to this three-amino acid motif adjacent to the catalytic triad. Molecular modeling suggested that the first residue of the motif may play an important role in benzyl alcohol binding via π - π -stacking. Engineering this motif in a related lovastatin hydrolase (WGG motif) indicated that the tryptophan residue is important for the hydrogen-bond network around the active site and therefore for hydrolase activity.⁷¹ In line with this, changing the EstCE1 WGG motif to YGG or FGG dramatically reduced acyl donor hydrolysis rate while maintaining most acyltransferase activity.²² Interestingly, numerous acyltransferases structurally related to family VIII carboxylesterases, like the Lovastatin synthase LovD, also have the FGG motif.⁷¹ As this three-residue motif was found to be important for selectivity, future engineering may be focused around this part of the active site.

Exchange of the catalytic serine with cysteine (S11C) enabled MsAcT to catalyze the formation of thioesters like acetyl-CoA in water, with vinyl acetate as acyl donor. Interestingly, hydrolysis of the thioesters was not observed. The S11C variant can also catalyze the acetylation of secondary amines to produce tertiary amides.⁶⁵

It must be noted that the AT/H ratio of a given enzyme can also be influenced by the type of acyl donor and/or acceptor substrates. For EstCE1, it was demonstrated that the AT/H ratio highly depends on the acyl acceptor substrate, with a strong preference for aromatic acyl acceptors.²² This dependence on the nature and concentration of the acyl acceptor substrate seems to be a general feature of promiscuous hydrolases/acyltransferases.^{14,24,42,60,62,66} Acyltransferase activity also depends on the acyl donor substrate, as demonstrated for MsAcT, several MsAcT variants, EstCE1, and several other family VIII carboxylesterases/acyltransferases. For example, EstA does not acetylate benzyl alcohol but can acylate it using longer chain acyl donors.²² MsAcT shows a higher AT/H activity ratio when assayed with *p*NP-butyrate compared to *p*NP-acetate as acyl donor.²⁵ This was explained by the larger acyl group hindering binding of water in the active site, similar to the case of lecithin:retinol acyltransferase, where a tight-fitting acyl group excludes hydrolytic water from the active site, thereby promoting acyl transfer.⁵³ This dependence of acyl transfer on the acyl donor substrate seems to be a general feature of promiscuous hydrolases/acyltransferases.^{25,30,72-75}

Since the investigation of multiple enzymes, substrates, concentrations, and time points can be analytically demanding, some convenient colorimetric assays have been developed to facilitate acyltransferase engineering. The simplest of these is based on the release of chromophores like *p*-nitrophenolate, which can be followed at 405 nm, from chromogenic substrate surrogates like *p*-nitrophenyl esters. Acyltransferase activity

corresponds to accelerated turnover of the acyl-enzyme intermediate, which in turn corresponds to faster release of *p*-nitrophenolate, in the presence of an acyl acceptor. Therefore, AT/H ratios for several acyl acceptors (and concentrations) can be simultaneously determined using a microtiter plate reader.^{14,21,22,25,76} Mestrom et al. reported a coupled enzymatic assay for the acetaldehyde released from vinyl esters. This assay is useful since vinyl esters are the most widely used acyl donors in synthetic reactions but may be limited by incompatibility between the acyl acceptors and dehydrogenases employed.^{21,44}

■ SUMMARY AND OUTLOOK

Promiscuous hydrolases/acetyltransferases have the potential to dramatically impact the development and application of biocatalytic cascades for the synthesis of a myriad of valuable esters, thioesters, amides, carbonates, and carbamates in water. This raises the question why transesterification in water is not more often applied in organic synthesis. Our view is that this is because only a few useful enzymes are known, which is because the prevalence of promiscuous hydrolases/acetyltransferases has been underestimated. Recent research on biocatalytic ester and amide synthesis in water has focused on the small number of promiscuous hydrolases/acetyltransferases identified since 1993. However, promiscuous acetyltransferase activity of hydrolases has been observed many times over the last century.^{14,15,19–24,66,72,77–79} In fact, we believe it is possible that some researchers have unknowingly studied promiscuous hydrolases/acetyltransferases. There are several examples of hydrolases that are stimulated by the presence of alcohols like methanol but not by other solvents like DMSO.^{80–83} Therefore, many of these “solvent-stimulated” enzymes may in fact be promiscuous hydrolases/acetyltransferases waiting to be reinvestigated.

On the basis of previous work,^{20,35} we have shown that simple precipitation-based assays can be used to deliberately screen libraries for enzymes with acetyltransferase activity.^{21,23} This simple concept could be used to screen larger metagenome libraries, which would dramatically expand the range of synthetically valuable acetyltransferases available to chemists. We have shown that acetyltransferase activity in the bacterial hormone-sensitive lipases could be predicted from amino acid sequence alone. In principle, this approach could be applied to other enzyme families by developing pipelines for automated structure prediction, using tools like AlphaFold or RoseTTAFold,^{84,85} identification of the active site residues, and ranking by active-site hydrophobicity. However, this method is currently unsuitable for predicting promiscuous acetyltransferase activity toward polar acceptors like sugars, since hydrophilic active sites do not imply affinity for hydrophilic substrates in the same general way a hydrophobic active site in water implies affinity for hydrophobic substrates. Predicting acetyltransferase activity toward hydrophilic compounds is therefore an exciting topic for future research. Because the same protein can be either a hydrolase or an acetyltransferase, depending only on conformational changes^{53,66,76} we anticipate that the success of future algorithms for sequence-based prediction of acetyltransferase activity will depend on sophisticated structure-based models. Therefore, we need to gain more detailed insight into the relationship between sequence, structure, and promiscuous acetyltransferase activity, so it is important that more of these enzymes be characterized. Of particular interest is the correlation between promiscuous

acetyltransferase activity and the half-lives of the acyl-enzyme intermediates of hydrolases in the absence of acyl acceptor substrates. Furthermore, binding affinity for acyl acceptor substrates is seldom determined, and more data would clarify the relative contributions of binding affinity and active site hydrophobicity.

We have shown that many family VIII carboxylesterases are very good acetyltransferases, with AT/H ratios much higher than even the best MsAcT variants. The family VIII carboxylesterases/acetyltransferases do not have very hydrophobic active sites as is typical of MsAcT and the CpLIP2-related lipases/acetyltransferases, and naturally occurring members like EstA can acylate sugars. Protein engineering could also convert EstCE1 into an efficient glucose, maltose, and maltotriose acetylation catalyst. Activity toward polar substrates opens up a wide field of potential applications like modification of the physicochemical properties of starch to produce food grade emulsifiers. Polysaccharide-deacetylating enzymes with promiscuous acetyltransferase activity are known and may present valuable starting points for engineering starch-acylating enzymes.^{20,62,86}

■ AUTHOR INFORMATION

Corresponding Authors

Uwe T. Bornscheuer – Department of Biotechnology & Enzyme Catalysis, Institute of Biochemistry, University of Greifswald, 17487 Greifswald, Germany; orcid.org/0000-0003-0685-2696; Email: uwe.bornscheuer@uni-greifswald.de

Christoffel P. S. Badenhorst – Department of Biotechnology & Enzyme Catalysis, Institute of Biochemistry, University of Greifswald, 17487 Greifswald, Germany; orcid.org/0000-0002-5874-4577; Email: chris.badenhorst@uni-greifswald.de

Authors

Henrik Müller – Department of Biotechnology & Enzyme Catalysis, Institute of Biochemistry, University of Greifswald, 17487 Greifswald, Germany; Competence Center for Biocatalysis, Institute of Chemistry and Biotechnology, Zurich University of Applied Sciences, 8820 Wädenswil, Switzerland

Henrik Terholsen – Department of Biotechnology & Enzyme Catalysis, Institute of Biochemistry, University of Greifswald, 17487 Greifswald, Germany

Simon P. Godehard – Department of Biotechnology & Enzyme Catalysis, Institute of Biochemistry, University of Greifswald, 17487 Greifswald, Germany

Complete contact information is available at: <https://pubs.acs.org/10.1021/acscatal.1c04543>

Notes

The authors declare the following competing financial interest(s): S.P.G. is an employee of BRAIN Biotech AG (Zwingenberg, Germany).

■ REFERENCES

- (1) Bell, E. L.; Finnigan, W.; France, S. P.; Green, A. P.; Hayes, M. A.; Hepworth, L. J.; Lovelock, S. L.; Niikura, H.; Osuna, S.; Romero, E.; Ryan, K. S.; Turner, N. J.; Flitsch, S. L. *Biocatalysis*. *Nat. Rev. Methods Primers* **2021**, *1*, 46.
- (2) Bornscheuer, U. T.; Kazlauskas, R. J. *Hydrolases in Organic Synthesis*; Wiley-VCH: 2006; pp 1–368.

- (3) Wu, S.; Snajdrova, R.; Moore, J. C.; Baldenius, K.; Bornscheuer, U. T. Biocatalysis: Enzymatic Synthesis for Industrial Applications. *Angew. Chem., Int. Ed.* **2021**, *60*, 88–119.
- (4) Zaks, A.; Klibanov, A. M. Enzymatic Catalysis in Organic Media at 100 Degrees C. *Science* **1984**, *224*, 1249–1251.
- (5) Prat, D.; Hayler, J.; Wells, A. A Survey of Solvent Selection Guides. *Green Chem.* **2014**, *16*, 4546–4551.
- (6) Therisod, M.; Klibanov, A. M. Facile Enzymatic Preparation of Monoacylated Sugars in Pyridine. *J. Am. Chem. Soc.* **1986**, *108*, 5638–5640.
- (7) Benkovics, T.; McIntosh, J.; Silverman, S.; Kong, J.; Maligres, P.; Itoh, T.; Yang, H.; Huffman, M.; Verma, D.; Pan, W.; Ho, H.-I.; Vroom, J.; Knight, A.; Hurtak, J.; Morris, W.; Strotman, N.; Murphy, G.; Maloney, K.; Fier, P. Evolving to an Ideal Synthesis of Molnupiravir, an Investigational Treatment for COVID-19. *ChemRxiv*, Dec. 22, **2020**, ver. 1. DOI: 10.26434/chemrxiv.13472373.v1.
- (8) Jiménez-Osés, G.; Osuna, S.; Gao, X.; Sawaya, M. R.; Gilson, L.; Collier, S. J.; Huisman, G. W.; Yeates, T. O.; Tang, Y.; Houk, K. N. The Role of Distant Mutations and Allosteric Regulation on LovD Active Site Dynamics. *Nat. Chem. Biol.* **2014**, *10*, 431–436.
- (9) Philpott, H. K.; Thomas, P. J.; Tew, D.; Fuerst, D. E.; Lovelock, S. L. A Versatile Biosynthetic Approach to Amide Bond Formation. *Green Chem.* **2018**, *20*, 3426–3431.
- (10) D'Auria, J. C. Acyltransferases in Plants: A Good Time to be BAHD. *Curr. Opin. Plant Biol.* **2006**, *9*, 331–340.
- (11) Jiang, Y.; Morley, K. L.; Schrag, J. D.; Kazlauskas, R. J. Different Active-Site Loop Orientation in Serine Hydrolases versus Acyltransferases. *ChemBioChem* **2011**, *12*, 768–776.
- (12) Jencks, W. P.; Gresser, M.; Valenzuela, M. S.; Huneeus, F. C. Acetyl Coenzyme A: Arylamine Acetyltransferase. *J. Biol. Chem.* **1972**, *247*, 3756–3760.
- (13) Kasche, V. Mechanism and Yields in Enzyme Catalysed Equilibrium and Kinetically Controlled Synthesis of β -Lactam Antibiotics, Peptides and other Condensation Products. *Enzyme Microb. Technol.* **1986**, *8*, 4–16.
- (14) Fitch, W. M. Studies on a Cholinesterase of *Pseudomonas fluorescens*: III. Acetyltransferase Activity. *J. Biol. Chem.* **1964**, *239*, 1328–1334.
- (15) Wilson, I. B.; Bergmann, F.; Nachmansohn, D. Acetylcholinesterase X. Mechanism of the Catalysis of Acylation Reactions. *J. Biol. Chem.* **1950**, *186*, 781–790.
- (16) Fournand, D.; Arnaud, A. Aliphatic and Enantioselective Amidases: From Hydrolysis to Acyl Transfer Activity. *J. Appl. Microbiol.* **2001**, *91*, 381–393.
- (17) Liu, M.; Subbaiah, P. V. Hydrolysis and Transesterification of Platelet-Activating Factor by Lecithin-Cholesterol Acyltransferase. *Proc. Natl. Acad. Sci. U. S. A.* **1994**, *91*, 6035–6039.
- (18) Wiktor, M.; Weichert, D.; Howe, N.; Huang, C.-Y.; Olierik, V.; Boland, C.; Bailey, J.; Voageley, L.; Stansfeld, P. J.; Buddelmeijer, N.; Wang, M.; Caffrey, M. Structural Insights into the Mechanism of the Membrane Integral N-Acyltransferase Step in Bacterial Lipoprotein Synthesis. *Nat. Commun.* **2017**, *8*, 15952.
- (19) Willstätter, R.; Stoll, A. Untersuchungen über Chlorophyll. XI. Über Chlorophyllase. *Justus Liebigs Ann. Chem.* **1911**, *378*, 18–72.
- (20) Mathews, I.; Soltis, M.; Saldajeno, M.; Ganshaw, G.; Sala, R.; Weyler, W.; Cervin, M. A.; Whited, G.; Bott, R. Structure of a Novel Enzyme that Catalyzes Acyl Transfer to Alcohols in Aqueous Conditions. *Biochemistry* **2007**, *46*, 8969–8979.
- (21) Müller, H.; Becker, A.-K.; Palm, G. J.; Berndt, L.; Badenhorst, C. P. S.; Godehard, S. P.; Reisky, L.; Lammers, M.; Bornscheuer, U. T. Sequence-Based Prediction of Promiscuous Acyltransferase Activity in Hydrolases. *Angew. Chem., Int. Ed.* **2020**, *59*, 11607–11612.
- (22) Müller, H.; Godehard, S. P.; Palm, G. J.; Berndt, L.; Badenhorst, C. P. S.; Becker, A.-K.; Lammers, M.; Bornscheuer, U. T. Discovery and Design of Family VIII Carboxylesterases as Highly Efficient Acyltransferases. *Angew. Chem., Int. Ed.* **2021**, *60*, 2013–2017.
- (23) Reisky, L.; Srinivasamurthy, V. S. T.; Badenhorst, C. P. S.; Godehard, S. P.; Bornscheuer, U. T. A Novel High-Throughput Assay Enables the Direct Identification of Acyltransferases. *Catalysts* **2019**, *9*, 64.
- (24) Riaublanc, A.; Ratomahenina, R.; Galzy, P.; Nicolas, M. Peculiar Properties of Lipase from *Candida parapsilosis* (Ashford) Langeron and Talice. *J. Am. Oil Chem. Soc.* **1993**, *70*, 497–500.
- (25) Godehard, S. P.; Badenhorst, C. P. S.; Müller, H.; Bornscheuer, U. T. Protein Engineering for Enhanced Acyltransferase Activity, Substrate Scope, and Selectivity of the *Mycobacterium smegmatis* Acyltransferase MsAcT. *ACS Catal.* **2020**, *10*, 7552–7562.
- (26) Jan, A. H.; Subileau, M.; Deyrieux, C.; Perrier, V.; Dubreucq, E. Elucidation of a Key Position for Acyltransfer Activity in *Candida parapsilosis* Lipase/Acyltransferase (CpLIP2) and in *Pseudozyma antarctica* Lipase A (CAL-A) by Rational Design. *Biochim. Biophys. Acta, Proteins Proteomics* **2016**, *1864*, 187–194.
- (27) Larsen, M. W.; Zielinska, D. F.; Martinelle, M.; Hidalgo, A.; Jensen, L. J.; Bornscheuer, U. T.; Hult, K. Suppression of Water as a Nucleophile in *Candida antarctica* Lipase B Catalysis. *ChemBioChem* **2010**, *11*, 796–801.
- (28) Yeats, T. H.; Martin, L. B. B.; Viart, H. M. F.; Isaacson, T.; He, Y.; Zhao, L.; Matas, A. J.; Buda, G. J.; Domozych, D. S.; Clausen, M. H.; Rose, J. K. C. The Identification of Cutin Synthase: Formation of the Plant Polyester Cutin. *Nat. Chem. Biol.* **2012**, *8*, 609–611.
- (29) Li, A. X.; Steffens, J. C. An Acyltransferase Catalyzing the Formation of Diacylglycerol is a Serine Carboxypeptidase-Like Protein. *Proc. Natl. Acad. Sci. U. S. A.* **2000**, *97*, 6902–6907.
- (30) Teutschbein, J.; Gross, W.; Nimtz, M.; Milkowski, C.; Hause, B.; Strack, D. Identification and Localization of a Lipase-Like Acyltransferase in Phenylpropanoid Metabolism of Tomato (*Solanum lycopersicum*). *J. Biol. Chem.* **2010**, *285*, 38374–38381.
- (31) Jan, A.-H.; Dubreucq, E.; Drone, J.; Subileau, M. A Glimpse into the Specialization History of the Lipases/Acyltransferases Family of CpLIP2. *Biochim. Biophys. Acta, Proteins Proteomics* **2017**, *1865*, 1105–1113.
- (32) Müller, J.; Sowa, M. A.; Dörr, M.; Bornscheuer, U. T. The Acyltransferase Activity of Lipase CAL-A Allows Efficient Fatty Acid Esters Formation from Plant Oil even in an Aqueous Environment. *Eur. J. Lipid Sci. Technol.* **2015**, *117*, 1903–1907.
- (33) Müller, J.; Sowa, M. A.; Fredrich, B.; Brundiek, H.; Bornscheuer, U. T. Enhancing the Acyltransferase Activity of *Candida antarctica* Lipase A by Rational Design. *ChemBioChem* **2015**, *16*, 1791–1796.
- (34) Biermann, U.; Bornscheuer, U. T.; Feussner, I.; Meier, M. A. R.; Metzger, J. O. Fatty Acids and their Derivatives as Renewable Platform Molecules for the Chemical Industry. *Angew. Chem., Int. Ed.* **2021**, *60*, 20144–20165.
- (35) Schmidt, S.; Scherkus, C.; Muschiol, J.; Menyés, U.; Winkler, T.; Hummel, W.; Gröger, H.; Liese, A.; Herz, H.-G.; Bornscheuer, U. T. An Enzyme Cascade Synthesis of ϵ -Caprolactone and its Oligomers. *Angew. Chem., Int. Ed.* **2015**, *54*, 2784–2787.
- (36) Land, H.; Hendil-Forsell, P.; Martinelle, M.; Berglund, P. One-Pot Biocatalytic Amine Transaminase/Acyl Transferase Cascade for Aqueous Formation of Amides from Aldehydes or Ketones. *Catal. Sci. Technol.* **2016**, *6*, 2897–2900.
- (37) Wiermans, L.; Hofzumahaus, S.; Schotten, C.; Weigand, L.; Schallmeyer, M.; Schallmeyer, A.; Domínguez de María, P. Transesterifications and Peracid-Assisted Oxidations in Aqueous Media Catalyzed by *Mycobacterium smegmatis* Acyl Transferase. *ChemCatChem* **2013**, *5*, 3719–3724.
- (38) Finnveden, M.; Semlitsch, S.; He, O.; Martinelle, M. Mono-Substitution of Symmetric Diesters: Selectivity of *Mycobacterium smegmatis* Acyltransferase Variants. *Catal. Sci. Technol.* **2019**, *9*, 4920–4927.
- (39) Perdomo, I. C.; Gianolio, S.; Pinto, A.; Romano, D.; Contente, M. L.; Paradisi, F.; Molinari, F. Efficient Enzymatic Preparation of Flavor Esters in Water. *J. Agric. Food Chem.* **2019**, *67*, 6517–6522.
- (40) Annunziata, F.; Contente, M. L.; Pinna, C.; Tamborini, L.; Pinto, A. Biocatalyzed Flow Oxidation of Tyrosol to Hydroxytyrosol

- and Efficient Production of their Acetate Esters. *Antioxidants* **2021**, *10*, 1142.
- (41) Jost, E.; Kazemi, M.; Mrkonjić, V.; Himo, F.; Winkler, C. K.; Kroutil, W. Variants of the Acyltransferase from *Mycobacterium smegmatis* Enable Enantioselective Acyl Transfer in Water. *ACS Catal.* **2020**, *10*, 10500–10507.
- (42) de Leeuw, N.; Torrelo, G.; Bisterfeld, C.; Resch, V.; Mestrom, L.; Straulino, E.; van der Weel, L.; Hanefeld, U. Ester Synthesis in Water: *Mycobacterium smegmatis* Acyl Transferase for Kinetic Resolutions. *Adv. Synth. Catal.* **2018**, *360*, 242–249.
- (43) Tswett, M. Über die Natur des Sogenannten “Krystallisierbaren Chlorophylls” (Metachlorophyllins). *Biochem. Z.* **1908**, *10*, 414–425.
- (44) Mestrom, L.; Claessen, J. G. R.; Hanefeld, U. Enzyme-Catalyzed Synthesis of Esters in Water. *ChemCatChem* **2019**, *11*, 2004–2010.
- (45) Funabashi, M.; Yang, Z.; Nonaka, K.; Hosobuchi, M.; Fujita, Y.; Shibata, T.; Chi, X.; Van Lanen, S. G. An ATP-Independent Strategy for Amide Bond Formation in Antibiotic Biosynthesis. *Nat. Chem. Biol.* **2010**, *6*, 581–586.
- (46) Liu, X.; Jin, Y.; Cai, W.; Green, K. D.; Goswami, A.; Garneau-Tsodikova, S.; Nonaka, K.; Baba, S.; Funabashi, M.; Yang, Z.; Van Lanen, S. G. A Biocatalytic Approach to Capuramycin Analogues by Exploiting a Substrate Permissive *N*-Transacylase CapW. *Org. Biomol. Chem.* **2016**, *14*, 3956–3962.
- (47) Hult, K.; Berglund, P. Enzyme Promiscuity: Mechanism and Applications. *Trends Biotechnol.* **2007**, *25*, 231–238.
- (48) Köller, W.; Kolattukudy, P. E. Mechanism of Action of Cutinase: Chemical Modification of the Catalytic Triad Characteristic for Serine Hydrolases. *Biochemistry* **1982**, *21*, 3083–3090.
- (49) Subileau, M.; Jan, A. H.; Nozac'h, H.; Perez-Gordo, M.; Perrier, V.; Dubreucq, E. The 3D Model of the Lipase/Acyltransferase from *Candida parapsilosis*, a Tool for the Elucidation of Structural Determinants in CAL-A Lipase Superfamily. *Biochim. Biophys. Acta, Proteins Proteomics* **2015**, *1854*, 1400–1411.
- (50) Bruner, S. D.; Weber, T.; Kohli, R. M.; Schwarzer, D.; Marahiel, M. A.; Walsh, C. T.; Stubbs, M. T. Structural Basis for the Cyclization of the Lipopeptide Antibiotic Surfactin by the Thioesterase Domain SrfTE. *Structure* **2002**, *10*, 301–310.
- (51) Poust, S.; Yoon, I.; Adams, P. D.; Katz, L.; Petzold, C. J.; Keasling, J. D. Understanding the Role of Histidine in the GHSxG Acyltransferase Active Site Motif: Evidence for Histidine Stabilization of the Malonyl-Enzyme Intermediate. *PLoS One* **2014**, *9*, No. e109421.
- (52) Jones, C. S.; Sychantha, D.; Howell, P. L.; Clarke, A. J. Structural Basis for the *O*-Acetyltransferase Function of the Extracytoplasmic Domain of OatA from *Staphylococcus aureus*. *J. Biol. Chem.* **2020**, *295*, 8204–8213.
- (53) Golczak, M.; Sears, A. E.; Kiser, P. D.; Palczewski, K. LRAT-Specific Domain Facilitates Vitamin A Metabolism by Domain Swapping in HRASLS3. *Nat. Chem. Biol.* **2015**, *11*, 26–32.
- (54) Mirza, I. A.; Nazi, I.; Korczynska, M.; Wright, G. D.; Berghuis, A. M. Crystal Structure of Homoserine Transacetylase from *Haemophilus influenzae* Reveals a New Family of Alpha/Beta-Hydrolases. *Biochemistry* **2005**, *44*, 15768–15773.
- (55) Kazemi, M.; Sheng, X.; Kroutil, W.; Himo, F. Computational Study of *Mycobacterium smegmatis* Acyl Transferase Reaction Mechanism and Specificity. *ACS Catal.* **2018**, *8*, 10698–10706.
- (56) Lejon, S.; Ellis, J.; Valegard, K. The Last Step in Cephalosporin C Formation Revealed: Crystal Structures of Deacetylcephalosporin C Acetyltransferase from *Acremonium chrysogenum* in Complexes with Reaction Intermediates. *J. Mol. Biol.* **2008**, *377*, 935–944.
- (57) Iqbal, A.; Clifton, I. J.; Bagonis, M.; Kershaw, N. J.; Domene, C.; Claridge, T. D.; Wharton, C. W.; Schofield, C. J. Anatomy of a Simple Acyl Intermediate in Enzyme Catalysis: Combined Biophysical and Modeling Studies on Ornithine Acetyl Transferase. *J. Am. Chem. Soc.* **2009**, *131*, 749–757.
- (58) Lima, C. G. S.; Monteiro, J. L.; de Melo Lima, T.; Weber Paixao, M.; Correa, A. G. Angelica Lactones: From Biomass-Derived Platform Chemicals to Value-Added Products. *ChemSusChem* **2018**, *11*, 25–47.
- (59) Poterala, M.; Borowiecki, P. From Waste to Value-Direct Utilization of α -Angelica Lactone as a Nonconventional Irreversible Acylating Agent in a Chromatography-Free Lipase-Catalyzed KR Approach toward *sec*-Alcohols. *ACS Sustainable Chem. Eng.* **2021**, *9*, 10276–10290.
- (60) Staudt, A.; Terholsen, H.; Kaur, J.; Müller, H.; Godehard, S. P.; Itabaiana, I.; Leal, I. C. R.; Bornscheuer, U. T. Rational Design for Enhanced Acyltransferase Activity in Water Catalyzed by the *Pyrobaculum calidifontis* VA1 Esterase. *Microorganisms* **2021**, *9*, 1790.
- (61) Rodrigues, J.; Perrier, V.; Lecomte, J.; Dubreucq, E.; Ferreira-Dias, S. Biodiesel Production from Crude Jatropha Oil Catalyzed by Immobilized Lipase/Acyltransferase from *Candida parapsilosis* in Aqueous Medium. *Bioresour. Technol.* **2016**, *218*, 1224–1229.
- (62) Godehard, S. P.; Müller, H.; Badendorst, C. P. S.; Stanetty, C.; Suster, C.; Mihovilovic, M. D.; Bornscheuer, U. T. Efficient Acylation of Sugars and Oligosaccharides in Aqueous Environment Using Engineered Acyltransferases. *ACS Catal.* **2021**, *11*, 2831–2836.
- (63) Contente, M. L.; Farris, S.; Tamborini, L.; Molinari, F.; Paradisi, F. Flow-Based Enzymatic Synthesis of Melatonin and other High Value Tryptamine Derivatives: a Five-Minute Intensified Process. *Green Chem.* **2019**, *21*, 3263–3266.
- (64) Okachi, R.; Hashimoto, Y.; Kawamori, M.; Katsumata, R.; Takayama, K.; Nara, T. In *Enzyme Engineering*; Chibata, I., Fukui, S., Wingard, L. B., Eds.; Springer: Boston, MA, 1982; pp 81–90.
- (65) Contente, M. L.; Roura Padrosa, D.; Molinari, F.; Paradisi, F. A Strategic Ser/Cys Exchange in the Catalytic Triad Unlocks an Acyltransferase-Mediated Synthesis of Thioesters and Tertiary Amides. *Nat. Catal.* **2020**, *3*, 1020–1026.
- (66) Carey, L. M.; Rodriguez, A.; Meighen, E. Generation of Fatty Acids by an Acyl Esterase in the Bioluminescent System of *Photobacterium phosphoreum*. *J. Biol. Chem.* **1984**, *259*, 10216–10221.
- (67) Michalski, T. J.; Hunt, J. E.; Bradshaw, C.; Wagner, A. M.; Norris, J. R.; Katz, J. J. Enzyme-Catalyzed Organic Syntheses: Transesterification Reactions of Chlorophyll a, Bacteriochlorophyll a, and Derivatives with Chlorophyllase. *J. Am. Chem. Soc.* **1988**, *110*, 5888–5891.
- (68) Zhang, Y.; Ding, L.; Yan, Z.; Zhou, D.; Jiang, J.; Qiu, J.; Xin, Z., Identification and Characterization of a Novel Carboxylesterase Belonging to Family VIII with Promiscuous Acyltransferase Activity toward Cyanidin-3-*O*-glucoside from a Soil Metagenomic Library. *Appl. Biochem. Biotechnol.* **2021**, DOI: 10.1007/s12010-021-03614-9.
- (69) Subileau, M.; Jan, A. H.; Drone, J.; Rutyna, C.; Perrier, V.; Dubreucq, E. What Makes a Lipase a Valuable Acyltransferase in Water Abundant Medium? *Catal. Sci. Technol.* **2017**, *7*, 2566–2578.
- (70) Contente, M. L.; Tamborini, L.; Molinari, F.; Paradisi, F. Aromas Flow: Eco-Friendly, Continuous, and Scalable Preparation of Flavour Esters. *J. Flow Chem.* **2020**, *10*, 235–240.
- (71) Liang, Y.; Lu, X. Structural Insights into the Catalytic Mechanism of Lovastatin Hydrolase. *J. Biol. Chem.* **2020**, *295*, 1047–1055.
- (72) Goldberg, M. I.; Fruton, J. S. Beef Liver Esterase as a Catalyst of Acyl Transfer to Amino Acid Esters. *Biochemistry* **1969**, *8*, 86–97.
- (73) Clarke, P. H. The Aliphatic Amidases of *Pseudomonas aeruginosa*. *Adv. Microb. Physiol.* **1969**, *4*, 179–222.
- (74) Kikuta, Y.; Ueda, H.; Takahashi, M.; Mitsumori, T.; Yamada, G.; Sakamori, K.; Takeda, K.; Furutani, S.; Nakayama, K.; Katsuda, Y.; Hatanaka, A.; Matsuda, K. Identification and Characterization of a GDSL Lipase-Like Protein that Catalyzes the Ester-Forming Reaction for Pyrethrin Biosynthesis in *Tanacetum cinerariifolium* - a New Target for Plant Protection. *Plant J.* **2012**, *71*, 183–193.
- (75) Mattson, A.; Boutelje, J.; Csöreg, I.; Hjalmarsson, M.; Jacobsson, U.; Lindbäck, M.; Norin, T.; Szmulik, P.; Hult, K. Enhanced Stereoselectivity in Pig Liver Esterase Catalysed Diester Hydrolysis. The Role of a Competitive Nucleophile. *Bioorg. Med. Chem.* **1994**, *2*, 501–508.

- (76) Ferri, S. R.; Meighen, E. A. An Essential Histidine Residue Required for Fatty Acylation and Acyl Transfer by Myristoyltransferase from Luminescent Bacteria. *J. Biol. Chem.* **1994**, *269*, 6683–6688.
- (77) Glazer, A. N. Transesterification Reactions Catalyzed by Trypsin. *J. Biol. Chem.* **1965**, *240*, 1135–1137.
- (78) Glazer, A. N. Transesterification Reactions Catalyzed by Papain. *J. Biol. Chem.* **1966**, *241*, 3811–3817.
- (79) Glazer, A. N. Transesterification Reactions Catalyzed by Subtilisins. *J. Biol. Chem.* **1966**, *241*, 635–638.
- (80) Lee, H. W.; Jung, W. K.; Kim, Y. H.; Ryu, B. H.; Kim, T. D.; Kim, J.; Kim, H. Characterization of a Novel Alkaline Family VIII Esterase with S-Enantiomer Preference from a Compost Metagenomic Library. *J. Microbiol. Biotechnol.* **2016**, *26*, 315–325.
- (81) Ouyang, L. M.; Liu, J. Y.; Qiao, M.; Xu, J. H. Isolation and Biochemical Characterization of Two Novel Metagenome-Derived Esterases. *Appl. Biochem. Biotechnol.* **2013**, *169*, 15–28.
- (82) Rashamuse, K.; Magomani, V.; Ronneburg, T.; Brady, D. A Novel Family VIII Carboxylesterase Derived from a Leachate Metagenome Library Exhibits Promiscuous Beta-Lactamase Activity on Nitrocefin. *Appl. Microbiol. Biotechnol.* **2009**, *83*, 491–500.
- (83) Selvin, J.; Kennedy, J.; Lejon, D. P. H.; Kiran, G. S.; Dobson, A. D. W. Isolation Identification and Biochemical Characterization of a Novel Halo-Tolerant Lipase from the Metagenome of the Marine Sponge *Haliclona simulans*. *Microb. Cell Fact.* **2012**, *11*, 72.
- (84) Baek, M.; DiMaio, F.; Anishchenko, I.; Dauparas, J.; Ovchinnikov, S.; Lee, G. R.; Wang, J.; Cong, Q.; Kinch, L. N.; Schaeffer, R. D.; Millán, C.; Park, H.; Adams, C.; Glassman, C. R.; DeGiovanni, A.; Pereira, J. H.; Rodrigues, A. V.; van Dijk, A. A.; Ebrecht, A. C.; Opperman, D. J.; Sagmeister, T.; Buhlheller, C.; Pavkov-Keller, T.; Rathinaswamy, M. K.; Dalwadi, U.; Yip, C. K.; Burke, J. E.; Garcia, K. C.; Grishin, N. V.; Adams, P. D.; Read, R. J.; Baker, D. Accurate Prediction of Protein Structures and Interactions Using a Three-Track Neural Network. *Science* **2021**, *373*, 871–876.
- (85) Jumper, J.; Evans, R.; Pritzel, A.; Green, T.; Figurnov, M.; Ronneberger, O.; Tunyasuvunakool, K.; Bates, R.; Zidek, A.; Potapenko, A.; Bridgland, A.; Meyer, C.; Kohl, S. A. A.; Ballard, A. J.; Cowie, A.; Romera-Paredes, B.; Nikolov, S.; Jain, R.; Adler, J.; Back, T.; Petersen, S.; Reiman, D.; Clancy, E.; Zielinski, M.; Steinegger, M.; Pacholska, M.; Berghammer, T.; Bodenstein, S.; Silver, D.; Vinyals, O.; Senior, A. W.; Kavukcuoglu, K.; Kohli, P.; Hassabis, D. Highly Accurate Protein Structure Prediction with AlphaFold. *Nature* **2021**, *596*, 583–589.
- (86) Oh, C.; Ryu, B. H.; An, D. R.; Nguyen, D. D.; Yoo, W.; Kim, T.; Ngo, T. D.; Kim, H. S.; Kim, K. K.; Kim, T. D. Structural and Biochemical Characterization of an Octameric Carbohydrate Acetyltransferase from *Sinorhizobium meliloti*. *FEBS Lett.* **2016**, *590*, 1242–1252.

Article IV



Article

Rational Design for Enhanced Acyltransferase Activity in Water Catalyzed by the *Pyrobaculum calidifontis* VA1 Esterase

Amanda Staudt^{1,2}, Henrik Terholsen¹, Jasmin Kaur¹, Henrik Müller¹, Simon P. Godehard¹,IVALDO ITABAIANA, JR.³, IVANA C. R. LEAL² and Uwe T. Bornscheuer^{1,*}

¹ Department of Biotechnology & Enzyme Catalysis, Institute of Biochemistry, University of Greifswald, 17487 Greifswald, Germany; amanda_staudt@hotmail.com (A.S.);

henrik.terholsen@uni-greifswald.de (H.T.); jasmin.kaur@stud.uni-greifswald.de (J.K.); henrikmuller1301@gmail.com (H.M.); simon_godehard@icloud.com (S.P.G.)

² Laboratory of Natural Products and Biological Assays, Department of Natural Products and Food, Faculty of Pharmacy, Federal University of Rio de Janeiro, Rio de Janeiro 21941-902, Brazil; ivanafarma@yahoo.com.br

³ Laboratory of Technological Biochemistry and Biocatalysis, Department of Biochemical Engineering, School of Chemistry, Federal University of Rio de Janeiro, Rio de Janeiro 21941-909, Brazil; ivaldoufrj@gmail.com

* Correspondence: uwe.bornscheuer@uni-greifswald.de

Citation: Staudt, A.; Terholsen, H.; Kaur, J.; Müller, H.; Godehard, S.P.; Itabaiana, I., Jr.; Leal, I.C.R.; Bornscheuer, U.T. Rational Design for Enhanced Acyltransferase Activity in Water Catalyzed by the *Pyrobaculum calidifontis* VA1 Esterase. *Microorganisms* **2021**, *9*, 1790. <https://doi.org/10.3390/microorganisms9081790>

Academic Editors: Dietmar Haltrich and Daniel Kracher

Received: 26 July 2021

Accepted: 20 August 2021

Published: 23 August 2021

Publisher's Note: MDPI stays neutral with regard to jurisdictional claims in published maps and institutional affiliations.



Copyright: © 2021 by the authors. Licensee MDPI, Basel, Switzerland. This article is an open access article distributed under the terms and conditions of the Creative Commons Attribution (CC BY) license (<http://creativecommons.org/licenses/by/4.0/>).

Abstract: Biocatalytic transesterification is commonly carried out employing lipases in anhydrous organic solvents since hydrolases usually prefer hydrolysis over acyl transfer in bulk water. However, some promiscuous acyltransferases can catalyze acylation in an aqueous solution. In this study, a rational design was performed to enhance the acyltransferase selectivity and substrate scope of the *Pyrobaculum calidifontis* VA1 esterase (PestE). PestE wild type and variants were applied for the acylation of monoterpene alcohols. The mutant PestE_I208A is selective for (–)-menthyl acetate (E-Value = 55). Highly active acyltransferases were designed, allowing for complete conversion of (–)-citronellol to citronellyl acetate. Additionally, carvacrol was acetylated but with lower conversions. To the best of our knowledge, this is the first example of the biocatalytic acylation of a phenolic alcohol in bulk water. In addition, a high citronellol conversion of 92% was achieved with the more environmentally friendly and inexpensive acyl donor ethyl acetate using PestE_N288F as a catalyst. PestE_N288F exhibits good acyl transfer activity in an aqueous medium and low hydrolysis activity at the same time. Thus, our study demonstrates an alternative synthetic strategy for acylation of compounds without organic solvents.

Keywords: PestE; acyltransferase; protein engineering; biocatalysis; acyl transfer; transesterification; monoterpene acylation

1. Introduction

Hydrolytic enzymes are versatile biocatalysts with many industrial applications, due to their broad substrate scope, absence of cofactor requirements, stability in organic solvents, and good chemo-, regio-, and stereoselectivity [1–3]. Usually, these enzymes are applied for the hydrolysis of esters, amides, or lipids in aqueous systems, since water acts as a nucleophile in the reaction [4,5]. Still, these enzymes can also act as biocatalysts for condensation reactions and in alcoholysis [1].

The capacity of some hydrolases, especially lipases, to synthesize esters and amides under anhydrous conditions increases the applicability of these enzymes [1,6,7]. Nevertheless, hydrolases typically favor a hydrolytic reaction over acyl transfer in water [8–11], limiting the direct acylation of interesting substances found naturally in aqueous raw materials.

In contrast to conventional hydrolases, some promiscuous hydrolases/acyltransferases are able to catalyze acyl transfer in aqueous systems, presenting an opportunity for cascade reactions in aqueous solutions. This is also more environmentally friendly than ionic liquids [12] or often hazardous and expensive organic solvents [5,13], which are then no longer required. Examples of promiscuous acyltransferases are enzymes from the CAL-A superfamily [14], an aryl esterase from *Mycobacterium smegmatis* (MsAcT) [13,15,16], family VIII carboxylesterases [17], and the enzymes from the bacterial hormone-sensitive lipase (bHSL) family [5,18].

Due to their acyltransferase activity in water, a lipase from *Sphingomonas* sp. (SpL) and the lipase A from *Pseudozyma antarctica* (CAL-A) were used for amide and ester synthesis in the presence of 4% and 50% water, respectively [19,20]. Regarding cascade reactions, the acyltransferase MsAcT was applied in a combination with a transaminase to synthesize *N*-benzylacetamide from benzaldehyde [21]. Furthermore, MsAcT was investigated in our group, and we observed approximately 50% conversion in the synthesis of benzyl acetate in a transesterification reaction between vinyl acetate and benzyl alcohol at an equimolar ratio in an aqueous environment [13].

Recently, our group also discovered esterase Est8 as a promiscuous hydrolase/acyltransferase. Est8 was the first enzyme from the bacterial hormone-sensitive lipase (bHSL) family, for which promiscuous acyltransferase activity was described [18]. Subsequently, we developed a sequence-based prediction method for acyltransferase activity, demonstrating that the active site hydrophobicity is directly related to the acyltransferase activity towards non-polar acyl acceptors. This analysis made it possible to identify and biochemically characterize five bHSLs with high acyltransferase activity [5].

One of the most promising acyltransferases identified in the study by Müller et al. [5] was the *Pyrobaculum calidifontis* VA1 esterase (PestE). This carboxylesterase (PDB code: 3ZWQ), first reported by Hotta et al. [22], is a highly thermostable biocatalyst. It has been shown to catalyze the hydrolysis of bulky substrates [22,23] and notably presents activity towards tertiary alcohols in transesterification reactions in organic solvents [6], which was associated with the high hydrophobicity inside the substrate-binding pocket [5,24]. Recognizing the high potential of this enzyme, in this work, we performed a rational design to enhance its acyltransferase activity for the biocatalytic synthesis of monoterpene esters in an aqueous solution without organic solvents.

2. Materials and Methods

2.1. Material

(±)-Linalool (97%), (±)-menthol (≥ 98.0%), (±)-citronellol (analytical standard), carvacrol (99%), (–)-menthol (99%), and vinyl acetate were purchased from Sigma-Aldrich. All other chemicals and solvents were purchased from Sigma, VWR, or Carl Roth. The synthetic gene encoding PestE for expression in *Escherichia coli*—subcloned into the pET-21a vector—was based on the gene reported by Hotta et al. [22].

2.2. Gene Expression and Protein Purification

Chemically competent *E. coli* BL21(DE3) cells were transformed with expression vectors by heat shock followed by cooling and then plated on LB agar containing 50 µg·mL⁻¹ ampicillin. Pre-cultures (4 mL LB containing 50 µg·mL⁻¹ ampicillin) were inoculated with single colonies and incubated overnight (37 °C, 180 rpm). LB medium (200 mL containing 50 µg·mL⁻¹ ampicillin) was inoculated with 0.1% (*v/v*) of the pre-culture and incubated (37 °C, 180 rpm) until it reached an OD₆₀₀ of 0.6. Protein expression was induced by the addition of isopropyl-β-D-thiogalactopyranoside (IPTG) to a final concentration of 0.4 mM followed by incubation for ~20 h at 20 °C at 180 rpm.

Cells were harvested by centrifugation at 4000× *g* and 4 °C for 15 min, and the cell pellets were resuspended with 4 mL equilibration buffer (50 mM potassium phosphate,

300 mM sodium chloride, 10 mM imidazole, pH 8.0). Cells were disrupted by sonication on ice (two cycles of 5 min sonication (30% intensity, 50% pulsed cycle)) using a SONOPULS HD 2070 (BANDELIN Electronic GmbH & Co. KG, Berlin, Germany), and the lysates were clarified by centrifugation at 10,000× *g* and 4 °C for 30 min. For purification, the crude lysates were applied to 1.5 mL Roti® Garose-His/Ni Beads (Carl Roth, Karlsruhe, Germany). The resins were washed with 15 mL washing buffer (50 mM sodium phosphate, 300 mM sodium chloride, 20 mM imidazole, pH 8.0) before target proteins were eluted with elution buffer (50 mM sodium phosphate, 300 mM sodium chloride, 250 mM imidazole, pH 8.0). Elution fractions were treated at 80 °C for 20 min (500 rpm), centrifuged (17,000× *g*, 4 °C for 5 min), and the supernatant transferred to the storage buffer (50 mM potassium phosphate, 300 mM sodium chloride, pH 8.0) using PD-10 desalting columns (GE Healthcare, Chalfont St Giles, UK). Protein concentrations were determined at 280 nm using a NanoDrop™ 1000 spectrophotometer (ThermoFisher, Darmstadt, Germany), while the purity of the proteins was investigated by SDS-PAGE. The purified enzymes were mixed with 0.1% (*v/v*) Triton-X-100 for storage at 4 °C.

2.3. In Silico Methods

Structural analysis and molecular modeling experiments of the structure of PestE (PDB entry: 3ZWQ) were performed using YASARA (Vienna, Austria) [25] and UCSF Chimera (San Francisco, CA, USA) [26]. The substrate-binding sites in the PestE crystal structure were identified and analyzed using the VINA docking tool [27] of the YASARA software. Molecular modeling was performed by two different approaches: the first was by evaluating the residues responsible for the water network and changing the structure to minimize hydrolase activity. The second was by increasing the hydrophobicity using the Chimera software with visualization of hydrophobic and hydrophilic regions.

2.4. Site-Directed Mutagenesis

Variants were constructed using the Q5® Site-Directed Mutagenesis Kit (New England Biolabs GmbH, Ipswich, UK). Non-overlapping DNA-oligonucleotides were designed using the online NEBaseChanger tool for the mutations: H95A: forward primer (5'→3'): CGTGGAGACTgcgGACCACGTGTGTAGGC; reverse primer (5'→3'): CTCCCCAA GACGAAGCCC; I208A: forward primer (5'→3'): CGAATACGTCgcg CTCACCGCCGACTTAATGG; reverse primer (5'→3'): GGCCCGCTGTACTCCACT; N288F: forward primer (5'→3'): CGGCTTCGTCtttTTCTACCCCATATTAGAAG, reverse primer (5'→3'): TGGATGACGCCGTTGTAC. PCR amplification and KLD reactions were performed according to the manufacturer's protocol. The correct introduction of the desired mutations was confirmed by sequencing by Eurofins Genomics GmbH (Ebersberg, Germany).

2.5. SDS-PAGE Analysis

The protein purity was analyzed by SDS-PAGE. Purified proteins were denatured by heating (95 °C, 10 min) in a 10% (*w/v*) sodium dodecyl sulfate (SDS) solution followed by centrifugation at 13,000× *g* for 5 min. The proteins were separated on 12.5% acrylamide gels at a constant voltage of 200 V. A protein standard was added for protein size comparison (Pierce™ Unstained Protein MW Marker, ThermoFisher, Darmstadt, Germany) and stained by Coomassie Brilliant Blue G-250.

2.6. Biocatalytic Experiments

Purified PestEs (wild type and variants) were applied for transesterification of linalool, menthol, carvacrol, and citronellol. For the reactions, a mixture of 20 mM monoterpene (from a 1 M stock in acetonitrile), vinyl acetate at a molar ratio of 1:10 (monoterpene:acyl donor), 0.1% (*v/v*) Triton-X-100 (from a 10% (*v/v*) stock in water), and 0.2 µg·mL⁻¹ of the purified PestE variants were adjusted to a total volume of 1 mL with

buffer (50 mM potassium phosphate, 300 mM sodium chloride, pH 8.0). Reactions were performed in 1.5 mL reaction tubes and incubated at 40 °C and 1000 rpm in a ThermoMixer Comfort (Eppendorf AG, Hamburg, Germany). Reactions without enzymes were performed to determine background transesterification and served as control. Time samples (10 µL) were taken, quenched with 10 µL of 2 M HCl, and extracted with 200 µL ethyl acetate (EtOAc). After drying with anhydrous MgSO₄, samples were analyzed by GC. In order to evaluate the possibility of producing monoterpene esters with a more environmentally friendly and cheaper acyl donor, reactions were also performed for (±)-citronellol with ethyl acetate as acyl donor. The reaction conditions were described above, with 20 µg·mL⁻¹ of the purified PestE variants.

2.7. GC Analysis

Reactions with linalool, carvacrol, and citronellol were analyzed by GC-MS using a GC-QP2010 SE (Shimadzu, Kyoto, Japan) equipped with a ZB-5MSi column (30.0 m × 0.25 mm, 0.25 µm film thickness, Phenomenex, Torrance, CA, USA). Injector temperature was 220 °C, a flow rate of 1.20 mL·min⁻¹ was used, and 1 µL sample at a split ratio of 10 was injected. The column temperature was held at 80 °C for 3 min, increased to 260 °C at 10 °C·min⁻¹, totalizing a 21 min method. Mass spectrum ion source and interface temperature was 220 °C, and the identification started after 3 min of the run.

Biocatalysis reactions with menthol were analyzed by GC-MS using a GC-QP2010 SE (Shimadzu, Kyoto, Japan) equipped with a β-TBDAC column (25.0 m × 0.25 mm, Macherey-Nagel, Düren, Germany). Injector temperature was 220 °C, a flow rate of 2.06 mL·min⁻¹ was used, and 1 µL sample at a split ratio of 30 was injected. The column temperature was held at 80 °C for 5 min, increased to 145 °C at 1.75 °C·min⁻¹, held for 5 min, and then increased to 180 °C at 20 °C·min⁻¹ and kept for 6.11 min, resulting in a 55 min method. Mass spectrum ion source and interface temperature were 220 °C.

3. Results

An initial study regarding menthol acylation with known hydrolases/acyltransferases was performed in order to verify potential acyltransferases for monoterpene ester synthesis. For this, the enzymes PestE, 1EVQ (Est2 from *Alicyclobacillus acidocaldarius*), CAL-A (lipase A from *Pseudozyma antarctica*), and PLE-6 (Pig Liver Esterase 6) were applied as catalysts. PestE showed the highest activity in menthol acylation (Figure S1), achieving 81% of the esterified product but with undesired subsequent hydrolysis. This behavior is known as an obstacle for biocatalytic ester production in water, in view that the optimum time point for the highest conversion needs to be determined to stop the reaction immediately; this makes enzymatic acyl transfer reactions in water somewhat challenging [5]. In addition, the possibility of enabling enantioselective acylation of (±)-menthol by mutagenesis has been investigated.

Aiming to decrease product hydrolysis, PestE was used as an object for the rational design. To identify target residues for site-directed mutagenesis, molecular docking was performed using (–)-menthol as a model substrate to study its binding in the PestE active site, as shown in Figure 1.

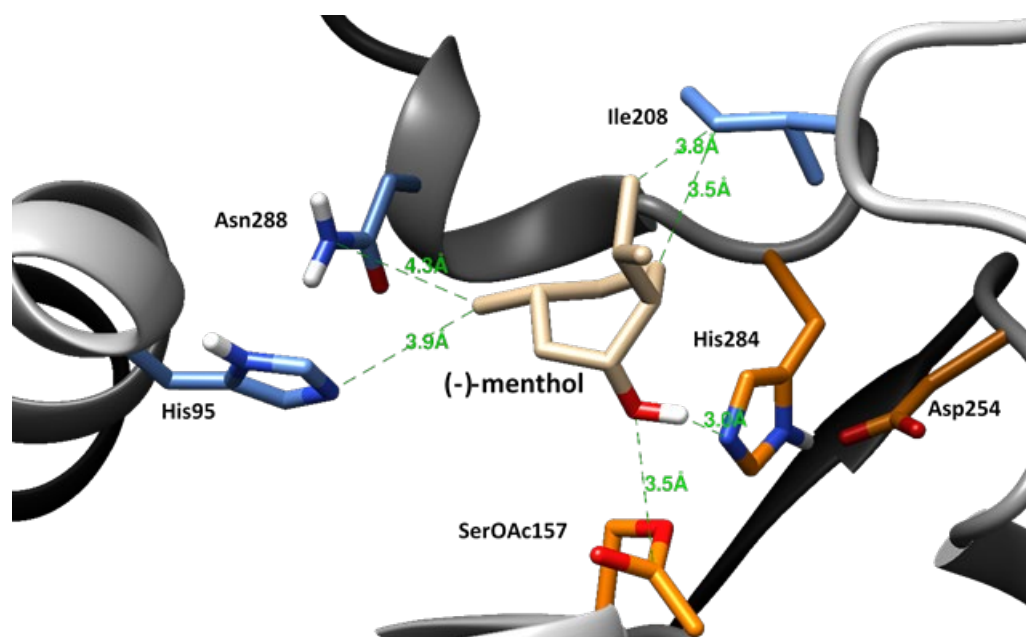


Figure 1. Interaction network for (–)-menthol within PestE (PDB code: 3ZWQ, [24]) based on a substrate docking. Residues interacting with (–)-menthol are shown in light blue, residues of the catalytic triad Ser157, His284, Asp254 are in orange. The model was created based on an acetylated Ser157.

Residues composing the substrate binding of (–)-menthol in the active site of PestE were examined. Three residues were selected, His95, Ile208, and Asn288, to perform rational protein engineering aiming to increase active site hydrophobicity and/or tunnel size. To enhance the hydrophobicity, the residues His95 and Asn288 were selected, while Ile208 was selected to increase the tunnel size. The increase in the active site region hydrophobicity can promote a more favorable surrounding for organic nucleophiles than for water. Moreover, the tunnel is the cavity space that connects the protein surface to the active site, and the residues forming this tunnel can have a significant influence on the biocatalytic properties so that the decrease in the residue size in these positions can increase the acceptance of larger substrates and the flux of substrates and products [28].

PestE wild type and variants were purified by a two-step approach consisting of affinity chromatography followed by heat precipitation. The purity of the purified enzymes was evaluated by SDS-PAGE (Figure S2). Subsequently, several monoterpenes were used as model compounds to determine the acyltransferase activity of PestE enzymes towards these primary (citronellol—Figure 2a and Table S1), secondary (menthol—Table 1), tertiary (linalool—data not shown), and phenolic (carvacrol—Table S3) alcohols with vinyl acetate as an acyl donor. In all reactions, 0.1% (*v/v*) Triton-X-100 was added because previous studies found that Triton-X-100 prevented the protein instability that occurs at low concentrations of purified PestE [22].

The results revealed that only the tertiary alcohol linalool was not converted, despite the efforts to increase the substrate entrance space, possibly due to the high steric hindrance and less reactivity of this tertiary alcohol. Reactions with primary and secondary alcohols showed similar conversions for all variants, although the conversion rate was lower for PestE_N288F. It is also obvious that the variant PestE_N288F decreased the undesired product hydrolysis (Tables S1 and 1). Regarding the phenolic alcohol carvacrol, low conversions were obtained for all PestE variants, still, this is the first time a promiscuous acyltransferase was reported to acylate a phenolic alcohol in an aqueous environment (Table S3).

Table 1 shows that all investigated variants catalyze the conversion of menthol to menthyl acetate with similar maximum conversions. The results (Table 1) confirmed low enantioselectivity for the wild type and PestE_H95A, and moderate E-values for the

PestE_N288F mutant. Contrary to this, PestE_I208A is highly enantioselective for the acetylation of (–)-menthol, showing an enantiomeric excess of 94%*ee* and an E-value over 55. Additionally, the initial acylation is higher for PestE_I208A compared to the wild type. These results suggest that the increase of the tunnel size by rational design facilitated the access of (–)-menthol to the enzyme’s active site.

Table 1. Menthyl acetate conversion and product enantiomeric excess from transesterification reactions catalyzed by PestE wild type and mutants.

Time (min)	PestE_wt		PestE_H95A		PestE_I208A		PestE_N288F	
	Conv (%)	% <i>ee</i> (E)	Conv (%)	% <i>ee</i> (E)	Conv (%)	% <i>ee</i> (E)	Conv (%)	% <i>ee</i> (E)
10	0	-	0	-	12	100	0	-
30	7	74	3	67	17	100	3	100
60	18	67	8	81	31	95 (59)	9	97
120	32	59 (5)	24	66	36	94 (55)	20	89
180	37	58 (5)	31	62 (6)	38	94 (58)	29	81
240	38	57 (5)	28	66	36	95 (67)	35	79 (13)
480	32	68 (7)	31	71 (8)	24	100	44	80 (17)
1440	19	80	9	67	13	100	38	79 (14)

Conversion (%) and optical purity (%*ee*) were determined from GC-MS analytical data using a chiral column; The E-value was determined according to Rakels, Straathof, and Heijnen [29]. Reaction conditions: molar ratio 1:10 ((±)-menthol:vinyl acetate), using 20 mM (±)-menthol, 0.1% (*v/v*) Triton-X-100, 0.2 µg·mL⁻¹ of the purified enzymes in 1 mL of an aqueous buffer (50 mM potassium phosphate, 300 mM sodium chloride, pH 8.0) at 1000 rpm and 40 °C. Reactions were conducted in triplicate, and the average values are shown. Reactions without enzymes did not result in ester products.

Transesterification reactions with ethyl acetate, a much less activated acyl donor compared to vinyl acetate, are reversible and, hence, could lead to lower conversion to esterified products. As all the PestE variants were shown to be efficient biocatalysts for the acylation of citronellol, this substrate was used in reactions with ethyl acetate. The results, shown in Figure 2b and Table S2, demonstrate that all PestE variants studied can perform the acylation with ethyl acetate as an acyl donor almost equally as well as with vinyl acetate. The PestE_N288F variant enabled higher conversion (92% ester formed within 4 h) in comparison to the other acyltransferase variants, where a maximum of 83% was observed together with subsequent hydrolysis of the ester product (Table S2). This finding could be linked to a potential reorganization of the water network (Figures S3–S5). Thus, the undesired and commonly observed hydrolysis of ester products was slowed down, which can be explained by its disrupted water network (Figure S5), decreasing the hydrolytic activity.

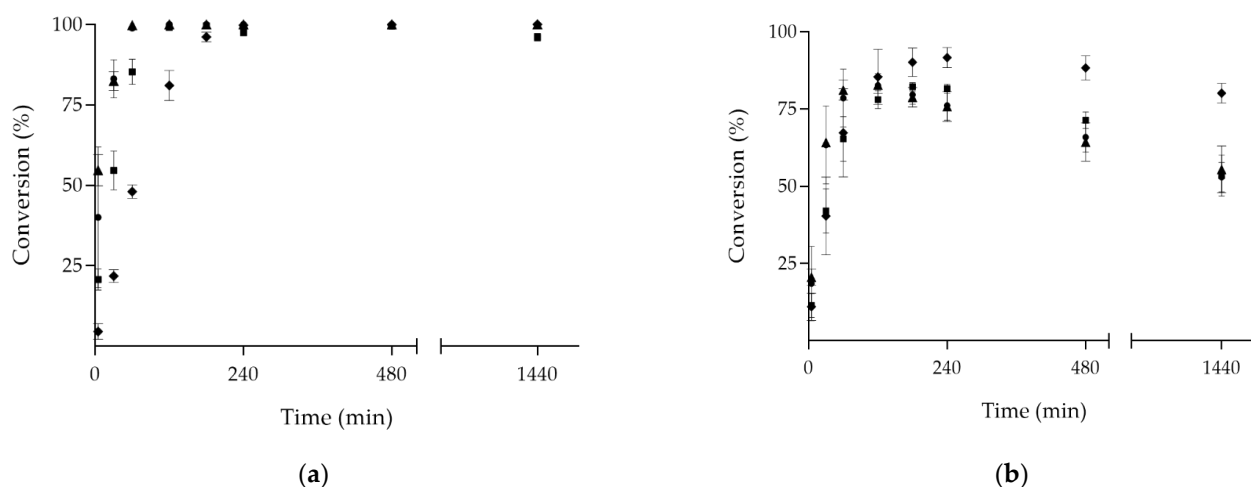


Figure 2. Enzymatic acylation of (±)-citronellol over time with (a) vinyl acetate and (b) ethyl acetate as acyl donors. Where: (●) PestE_wt; (■) PestE_H95A; (▲) PestE_I208A; (▼) PestE_N288F. Reaction conditions: Molar ratio 1:10 ((±)-citronellol:acyl donor), using 20 mM (±)-citronellol, 0.1% (*v/v*) Triton-X-100, 20 $\mu\text{g}\cdot\text{mL}^{-1}$ of the purified enzymes when ethyl acetate was used, or 0.2 $\mu\text{g}\cdot\text{mL}^{-1}$ of the purified enzymes when vinyl acetate was used, in 1 mL of an aqueous buffer (50 mM potassium phosphate, 300 mM sodium chloride, pH 8.0) at 1000 rpm and 40 °C. Reactions were conducted in triplicate, and the average values are shown. Reactions without enzymes did not result in ester products.

4. Discussion

In this study, we performed rational protein engineering of the *Pyrobaculum calidifontis* VA1 esterase (PestE) using two different concepts, the first to increase the hydrophobicity of the active site, with the mutations H95A and N288F, aiming to disrupt the water network and to increase affinity to organic nucleophiles. The second approach was to increase the tunnel size by the mutation I208A. Interestingly, the increased hydrophobicity with the mutations H95A and N288F did not increase the acyltransferase activity, although it is believed that increased hydrophobicity facilitates binding of (non-polar) acyl acceptors [5,15,30]. However, the undesired subsequent hydrolysis of the acylated product was substantially reduced by the variant PestE_N288F, which showed very high up to complete conversions to the ester products and reduced subsequent hydrolysis. The reduced hydrolysis could be due to inactivation of the water molecules in the active site by the introduction of phenylalanine (Figure S5). In the same way, the variant PestE_H95A showed higher hydrolysis as the water network was strengthened (Figure S4), although the hydrophobicity increased. Thus, the reorganized water network in the active site seems to affect hydrolysis activity stronger than the increase in hydrophobicity. For completeness, it has to be mentioned that the PestE_N288F variant presented higher electrophoretic mobility (Figure S2), which might be caused by protein digestion; nevertheless, this variant still showed very high activity. Meanwhile, the variant I208A is highly selective on the (–)-menthol acylation, which can be related to a better access or a better binding of the substrate into the enzyme active site. Again, the decreased hydrophobicity did not decrease but increased the acyltransferase activity in the mutant PestE_I208A, emphasizing that factors such as the access to the binding site are, in this particular case, more relevant for the conversion of monoterpene substrates. Consequently, the highest conversion of the challenging substrate carvacrol was achieved with PestE_I208A, demonstrating not only acyltransferase activity on phenolic alcohols for the first time, but also that enzyme activity is limited by access to the active site. In the same manner, the conversion of tertiary alcohols is eventually only limited by the accessibility of the active site. These findings might help to develop effective acyltransferases for further applications. The outstanding enzymatic activities of the PestE variants for good substrates as citronellol underline the synthetic potential of acyltransferase-catalyzed acylation reactions in aqueous solutions. Even though the

protocol presented in this paper requires the addition of Triton-X-100 for the protein stabilization [22], in experiments with heat shock-enriched lysate (without affinity chromatography purification, data not shown) this was not necessary, which can facilitate the enzyme application. Furthermore, we could show that the acyl donor vinyl acetate can be replaced by the less toxic and more environmentally friendly ethyl acetate, in relation to vinyl acetate [31], still leading to high conversions at relatively short reaction times.

5. Conclusions

In this study, novel PestE variants have been designed for the acylation of monoterpene in water. All variants represented high activity for citronellol. PestE_I208A presented high enantioselectivity for the acetylation of (–)-menthol. PestE_N288F showed good acyl transfer in water, reducing the commonly observed hydrolysis of the monoterpene esters formed upon prolonged reaction times. This variant also catalyzes acylation successfully with the cheaper and environmentally friendly acyl donor ethyl acetate. With carvacrol, a phenolic alcohol was acylated with a promiscuous acyltransferase for the first time.

Supplementary Materials: The following are available online at www.mdpi.com/article/10.3390/microorganisms9081790/s1, Figure S1: Enzymatic acylation of (±)-menthol over time with vinyl acetate as acyl donor, Figure S2: SDS-PAGE analysis of samples of the purified PestE (wt and variants) used in this study, Table S1: Conversion (%) of (±)-citronellol and vinyl acetate to citronellyl acetate over time using PestE wild type and mutants as biocatalysts, Table S2: Conversion (%) of (±)-citronellol and ethyl acetate to citronellyl acetate over time using PestE wild type and mutants as biocatalysts, Table S3: Conversion (%) of carvacrol to carvacryl acetate over time using PestE wild type and mutants as biocatalysts, Figure S3: Water network of PestE wild type active site, Figure S4: Water network of PestE_H95A active site, Figure S5: Water network of PestE_N288F active site.

Author Contributions: U.T.B. and A.S. conceived the project; A.S. and H.T. equally designed the methodology and performed the investigation; J.K. performed the investigation; H.M. executed formal analysis; S.P.G. contributed to the methodology; I.I.J., I.C.R.L., and U.T.B. accomplished the funding; U.T.B. administered and supervised the project; A.S. and H.T. wrote the original draft that all authors contributed to. All authors have read and agreed to the published version of the manuscript.

Funding: A.S. received funding from the Coordenação de Aperfeiçoamento de Pessoal de Nível Superior—Brasil (Capes)—Finance Code 001. H.T. was funded by the Leibniz Association's strategic networking funding program Leibniz ScienceCampus ComBioCat.

Institutional Review Board Statement: Not applicable.

Informed Consent Statement: Not applicable.

Data Availability Statement: Data are contained within the article and the supplementary material.

Acknowledgments: The authors are grateful to Haruyuki Atomi, Kyoto University (Kyoto, Japan) for providing the gene encoding PestE.

Conflicts of Interest: The authors declare no conflict of interest. Additionally, the funders had no role in the design of the study; in the collection, analyses, or interpretation of data; in the writing of the manuscript, or in the decision to publish the results.

References

1. Bornscheuer, U.T.; Kazlauskas, R.J. *Hydrolases in Organic Synthesis*, 2nd ed.; Wiley-VCH: Weinheim, Germany, 2006.
2. Henke, E.; Pleiss, J.; Bornscheuer, U.T. Activity of lipases and esterases towards tertiary alcohols: Insights into structure-function relationships. *Angew. Chem. Int. Ed.* **2002**, *41*, 3211–3213.
3. Liese, A.; Seelbach, K.; Wandrey, C. (Eds.) *Industrial Biotransformations*, 2nd ed.; Wiley-VCH: Weinheim, Germany, 2006.
4. Bornscheuer, U.T.; Kazlauskas, R.J. Catalytic promiscuity in biocatalysis: Using old enzymes to form new bonds and follow new pathways. *Angew. Chem. Int. Ed.* **2004**, *43*, 6032–6040.
5. Müller, H.; Becker, A.-K.; Palm, G.J.; Berndt, L.; Badenhorst, C.P.S.; Godehard, S.P.; Reisky, L.; Lammers, M.; Bornscheuer, U.T. Sequence-based prediction of promiscuous acyltransferase activity in hydrolases. *Angew. Chem. Int. Ed.* **2020**, *59*, 11607–11612.

6. Krishna, S.H.; Persson, M.; Bornscheuer, U.T. Enantioselective transesterification of a tertiary alcohol by lipase A from *Candida antarctica*. *Tetrahedron Asymmetry* **2002**, *13*, 2693–2696.
7. Wikmark, Y.; Humble, M.S.; Bäckvall, J.-E. Combinatorial library based engineering of *Candida antarctica* lipase A for enantioselective transacylation of *sec*-alcohols in organic solvent. *Angew. Chem. Int. Ed.* **2015**, *54*, 4284–4288.
8. Herbst, D.; Peper, S.; Niemeyer, B. Enzyme catalysis in organic solvents: Influence of water content, solvent composition and temperature on *Candida rugosa* lipase catalyzed transesterification. *J. Biotechnol.* **2012**, *162*, 398–403.
9. Holmberg, E.; Szmulik, P.; Norin, T.; Hult, K. Hydrolysis and esterification with lipase from *Candida cylindracea*. Influence of the reaction conditions and acid moiety on the enantiomeric excess. *Biocatalysis* **1989**, *2*, 217–223.
10. Wu, X.Y.; Jääskeläinen, S.; Linko, Y.-Y. An investigation of crude lipases for hydrolysis, esterification and transesterification. *Enzym. Microb. Technol.* **1996**, *19*, 226–231.
11. van Rantwijk, F.; Hacking, M.A.P.J.; Sheldon, R.A. Lipase-catalyzed synthesis of carboxylic amides: Nitrogen nucleophiles as acyl acceptor. *Monatsh. Chem.* **2000**, *131*, 549–569.
12. Yang, Z.; Huang, Z.-L. Enzymatic synthesis of sugar fatty acid esters in ionic liquids. *Catal. Sci. Technol.* **2012**, *2*, 1767–1775.
13. Godehard, S.P.; Badenhorst, C.P.S.; Müller, H.; Bornscheuer, U.T. Protein engineering for enhanced acyltransferase activity, substrate scope, and selectivity of the *Mycobacterium smegmatis* acyltransferase MsAcT. *ACS Catal.* **2020**, *10*, 7552–7562.
14. Neungot, V.; Moulin, G.; Dubreucq, E.; Bigey, F. The lipase/acyltransferase from *Candida prapsilosis*—Molecular cloning and characterization of purified recombinant enzymes. *Eur. J. Biochem.* **2002**, *269*, 1734–1745.
15. Mathews, I.; Soltis, M.; Saldajeno, M.; Ganshaw, G.; Sala, R.; Weyler, W.; Cervin, M.A.; Whited, G.; Bott, R. Structure of a novel enzyme that catalyzes acyl transfer to alcohols in aqueous conditions. *Biochemistry* **2007**, *46*, 8969–8979.
16. Godehard, S.P.; Müller, H.; Badenhorst, C.P.S.; Stanetty, C.; Suster, C.; Mihovilovic, M.D.; Bornscheuer, U.T. Efficient acylation of sugars and oligosaccharides in aqueous environment using engineered acyltransferases. *ACS Catal.* **2021**, *11*, 2831–2836.
17. Müller, H.; Godehard, S.P.; Palm, G.J.; Berndt, L.; Badenhorst, C.P.S.; Becker, A.-K.; Lammers, M.; Bornscheuer, U.T. Discovery and design of family VIII carboxylesterases as highly efficient acyltransferases. *Angew. Chem. Int. Ed.* **2021**, *60*, 2013–2017.
18. Reisky, L.; Srinivasamurthy, V.S.T.; Badenhorst, C.P.S.; Godehard, S.P.; Bornscheuer, U.T. A novel high-throughput assay enables the direct identification of acyltransferases. *Catalysts* **2019**, *9*, 64.
19. Zeng, S.; Liu, J.; Anankanbil, S.; Chen, M.; Guo, Z.; Adams, J.P.; Snajdrova, R.; Li, Z. Amide synthesis via aminolysis of ester or acid with an intracellular lipase. *ACS Catal.* **2018**, *8*, 8856–8865.
20. Müller, J.; Sowa, M.A.; Dörr, M.; Bornscheuer, U.T. The acyltransferase activity of lipase CAL-A allows efficient fatty acid esters formation from plant oil even in an aqueous environment. *Eur. J. Lipid Sci. Technol.* **2015**, *117*, 1903–1907.
21. Land, H.; Hendil-Forsell, P.; Martinelle, M.; Berglund, P. One-pot biocatalytic amine transaminase/acyl transferase cascade for aqueous formation of amides from aldehydes or ketones. *Catal. Sci. Technol.* **2016**, *6*, 2897–2900.
22. Hotta, Y.; Ezaki, S.; Atomi, H.; Imanaka, T. Extremely stable and versatile carboxylesterase from a hyperthermophilic archaeon. *Appl. Environ. Microbiol.* **2002**, *68*, 3925–3931.
23. Kourist, R.; de María, P.D.; Bornscheuer, U.T. Enzymatic synthesis of optically active tertiary alcohols: Expanding the biocatalysis toolbox. *ChemBioChem* **2008**, *9*, 491–498.
24. Palm, G.J.; Fernandez-Álvaro, E.; Bogdanović, X.; Bartsch, S.; Sczodrok, J.; Singh, R.K.; Böttcher, D.; Atomi, H.; Bornscheuer, U.T.; Hinrichs, W. The crystal structure of an esterase from the hyperthermophilic microorganism *Pyrobaculum calidifontis* VA1 explains its enantioselectivity. *Appl. Environ. Microbiol.* **2011**, *91*, 1061–1072.
25. Krieger, E.; Darden, T.; Nabuurs, S.B.; Finkelstein, A.; Wriend, G. Making optimal use of empirical energy functions: Force-field parameterization in crystal space. *Proteins* **2004**, *57*, 678–683.
26. Pettersen, E.F.; Goddard, T.D.; Huang, C.C.; Couch, G.S.; Greenblatt, D.M.; Meng, E.C.; Ferrin, T.E. UCSF chimera—A visualization system for exploratory research and analysis. *J. Comput. Chem.* **2004**, *25*, 1605–1612.
27. Trott, O.; Olson, A.J. AutoDock Vina: Improving the speed and accuracy of docking with a new scoring function, efficient optimization and multithreading. *J. Comput. Chem.* **2010**, *31*, 455–461.
28. Kokkonen, P.; Bednar, D.; Pinto, G.; Prokop, Z.; Damborsky, J. Engineering enzymes access tunnels. *Biotechnol. Adv.* **2019**, *37*, 107386.
29. Rakels, J.L.L.; Straathof, A.J.J.; Heijnen, J.J. A simple method to determine the enantiomeric ratio in enantioselective biocatalysis. *Enzym. Microb. Technol.* **1993**, *15*, 1051–1056.
30. Kazemi, M.; Sheng, X.; Kroutil, W.; Himo, F. Computational study of *Mycobacterium smegmatis* acyl transferase reaction mechanism and specificity. *ACS Catal.* **2018**, *8*, 10698–10706.
31. Paravidino, M.; Hanefeld, U. Enzymatic acylation: Assessing the greenness of different acyl donors. *Green Chem.* **2011**, *13*, 2651–2657.

Supplementary Material

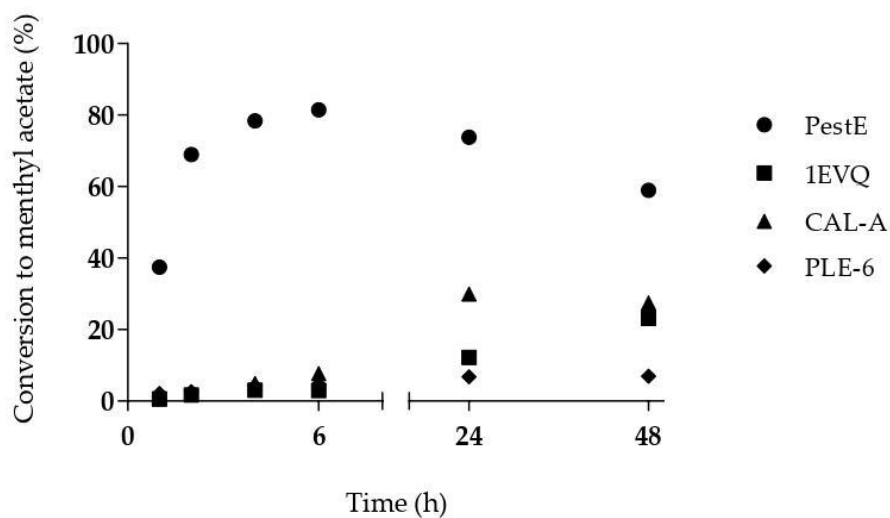


Figure S1. Enzymatic acylation of (\pm)-menthol over time with vinyl acetate as acyl donor. Reaction conditions: molar ratio 1:100 (alcohol: acyl donor), concentration of 20 mM of (\pm)-menthol in 1 mg of lyophilized enzyme per mL of aqueous buffer (200 mM potassium phosphate, pH 8.0), 1000 rpm and 40°C, for reactions conducted with PestE, 1EVQ and CAL-A. For reactions conducted with PLE-6 the molar ratio was reduced to 1:10 (alcohol: acyl donor). In control reactions without enzymes no ester product formation was observed.

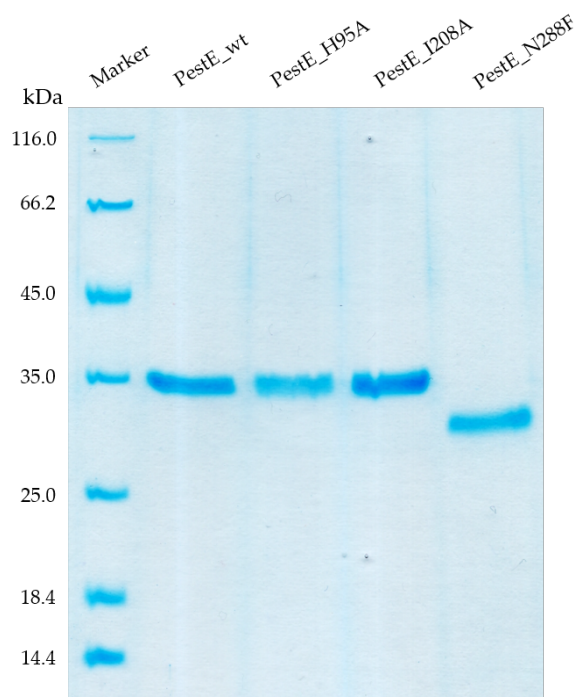


Figure S2. SDS-PAGE analysis of samples of the purified PestE (wt and variants) used in this study. Pierce™ Unstained Protein MW Marker (ThermoFisher, Germany) was used as reference.

Table S1. Conversion (%) of (\pm)-citronellol to citronellyl acetate over time using PestE wild type and mutants as biocatalysts

Time (min)	PestE_wt	PestE_H95A	PestE_I208A	PestE_N288F
5	40	21	55	5
20	71	42	63	15
30	83	55	82	22
45	93	73	97	35
60	99	85	100	48
120	100	99	100	81
240	100	97	100	100
1440	100	96	100	100

Conversion (%) was determined by GC-MS. Reaction conditions: molar ratio 1:10 (\pm)-citronellol: vinyl acetate), using 20 mM (\pm)-citronellol, 0.1 % (v/v) Triton-X-100, 0.2 $\mu\text{g}\cdot\text{mL}^{-1}$ of the purified enzymes, in 1 mL of aqueous buffer (50 mM potassium phosphate, 300 mM sodium chloride, pH 8.0) at 1000 rpm and 40°C. Reactions without enzymes did not show the formation of ester product.

Table S2. Conversion (%) of carvacrol to carvacryl acetate over time using PestE wild type and mutants as biocatalysts

Time (min)	Without enz	PestE_wt	PestE_H95A	PestE_I208A	PestE_N288F
5	0	1	<1	1	1
20	0	2	2	2	2
30	0	4	2	5	1
45	<1	7	6	11	5
60	1	4	4	5	4
120	2	4	3	3	2
240	3	2	2	3	1
1440	2	2	1	1	1

Conversion (%) was determined by GC-MS. Reaction conditions: molar ratio 1:10 (carvacrol: vinyl acetate), using 20 mM carvacrol, 0.1 % (v/v) Triton-X-100, 0.2 $\mu\text{g}\cdot\text{mL}^{-1}$ of the purified enzymes, in 1 mL of aqueous buffer (50 mM potassium phosphate, 300 mM sodium chloride, pH 8.0) at 1000 rpm and 40°C.

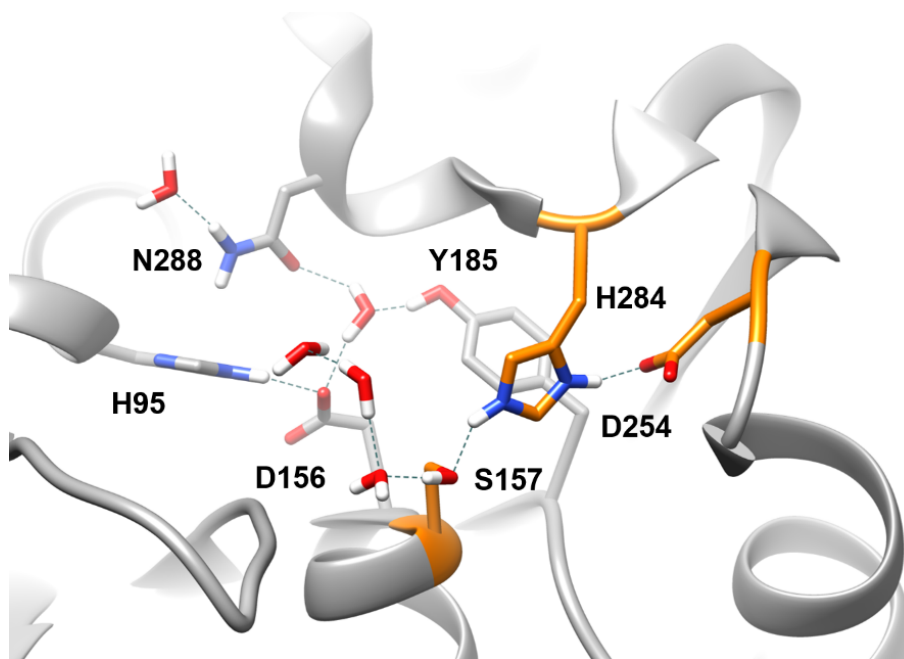


Figure S3. Water network of PestE wild type active site.

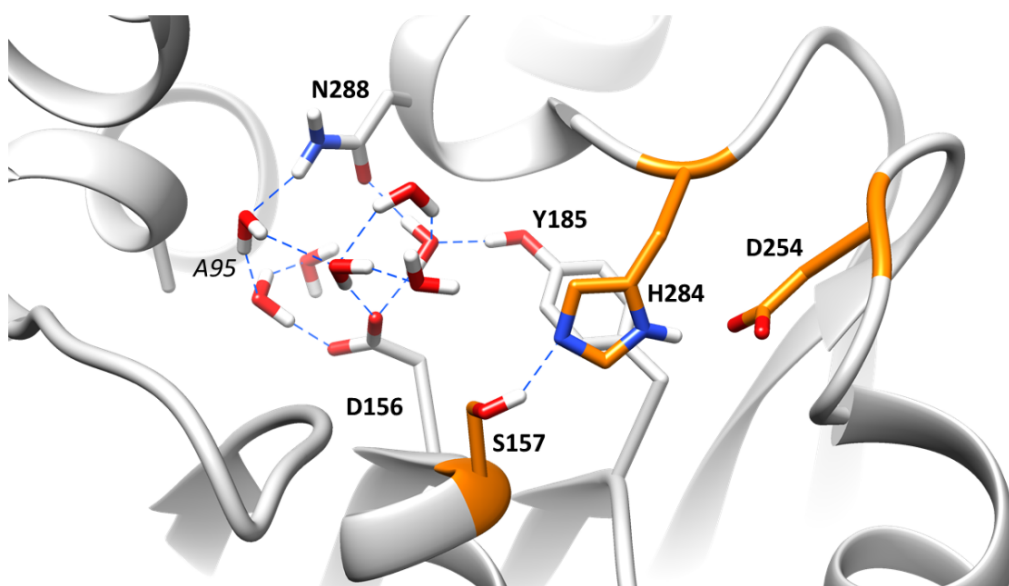


Figure S4. Water network of PestE_H95A active site. Simulated by Molecular Dynamics with YASARA Software.

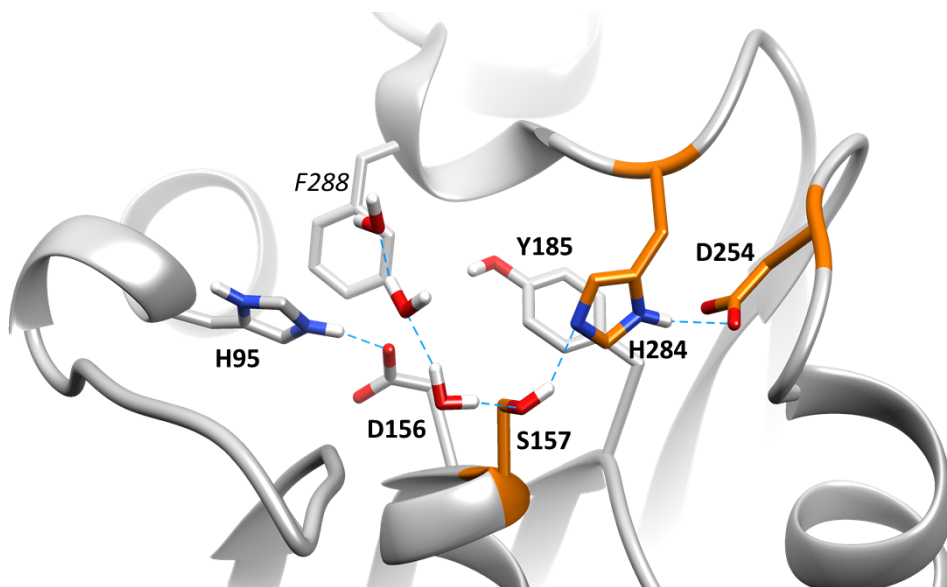


Figure S5. Water network of PestE_N288F active site. Simulated by Molecular Dynamics with YASARA Software.

Article V

Special
Collection

Recovery of Hydroxytyrosol from Olive Mill Wastewater Using the Promiscuous Hydrolase/Acyltransferase PestE

Henrik Terholsen,^[a] Jasmin Kaur,^[a] Nikolaos Kaloudis,^[b] Amanda Staudt,^[a] Henrik Müller,^[a] Ioannis V. Pavlidis,^[b] and Uwe T. Bornscheuer^{*,[a]}

Olive mill wastewater (OMWW) is produced annually during olive oil extraction and contains most of the health-promoting 3-hydroxytyrosol of the olive fruit. To facilitate its recovery, enzymatic transesterification of hydroxytyrosol (HT) was directly performed in an aqueous system in the presence of ethyl acetate, yielding a 3-hydroxytyrosol acetate rich extract. For this, the promiscuous acyltransferase from *Pyrobaculum calidifontis* VA1 (PestE) was engineered by rational design. The best mutant for the acetylation of hydroxytyrosol (PestE_

I208A_L209F_N288A) was immobilized on EziG² beads, resulting in hydroxytyrosol conversions between 82 and 89% in one hour, for at least ten reaction cycles in a buffered hydroxytyrosol solution. Due to inhibition by other phenols in OMWW the conversions of hydroxytyrosol from this source were between 51 and 62%. In a preparative scale reaction, 13.8 mg (57%) of 3-hydroxytyrosol acetate was extracted from 60 mL OMWW.

Introduction

Olive mill wastewater (OMWW) is an industrial sewage produced besides olive oil and solid pomace in three-phase olive mills. Annually, 30 million m³ of OMWW are produced worldwide within a few months (October to February). The wastewater causes environmental problems as it has a high polluting organic load, including polyphenolics, sugars, and lipids.^[1] In addition to the acidity of the OMWW (pH ~5), the phytotoxic and antimicrobial activities of polyphenolics hinder the biodegradation of organic compounds.^[2,3] Therefore, in addition to illegal disposal, incubation of OMWW in open ponds to decompose the organic matter is still widespread. Besides the unpleasant odor and the land requirements of open pond OMWW treatment, the economic value of the phenols is also lost. The phenols of olives have several health-promoting properties, e.g., neuroprotective, which are associated with their antioxidant and anti-inflammatory benefits.^[4–8] Several methods have been developed to facilitate the degradation or extraction of phenolic compounds, such as

chemical oxidation, solvent extraction, membrane systems or adsorbents.^[9–20] However, all these systems require several laborious steps. In the case of solvent extraction, several extraction steps are required due to the hydrophilic nature of the contained phenols, e.g., the major phenolic compound 3-hydroxytyrosol (HT).^[11] Lipophilization of HT by acetylation could facilitate the extraction and increase the bioavailability of the extracted health-promoting 3-hydroxytyrosol acetate (HTA).^[4,21] However, acetylation/transesterification in an aqueous medium is challenging, as the hydrolysis of the formed ester and acyl donor is thermodynamically favored and thus pure organic solvents must be used for lipase-catalyzed acetylation.^[22] As an alternative, promiscuous acyltransferases are able to catalyze the acetylation of nucleophiles with an acyl donor in a kinetically controlled manner in an aqueous system, thus favoring acetylation over hydrolysis.^[22] The most studied promiscuous acyltransferase from *Mycobacterium smegmatis* (MsAcT) has been shown to catalyze the acetylation of HT.^[23] However, MsAcT cannot be used in this process, because the pH optimum of MsAcT is in the basic range^[24] and the pH of OMWW is acidic. The hyperthermostable esterase from the archaeon *Pyrobaculum calidifontis* VA1 (PestE) is a very robust biocatalyst exhibiting activity down to pH 3.5.^[25] Our group recently discovered PestE as a promiscuous hydrolase/acyltransferase and demonstrated high acetylation activity and acyltransferase efficiency toward monoterpene alcohols.^[26,27] Therefore, PestE was used in this study to catalyze the acetylation of HT in untreated aqueous OMWW in order to facilitate direct extraction of the HTA formed. Extraction of HT(A) from OMWW could provide an alternative to petrol-based chemical synthesis pathways of these compounds.^[28,29]

[a] H. Terholsen, J. Kaur, Dr. A. Staudt, Dr. H. Müller, Prof. Dr. U. T. Bornscheuer
Department of Biotechnology and Enzyme Catalysis,
University Greifswald, Felix-Hausdorff-Straße 4,
17487 Greifswald (Germany)
E-mail: uwe.bornscheuer@uni-greifswald.de

[b] N. Kaloudis, Prof. Dr. I. V. Pavlidis
Department of Chemistry, University of Crete,
Voutes University Campus, 70013, Heraklion (Greece)

Supporting information for this article is available on the WWW under
<https://doi.org/10.1002/cbic.202200254>

This article is part of the Special Collection based on the IBPRO2022 conference on biocatalytic processes. Please see our homepage for more articles in the collection.

© 2022 The Authors. ChemBioChem published by Wiley-VCH GmbH. This is an open access article under the terms of the Creative Commons Attribution Non-Commercial NoDerivs License, which permits use and distribution in any medium, provided the original work is properly cited, the use is non-commercial and no modifications or adaptations are made.

Results and Discussion

In a first screening, the PestE wild type (wt) and the variants PestE_H95 A, PestE_I208A, and PestE_N288F, created in a previous study to improve the activity of PestE towards monoterpene alcohols,^[26] were screened for HT acetylation with ethyl acetate. All PestE variants were found to be active, but the weak spots on thin-layer chromatography (TLC) indicates only low acyltransferase activity (Figure S1). Among the tested variants, PestE_I208A showed a stronger spot, indicating a higher activity and was therefore included in further investigations. The N288 position putatively has an impact on the water network and increases the conversions achieved with ethyl acetate as an acyl donor.^[26] However, docking HT in the binding pocket of PestE revealed that N288 may interact with the phenolic alcohol groups of HT (Figure S2). To find a compromise between the conflicting requirements for water network suppression and polar interactions with HT, the N288A mutant was created. Additionally, the binding of HT in the active site was investigated by molecular docking, as Kazemi *et al.* found that a high binding affinity is the basis of promiscuous hydrolases/acetyltransferase.^[30] To increase the binding affinity of HT, the structures of several PestE variants were modelled and analyzed. Molecular docking suggested that PestE_G86A and PestE_L209F bind the substrate stronger than the wild-type enzyme (Figure S2).

All PestE variants were studied in an aqueous/organic two-phase system (2:1) with ethyl acetate (EtOAc; Scheme 1). EtOAc is proved to be the best solvent for the extraction of the OMWW phenols^[11] and it can act simultaneously as an acyl donor for PestE. In contrast to vinyl acetate, which is a much better acyl donor, EtOAc is less toxic to aquatic organisms and therefore more suitable for OMWW treatment and subsequent use of the extracted phenols in the food industry.^[22,31]

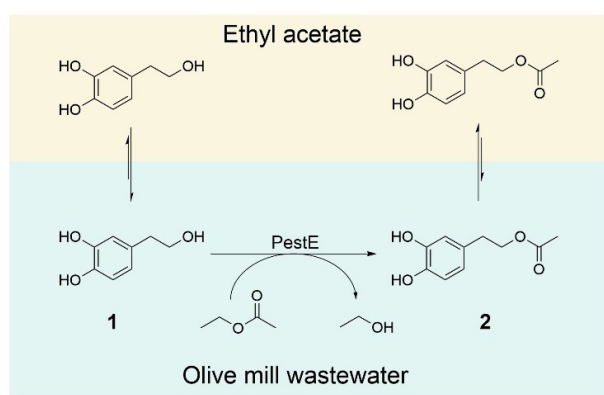
Mutations I208A, L209F, and N288A improved HT conversion from 18% (PestE_wt) to 22, 52, and 21%, respectively, while G86A was neutral. It was demonstrated by thin-layer chromatography (TLC) that the maximum conversions were not reached at an earlier time point examined (data not

shown). To investigate possible synergistic effects, mutations were combined iteratively and the resulting variants were used for HT acetylation (Figure 1).

Although G86A is a neutral mutation, combination with I208A and L209F resulted in a decreased turnover. Only PestE_G86A_N288A showed higher turnover than the single mutant alone. Since PestE_G86A_N288A was still less active than other double mutants and the combination with other mutations was deleterious, G86A was not further included in the combinatorial approach. PestE_I208A_L209F_N288A showed the best performance among the tested variants, reaching 86% conversion after 24 h (Figure 1). Further investigation revealed that over 80% conversion was reached already after 4 h and no hydrolysis of hydroxytyrosol acetate was observed even after 24 h (Figure S3).

When using acyltransferases for the treatment of OMWW, the enzyme production would be a major economical cost factor.

Enzyme immobilization can reduce these costs by allowing easy separation and reuse of the catalyst.^[32] Therefore, immobilization on EziG beads was investigated. EziG beads have different surface polarities and bind the target proteins via their polyhistidine tag. EziG¹ has a hydrophilic surface, EziG² is coated with a hydrophobic polymer, while the surface polarity of EziG³ is intermediate. Further immobilization properties according to the product specification are listed in the SI (Table S3). The immobilization efficiency using EziG¹ beads was very low, so EziG² and EziG³, both of which had an immobilization efficiency of about 50% (0.3 mg_{enzyme}/mg_{carrier}), were further evaluated. PestE_I208A_L209F_N288A immobilized on EziG² beads (PestE_I208A_L209F_N288A-EziG²) showed slightly better performance over ten reaction cycles studied compared to PestE_I208A_L209F_N288A immobilized on EziG³ beads and was used for the following experiments (Figure 2).



Scheme 1. Two-phase system for acetylation of HT (1) in OMWW by PestE and extraction of HTA (2) into the ethyl acetate phase.

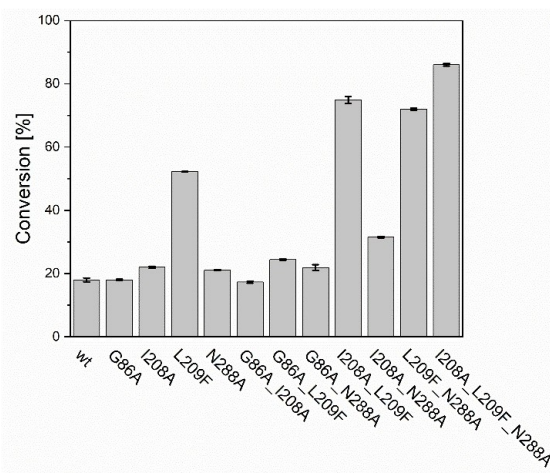


Figure 1. Conversion of HT to HTA after 24 h at 25 °C (1000 rpm) by 0.1 mg mL⁻¹ of each PestE variant in a two-phase system with EtOAc.

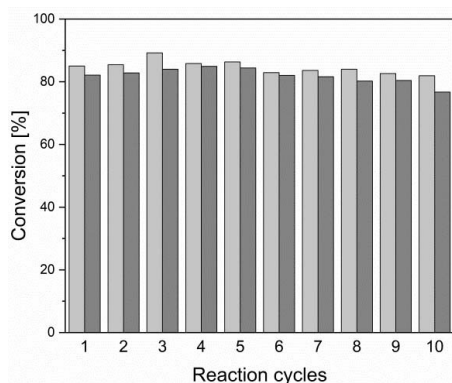


Figure 2. Conversion of HT to HTA by PestE_I208A_L209F_N288A immobilized on EziG² (light gray) or EziG³ (dark gray) in a two-phase system with EtOAc over ten reaction cycles. Reactions were performed for 1 h at 25 °C and 1000 rpm with 1.0 mg mL⁻¹ enzyme (in the aqueous phase).

Batch reactions with promiscuous hydrolases/acetyltransferases usually result in maximum conversion before the product formed is hydrolyzed again.^[22] By using ethyl acetate as the organic phase, a large excess of the acyl donor is present and the product is removed from the reaction. Both lead to a shift of the reaction equilibrium and a flattening of the reaction curve after reaching the maximum conversion (Figure S3). However, the maximum conversion of the reaction still depends on the efficiency of the acyltransferase. A comparison of the conversions achieved with PestE_I208A_L209F_N288A and MsACT, which was used by Annunziata *et al.* for HT acetylation,^[23] shows that our engineered PestE variant is a much more efficient acyltransferase for HT acetylation in water. Annunziata *et al.* could not overcome 29% conversion in their batch process with MsACT, while PestE_I208A_L209F_N288A allows conversion of over 80%. Moreover, the pH of this model system was adjusted to pH 5.0 with respect to the OMWW application, while Annunziata *et al.* worked at the optimal pH of MsACT, around pH 8.0.^[23,33] Therefore, PestE_I208A_L209F_N288A is a much better candidate than MsACT for acetylation of HT in OMWW.

However, OMWW is a challenging reaction medium because it is unbuffered and contains numerous other compounds.^[1] Therefore, it is necessary to determine whether immobilized PestE_I208A_L209F_N288A can indeed be used to acetylate HT in OMWW. Therefore, OMWW was obtained from three different three-phase olive mills in Crete (Greece) and used as HT source. The pre-test of the HT acetylation in OMWW already showed that the PestE activity in OMWW is strongly reduced (data not shown). Since the HT conversions were still increasing up to 24 hours, an inactivation of the enzyme in OMWW could be excluded. However, inhibition by structurally similar phenols to HT, e.g., ferulic acid, could explain the reduced activity. To confirm this theory, PestE activity was examined in the presence of ferulic acid. The hydrolysis of *p*-nitrophenyl acetate was decreased by up to 60% (Table S1). Consistently, the acyl transfer reaction of HT was decreased by 27% in the presence of 1 mM ferulic acid,

although no acetylation of ferulic acid was observed. Considering that other OMWW phenols besides ferulic acid might have an inhibitory effect on PestE, the reduced activity could be thus explained.

To compensate for the decreased activity, the reaction temperature was increased to 35 °C, the approximate temperature of fresh OMWW (Table S2), and the reaction time was extended to 24 h. Nevertheless, the conversions measured with HT in OMWW were lower than in reactions with HT (Figure 3).

Due to the large variety of potential inhibitors in OMWW, it might be difficult to address the inhibition by rational design. Nevertheless, a preparative scale reaction with 60 mL OMWW was performed to show the potential of using PestE for OMWW valorization. Using 72 µg mL⁻¹ heat shock enriched PestE_I208A_L209F_N288A on EziG², 13.8 mg of HTA could be extracted, corresponding to over 57% of the HT contained in the OMWW. Together with the 2.1 mg HT in the extract, 15.9 mg hydroxytyrosol derivatives were extracted. This value corresponds to 73 mol% of HT and HTA in the investigated OMWW mixture, which is comparable to the extraction yields reported in literature,^[10,11] although here only a simple one step liquid/liquid extraction procedure was performed.

However, the absolute amount of HT derivatives extracted per liter OMWW is relatively low.^[10,11] This could be explained by the ripeness status of olives at the time of sampling in the middle of the season (late November). During ripening, HT is released from oleuropein, so HT would have been higher in the late season.^[34] Accordingly, the darkest OMWW had the highest HT content (Figure S4; Table S2). Further studies could be conducted to couple HT-releasing enzymes, such as β-glucosidase, with PestE, to form HTA from the HT precursor, oleuropein.^[35] This could lead to better HTA yields regardless of the maturity of the olives. In addition, procedural measures, such as the application of the immobilized enzymes in a flow application, could increase the productivity and activity of PestE_I208A_L209F_N288A.^[18]

Although several other compounds were present in the organic extract, HTA is the major compound, as revealed by the ¹H-NMR study (Figure S5). Phenol-rich extracts are used as

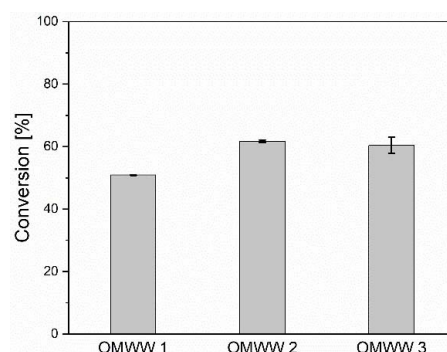


Figure 3. Conversion of HT in OMWW with EtOAc after 24 h at 35 °C (1000 rpm). PestE_I208A_L209F_N288A (0.5 mg mL⁻¹) on EziG² was used as catalyst.

dietary supplements, e.g., in fermented sausages, to stabilize the product or increase the health value of the product.^[36–38] HTA-enriched functional foods could have neuroprotective, anticoagulant, arthritis preventive and other health-promoting properties.^[4,8,39,40] For example, olive oil that contains 250 mg kg⁻¹ hydroxytyrosol derivatives can be called health-promoting according to an EU regulation (EU Commission Regulation No. 432/2012). However, further purification of the extracts may be required to meet the criteria for food applications. Taking into account that three to five liters of OMWW are produced per kilogram of olive oil, about 810 to 1,340 mg of HT and HTA can be obtained from the OMWW of one kilogram of oil. Using the example of the olive mills visited that produce 200,000 to 1,300,000 t olive oil annually, 160 to 1,740 t HT derivatives could be produced.

The recyclability of the immobilized enzymes is thus a first step towards a possible industrial application. The use of a simple heat shock enrichment of PestE could also help to reduce the cost of the process. However, further process engineering measures, e.g., recycling of ethyl acetate and more sophisticated extraction procedures, would be required to make the process economically viable and sustainable.

Conclusions

Since only 2% of olive phenols remain in olive oil and 53% are found in the OMWW, which is causing environmental problems, new methods of recovering the health-promoting phenols are needed to utilize the full power of the olive.^[41] Lipophilization of phenols such as HT using acyltransferases could be an important step to facilitate the recovery of phenols from OMWW. Immobilization and rational optimization of PestE led to the recyclable catalyst PestE_I208A_L209F_N288A-EziG², which is also active in untreated OMWW. We demonstrated that the phenol-rich extract obtained from OMWW provides sufficient HT and HTA to enrich the same amount of olive oil to phenol-rich olive oil according to the EU health claim.

Experimental Section

Enzyme preparation

Expression of PestE variants was performed according to a protocol previously described by our group.^[26]

Mutant screening

For screening of PestE variants, 160 μL of 50 mM citrate buffer pH 5.0 and 40 μL enzyme solution (0.1 mg mL⁻¹ final) were mixed. Then, 10 μL 200 mM HT in ethyl acetate (EtOAc) and 90 μL EtOAc were added. The reaction was incubated at 25 °C (1000 rpm) for 24 h. Reaction controls of 1 μL of the organic phase (OP) of each reaction were taken after 1, 2, 3, 4, 8, and 24 h and analyzed by TLC after 24 h to exclude that higher conversions were achieved at an earlier time point. TLC was performed using silica plates (Merck, Darmstadt, Germany) as solid and EtOAc as mobile phase.

The staining was done with iodine ($R_f(\text{HT})=0.71$; $R_f(\text{HTA})=0.91$). After 24 hours, the reaction was stopped by adding 50 μL 2 M HCl. Subsequently, the reactions were extracted three times with 200 μL EtOAc each. The organic phase was dried over sodium sulfate, and analyzed by GC-FID.

Selection and reuse of immobilization carriers

To a reaction tube, 5 mg EziG¹, EziG², and EziG³ were added and then 500 μL PestE_I208A_L209F_N288A solution (2.98 mg mL⁻¹ in 20 mM NaP_i with 500 mM NaCl pH 8.0). Immobilization was performed according to the manufacturer's protocol (<https://enginzyme.com/wp-content/uploads/2015/05/EziG%E2%84%A2-Detailed-Instruction-manual.pdf>; April 25, 2022). Briefly, incubation was performed for 2 h at 25 °C (1000 rpm) and the beads were washed twice with 500 μL 50 mM citrate buffer pH 5.0. Loading was calculated based on the residual protein concentration in the supernatant. Biocatalytic test reactions with the immobilisate were performed as described for mutant screening and stopped after 1 h by transferring the supernatant to a new vial containing 50 μL of 2 M HCl. The supernatant was extracted and analyzed by GC-FID, as described in the respective paragraph. The beads were reused by washing with 200 μL of citrate buffer pH 5.0, centrifuging and discarding of the supernatant. The reaction was repeated nine more times.

PestE_I208A_L209F_N288A immobilization for preparative scale reaction

Expression of PestE_I208A_L209F_N288A was performed according to a protocol previously described on a 400 mL scale.^[26] Deviating from this, the lysis was performed in 4 mL loading buffer (20 mM NaP_i+500 mM NaCl, pH 8.0) and the enzymes were enriched in the lysate using only heat shock (40 min, 80 °C). The enriched lysate was immobilized on 400 mg EziG²™ beads (EnginZyme, Solna, Sweden) as described above. After washing twice with 1 mL loading buffer (20 mM NaP_i+500 mM NaCl, pH 8.0), the immobilized material was stored moist at 4 °C before further use.

Small scale extraction of OMWW with PestE_I208A_L209F_N288A-EziG²

30 mg PestE_I208A_L209F_N288A-EziG² immobilisate (0.1 mg enzyme) was submitted in a reaction tube. Then, 200 μL of the filtered OMWW was added and incubated at 35 °C (1000 rpm) for 24 h after the addition of 100 μL ethyl acetate. Subsequently, the aqueous and organic phases were separated and each diluted tenfold in HPLC running medium (ddH₂O+2% v/v AcOH:methanol; 25:75). The samples were analyzed by reverse phase high performance liquid chromatography (RP-HPLC). Analogous reaction approaches without enzyme were performed to compare HT conversions and extraction. All experiments were performed in duplicates.

Preparative scale extraction of OMWW with PestE_I208A_L209F_N288A-EziG²

In a 250 mL round bottom flask, 1.310 g of the PestE-EziG² immobilisate (4.32 mg enzyme) was placed and 20 mL each of the filtered OMWW 1, 2, and 3 were added, to a total volume of 60 mL. After the addition of 30 mL of ethyl acetate, the reaction mixture was incubated for 24 h under vigorous stirring. A preparation without enzyme immobilisate was performed analo-

gously. The temperature was adjusted to 35 °C by an oil bath and controlled with a ground-glass thermometer. Subsequently, the organic phase was separated via a separating funnel, dried over magnesium sulfate, filtered, and the solvent was evaporated in vacuum. After additional drying for 16 h into a lyophilizer, the weight of the extracted substances (117.0 mg and 104.3 mg in the control without enzyme, respectively) was determined. The brown, highly viscous oil exhibited a spicy-bitter odor. The extract was dissolved in deuterated methanol (MeOD) and a ¹H-NMR spectrum was recorded. The HT and HTA content were quantified by gas chromatography with flame ionization detector (GC-FID). The natural HTA content in the OMWW was subtracted from the HTA measured in the organic phase, which would correspond to a complete extraction of the natural HTA. Accordingly, the conversion is to be evaluated as minimum conversion.

GC-FID analytics

Samples in 50 µL ethyl acetate were derivatized by adding 40 µL *N,O*-bis(trimethylsilyl)trifluoroacetamide and 10 µL pyridine. Analysis was performed with GC-FID (GC-2010, Shimadzu, Kyoto, Japan) equipped with a BPX5 column (25.0 m × 0.25 mm, 0.25 µm film thickness, Trajan Scientific and Medical, Ringwood, Australia). Injector and detector temperature was 250 °C, and 1 µL sample was injected. The column temperature was held at 150 °C for 3 min, increased to 220 °C with 14 °C min⁻¹, and held 2 min. Compounds were identified with authentic standards (retention times: HT 8.0 min; HTA 8.5 min).

RP-HPLC analytics

An Agilent 1260 Infinity II with a Lichosphere RP18-5 (250 × 46 mm, 5 µm) column was used for RP-HPLC analysis. For the first 30 minutes of the run, the flow was maintained at 0.5 mL min⁻¹ and 25% (v/v) methanol (MeOH). The flow was gradually decreased to 0.4 mL min⁻¹ and 50% (v/v) MeOH until 40 minutes and held for ten minutes. In the following five minutes, the MeOH was reduced again to 25% (v/v). Then the flow rate was gradually increased to 0.5 mL min⁻¹ until 60 min, followed by a final hold time of five minutes. Compounds were identified with authentic standards (retention times: HT 10.4 min; HTA 44.3 min). Naturally occurring HTA was subtracted to calculate HT conversions.

Acknowledgements

H.T. was funded by the Leibniz Association's strategic networking funding program Leibniz ScienceCampus ComBioCat. A.S. received funding from the Coordenação de Aperfeiçoamento de Pessoal de Nível Superior – Brasil (Capes) – Finance Code 001. We are very grateful for the support from Prof. Apostolos Spyros (University of Crete) and Charitomeni Aggeli (University of Crete) regarding the NMR analysis. Special thanks to the operators of the olive mills Melissourgakis, Politakis and Gaia (Crete, Greece). Open Access funding enabled and organized by Projekt DEAL.

Conflict of Interest

The authors declare no conflict of interest.

Data Availability Statement

The data that support the findings of this study are available in the supplementary material of this article.

Keywords: acyltransferases · biocatalysis · hydroxytyrosol · hydroxytyrosol acetate · olive mill wastewaters valorization

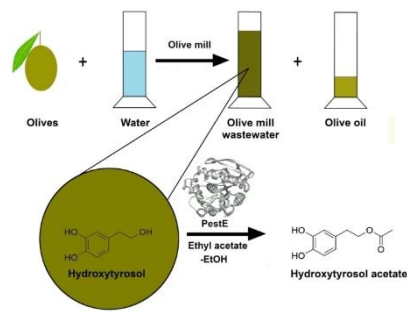
- [1] E. Tsagaraki, H. N. Lazarides, K. B. Petrotos, in *Utilization of By-Products and Treatment of Waste in the Food Industry* (Eds.: V. Oreopoulou, W. Russ), Springer US, Boston, **2007**, pp. 133–157.
- [2] A. Ramos-Cormenzana, M. Monteoliva-Sanchez, M. J. Lopez, *Int. Biodegrad. Biodegrad.* **1995**, *35*, 249–268.
- [3] H. Zbakh, A. El Abbassi, *J. Funct. Foods* **2012**, *4*, 53–65.
- [4] C. Qin, S. Hu, S. Zhang, D. Zhao, Y. Wang, H. Li, Y. Peng, L. Shi, X. Xu, C. Wang, J. Liu, Y. Cheng, J. Long, *Mol. Nutr. Food Res.* **2021**, *65*, 2000797.
- [5] A. H. Abuznait, H. Qosa, B. A. Busnena, K. A. El Sayed, A. Kaddoumi, *ACS Chem. Neurosci.* **2013**, *4*, 973–982.
- [6] G. K. Beauchamp, R. S. J. Keast, D. Morel, J. Lin, J. Pika, Q. Han, C.-H. Lee, A. B. Smith, P. A. S. Breslin, *Nature* **2005**, *437*, 45–46.
- [7] R. Fucelli, R. Fabiani, P. Rosignoli, *Molecules* **2018**, *23*, 3212.
- [8] M. A. Rosillo, M. Sánchez-Hidalgo, A. González-Benjumea, J. G. Fernández-Bolaños, E. Lubberts, C. Alarcón-de-la-Lastra, *Mol. Nutr. Food Res.* **2015**, *59*, 2537–2546.
- [9] C. Agabo-García, N. Calderón, G. Hodaifa, *Catalysts* **2021**, *11*, 557.
- [10] M. O. J. Azzam, S. A. Hazaimah, *Process Saf. Environ. Prot.* **2021**, *148*, 495–523.
- [11] N. Allouche, I. Fki, S. Sayadi, *J. Agric. Food Chem.* **2004**, *52*, 267–273.
- [12] A. El-Abbassi, M. Khayet, A. Hafidi, *Water Res.* **2011**, *45*, 4522–4530.
- [13] R. Tundis, C. Conidi, M. R. Loizzo, V. Sicari, A. Cassano, *Antioxidants* **2020**, *9*, 602.
- [14] K. Al-Malah, M. O. J. Azzam, N. I. Abu-Lail, *Sep. Purif. Technol.* **2000**, *20*, 225–234.
- [15] D. Frascari, G. Rubertelli, F. Arous, A. Ragini, L. Bresciani, A. Arzu, D. Pinelli, *Chem. Eng. J.* **2019**, *360*, 124–138.
- [16] R. Mazzei, E. Piacentini, M. Nardi, T. Poerio, F. Bazzarelli, A. Procopio, M. L. Di Gioia, P. Rizza, R. Ceraldi, C. Morelli, L. Giorno, M. Pellegrino, *Front. Bioeng. Biotechnol.* **2020**, *8*.
- [17] G. Ranieri, R. Mazzei, T. Poerio, F. Bazzarelli, Z. Wu, K. Li, L. Giorno, *Chem. Eng. Sci.* **2018**, *185*, 149–156.
- [18] N. Solomakou, A. M. Goula, *Rev. Environ. Sci. Bio/Technol.* **2021**, *20*, 839–863.
- [19] P. Tapia-Quirós, M. F. Montenegro-Landívar, M. Reig, X. Vecino, J. Saurina, M. Granados, J. L. Cortina, *J. Environ. Manage.* **2022**, *307*, 114555.
- [20] R. Tundis, C. Conidi, M. R. Loizzo, V. Sicari, R. Romeo, A. Cassano, *Molecules* **2021**, *26*, 1808.
- [21] D. Tofani, V. Balducci, T. Gasperi, S. Incerpi, A. Gambacorta, *J. Agric. Food Chem.* **2010**, *58*, 5292–5299.
- [22] H. Müller, H. Terholsen, S. P. Godehard, C. P. S. Badenhorst, U. T. Bornscheuer, *ACS Catal.* **2021**, *11*, 14906–14915.
- [23] F. Annunziata, M. L. Contente, C. Pinna, L. Tamborini, A. Pinto, *Antioxidants* **2021**, *10*, 1142.
- [24] H. Land, P. Hendil-Forsell, M. Martinelle, P. Berglund, *Catal. Sci. Technol.* **2016**, *6*, 2897–2900.
- [25] Y. Hotta, S. Ezaki, H. Atomi, T. Imanaka, *Appl. Environ. Microbiol.* **2002**, *68*, 3925–3931.
- [26] A. Staudt, H. Terholsen, J. Kaur, H. Müller, S. P. Godehard, I. Itabaiana, I. C. R. Leal, U. T. Bornscheuer, *Microorganisms* **2021**, *9*, 1790.
- [27] H. Müller, A.-K. Becker, G. J. Palm, L. Berndt, C. P. S. Badenhorst, S. P. Godehard, L. Reisky, M. Lammers, U. T. Bornscheuer, *Angew. Chem. Int. Ed.* **2020**, *59*, 11607–11612; *Angew. Chem.* **2020**, *132*, 11704–11709.
- [28] J. Britton, R. Davis, K. E. O'Connor, *Appl. Microbiol. Biotechnol.* **2019**, *103*, 5957–5974.
- [29] P. Ziosi, C. Paolucci, F. Santarelli, T. Tabanelli, S. Passeri, F. Cavani, P. Righi, *ChemSusChem* **2018**, *11*, 2202–2210.
- [30] M. Kazemi, X. Sheng, W. Kroutil, F. Himo, *ACS Catal.* **2018**, *8*, 10698–10706.
- [31] "GESTIS-Stoffdatenbank," can be found under <https://gestis.dguv.de/data?name=012040>, access February 15, 2022.

- [32] U. T. Bornscheuer, R. J. Kazlauskas, *Hydrolases in Organic Synthesis: Regio- and Stereoselective Biotransformations*, Wiley-VCH, Weinheim, **1999**.
- [33] L. Wiermans, S. Hofzumahaus, C. Schotten, L. Weigand, M. Schallmey, A. Schallmey, P. Domínguez de María, *ChemCatChem* **2013**, *5*, 3719–3724.
- [34] E. López-Huertas, J. Lozano-Sánchez, A. Segura-Carretero, *Food Chem.* **2021**, *342*, 128291.
- [35] G. Catinella, S. Donzella, G. Borgonovo, S. Dallavalle, M. L. Contente, A. Pinto, *Antioxidants* **2022**, *11*, 260.
- [36] P. Gullón, B. Gullón, G. Astray, M. Carpena, M. Fraga-Corral, M. A. Prieto, J. Simal-Gandara, *Food Res. Int.* **2020**, *137*, 109683.
- [37] C. Chaves-López, A. Serio, G. Mazzarrino, M. Martuscelli, E. Scarpone, A. Paparella, *Int. J. Food Microbiol.* **2015**, *207*, 49–56.
- [38] P. Conte, S. Pulina, A. Del Caro, C. Fadda, P. P. Urgeghe, A. De Bruno, G. Difonzo, F. Caponio, R. Romeo, A. Piga, *Food* **2021**, *10*, 923.
- [39] C. Romero, E. Medina, J. Vargas, M. Brenes, A. De Castro, *J. Agric. Food Chem.* **2007**, *55*, 680–686.
- [40] J. A. G. Correa, J. A. López-Villodres, R. Asensi, J. L. Espartero, G. Rodríguez-Gutiérrez, J. P. D. L. Cruz, *Br. J. Nutr.* **2008**, *101*, 1157–1164.
- [41] P. S. Rodis, V. T. Karathanos, A. Mantzavinou, *J. Agric. Food Chem.* **2002**, *50*, 596–601.

Manuscript received: May 2, 2022
Revised manuscript received: May 17, 2022
Accepted manuscript online: May 17, 2022
Version of record online: ■■■, ■■■■

RESEARCH ARTICLE

Use it all: Olive mill wastewater contains the majority of health-promoting olive phenols, but this resource has been little utilized. For the valorization of olive mill wastewater, the promiscuous acyltransferase PestE was engineered to acetylate hydroxytyrosol notably in an aqueous phase and to facilitate its extraction into the organic ethyl acetate phase.



*H. Terholsen, J. Kaur, N. Kaloudis, Dr. A. Staudt, Dr. H. Müller, Prof. Dr. I. V. Pavlidis, Prof. Dr. U. T. Bornscheuer**

1 – 7

Recovery of Hydroxytyrosol from Olive Mill Wastewater Using the Promiscuous Hydrolase/Acyltransferase PestE



ChemBioChem

Supporting Information

Recovery of Hydroxytyrosol from Olive Mill Wastewater Using the Promiscuous Hydrolase/Acyltransferase PestE

Henrik Terholsen, Jasmin Kaur, Nikolaos Kaloudis, Amanda Staudt, Henrik Müller,
Ioannis V. Pavlidis, and Uwe T. Bornscheuer*

Table of content

Methods	2
Materials	2
Prescreening of PestE_wt, PestE_H95A, PestE_I208A, and PestE_N288F	2
Inhibition of PestE by ferulic acid.....	2
OMWW sampling and preparation	2
Mutagenesis	3
<i>In silico</i> docking	3
Tables	3
Figures.....	4
Protein sequence of wild-type PestE	6

Methods

Materials

Hydroxytyrosol and *trans*-ferulic acid were purchased from Tokyo Chemical Industry Co. (Tokyo, Japan); hydroxytyrosol acetate was purchased from Santa Cruz Biotechnology (Dallas, Texas, USA). All other chemicals were purchased from Sigma-Aldrich (St. Louis, Missouri, USA) or Carl Roth (Karlsruhe, Germany) and were used without further purification.

Prescreening of PestE_wt, PestE_H95A, PestE_I208A, and PestE_N288F

To see if PestE variants can convert HT, 100 μL of enzyme solution (0.1 mg mL⁻¹) of PestE_wt, PestE_H95A, PestE_I208A, and PestE_N288F in 50 mM sodium phosphate buffer pH 8.0 were added to a reaction tube. Then, 100 μL of HT solution (10 mM in 50 mM sodium phosphate buffer pH 8.0) was added. The reactions were started by adding 100 μL of ethyl acetate. The reactions were incubated at 40°C for ten minutes and a sample of 1 μL from each ethyl acetate phase was analyzed by TLC. TLC was performed using silica gel plates (Merck, Darmstadt, Germany) as the solid and EtOAc as the mobile phase. The staining was performed with iodine ($R_f(\text{HT})=0.71$; $R_f(\text{HTA})=0.91$).

Inhibition of PestE by ferulic acid

To detect the inhibition of PestE_I208A_L209F_N288A by ferulic acid (FA), a *p*-nitrophenyl acetate hydrolysis assay (*p*NPA assay) and an acyl transfer reaction were performed. For the *p*NPA assay, 20 μL 10 mM *p*NPA in dimethyl sulfoxide was added to 180 μL enzyme solution (1 $\mu\text{g mL}^{-1}$) in phosphate buffer pH 7.5 containing FA to a final concentration of 0, 1, 2 or 5 mM. The absorbance was monitored at 405 nm using Tecan Reader Infinite 200 PRO (Tecan Trading AG; Männedorf, Switzerland).

The acyltransferase reaction was performed analogously to the conditions used for mutant screening, with and without 1 mM FA.

OMWW sampling and preparation

Olive mill wastewater (OMWW) samples were collected from three different three-phase olive oil mills in the Heraklion area (Crete, Greece). The temperature of the fresh OMWW was immediately determined and the solution was then cooled on ice. Samples were stored at -20°C when not used directly. To separate suspended solids, the OMWW was centrifuged (1 h, 10,000 $\times g$, 4°C), filtered through a sieve, centrifuged again, and the supernatant was finally ultrafiltrated with a 0.45 μm filter paper (Whatman®, Buckinghamshire, UK).

Mutagenesis

Variants were constructed based on pET21a_PestE using the Q5[®] Site-Directed Mutagenesis Kit (New England Biolabs GmbH, Ipswich, UK). Non-overlapping DNA-oligonucleotides were designed using the online NEBaseChanger tool for the mutations:

I208A: forward primer (5'→3'): CGAATACGTCgcgCTCACCGCCGACTTAATGG

reverse primer (5'→3'): GGCCCGCTGTACTCCACT

L209F: forward primer (5'→3'): ATACGTCATCtttACCGCCGACTTAATGGC

reverse primer (5'→3'): TCGGGCCCGCTGTACTCC

N288A: forward primer (5'→3'): CGGCTTCGTCgcgTTCTACCCCATATTAGAAG

reverse primer (5'→3'): CGGCTTCGTCgtcTTCTACCCCATATTAG.

PCR protocol was performed according to the manufacturer's description.

In silico docking

Structural analysis and molecular docking experiments of HT in PestE (PDB entry: 3ZWQ) were performed using YASARA (Vienna, Austria). UCSF Chimera (San Francisco, CA, USA) was used for visualization.

Tables

Table S1. Relative pNPA hydrolysis activity of PestE_I208A_L209F_N288A in the presence of ferulic acid.

Ferulic acid [mM]	0	1	2	5
Relative activity	100±5%	90±2%	67±21%	30±6%

Table S2. Characteristics of OMWW samples.

	OMWW 1 ^[a]	OMWW 2 ^[b]	OMWW 3 ^[c]
pH value	5.0	5.1	5.0
Temperature [°C]	38	32	32
HT [mM]	2.22	1.61	1.58

[a] Melissourgakis mill [b] Politakis mill [c] Gaia mill

Table S3. Specification of the EziG beads according to the manufacturer's data (<https://enginzyne.com/wp-content/uploads/2017/03/EziG%E2%84%A2-Product-Data-Sheet.pdf>). All beads are based on controlled porosity glass.

	EziG 1	EziG 2	EziG 3
Pore volume	~1.8 mL g ⁻¹	~1.8 mL g ⁻¹	~1.8 mL g ⁻¹
Surface	hydrophilic (glass)	hydrophobic (polymer)	semi- hydrophilic (polymer)
Pore diameter	500 +/- 50 Å	300 +/- 50 Å	300 +/- 50 Å

Figures

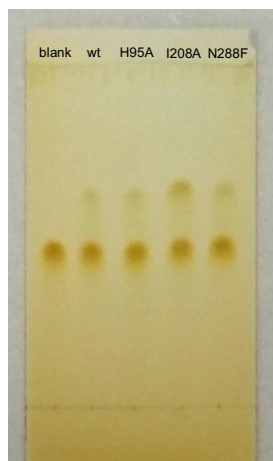


Figure S1. TLC of the initial screening of PestE_wt, PestE_H95A, PestE_I208A and PestE_N288F towards hydroxytyrosol.

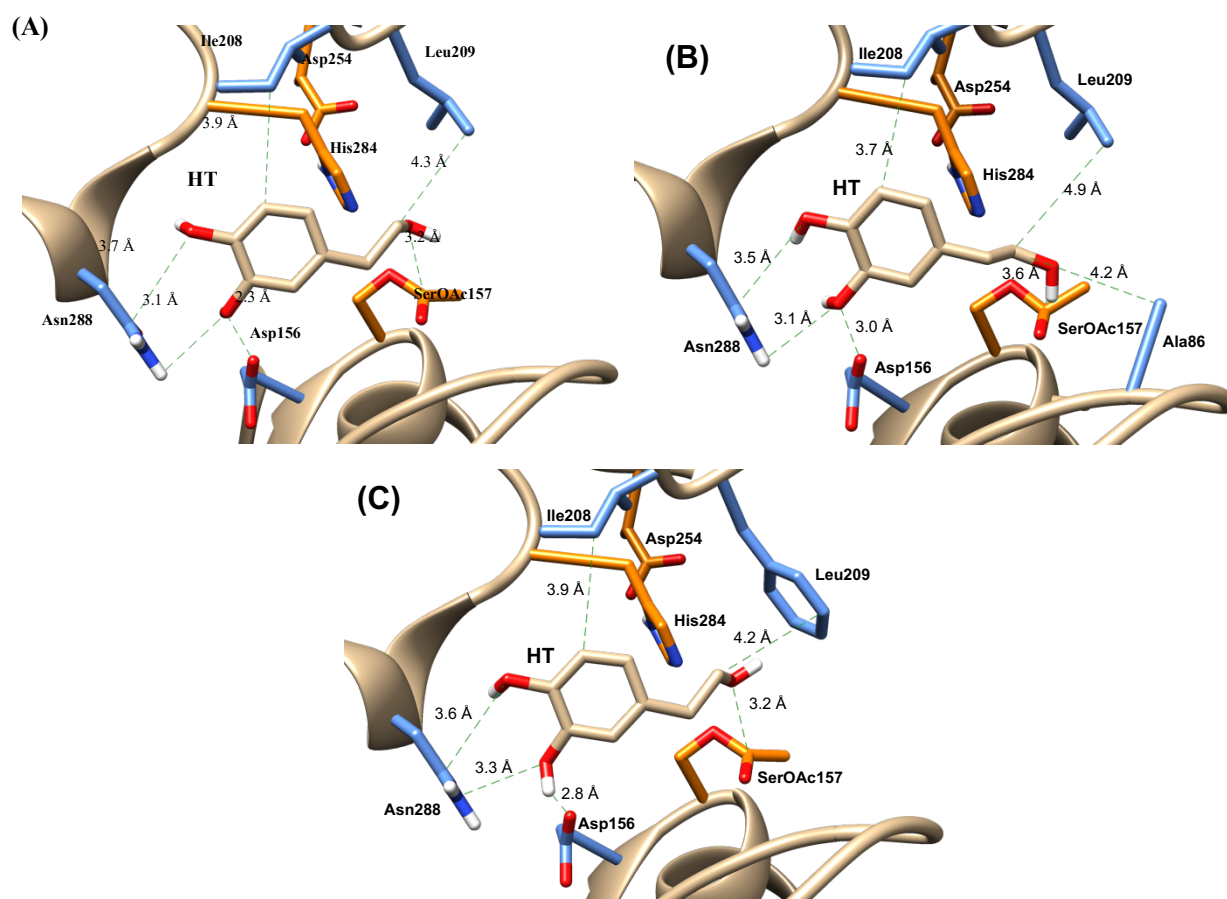


Figure S2. Docking structures of 3-hydroxytyrosol (HT) in PestE variants with the binding energies. Homology models are based on PDB 3ZWQ. Residues interacting with HT are shown in light blue, residues of the catalytic triad Ser157, His284, Asp254 are in orange. (A) PestE_wt. (B) PestE_G86A. (C) PestE_L209F.

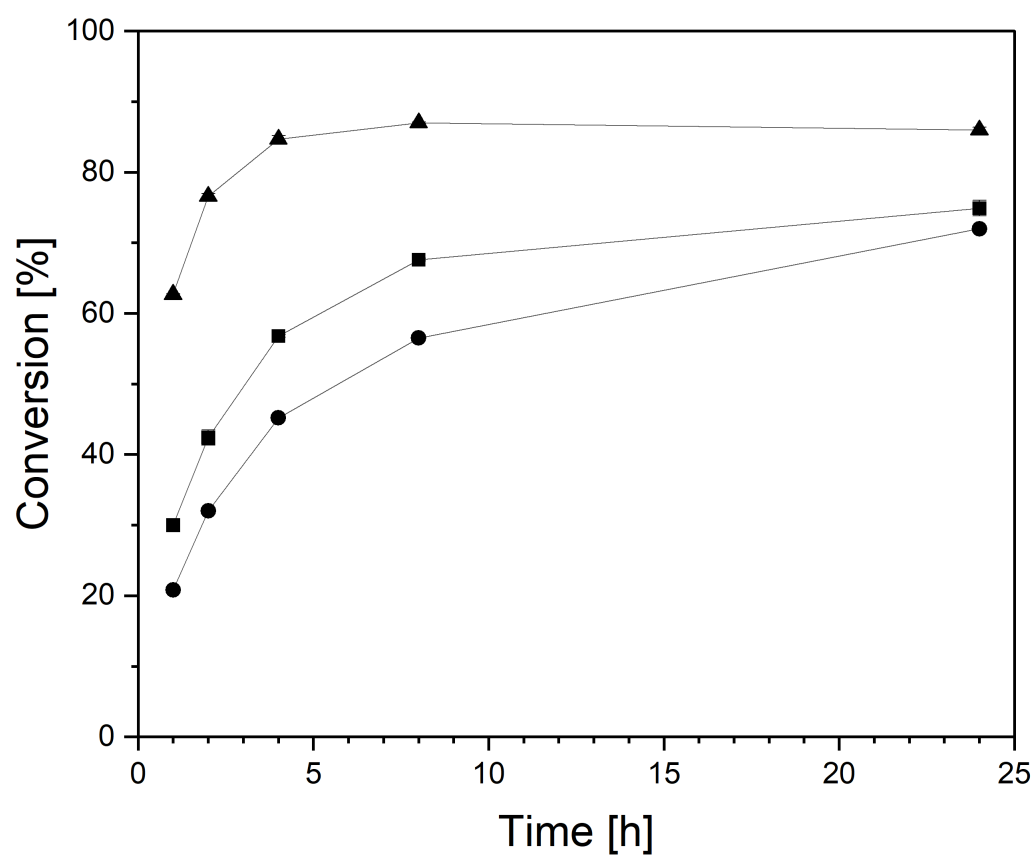


Figure S3. Conversions of HT by PestE_I208A_L209F (square), PestE_L209F_N288A (circle), and PestE_I208A_L209F_N288A (triangle) analyzed by GC-FID.

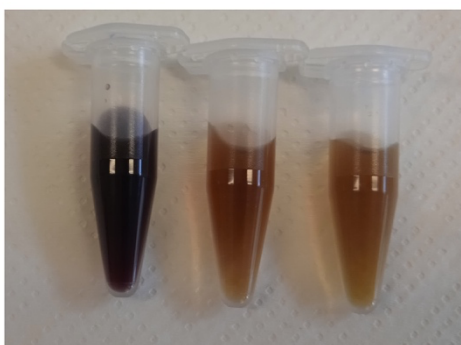


Figure S4. Color comparison of OMWW 1 to 3 (left to right).

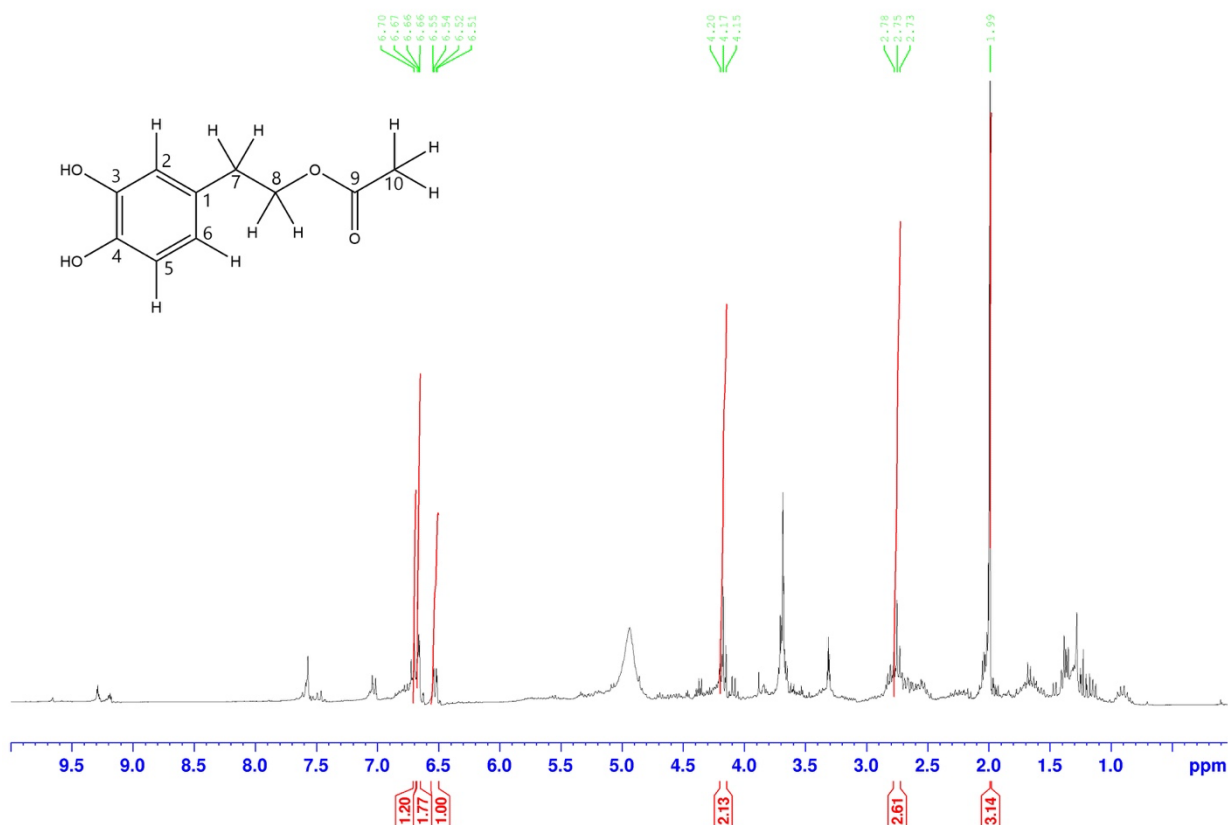


Figure S5. ^1H NMR profile of a phenolic extract obtained with PestE_I208A_L209F_N288A.

$^1\text{H-NMR}$ (300 MHz, $[\text{D}_4]$ MeOD): δ [ppm] = 1.99 (s, 3H, H-10 I-III), 2.75 (t, $^3J_{\text{H,H}}=7.1$ Hz, 2H, H-7 I&II), 4.17 (t, $^3J_{\text{H,H}}=7.1$ Hz, 2H, H-8 I&II), 6.52 (dd, $^3J_{\text{H,H}}=8.0$ Hz, $^4J_{\text{H,H}}=2.0$ Hz, 1H, H-6), 6.66 (d, $^3J_{\text{H,H}}=8.0$ Hz, 1H, H-5), 6.69 (d, $^4J_{\text{H,H}}=2.0$ Hz, 1H, H-2).

Protein sequence of wild-type PestE


MPLSPILRQILQQLAAQLQFRPDM DVKTVREQFEKSSLILVKMANEPIHRVEDITIPGRGGP
 IRARVYRPRDGERLPAVVYYHGGGFVLG SVETHDHVCRRLANLSGAVVVSVDYRLAPEH
 KFPAAVEDAYDAAKWWADNYDKLGV DNGKIAVAGDSAGGNLAAVTAIMARDRGESFVKY
 QVLIYPAVNLTGSPTVSRVEYSGPEYVILTADLMAWFG RQYFSKPQDALSPYASPIFADLSN
 LPPALVITAEYDPLRDEGELYAHLLKTRGVRAVAVRYNGVIHG FVNFYPILEEGREAVSQIAA
 SIKSMAVAHHHHH*

Article VI

An Enzyme Cascade Reaction for the Recovery of Hydroxytyrosol Derivatives from Olive Mill Wastewater

Henrik Terholsen¹, Jasmin Kaur¹, Nikolaos Kaloudis², Amanda Staudt¹, Ioannis V. Pavlidis², and Uwe T. Bornscheuer^{1,*}

DOI: 10.1002/cite.202200069

 This is an open access article under the terms of the Creative Commons Attribution-NonCommercial-NoDerivs License, which permits use and distribution in any medium, provided the original work is properly cited, the use is non-commercial and no modifications or adaptations are made.

The valorization of olive mill wastewaters (OMWW), a by-product of the olive milling, is getting rising attention. Lipophilization of the main phenolic compound 3-hydroxytyrosol (HT) could facilitate its extraction. An immobilized variant of the promiscuous hydrolase/acyltransferase from *Pyrobaculum calidifontis* VA1 (PestE) was used to perform acetylation in water using ethyl acetate as acyl donor. PestE was used in a segmented flow setting to allow continuous operation. Additionally, HT precursors were made accessible by pretreatment with almond β -glucosidase and the hydrolytic activity of PestE_I208A_L209F_N288A.

Keywords: Cascade reaction, Flow catalysis, Hydroxytyrosol, Olive mill wastewaters valorization, Promiscuous acyltransferase

Received: May 19, 2022; revised: June 16, 2022; accepted: June 29, 2022

1 Introduction

Olive oil is known for its health-promoting properties, which can be attributed to the phenolic substances it contains [1]. However, only 2% of the total olive fruit phenols are obtained in the olive oil due to the hydrophilic nature of these phenols [2]. More than half of the total phenols are disposed of with the olive mill wastewater (OMWW), which therefore has phytotoxic and antimicrobial properties and requires special treatment to degrade the organic matter [2, 3]. While various methods such as chemical oxidation, solvent extraction, membrane systems, or adsorbents have been investigated for phenol removal, open pond treatment is still widely used [4–10]. Recently, our group developed a system for the lipophilization and recovery of the main phenol 3-hydroxytyrosol (HT) in a biphasic ethyl acetate/OMWW system using an engineered variant of the promiscuous hydrolase/acyltransferase from the hyperthermophilic archaeum *Pyrobaculum calidifontis* VA1 (PestE) [11]. In contrast to commonly used lipases, promiscuous hydrolases/acyltransferases such as PestE can perform efficient transesterification reactions in bulk water [12, 13]. Moreover, PestE is a hyperthermostable enzyme that shows no decrease in activity at 100 °C [14] and can even be used in pure organic solvent [15]. Using the PestE variant optimized for HT, PestE_I208A_L209A_N288A, which was immobilized on EziG² beads, 265 mg L_{OMWW}⁻¹ HT and hydroxytyrosol acetate (HTA) were recovered from untreated OMWW [11]. It was possible to reuse the immobilized

PestE_I208A_L209A_N288A for at least ten reaction cycles without loss of activity, emphasizing the high process stability of the promiscuous hydrolase/acyltransferase PestE in this system [11]. The recovered HT derivatives from 1 L OMWW would be sufficient to fulfill the EU health claim for 1 kg of high-priced health-promoting olive oil, would it be added to any olive oil. However, the reaction was carried out in batch mode and with an incubation time of 24 h, which would require many large reaction vessels to apply this system to the huge volumes of OMWW continuously produced during the olive harvest. In this work, the biphasic batch system was transferred to a segmented flow system to allow continuous operation. Additionally, the release of HT from the HT glycoside oleuropein, another main olive phenol, was investigated by combining the almond (*Prunus amygdalus*) β -glucosidase with the acyltransferase activity of PestE (Fig. 1). The release of oleuropein from HT also occurs naturally during olive ripening, but olives for olive oil production are mostly green or unripe, especially in the

¹Henrik Terholsen, Jasmin Kaur, Dr. Amanda Staudt, Prof. Dr. Uwe T. Bornscheuer
uwe.bornscheuer@uni-greifswald.de

University Greifswald, Department of Biotechnology and Enzyme Catalysis, Felix-Hausdorff-Straße 4, 17487 Greifswald, Germany.

²Nikolaos Kaloudis, Prof. Dr. Ioannis V. Pavlidis

University of Crete, Department of Chemistry, Voutes University Campus, 70013 Heraklion, Greece.

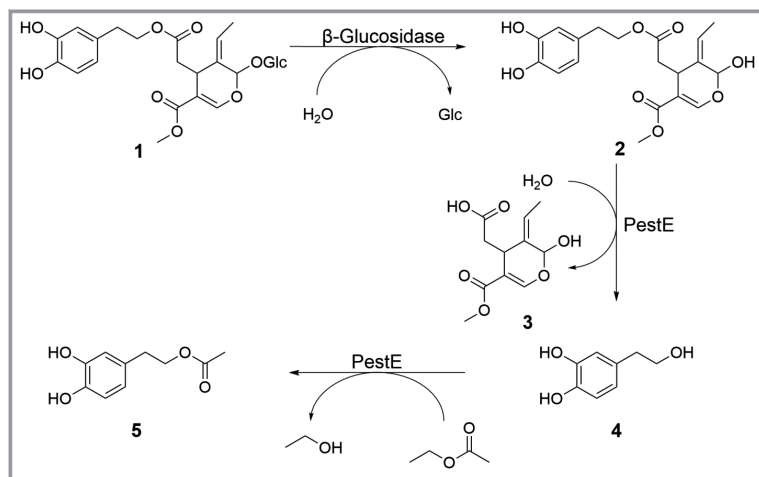


Figure 1. Reaction cascade for the conversion of oleuropein (1) to HTA (5). The almond β -glucosidase deglycosylates oleuropein (1) to the oleuropein aglycone (2) [17]. PestE_I208A_L209F_N288A is intended to release elenolic acid (3) and HT (4) by hydrolysis and to transesterify 4 to HTA (5) using ethyl acetate as acyl donor.

early season [16]. Degradation of oleuropein to HT would hence allow more efficient HT recovery even in the early season.

2 Experimental

2.1 Materials

OMWW samples were collected from different three-phase olive oil mills on Crete (Greece) and prepared as reported previously [11]. Ethyl acetate was purchased from VWR (Darmstadt, Germany) in HPLC grade (99.8+%). The β -glucosidase from almonds was purchased from Sigma-Aldrich (St. Louis, Missouri, USA).

2.2 Flow Settings

The ethyl acetate flow was controlled with a syringe pump (Perfusor[®] fm, Braun, Kronberg, Germany). The OMWW was pumped using a peristaltic pump (Minipuls 3, GILSON, Middleton, WI, USA). The ethyl acetate and OMWW phases were introduced into a packed-bed reactor of 0.5 mL volume (200 mg), which consisted of EziG² beads (Engin-Zyme, Solna, Sweden). A thin layer of sand was placed at the bottom and top of the packed bed. EziG² beads were loaded with 5 mg of PestE_I208A_L209A_N288A. The residence time on the column was approximately 10 min and the system was operated at room temperature. The ethyl acetate phase was separated, dried with anhydrous Na₂SO₄ and analyzed by gas chromatography, as described previously [11].

2.2.1 Acetylation/Extraction Setup

For the acetylation and extraction of HT in flow, ethyl acetate was pumped into the packed-bed reactor at 1.0 mL h⁻¹ and OMWW at 1.6 mL h⁻¹. OMWW was either untreated or pretreated with 1 U mL⁻¹ almond β -glucosidase for 1 h at room temperature.

2.2.2 Oleuropein Hydrolysis Setup

OMWW was pretreated with 1 U mL⁻¹ almond β -glucosidase for 1 h at room temperature and then added to the packed-bed reactor at a flow rate of 1.6 mL h⁻¹.

2.3 Protein Expression and Immobilization

Protein expression was performed as reported previously [13]. The purification of PestE_I208A_L209F_N288A was performed with heat shock for 40 min at 80 °C. The denatured proteins were separated by centrifugation (30 min, 17 000 g, 4 °C). The supernatant was added to the packed-bed reactor and the flow-through was collected and applied two more times. PestE_I208A_L209F_N288A (5.0 mg) were immobilized on the packed-bed beads.

3 Results and Discussion

The recovery of HT derivatives by acyltransferase-catalyzed lipophilization in batch mode was described previously [11]. HT was acetylated in the aqueous phase by PestE_I208A_L209F_N288A and then extracted into the organic ethyl acetate phase, which also functions as the acyl donor. In order to allow a continuous operation of the recovery of HT from OMWW, a segmented flow setup was used. In addition, ethanol, which is a by-product of enzymatic HT transesterification with ethyl acetate, cannot accumulate in a flow system and enhance the back reaction of the resulting product HTA. The packed-bed reactor was loaded with EziG² beads, porous glass beads coated with a semi-hydrophobic polymer that can bind His₆-tagged proteins. EziG² beads were found to be suitable for the immobilization of PestE_I208A_L209F_N288A and could be used for at least ten reaction cycles without loss of activity [11].

Using the flow system described in Fig. 2a, 93 mg L_{OMWW}⁻¹ HTA and 37 mg L_{OMWW}⁻¹ HT could be extracted in the organic phase. However, with 130 mg L_{OMWW}⁻¹ less HT derivatives were recovered compared to the batch process reported previously (265 mg L_{OMWW}⁻¹) [11], the reaction time could be reduced from 24 h to 10 min and elevated temperatures could be avoided.

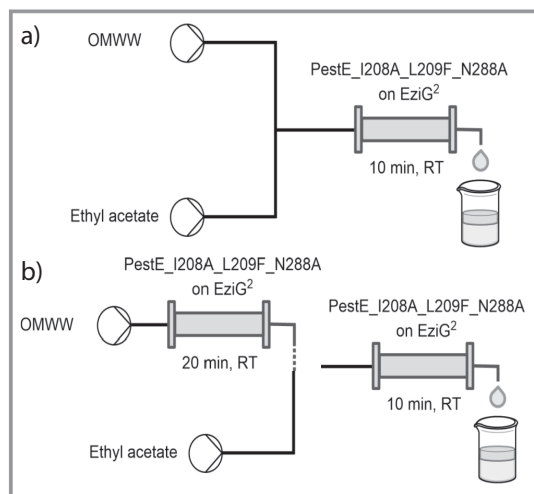


Figure 2. Schematic diagram of the flow settings. a) Acetylation/extraction setup. Ethyl acetate and OMWW were added to the packed-bed reactor at flow rates of 1.0 mL h^{-1} and 1.6 mL h^{-1} , respectively. b) Combined oleuropein hydrolysis and acetylation/extraction setup. Hydrolysis of oleuropein was performed in a separate flow-through reaction at a flow rate of 1.6 mL h^{-1} . The acetylation/extraction reaction (as described above) was performed sequentially.

The HT concentration of the OMWW was about 2 mM (300 mg L^{-1}), which is relatively low compared to literature [5, 6]. One reason for the low HT content could be the ripeness of the olives used for olive oil production. Since the olives were mostly unripe at the time of sampling in November, the HT could still be bound in the precursor oleuropein. Since β -glucosidase from almonds has already been used for the cleavage of oleuropein and has a pH optimum of about 5, as well as tolerance to potential impurities such as heavy metals [17, 18], almond β -glucosidase was used in this work. However, because limited data are available on the tolerance of almond β -glucosidase towards organic solvents in a two-phase system, pretreatment of the OMWW was performed before the OMWW was used for the flow reaction.

OMWW pretreated with almond β -glucosidase was used in the flow setting described in Fig. 2a. However, only $61 \text{ mg L}_{\text{OMWW}}^{-1}$ HTA and $38 \text{ mg L}_{\text{OMWW}}^{-1}$ HT could be extracted using this system, possibly due to the fact that the hydrolase activity of PestE towards the oleuropein aglycone is suppressed under acyltransferase conditions. The lower acyltransferase activity could possibly be explained by the inhibition of the acyltransferase reaction by the oleuropein aglycone. Inhibition of PestE by structurally similar phenols has been reported previously for ferulic acid [11]. Therefore, deglycosylation and hydrolysis of oleuropein and acetylation of HT must be carried out sequentially. For this purpose, pretreated OMWW was added to the packed-bed reactor without the addition of ethyl acetate (Fig. 2b). The resulting solution was again applied to the immobilized enzymes using the acetylation/extraction flow setting with

ethyl acetate. With this approach, $86 \text{ mg L}_{\text{OMWW}}^{-1}$ HTA and $69 \text{ mg L}_{\text{OMWW}}^{-1}$ HT could be extracted. In total, $155 \text{ mg L}_{\text{OMWW}}^{-1}$ HT derivatives could be extracted, which is more compared to the approach without β -glucosidase ($130 \text{ mg L}_{\text{OMWW}}^{-1}$), indicating successful release of HT from oleuropein by β -glucosidase and PestE. However, the acyltransferase reaction proved to be incomplete, as this approach extracted more unreacted HT than HTA despite its more hydrophilic properties. To convert the released HT to HTA, which is easier to extract, another acetylation/extraction run was performed with the separated ethyl acetate and OMWW phases. After this flow run, $166 \text{ mg L}_{\text{OMWW}}^{-1}$ HTA and $62 \text{ mg L}_{\text{OMWW}}^{-1}$ HT ($228 \text{ mg L}_{\text{OMWW}}^{-1}$ HT derivatives) were recovered, representing 75% improvement in extracted HT derivatives compared to the original flow system. Using the sequential flow approach, similar amounts of HT could be extracted as with the batch reaction [11], but without heating and with much shorter reaction times. For industrial application the system would have to be scaled up. Additionally, the sequential approach would have to be included in a flow system with two separate pack-bed reactions to allow continuous processing. However, the proof of concept of a flow system for the valorization of OMWW using β -glucosidase and both catalytic activities of promiscuous hydrolase/acyltransferase PestE_I208A_L209F_N288A was already successful as confirmed by our results. To further reduce the cost of the process, purified β -glucosidase could be co-immobilized [19] or, even cheaper, microbial pretreatment of OMWW could be applied to release HT from oleuropein [20].

4 Conclusion

Immobilized PestE_I208A_L209F_N288A was previously used for valorization of OMWW in a batch system. Herein we developed a flow system that shortens the reaction time and does not require heating. Using almond β -glucosidase and the hydrolase/acyltransferase activities of PestE_I208A_L209F_N288A, previously inaccessible HT precursors could be utilized. Using this system, 228 mg of HT derivatives could be extracted from 1 L OMWW.

H.T. was funded by the Leibniz Association's strategic networking funding program Leibniz ScienceCampus ComBioCat. A.S. received funding from the Coordenação de Aperfeiçoamento de Pessoal de Nível Superior – Brasil (Capes) – Finance Code 001. Special thanks to the operators of the olive mills Melissourgakis, Politakis and Gaia for the OMWW samples (Crete, Greece). Open access funding enabled and organized by Projekt DEAL.

Abbreviations

HT	3-Hydroxytyrosol
HTA	Hydroxytyrosol acetate
PestE	Promiscuous hydrolase/acyltransferase from <i>Pyrobaculum calidifontis</i> VA1

References

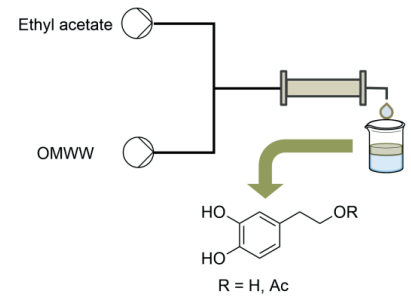
- [1] G. K. Beauchamp, R. S. J. Keast, D. Morel, J. Lin, J. Pika, Q. Han, C.-H. Lee, A. B. Smith, P. A. S. Breslin, *Nature* **2005**, *437*, 45–46.
- [2] A. Ramos-Cormenzana, M. Monteoliva-Sanchez, M. J. Lopez, *Int. Biodeterior. Biodegrad.* **1995**, *35*, 249–268.
- [3] H. Zbakh, A. El Abbassi, *J. Funct. Foods* **2012**, *4*, 53–65.
- [4] C. Agabo-García, N. Calderón, G. Hodaifa, *Catalysts* **2021**, *11*, 557.
- [5] M. O. J. Azzam, S. A. Hazaimah, *Process Saf. Environ. Prot.* **2021**, *148*, 495–523.
- [6] N. Allouche, I. Fki, S. Sayadi, *J. Agric. Food Chem.* **2004**, *52*, 267–273.
- [7] A. El-Abbassi, M. Khayet, A. Hafidi, *Water Res.* **2011**, *45*, 4522–4530.
- [8] R. Tundis, C. Conidi, M. R. Loizzo, V. Sicari, A. Cassano, *Antioxidants* **2020**, *9*, 602.
- [9] K. Al-Malah, M. O. J. Azzam, N. I. Abu-Lail, *Sep. Purif. Technol.* **2000**, *20*, 225–234.
- [10] D. Frascari, G. Rubertelli, F. Arous, A. Ragini, L. Bresciani, A. Arzu, D. Pinelli, *Chem. Eng. J.* **2019**, *360*, 124–138.
- [11] H. Terholsen, J. Kaur, N. Kaloudis, A. Staudt, H. Müller, I. V. Pavlidis, U. Bornscheuer, *ChemBioChem* **2022**, e202200254. DOI: <https://doi.org/10.1002/cbic.202200254>
- [12] H. Müller, H. Terholsen, S. P. Godehard, C. P. S. Badenhorst, U. T. Bornscheuer, *ACS Catal.* **2021**, *11*, 14906–14915.
- [13] A. Staudt, H. Terholsen, J. Kaur, H. Müller, S. P. Godehard, I. Itabaiana, I. C. R. Leal, U. T. Bornscheuer, *Microorganisms* **2021**, *9*, 1790.
- [14] Y. Hotta, S. Ezaki, H. Atomi, T. Imanaka, *Appl. Environ. Microbiol.* **2002**, *68*, 3925–3931.
- [15] S. Hari Krishna, M. Persson, U. T. Bornscheuer, *Tetrahedron: Asymmetry* **2002**, *13*, 2693–2696.
- [16] E. López-Huertas, J. Lozano-Sánchez, A. Segura-Carretero, *Food Chem.* **2021**, *342*, 128291.
- [17] R. Mazzei, L. Giorno, E. Piacentini, S. Mazzuca, E. Drioli, *J. Membr. Sci.* **2009**, *339*, 215–223.
- [18] G. Geiger, G. Furrer, F. Funk, H. Brandl, R. Schulin, *J. Enzym. Inhib.* **1999**, *14*, 365–379.
- [19] R. Briante, F. La Cara, F. Febbraio, R. Barone, G. Piccialli, R. Carolla, P. Mainolfi, L. De Napoli, M. Patumi, G. Fontanazza, R. Nucci, *J. Biotechnol.* **2000**, *77*, 275–286.
- [20] F. V. Romeo, G. Granuzzo, P. Foti, G. Ballistreri, C. Caggia, P. Rapisarda, *Molecules* **2021**, *26*, 1944.

DOI: 10.1002/cite.202200069

An Enzyme Cascade Reaction for the Recovery of Hydroxytyrosol Derivatives from Olive Mill Wastewater

Henrik Terholsen, Jasmin Kaur, Nikolaos Kaloudis, Amanda Staudt, Ioannis V. Pavlidis, Uwe T. Bornscheuer*

Short Communication: Olive mill wastewater (OMWW) is a major by-product of olive oil extraction and requires special treatment due to the polyphenolic compounds it contains. We developed an enzymatic cascade reaction for the deglycosylation and acetylation of oleuropein and 3-hydroxytyrosol to facilitate their extraction. ■



Article VII

Chemoenzymatic Cascade Reaction for the Valorization of the Lignin Depolymerization Product G-C2-Dioxolane Phenol

Henrik Terholsen^[a], Jule R. H. Meyer^[a], Zhenlei Zhang^[b], Peter J. Deuss^[b], and Uwe T. Bornscheuer^{*[a]}

[a] M.Sc. H. Terholsen, B.Sc. J. R. H. Meyer, Prof. Dr. U. T. Bornscheuer
Institute of Biochemistry, Department of Biotechnology and Enzyme Catalysis
University of Greifswald
Felix-Hausdorff-Straße 4, 17487 Greifswald (Germany)
E-mail: uwe.bornscheuer@uni-greifswald.de

[b] Dr. Z. Zhang, Prof. Dr. P.J. Deuss
Faculty of Science and Engineering
Chemical Technology — Engineering and Technology Institute Groningen
University of Groningen
Nijenborgh 4, 9747 AG Groningen (Netherlands)

Supporting information for this article is given via a link at the end of the document.

Abstract: Combining solid acid catalysts with enzyme reactions in aqueous environments is challenging because either very acidic conditions inactivate the enzymes or the solid acid catalyst is neutralized. Using Amberlyst-15 encapsulated in polydimethylsiloxane (Amb-15@PDMS), we were able to perform deprotection of the lignin depolymerization product G-C2 dioxolane phenol in a buffered system at pH 6.0. This reaction was directly coupled with the biocatalytic reduction of the released homovanillin to homovanillyl alcohol by recombinant horse liver alcohol dehydrogenase, which was subsequently acylated by a triple mutant of the promiscuous acyltransferase/hydrolase PestE in a one-pot system. The deprotection catalyzed with Amb-15@PDMS reached up to 97% conversion. Overall, this cascade enabled conversions of up to 57 %.

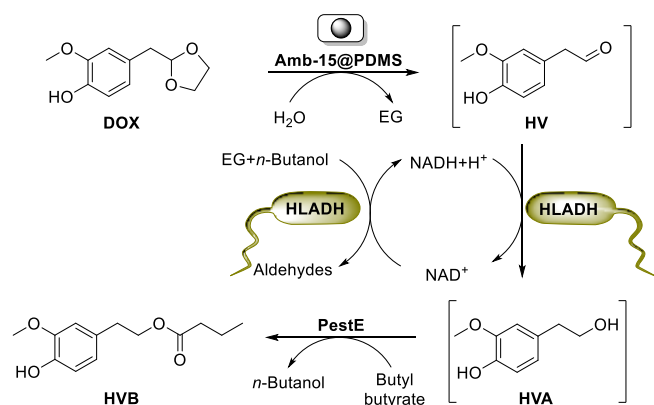
Introduction

Valorization of lignocellulose-derived lignin can provide a sustainable route for the production of phenolic compounds^[1]. However, in conventional pulp production, lignin extraction leads to an irreversibly altered complex structure that makes it impossible to produce defined depolymerization products^[2]. The "lignin first" approach aims to extract and depolymerize lignin from lignocellulose without compromising the utilization of cellulose and hemicellulose^[2,3]. Diol-assisted lignocellulose fractionation follows the lignin-first approach and prevents the repolymerization of reactive species formed during acid-catalyzed depolymerization by the formation of diol-based lignin mono- and oligomer acetals^[3–7]. Diol-assisted acidolysis of the β -O-4'-bond in lignin of softwoods such as pine, cedar, or spruce with ethylene glycol leads to the formation of an acetal derived from the lignin subunit G (G-C2-dioxolane phenol, DOX; Scheme 1)^[5].

In this work, we aim to further utilize the generated G-C2 acetal to produce homovanillyl butyrate (HVB), a lipophilized derivative of homovanillyl alcohol (HVA). Homovanillyl alcohol is an antioxidant with protective effects on cardiovascular diseases and a metabolite of hydroxytyrosol^[8,9]. A chemoenzymatic cascade involving a deacetalization, reduction, and acylation step was considered for the conversion of DOX to homovanillyl butyrate (Scheme 1). However, the product of the deacetalization, homovanillin (HV), is known to be labile under acidic conditions typically used for acetal deprotection^[10,11].

Furthermore, the reaction comes into equilibrium with the reverse reaction, resulting in incomplete deprotection. Therefore, acetone is usually added to shift the equilibrium for deprotection of this type of compounds^[12–14]. In contrast, we used horse liver alcohol dehydrogenase (HLADH), recombinantly produced in *E. coli*, to convert HV to HVA, thereby avoiding condensation of HV and shifting the equilibrium of the deacetalization. To further shift the equilibrium, we used an enzymatic acyltransferase reaction, which was carried out by the promiscuous acyltransferase/hydrolase from *Pyrobaculum calidifontis* VA1 (PestE)^[15]. The variant PestE_I208A_L209F_N288A was previously optimized by us for hydroxytyrosol acetylation in an aqueous/organic two-phase system and applied in a cascade reaction to obtain hydroxytyrosol acetate from olive mill wastewater^[16,17]. In the present study, we found that PestE_I208A_L209F_N288A also acylated the structurally related homovanillyl alcohol. Apart from shifting the equilibrium of the HLADH reaction, lipophilization of homovanillyl alcohol in homology to hydroxytyrosol could enhance the membrane permeability of this antioxidant^[18,19]. However, since strongly acidic conditions required for the deacetalization of the G-C2-dioxolane phenol are incompatible with the enzymatic reactions, a compartmentalization strategy was used to establish a one-pot reaction. For this purpose, the polymeric solid acid catalyst Amberlyst 15 (Merck KGaA, Darmstadt, Germany), which contains sulfonic acid residues, was encapsulated in the hydrophobic polydimethylsiloxane (PDMS) polymer, resulting in Amb-15@PDMS. The combination of enzyme reactions with solid acid catalysts in an aqueous one-pot reactions has so far been little explored. The only known one-pot cascade combining a solid acid catalyst and an enzyme could not be performed in buffered solution as this resulted in a rapid deactivation of the enzyme under the harsh reaction conditions^[20]. Here we report on the development of a catalytic cascade that starts with Amb-15@PDMS as solid acid catalyst in buffered water demonstrating its compatibility with a suitable environment for the desired enzymatic reactions.

Results and Discussion



Scheme 1. Chemoenzymatic cascade for the synthesis of homovanillyl butyrate from G-C2-dioxolane phenol (DOX). Amb-15@PDMS catalyzes the deprotection of DOX (accessible from the diol (EG)-assisted acidolysis of softwood lignin) to HV^[6]. HV is reduced to HVA by lyophilized *E. coli* whole cells containing HLADH. HLADH recycles NADH using ethylene glycol (EG) and *n*-butanol released during the other reaction steps. PestE_I208A_L209F_N288A finally acylates HVA to HVB.

The instability of phenolic compounds at basic pH is well known^[21,22]. Therefore, a sodium phosphate/citrate buffer (25 mM each, pH 6.0) was chosen to perform the cascade reaction. Both enzymes, HLADH and PestE_I208A_L209F_N288A, tolerated these conditions (Figures S1 and S3). However, Amberlyst-15 was inactive in our buffered aqueous system, although the solid acid catalyst Amberlyst-15 is water stable and has been used in several aqueous systems^[23–26]. Unlike systems containing pure water, a buffered system required for enzymatic reactions can completely neutralize the solid acid catalyst. To protect the solid acid catalyst, the Amberlyst-15 beads were encapsulated in PDMS, resulting in Amb-15@PDMS. PDMS retains buffer salts but allows organic compounds to enter^[27–29]. In addition, PDMS has low permeability to water, allowing deacetalization to occur without rapidly inactivating the acid catalyst^[30]. With ten Amb-15@PDMS punchings it was possible to reach 97% conversion in 24 h at 20°C without addition of the enzymes for the cascade (Table S1, entry 10).

However, due to the large differences in deprotection activity (Table S2), the conversions achieved in the initial cascade reactions varied widely (Table S1). Nevertheless, with careful selection of Amb 15@PDMS beads, where the catalyst is located in the center of the punching, DOX deacetalization efficiencies of up to 97% were achieved in the cascade reaction (Table 1; entry 1). In addition, Amb-15@PDMS can be recycled without further regeneration (Table S2). Interestingly, beads that showed low activity when first used showed no activity when reused, indicating that the beads were deactivated during the first reaction cycle, possibly due to the disintegration of the beads during the first use (Figure S4; e.g., beads 5 and 9). Apart from bead 6, similar conversions were achieved with reused beads (Table S2). This demonstrates the robustness of the newly developed Amb-15@PDMS catalyst making it a promising candidate for combining solid acid catalysts with various enzymatic reactions. From a practical point of view, washing Amb-15@PDMS twice with ethyl acetate was sufficient to efficiently extract the contained organic compounds. A third washing step performed in initial experiments did not contain

DOX, HV, HVA or HVB. DOX and HVB are mainly recovered from the Amb-15@PDMS beads, while HV and HVA are mainly recovered from the aqueous phase (data not shown).

Unfortunately, the presence of Amb-15@PDMS was not compatible to the commercial HLADH used in the initial experiments (data not shown), which may be attributed to its immobilization on the PDMS surface^[31,32]. Moreover, the addition of the acyl donor ethyl acetate, which was previously used to promote the subsequent acyltransferase reaction, is greatly reducing HLADH activity (Figure S2). To overcome these limitations, the less inhibitory acyl donor butyl butyrate was used and recombinantly expressed HLADH was used in lyophilized *E. coli* BL21 whole cells. The use of whole cells had the unexpected advantage that the endogenous enzymes also showed some activity in reducing HV to HVA, as seen in a control reaction with empty vector-containing *E. coli* BL21 whole cells (Table S1; entry 1). However, the activity of HLADH remained low, and large amounts of whole-cell lyophilizate were required to achieve 97% conversion of the HV produced to HVA (Table 1).

Promiscuous acyltransferases/hydrolases are capable of catalyzing transesterification reactions, usually carried out in organic solvents, in water. The robust promiscuous acyltransferase/hydrolase PestE_I208A_L209F_N288A is not inactivated by Amb-15@PDMS and can be added as an isolated enzyme, from (heat-treated) lysate or from lyophilized *E. coli* whole cells (Table S1). In the absence of PestE_I208A_L209F_N288A, only trace amounts of HVB were formed, indicating that HVB formation originates from the acyltransferase. Conversions of up to 61±0% were obtained for the acylation step, although solid acid catalysts are in principle capable of hydrolyzing esters^[33,34]. Moreover, complete conversions with butyl butyrate as the acyl donor are not expected because the butanol released during the acyl transfer and hydrolysis of the acyl donor favors the reverse reaction. Conversions of 68±1% were achieved when 5 mM HVA was converted by PestE_I208A_L209F_N288A in the presence of ten Amb 15@PDMS beads, indicating that the 61% conversion achieved in the cascade is close to the maximum conversions expected for this system. However, it is worth noting that PestE_I208A_L209F_N288A is the HVB-forming catalyst and not Amb-15@PDMS (Table S1, entry 2). To achieve good conversions with acyl donors from aliphatic esters or poor acyltransferase substrates, a large excess of acyl donor is usually added to form a second phase, shifting the equilibrium and preventing hydrolysis of the product by extraction^[35]. Therefore, 20% (v/v) butyl butyrate was added to the reaction. However, in the system described, the liquid organic phase was rapidly absorbed by the Amb-15@PDMS beads, resulting in a two-phase system consisting of an organic-solid phase and an aqueous-liquid phase. Increasing the amount of butyl butyrate to 50% (v/v) did not increase the conversion of the acyl transfer step (Table S1, entry 6), indicating that 20% acyl donor is already sufficient to achieve maximal conversions.

The use of PestE_I208A_L209F_N288A emphasized that the coupling of Amb-15@PDMS with enzymes is possible, however, as learned from HLADH, not all enzymes can be applied as purified enzymes. Most importantly, this chemoenzymatic cascade reaction showed a potential valorization strategy for the lignin depolymerization product DOX

and potentially further acetal compounds originating from the H and S subunits of lignin.

WILEY-VCH

Table 1. Chemoenzymatic cascade reaction for the synthesis of HVB.

Entry	HLADH	PestE	DOX	HV	HVA	HVB
1	OD ₆₀₀ 500	20 µg	3±1%	3±2%	37±1%	57±0%
2	OD ₆₀₀ 100	20 µg	14±6%	50±2%	13±3%	23±2%
3	OD ₆₀₀ 15	20 µg	13±7%	75±7%	4±0%	8±0%
4	–	–	3±0%	97±0%	n.d.	n.d.

Reaction conditions: 5 mM G-C2 dioxolane phenol, 7 mg Amb-15@PDMS (containing approximately 1.4 mg Amb-15; 10 beads), 20% (v/v) butyl butyrate, and purified PestE_I208A_L209F_N288A were added. The 100-µL-scale reaction in sodium phosphate/citrate buffer (25 mM each; pH 6.0) was performed at 20°C (1000 rpm) for 24 hours. The conversions are relative to the recovered molecules, the recovery rate was about 80%. HLADH was expressed in *E. coli* whole cells and used as a lyophilizate. All reactions were extracted twice with 200 µL ethyl acetate and Amb-15@PDMS was also washed twice. Values shown are means of duplicates. OD₆₀₀ was measured before lyophilization and the amount of lyophilisate added was adjusted accordingly. Experiments were performed with beads where accurate Amb-15@PDMS punching was double checked.

Conclusion

A cascade chemoenzymatic reaction in an aqueous system was successfully developed for the deacetalization, reduction, and acylation of the lignin depolymerization product G-C2 dioxolane phenol. Up to 57% conversion to HVB were achieved using Amb-15@PDMS, *E. coli* BL21 whole cells containing HLADH, and PestE_I208A_L209F_N288A. With deacetalization and transesterification, two reactions that are typically incompatible with buffered aqueous systems were combined in a cascade reaction under mild reaction conditions. Amb-15@PDMS was developed as a solid acid catalyst that can work in buffered aqueous solution and is compatible with enzymatic reactions. Therefore, Amb-15@PDMS can be a pioneer for coupling solid acid catalysts and enzymatic reactions under mild aqueous conditions. The combination of Amb-15@PDMS with the labile HLADH was demonstrated, even if the enzyme had to be protected in whole cells. In contrast, PestE_I208A_L209F_N288A could be used as a free biocatalyst, highlighting the robustness and compatibility of this enzyme in cascade reactions.

Experimental Section

Protein preparation

Chemically competent *E. coli* BL21 (DE3) cells were transformed with the expression vectors pET21a_PestE_I208A_L209F_N288A or pET28a_HLADH by heat shock and plated on LB agar containing 100 µg/mL ampicillin (Amp) or 50 µg/mL kanamycin (Kan), respectively. 4 mL Lysogeny broth (LB) pre-cultures containing Amp or Kan were inoculated and incubated overnight (37°C, 140 rpm). LB medium (50-600 mL) was inoculated with 1% (v/v) of the pre-culture and incubated (37°C, 140 rpm) until it reached OD₆₀₀ of 0.6. Protein expression was induced by the addition of isopropyl-β-D-thiogalactopyranoside (IPTG) to a final concentration of 0.5 mM and incubated overnight (~20 h) at 20°C and 140 rpm. Cells were harvested by centrifugation at 10,000 g and 4°C for 5 min.

For the preparation of HLADH, *E. coli* cells were resuspended in 4 mL reaction buffer (50 mM sodium phosphate, 50 mM sodium citrate buffer, pH 6.0) per gram of cells to produce whole cells, and OD₆₀₀ was measured. The resuspension was lyophilized for the cascade reaction. Preparation of whole cells containing the empty pET28a vector was performed accordingly.

For the purification of PestE_I208A_L209F_N288A, cell pellets were resuspended with 4 mL lysis buffer (10 mM imidazole, 50 mM potassium phosphate, 300 mM sodium chloride, pH 8.0) per gram of cells. The cell solutions were lysed by sonification on ice (two cycles of 5 min sonication (50% intensity, 50% pulsed cycle)) using a SONOPULS HD 2070

(BANDELIN Electronic GmbH & Co. KG, Berlin, Germany). After centrifugation at 10,000 g and 4°C for 30 min. For purification, the crude lysates were applied to 1.5 mL Roti®Garose-His/Ni Beads (Carl Roth, Karlsruhe, Germany). The resins were washed with 15 mL washing buffer (20 mM imidazole, 50 mM sodium phosphate, 300 mM sodium chloride, pH 8.0) before target proteins were eluted with elution buffer (250 mM imidazole, 50 mM sodium phosphate, 300 mM sodium chloride, pH 8.0). Elution fractions were treated at 80°C for 20 min (500 rpm), centrifuged (17,000 g, 4°C for 5 min), and the supernatant transferred to the storage buffer (50 mM sodium phosphate, pH 7.5) using PD-10 desalting columns (GE Healthcare, UK). Protein concentrations were determined at 280 nm using a NanoDrop™ 1000 spectrophotometer (ThermoFisher, Germany).

Lyophilization, when appropriate, was performed overnight in a Christ™ Alpha 1-2 lyophilizer (Martin Christ Gefrierrocknungsanlagen GmbH, Osterode am Harz, Germany).

Deprotection with Amb-15@PDMS

Ten Amb-15@PDMS beads (approximately 7 mg containing 1.4 mg Amb-15), 10 µL DOX solution (from a 50 mM stock in butyl butyrate; 5 mM final concentration), 10 µL butyl butyrate, and 80 µL sodium phosphate/citrate buffer (25 mM each; pH 6.0) were added to a 1.5-mL GC vial and incubated for 24 h at 20°C (1000 rpm). The aqueous phase was separated and extracted twice with 200 µL ethyl acetate. The beads were washed twice with 200 µL ethyl acetate (10 min, 20°C, 1000 rpm). The ethyl acetate phases were combined and dried with anhydrous sodium sulfate before gas chromatography (GC) analysis.

Cascade reactions

Reactions were performed according to the following protocol unless stated differently. Ten Amb-15@PDMS beads (approximately 7 mg containing 1.4 mg Amb-15), 2.5 µL DOX solution (from a 200 mM stock in butyl butyrate; 5 mM final concentration), 17.5 µL butyl butyrate, and 80 µL sodium phosphate/citrate buffer (25 mM each; pH 6.0) with 20 µg PestE_I208A_L209F_N288A and lyophilized *E. coli* BL21 (DE3) containing HLADH (final OD₆₀₀ = 500 calculated on the basis of cell density before lyophilization) were added to a 1.5-mL GC vial. The reaction was incubated for 24 h at 20°C (1000 rpm), the aqueous phase was separated and extracted twice with 200 µL ethyl acetate. The beads were washed twice with 200 µL ethyl acetate (15 min, 20°C, 1000 rpm). The ethyl acetate phases were combined and dried with anhydrous sodium sulfate before gas chromatography (GC) analysis.

GC-FID analytics

Analysis was performed with a GC-FID (GC-2010, Shimadzu, Kyoto, Japan) equipped with a ZB 5MSi column (25.0 m x 0.25 mm, 0.25 µm film thickness, Phenomenex, Torrance, California, USA). Injector and detector temperature was 250°C, and 1 µL sample was injected. The column temperature was held at 160°C for 3.0 min, increased to 190°C

with 14°C min⁻¹, and held 4.9 min. Total time: 10 min. Retention times: DOX: 6.75 min, HV: 3.97 min; HVA: 4.65 min; HVB: 8.67 min.

Preparation of Amb-15@PDMS

The commercial PDMS Sylgard[®] 184 (Merck KGaA, Darmstadt, Germany) was prepared by adding 1 part of hardener to 10 parts of PDMS base (total volume: 12 mL). After mixing the reagents, the mixture was added to 100 mg dry Amberlyst-15 (Sigma-Aldrich) in a Petri dish. The dish was inverted several times and quickly inverted back to ensure that the Amberlyst-15 was completely surrounded by PDMS. The reaction product cured overnight at room temperature and for an additional 4 hours 60°C. The Amb-15@PDMS beads were cut using a 1.5 mm diameter biopsy punch.

Synthesis of G-C2-dioxolane phenol

The G-C2-dioxolane phenol can be isolated from the reaction mixture of diol (EG)-assisted softwood lignin acidolysis^[7] or a reaction mixture under a diol (EG)-assisted lignin-first approach^[5]. Separation of G-C2-dioxolane phenol via column chromatography from beech ethanosolv lignin has been demonstrated in our previous study^[4]. In this study, we used a synthesized model by applying a modified literature procedure^[36]. Under N₂ atmosphere, 3.25 g of *N*-bromosuccinimide (18.5 mmol, NBS) and 4.75 g of silver trifluoromethanesulfonate (18.5 mmol) were dispersed in 30 mL DCM and 15 mL ethylene glycol. Subsequently, 2.5 mL (18.5 mmol) 4-vinyl guaiacol was added dropwise to the mixture and allowed to stir for 30 min. The reaction was quenched by adding 10 mL H₂O, 10 mL saturated NaHCO₃ solution, and 40 mL saturated Na₂S₂O₃ solution. The mixture was then extracted with DCM (20 mL x 3) and purified by column chromatography (ethyl acetate/pentane 5-30%). G-C2-dioxolane was obtained as yellowish oil (0.01 mol, 54% yield, ¹H-NMR purity: 95%). The obtained data are consistent with literature. ¹H NMR (400 MHz, Chloroform-*d*) δ 6.85 (d, *J* = 8.0 Hz, 1H), 6.81 – 6.73 (m, 2H), 5.52 (s, 1H), 5.03 (t, *J* = 4.8 Hz, 1H), 4.00 – 3.79 (m, 7H), 2.89 (d, *J* = 4.8 Hz, 2H). ¹³C NMR (101 MHz, Chloroform-*d*) δ 148.96, 147.02, 130.61, 125.03, 116.88, 114.84, 107.49, 67.63, 58.54, 43.05.

Acknowledgements

H.T. was funded by the Leibniz Association's strategic networking funding program Leibniz ScienceCampus ComBioCat. We thank Dr. Alessandra De Santi for initiating the synthesis of G-C2-dioxolane.

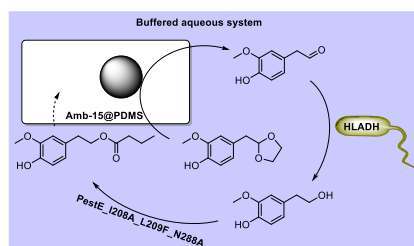
Keywords: biocatalysis • chemoenzymatic cascade • lignin valorization • promiscuous acyltransferases/hydrolases • solid acid catalyst

References

- [1] M. Al-Naji, F. Brandi, M. Drieß, F. Rosowski, *Chem. Ing. Tech.* **2022**, *94*, 1611–1627.
- [2] T. Renders, S. V. den Bosch, S.-F. Koelewijn, W. Schutyser, B. F. Sels, *Energy Environ. Sci.* **2017**, *10*, 1551–1557.
- [3] M. M. Abu-Omar, K. Barta, G. T. Beckham, J. S. Luterbacher, J. Ralph, R. Rinaldi, Y. Román-Leshkov, J. S. M. Samec, B. F. Sels, F. Wang, *Energy Environ. Sci.* **2021**, *14*, 262–292.
- [4] P. J. Deuss, M. Scott, F. Tran, N. J. Westwood, J. G. de Vries, K. Barta, *J. Am. Chem. Soc.* **2015**, *137*, 7456–7467.
- [5] A. De Santi, M. V. Galkin, C. W. Lahive, P. J. Deuss, K. Barta, *ChemSusChem* **2020**, *13*, 4468–4477.
- [6] P. J. Deuss, C. W. Lahive, C. S. Lancefield, N. J. Westwood, P. C. J. Kamer, K. Barta, J. G. de Vries, *ChemSusChem* **2016**, *9*, 2974–2981.
- [7] Z. Zhang, C. W. Lahive, J. G. M. Winkelman, K. Barta, P. J. Deuss, *Green Chem.* **2022**, *24*, 3193–3207.
- [8] R. De la Torre, D. Corella, O. Castañer, M. A. Martínez-González, J. Salas-Salvador, J. Vila, R. Estruch, J. V. Sorli, F. Arós, M. Fiol, E. Ros, L. Serra-Majem, X. Pintó, E. Gómez-Gracia, J. Lapetra, M. Ruiz-

- [9] Canela, J. Basora, E. M. Asensio, M. I. Covas, M. Fitó, *Am. J. Clin. Nutr.* **2017**, *105*, 1297–1304.
- [10] R. Mateos, L. Goya, L. Bravo, *J. Agric. Food Chem.* **2005**, *53*, 9897–9905.
- [11] P. J. Deuss, C. S. Lancefield, A. Narani, J. G. de Vries, N. J. Westwood, K. Barta, *Green Chem.* **2017**, *19*, 2774–2782.
- [12] K. P. C. Vollhardt, N. E. Schore, *Organische Chemie. Hauptbd.*, Wiley-VCH, Weinheim, **2020**.
- [13] B. T. Gregg, K. C. Golden, J. F. Quinn, *J. Org. Chem.* **2007**, *72*, 5890–5893.
- [14] T. Kawabata, M. Kato, T. Mizugaki, K. Ebitani, K. Kaneda, *Chem. Lett.* **2003**, *32*, 648–649.
- [15] R. K. Wolford, *J. Phys. Chem.* **1963**, *67*, 632–636.
- [16] H. Müller, A.-K. Becker, G. J. Palm, L. Berndt, C. P. S. Badenhorst, S. P. Godehard, L. Reisky, M. Lammers, U. T. Bornscheuer, *Angew. Chem. Int. Ed.* **2020**, *59*, 11607–11612; *Angew. Chem.* **2020**, *132*, 11704–11709.
- [17] H. Terholsen, J. Kaur, N. Kaloudis, A. Staudt, H. Müller, I. V. Pavlidis, U. T. Bornscheuer, *ChemBioChem* **2022**, *23*, e202200254.
- [18] H. Terholsen, J. Kaur, N. Kaloudis, A. Staudt, I. V. Pavlidis, U. T. Bornscheuer, *Chem. Ing. Tech.* **2022**, *94*, 1860–1863.
- [19] R. Mateos, G. Pereira-Caro, S. Saha, R. Cert, M. Redondo-Horcajo, L. Bravo, P. A. Kroon, *Food Chem.* **2011**, *125*, 865–872.
- [20] R. Bernini, E. Mincione, M. Barontini, F. Crisante, *J. Agric. Food Chem.* **2008**, *56*, 8897–8904.
- [21] H. Huang, C. A. Denard, R. Alamillo, A. J. Crisci, Y. Miao, James. A. Dumesic, S. L. Scott, H. Zhao, *ACS Catal.* **2014**, *4*, 2165–2168.
- [22] C. Giulivi, N. J. Traaseth, K. J. A. Davies, *Amino Acids* **2003**, *25*, 227–232.
- [23] E. Herlinger, R. F. Jameson, W. Linert, *J. Chem. Soc. Perkin Trans. 2* **1995**, 259.
- [24] G. M. Coppola, *Synthesis* **1984**, *1984*, 1021–1023.
- [25] S. Kiran Kumar, D. Rambabu, C. H. Vijay Kumar, B. Yogi Sreenivas, K. R. S. Prasad, M. V. Basaveswara Rao, M. Pal, *RSC Adv.* **2013**, *3*, 24863–24867.
- [26] R. Reddy Kuchukulla, F. Li, Z. He, L. Zhou, Q. Zeng, *Green Chem.* **2019**, *21*, 5808–5812.
- [27] T. Okuhara, *Chem. Rev.* **2002**, *102*, 3641–3666.
- [28] F. Uthoff, H. Gröger, *J. Org. Chem.* **2018**, *83*, 9517–9521.
- [29] F. Uthoff, H. Sato, H. Gröger, *ChemCatChem* **2017**, *9*, 555–558.
- [30] H. Sato, W. Hummel, H. Gröger, *Angew. Chem. Int. Ed.* **2015**, *54*, 4488–4492; *Angew. Chem.* **2015**, *127*, 4570–4574.
- [31] A. Hasanoğlu, Y. Salt, S. Keleşer, S. Dinçer, *Desalination* **2009**, *245*, 662–669.
- [32] K. A. Heyries, C. A. Marquette, L. J. Blum, *Langmuir* **2007**, *23*, 4523–4527.
- [33] A. Gökaltun, Y. B. (Abraham) Kang, M. L. Yarmush, O. B. Usta, A. Asatekin, *Sci. Rep.* **2019**, *9*, 7377.
- [34] M. Kimura, T. Nakato, T. Okuhara, *Appl. Catal. Gen.* **1997**, *165*, 227–240.
- [35] W. Long, C. W. Jones, *ACS Catal.* **2011**, *1*, 674–681.
- [36] H. Müller, H. Terholsen, S. P. Godehard, C. P. S. Badenhorst, U. T. Bornscheuer, *ACS Catal.* **2021**, *11*, 14906–14915.
- [37] P. V. Balaji, S. Chandrasekaran, *Eur. J. Org. Chem.* **2016**, *2016*, 2547–2554.

Entry for the Table of Contents



A chemoenzymatic cascade reaction in an aqueous system was developed for the valorization of the lignin depolymerization product G-C2 dioxolane phenol. The PDMS-protected solid acid catalyst Amberlyst-15 enabled the deacetalization at pH 6.0 and allows coupling with the enzymatic reduction and acylation reactions performed by recombinant horse liver alcohol dehydrogenase and a promiscuous acyltransferase/hydrolase PestE_I208A_L209F_N288A yielding homovanillyl butyrate at a total conversion up to 57%.

Supporting Information

Chemoenzymatic Cascade Reaction for the Valorization of the Lignin Depolymerization Product G-C2-Dioxolane Phenol

Henrik Terholsen, Jule R. H. Meyer, Zhenlei Zhang, Peter J. Deuss, and Uwe T. Bornscheuer

Table of content

Materials	2
Supporting methods	2
Solvent and pH tolerance of HLADH	2
pH tolerance of PestE_I208A_L209F_N288A	2
Transesterification of HVA with butyl butyrate in the presence of Amb-15@PDMS catalyzed by PestE_I208A_L209F_N288A	2
Deprotection and reuse of single Amb-15@PDMS beads.....	2
Figures.....	3
Tables	4

Materials

All materials were ordered from Sigma-Aldrich/Merck, VWR or Carl Roth unless stated otherwise, and were used without further purification.

Supporting methods

Solvent and pH tolerance of HLADH

In preliminary experiments, HLADH showed very little activity below pH 5. For pH screening, 50 mM sodium citrate buffer was used for pH 5 to 6 and 50 mM sodium phosphate buffer for pH 6 to 8. 200 µg/mL HLADH, 1 mM NAD⁺, 100 mM acetaldehyde, and 5 mM HVA were added to a total volume of 1 mL. After 24 h at 20°C (1000 rpm), a sample of 100 µL was extracted with 200 µL ethyl acetate. The samples were dried with anhydrous sodium sulfate and analyzed by GC-FID.

Two-phase systems of 50 mM sodium citrate/phosphate buffer (25 mM each) pH 6.0 and *n*-hexane, ethyl acetate, phenyl acetate, and butyl butyrate were used for solvent tolerance screening. Although *n*-hexane is not an acyl donor for the acyltransferase reaction, it was chosen as a control solvent because of the known stability of HLADH to *n*-hexane^[1]. 100 µg/mL HLADH (1.5 U/mg toward benzaldehyde, Sigma-Aldrich, Saint Louis, MO, USA), 1 mM NAD⁺, 12.1 mM acetaldehyde, 5 mM HVA, and 15% (v/v) organic solvent were added to a total volume of 1.5 mL. After 24 h at 20°C (1000 rpm), the organic phase was removed and the aqueous phase was extracted with 250 µL ethyl acetate. The organic phases were combined, dried with anhydrous sodium sulfate, and analyzed by GC-FID.

To detect the solvent and pH tolerance of HLADH, the oxidation of HVA to HV was investigated since HVA was available in larger amounts.

pH tolerance of PestE_I208A_L209F_N288A

For pH screening, 50 mM sodium citrate buffer was used for pH 3 to 6 and 50 mM sodium phosphate buffer for pH 6 to 8. 20 µg/mL PestE_I208A_L209F_N288A, 5 mM HVA, and 50% (v/v) were added to a total volume of 0.4 mL. After 24 h at 20°C (1000 rpm), the organic phase was removed, dried with anhydrous sodium sulfate, and analyzed by GC-FID.

Transesterification of HVA with butyl butyrate in the presence of Amb-15@PDMS catalyzed by PestE_I208A_L209F_N288A

Ten Amb-15@PDMS (~7 mg, containing 1.4 mg Amb-15), 10 µL HVA solution (from a 50 mM stock in butyl butyrate; 5 mM final concentration), 10 µL butyl butyrate, and 80 µL sodium phosphate/citrate buffer (25 mM each; pH 6.0) with 20 µg PestE_I208A_L209F_N288A were added to a 1.5-mL GC vial and incubated for 24 h at 20°C (1000 rpm). The aqueous phase was separated and extracted twice with 200 µL ethyl acetate. The beads were washed twice with 200 µL ethyl acetate (10 min, 20°C, 1000 rpm). The ethyl acetate phases were combined and dried with anhydrous sodium sulfate before GC analysis. The reaction was carried out in duplicates. Conversions of 68±1% were achieved.

Deprotection and reuse of single Amb-15@PDMS beads

For the experiment with a single Amb-15@PDMS, the reaction was performed as described above, but with only one bead. After the extraction and washing the Amb-15@PDMS beads used were dried for 3 hours at 60°C and reused for the same reaction as before. The results are described in Table S2 and the beads used are shown in Figure S4.

Figures

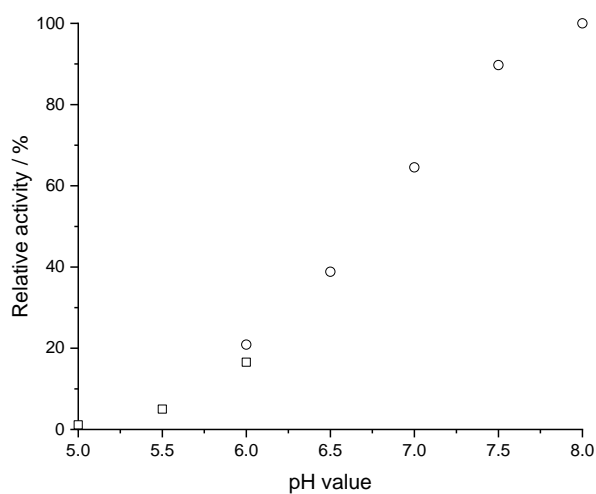


Figure S1. Relative activity of HLADH in sodium citrate buffer pH 5 to 6 (squares) and sodium phosphate buffer pH 6 to 8 (circles).

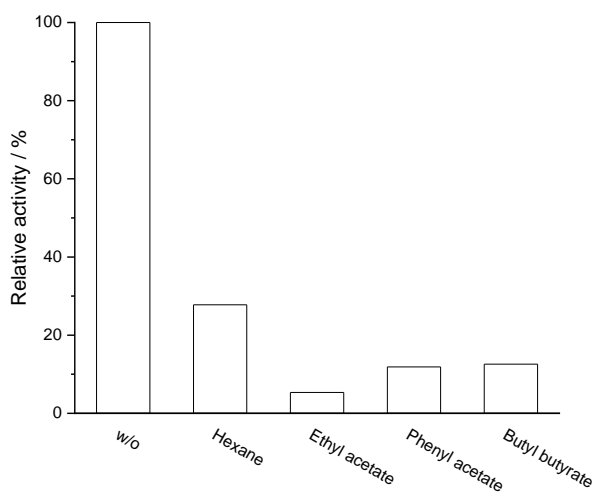


Figure S2. Relative activity of HLADH in a two-phasic of 50 mM sodium citrate/phosphate buffer and 15 % (v/v) organic solvent.

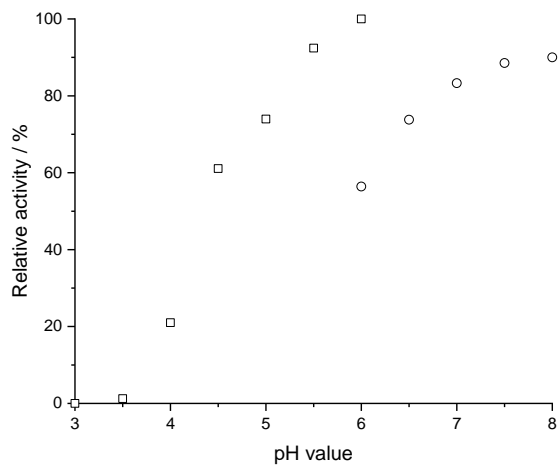


Figure S3. Relative activity of PestE_I208A_L209F_N288A in sodium citrate buffer pH 3 to 6 (squares) and sodium phosphate buffer pH 6 to 8 (circles).

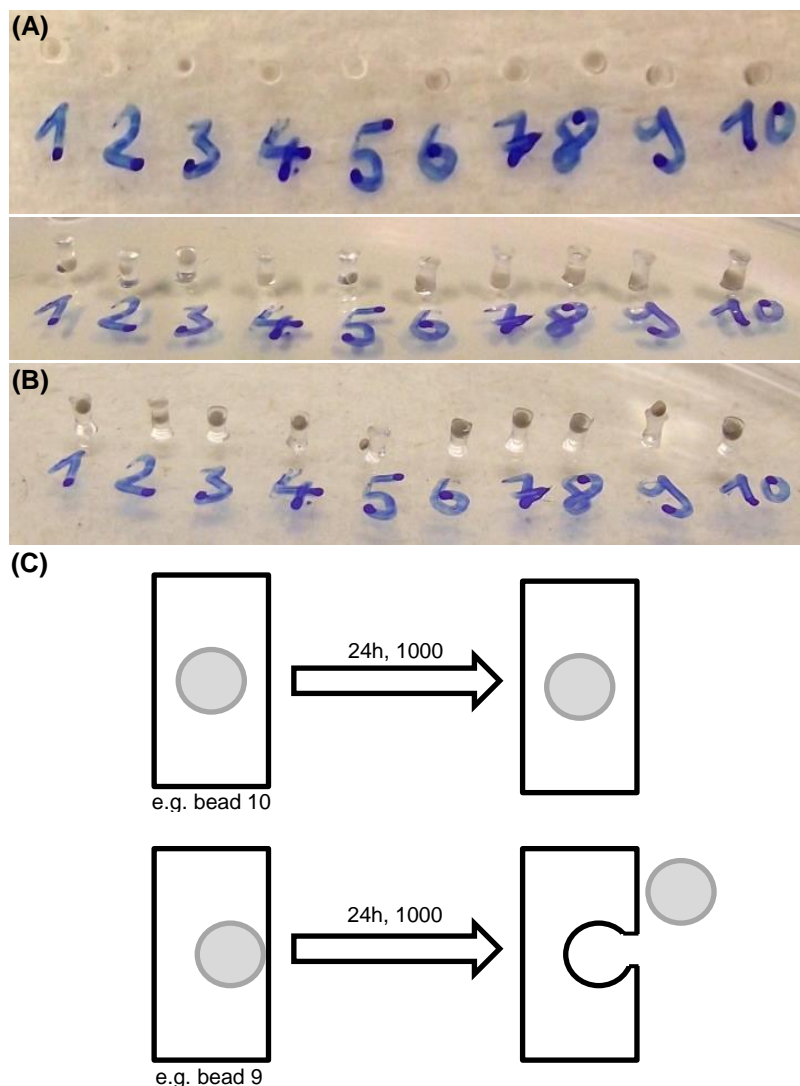


Figure S4. Amb-15@PDMS punches with smaller (1-5, about 0.1 mg) and larger (6-10, about 0.2 mg) holes. (A) Amb-15@PDMS beads before the reaction described in Table S2 in top and side view. (B) The same Amb-15@PDMS beads after the reaction described in Table S2. The numbering corresponds to the entries in Table S2. (C) Schematic representation of the disintegration of Amb-15@PDMS when the solid acid catalyst is not in the center of the punching (e.g., bead 9).

Tables

Table S1. Initial cascade reactions with Amb-15@PDMS.

Entry	HLADH	PestE	DOX	HV	HVA	HVB
1 ^a	-	20 µg	32±14%	57±15%	9±1%	2±0%
2	OD ₆₀₀ 500	-	64±6%	1±0%	34±6%	Traces
3	OD ₆₀₀ 500	10 µg	26±18%	37±5%	32±8%	32±10%
4	OD ₆₀₀ 500	20 µg	37±5%	15±5%	21±1%	27±1%
5	OD ₆₀₀ 500	40 µg	87±7%	4±4%	3±1%	6±2%
6 ^b	OD ₆₀₀ 500	20 µg	65±2%	4±1%	16±4%	15±2%
7 ^c	OD ₆₀₀ 500	20 µg	57±0%	8±6%	18±4%	17±2%
8 ^d	OD ₆₀₀ 500	20 µg	84±3%	1±0%	9±3%	6±0%
9 ^e	OD ₆₀₀ 500	20 µg	61±21%	6±5%	20±10%	13±6%
10	-	-	3±0%	97±0%	-	-

Reaction conditions: 5 mM G-C2 dioxolane phenol, 7 mg Amb-15@PDMS (containing approximately 1.4 mg Amb-15; 10 beads), 20% (v/v) butyl butyrate, and purified PestE I208A_L209F_N288A were added. The 100-µL-scale reaction in sodium phosphate/citrate buffer (25 mM each) was performed at 20°C (1000 rpm) for 24 hours. HLADH was expressed in *E. coli* whole cells and used as a lyophilizate. All reactions were extracted twice with 200 µL ethyl acetate and Amb-15@PDMS was also washed twice. Values shown are means of duplicates. OD₆₀₀ was measured before lyophilization and the amount of lyophilisate added was adjusted accordingly. a) 150 OD₆₀₀ *E. coli* whole cells containing empty vector pET28a. b) 50% (v/v) butyl butyrate. (c) Addition of PestE as lyophilisate of *E. coli* BL21 (DE3) containing 20 µg PestE. (d) Addition of PestE as lyophilisate of crude lysate containing 20 µg PestE. (e) Addition of PestE as lyophilisate of supernatant of lysate heated to 80°C for 40 min.

Table S2. DOX deprotection efficiency of single Amb-15@PDMS beads (see also Figure S4).

Entry	Conversion (first use)	Conversion (second use)
1	23%	29%
2	4%	0%
3	24%	33%
4	21%	18%
5	<1%	0%
6	31%	7%
7	26%	21%
8	34%	43%
9	1%	0%
10	42%	46%

Reaction conditions: 5 mM G-C2 dioxolane phenol, one Amb-15@PDMS bead (about 0.7 mg; 0.1-0.2 mg Amberlyst-15), and 20% (v/v) butyl butyrate were added. The 100- μ L-scale reaction in sodium phosphate/citrate buffer (25 mM each; pH 6.0) was performed at 20°C (1000 rpm) for 24 hours. The conversions are relative to the recovered molecules, the recovery rate was about 80%. Beads 1 to 5 were smaller (about 0.1 mg per bead) and beads 6-10 were bigger (about 0.2 mg per bead, see also Figure S4).

Manual punching of the Amb-15@PDMS beads is a critical factor and resulted in stronger variations in the deprotection efficiency of initial cascade reactions (Table S1). To estimate the activity variation between Amb-15@PDMS punchings, single beads (instead of 10) were used for the deprotection experiments (Figure S4). One bead showed below 1% conversion, while others showed up to 42% conversions (entries 5 and 10). On average, 21% conversion was achieved, but the standard deviation was high (13%). Larger Amberlyst-15 beads generally gave higher conversion than smaller beads (entries 6 to 10 and 1 to 5, respectively), probably due to a thinner PDMS layer and thus a shorter diffusion path. On the other hand, care had to be taken to ensure that the Amberlyst-15 beads were located in the center of the punch-outs, otherwise PDMS layers that were too thin would break open during shaking and release the Amberlyst-15 bead (Figure S4), leading to a loss of activity and acidification of the medium (entries 5 and 9).

Protein sequences

PestE_I208A_L209F_N288A (in pET28a):

MPLSPILRQILQQLAAQLQFRPDMVDVKTVREQFEKSSLILVKMANEPIHRVEDITIPGRGGPIRARVYRPRDGERLPAVVYY
HGGGFVLGVSVDHVCRRANLSGAVVSVDYRLAPEHKFPAAVEDAYDAAKWVADNYDKLGVDNGKIAVAGDSAGG
NLAAVTAIMARDRGESFVKYQVLIYPAVNLTGSPTVSRVEYSGPEYVAFTADLMAWFGRQYFSKPDALSPYASPIFADLS
NLPPALVITAEYDPLRDEGELYAHLKTRGVRAVAVRYNGVIHGFVFFYPILEEGREAVSQIAASIKSMAVALEHHHHHH*

HLADH (in pET28a):

MSTAGKVIKCKAAVLWEEKKPFSEIEVEVAPPKAHEVRIKMVATGICRSDDHVSGTLVTPLPVIAGHEAAGIVESIGEGVTT
VRPGDKVIPLFTPQCCKRVCVCKHPEGNFCLKNDLSMPRGTMQDGTSRFTCRGKPIHHFLGTSTFSQYTVVDEISVAKIDA
ASPLEKVCLIGCFSTGYGSAVKAVTQGSTCAVFLGGVGLSVIMGCKAAGAARIIGVDINKDKFAKAKEVGATECVNP
QDYKKPIQEVLTMSNGGVDFSFVEVIGRLDTMVTALSCCQEAYGVSIVGVPPDSQNLMSNPMLLLSGRTWKGAIFGGFK
SKDSVPKLVADFMKKFALDPLITHVLPFEKINEGFDLLRSGESIRTILTFFHHHHHH*

Literature

[1] D. Quaglia, M. Pori, P. Galletti, E. Emer, F. Paradisi, D. Giacomini, *Proc. Biochem.* **2013**, *48*, 810–818.

7. List of Publications

1. T. Bayer, A. Becker, H. Terholsen, I. J. Kim, I. Menyes, S. Buchwald, K. Balke, S. Santala, S. C. Almo, U. T. Bornscheuer, LuxAB-Based Microbial Cell Factories for the Sensing, Manufacturing and Transformation of Industrial Aldehydes. *Catalysts* **2021**, *11*, 953
2. H. Müller, H. Terholsen, S. P. Godehard, C. P. S. Badenhorst, U. T. Bornscheuer, Recent Insights and Future Perspectives on Promiscuous Hydrolases/Acyltransferases. *ACS Catal.* **2021**, *11*, 14906–14915.
3. A. Staudt, H. Terholsen, J. Kaur, H. Müller, S. P. Godehard, I. Itabaiana, I. C. R. Leal, U. T. Bornscheuer, Rational Design for Enhanced Acyltransferase Activity in Water Catalyzed by the *Pyrobaculum calidifontis* VA1 Esterase. *Microorganisms* **2021**, *9*, 1790.
4. I. J. Kim, T. Bayer, H. Terholsen, U. T. Bornscheuer, α -Dioxygenases (α -DOXs): Promising Biocatalysts for the Environmentally Friendly Production of Aroma Compounds. *ChemBioChem* **2022**, *23*, e202100693.
5. H. Terholsen, J. Kaur, N. Kaloudis, A. Staudt, H. Müller, I. V. Pavlidis, U. T. Bornscheuer, Recovery of Hydroxytyrosol from Olive Mill Wastewater Using the Promiscuous Hydrolase/Acyltransferase PestE. *ChemBioChem* **2022**, *23*, e202200254.
6. H. Terholsen, J. Kaur, N. Kaloudis, A. Staudt, I. V. Pavlidis, U. T. Bornscheuer, An Enzyme Cascade Reaction for the Recovery of Hydroxytyrosol Derivatives from Olive Mill Wastewater. *Chem. Ing. Tech.* **2022**, *94*, 1860–1863.
7. S. Roda*, H. Terholsen*, J. R. H. Meyer, A. Cañellas, V. Guallar, U. T. Bornscheuer, M. Kazemi, AsiteDesign: A semi-rational algorithm for automated enzyme design. *J. Phys. Chem. B* **2023**, *Minor revision*
*with equal contribution
8. H. Terholsen*, H. D. Huerta-Zerón*, C. Möller, H. Junge, U. Bornscheuer, M. Beller, Photo-enzymatic Catalytic CO₂ Reduction Using a Promiscuous Decarboxylase as Protein Scaffold. *Nat. Catal.* **2023**, *submitted*
*with equal contribution
9. H. Terholsen, J. R. H. Meyer, Z. Zhang, P. J. Deuss, and U. T. Bornscheuer, Chemoenzymatic Cascade Reaction for the Valorization of the Lignin Depolymerization Product G-C2-Dioxolane Phenol. *ChemSusChem* **2023**, *submitted*
10. H. Terholsen*, K. Myrtiollari*, C. Möller, R. Kourist, U. T. Bornscheuer, D. Kracher, Spectrophotometric and Fluorimetric High-Throughput Assays for Phenolic Acid Decarboxylase. *Manuscript in preparation*
*with equal contribution
11. H. Terholsen, L. Koch, I. Somvilla, S.C. Almo, U. T. Bornscheuer, T. Bayer, Protein-ligand Interaction-guided Expansion of Inducible Expression Systems in *Escherichia coli*. *Manuscript in preparation*

8. Acknowledgement

Mein besonderer Dank gilt denen, die mich auf meinem Weg unterstützt haben. Zum einen danke ich Uwe dafür, dass er mir 2018 die Möglichkeit gegeben hat mein Forschungspraktikum in seiner Arbeitsgruppe zu machen. Die positiven Eindrücke fachlicher und persönlicher Natur haben mir den Weg zur Promotion in Greifswald überhaupt erst eröffnet. Den Schritt für die Stelle in deiner Arbeitsgruppe nach Greifswald zu kommen habe ich nie bereut. Besonders genossen habe ich die Möglichkeit zur Umsetzung vieler eigener Ideen und Mitwirkung an diversen Projekten, selbst wenn diese nicht immer unbedingt zum selben Ast des Promotionsbaums gehörten -was sich im Bezug auf den Projektverlauf des ursprüngliche Hauptprojekts als großer Glücksfall herausstellte-. Zudem möchte ich mich dafür bedanken, dass mir Konferenzen, Dienstreisen, etc. ermöglicht wurden, die meinen persönlichen und wissenschaftlichen Horizont erweitert haben. Im Hinblick auf meinen Aufenthalt in Kreta möchte ich Ioannis (Pavlidis) und seiner ganzen Arbeitsgruppe, besonders aber Nikos (Kaloudis), für die herzliche Aufnahme und den Beitrag zum Olivenölabwasserprojekt bedanken.

Meinen hart arbeitenden Bachelorstudentinnen Jasmin (Kaur) und Jule (Meyer) möchte ich einen besonderen Dank aussprechen, da sie mit ihrer Arbeit einen wesentlich Beitrag zum Gelingen der PestE-Projekte geleistet haben. Meiner ehemaligen Masterandin und Freundin Christina (Möller) möchte ich neben ihrem fachlichen Beitrag zum BsPAD und Universal-Thrombozytenkonzentrat-Projekt für viele gemeinsame, motivierende Kaffeepausen, Squashspiele und sonstige außeruniversitäre Aktivitäten danken. Als erster Ansprechpartner im Labor hast du zur Lösung vieler großer und kleiner Probleme beigetragen.

Mit Thomas (Bayer) habe ich nicht nur mein erstes Paper publiziert, sondern auch viel über wissenschaftliches Arbeiten gelernt. Bei Kaffee und manchmal Kuchen/Milchhörnchen haben wir spannende Projekte geplant, Ergebnisse diskutiert und über Gott und die Welt geredet. Dich konnte ich auch immer fragen, wenn ich mal nicht weiter wusste, wofür ich dir ganz herzlich danken möchte.

Meinen Kooperationspartnern aus der Transfusionsmedizin und dem LIKAT Rostock möchte ich gerne für den regen und konstruktiven Austausch danken. Ina (Menyes) möchte ich danken, dass ich so viel über analytische Methoden lernen

8. Acknowledgement

durfte (ich habe tatsächlich alle Geräte außer GC1 und HPLC4 in meinem PhD benutzt).

Mark und Dominique möchte ich für die Labororganisation und hilfreiche Anmerkungen bei Projektmeetings und Vorträgen danken.

Besonderer Dank gilt meiner Familie und Freunden, die mich auch an den harten Tagen auf meinem Weg unterstützten und Kraft gegeben haben. Auf euch konnte ich mich immer verlassen!

Generell habe ich die offene und hilfsbereite Atmosphäre der Arbeitsgruppe stets genossen und möchte mich bei allen bedanken die auf unterschiedlichster Weise, bspw. einem kurzen Austausch auf dem Gang oder eine Gemeinschaftsaktivität, zu meiner Promotion beigetragen haben.

Zu letzt möchte ich dem Leibniz-Wissenschaftscampus ComBioCat für die Finanzierung meines PhDs danken.